Simulation of Net Infiltration and Potential Recharge Using a Distributed-Parameter Watershed Model of the Death Valley Region, Nevada and California

By Joseph A. Hevesi, Alan L. Flint, *and* Lorraine E. Flint

U.S. GEOLOGICAL SURVEY

Water-Resources Investigations Report 03-4090

Prepared in cooperation with the
Office of Environmental Management
U.S. Department of Energy
National Nuclear Security Administration
Nevada Operation Office, under
Interagency Agreement DE-AI08 01NV13944

8035-82

Sacramento, California
2003

U.S. DEPARTMENT OF THE INTERIOR
GALE A. NORTON, *Secretary*

U.S. GEOLOGICAL SURVEY
Charles G. Groat, *Director*

The authors wish to thank the many individuals who contributed to the development of this report. Claudia Faunt and Thomas Haltom (USGS), and Frank D'Agnese and Grady O'Brien (formerly with USGS), provided support and expertise in the application of the geographic information systems (GIS) used to develop the model inputs and to help analyze the model results. Helpful suggestions were provided by Daniel Bright (USGS), Robert Meyer (USGS), Devin Galloway (USGS), Richard Waddell (GeoTrans Inc.), Tony Buono (retired USGS), Doug Bedinger (formerly with USGS), and James Harrill (formerly with USGS). Glenn Schwegmann (formerly with USGS) and Myrna DeBortoli (USGS) provided editorial reviews of the manuscript and also contributed to the development of the manuscript. David Uyematsu (USGS) contributed to the development of illustrations. James Baker (USGS) prepared the final version of the manuscript for the web-based publication.

For additional information write to:

U.S. Geological Survey
Water Resources
Placer Hall, Suite 2012
6000 J Street
Sacramento, California 95819-6129
http://ca.water.usgs.gov

Copies of this report can be purchased from:

U.S. Geological Survey
Information Services
Building 810
Box 25286, Federal Center
Denver, CO 80225-0286

CONTENTS

FIGURES

TABLES

CONVERSION FACTORS, DATUM, AND ABBREVIATIONS

CONVERSION FACTORS

Multiply	By	To obtain
	Length	
meter (m)	3.281	foot
millimeter (mm)	0.03937	inch
	Area	
square kilometer (km^2)	247.1054	acre
square meter ($m^{2)}$	0.0002471	acre
	Volume	
cubic meter (m^3)	0.0002642	gallons
cubic meter (m^3)	0.000810713	acre-feet
	Flow rate	
cubic meter per day (m^3/d)	0.296113	acre-feet per year
cubic meter per day (m^3/d)	0.000408731	cubic-feet per second
millimeter per day (mm/d)	0.03937	inch per day
millimeter per year (mm/yr)	0.03937	inch per year

Temperature in degrees Celsius (^oC) may be converted to degrees Fahrenheit (^oF) as follows:

$$^oF=1.8\ ^oC+32.$$

VERTICAL DATUM

Sea level: In this report, "sea level" refers to the National Geodetic Vertical Datum of 1929 (NGVD of 1929)—a geodetic datum *derived* from a general adjustment of the first-order level nets of both the United States and Canada, formerly called Sea Level Datum of 1929.

VERTICAL DATUM

All map units and projections in this report are in the Universal Transverse Mercator system, North American Datum of 1927 (NA27D), zone 11, in meters.

ABBREVIATIONS

ADRS	Amargosa Desert Research Site
BR	Biological Resources
CMB	chloride mass balance
DEM	digital elevation model
DVRFS	Death Valley regional flow system
ENSO	El Niño Southern Oscillation
GAP	Gap Analysis Program
GIS	geographic information system
INFIL	Net infiltration model
INFILv3	Net infiltration model version 3
NOAA/NCDC	National Oceanic and Atmospheric Administration/National Climatic Data Center
NTS	Nevada Test Site
NWS	National Weather Service
PDO	Pacific Decadal Oscillation
STATSGO MUID	State Soil Geographic map unit identifier
USGS	U.S. Geological Survey
UTM	Universal transverse Mercator
WESTVEG	western region vegetation

Simulation of Net Infiltration and Potential Recharge Using a Distributed-Parameter Watershed Model of the Death Valley Region, Nevada and California

By Joseph A. Hevesi, Alan L. Flint, *and* Lorraine E. Flint

ABSTRACT

This report presents the development and application of the distributed-parameter watershed model, INFILv3, for estimating the temporal and spatial distribution of net infiltration and potential recharge in the Death Valley region, Nevada and California. The estimates of net infiltration quantify the downward drainage of water across the lower boundary of the root zone and are used to indicate potential recharge under variable climate conditions and drainage basin characteristics. Spatial variability in recharge in the Death Valley region likely is high owing to large differences in precipitation, potential evapotranspiration, bedrock permeability, soil thickness, vegetation characteristics, and contributions to recharge along active stream channels. The quantity and spatial distribution of recharge representing the effects of variable climatic conditions and drainage basin characteristics on recharge are needed to reduce uncertainty in modeling ground-water flow. The U.S. Geological Survey, in cooperation with the Department of Energy, developed a regional saturated-zone ground-water flow model of the Death Valley regional ground-water flow system to help evaluate the current hydrogeologic system and the potential effects of natural or human-induced changes. Although previous estimates of recharge have been made for most areas of the Death Valley region, including the area defined by the boundary of the Death Valley regional ground-water flow system, the uncertainty of these estimates is high, and the spatial and temporal variability of the recharge in these basins has not been quantified.

To estimate the magnitude and distribution of potential recharge in response to variable climate and spatially varying drainage basin characteristics, the INFILv3 model uses a daily water-balance model of the root zone with a primarily deterministic representation of the processes controlling net infiltration and potential recharge. The daily water balance includes precipitation (as either rain or snow), snow accumulation, sublimation, snowmelt, infiltration into the root zone, evapotranspiration, drainage, water content change throughout the root-zone profile (represented as a 6-layered system), runoff (defined as excess rainfall and snowmelt) and surface water run-on (defined as runoff that is routed downstream), and net infiltration (simulated as drainage from the bottom root-zone layer). Potential evapotranspiration is simulated using an hourly solar radiation model to simulate daily net radiation, and daily evapotranspiration is simulated as an empirical function of root zone water content and potential evapotranspiration. The model uses daily climate records of precipitation and air temperature from a regionally distributed network of 132 climate stations and a spatially distributed representation of drainage basin characteristics defined by topography, geology, soils, and vegetation to simulate daily net

infiltration at all locations, including stream channels with intermittent streamflow in response to runoff from rain and snowmelt. The temporal distribution of daily, monthly, and annual net infiltration can be used to evaluate the potential effect of future climatic conditions on potential recharge.

The INFILv3 model inputs representing drainage basin characteristics were developed using a geographic information system (GIS) to define a set of spatially distributed input parameters uniquely assigned to each grid cell of the INFILv3 model grid. The model grid, which was defined by a digital elevation model (DEM) of the Death Valley region, consists of 1,252,418 model grid cells with a uniform grid cell dimension of 278.5 meters in the north–south and east–west directions. The elevation values from the DEM were used with monthly regression models developed from the daily climate data to estimate the spatial distribution of daily precipitation and air temperature. The elevation values were also used to simulate atmospheric effects on potential evapotranspiration, to develop topographic parameters to simulate the effects of shading on potential evapotranspiration, and to develop parameters to simulate surface-water flow. Surface-water flow was modeled as a downstream redistribution of runoff generated by rain or snowmelt and was routed across all the model grid cells as a daily surface-water run-on component of the water balance (for days when runoff was generated) using an eight-directional (D-8), convergent-flow routing algorithm. A six-layer root-zone system— five soil layers and one bedrock layer—was used to simulated the daily root-zone water balance, including evapotranspiration, infiltration, drainage, and redistribution of moisture in the root zone. Evapotranspiration from each root-zone layer was modeled as a function of potential evapotranspiration, the estimated root density for each layer, and the simulated water content for each layer. Downward drainage through each layer was modeled as a function of soil saturated hydraulic conductivity, soil texture, and the simulated water content. Snowfall, sublimation, and snowmelt were modeled as functions of the spatially distributed daily climate input and the simulated solar radiation component of the potential evapotranspiration model.

The model was calibrated using comparisons of (1) simulated streamflow with historical streamflow data from 31 gaging stations in the Death Valley region, and (2) simulated 50-year (1950–99) basinwide average net infiltration with previous estimates of basinwide average recharge for 42 basin areas (defined in previous studies as hydrographic areas and subareas) in the Death Valley region. Parameters adjusted during model calibration included bedrock saturated hydraulic conductivity, root density, average storm duration (for summer and winter storms), and soil saturated hydraulic conductivity and wetted area used to represent stream-channel characteristics. Model calibration using the streamflow records was difficult because the spatial coverage of the daily climate records for many locations in the Death Valley region is not sufficient for simulating local-scale, high-intensity summer storms. In addition, calibration results based on streamflow were sensitive to the parameters representing stream-channel characteristics, and these characteristics were assumed (and thus highly uncertain). Comparison of simulated basinwide net infiltration with previous basinwide estimates of recharge provided better calibration results than comparisons using simulated and measured streamflow. Overall calibration of the INFILv3 model incorporated the results from both methods of calibration because of the uncertainty of the previous estimates of recharge and because of the need to develop independent estimates of potential recharge,

The 50-year INFILv3 simulation results for four different models (where model differences were defined by differences in input parameters were evaluated using a comparison of net-infiltration estimates with the streamflow records and the previous basinwide recharge estimates for the 42 hydrographic areas and subareas. For the model providing the best overall calibration, a total net-infiltration estimate of 413,000 m^3/d was simulated for the total area covered by the 42 hydrographic areas and subareas; this estimate is in good agreement with the total estimated basinwide recharge of 431,000 m^3/d for the same area. The net-infiltration results generally are consistent with the recharge estimates, although net

infiltration had less variability on a basinwide scale. Basinwide net-infiltration volumes are lower than recharge volumes for most of the hydrographic areas and subareas that have high recharge estimates and higher than recharge for most hydrographic areas and subareas that have low recharge estimates. The model comparisons indicate that simulated daily streamflow is sensitive to uncertainty in estimates of storm duration, stream-channel characteristics, and bedrock hydraulic conductivity. Net infiltration is sensitive to uncertainty in bedrock hydraulic conductivity and parameters controlling evapotranspiration (such as root density). Both streamflow and net infiltration are sensitive to uncertainty in spatially distributed precipitation and estimated soil thickness.

For the model providing the best overall calibration, model application results for the Death Valley regional ground-water flow system (based on the 1950–99 simulation) include an average net infiltration rate of 2.8 millimeters per year (mm/yr), or a total potential recharge volume of 342,000 cubic meters per day (m^3/d). The simulated potential recharge is 1.6 percent of the 1950–99 simulated average annual precipitation rate of 171.3 mm/yr. Net-infiltration results for individual model cells were highly variable across the Death Valley regional ground-water flow system, with a maximum net-infiltration rate of 1,262 mm/yr for an active stream-channel location. Simulation results also include an average runoff-generation rate of 2.2 mm/yr and an average run-on infiltration rate of 2.0 mm/yr, indicating that most of the runoff infiltrates back into the root zone during downstream routing (as run-on) rather than discharging to playas. Infiltration from surface-water run-on accounts for about 14 percent of the total net-infiltration volume for the Death Valley regional ground-water flow system. However, in some areas of the regional flow system, surface-water flow may contribute as much as 40 percent to the total net-infiltration volume. The simulated average surface-water inflow into playa lakebeds is 0.20 mm/yr and is assumed to evaporate from the playas.

INTRODUCTION

The purpose of this report is to document the development and application of the distributed-parameter, deterministic watershed model, INFILv3 (henceforth referred to as the INFILv3 model), for estimating the magnitude and the spatial and temporal distribution of net infiltration in the Death Valley region of Nevada and California. Net infiltration, defined as the downward drainage of water across the lower boundary of the root zone, was used to estimate potential recharge. Estimates of the magnitude and the spatial and temporal distribution of potential recharge were needed to reduce the uncertainties in calibrating and applying ground-water flow models for the Death Valley regional ground-water flow system (following D'Agnese and others [1997, 2002], the Death Valley regional ground-water flow system is referred to as the Death Valley regional flow system, or DVRFS). Ground-water flow models of the saturated zone of the DVRFS were developed by the U.S. Geological Survey (USGS), in cooperation with the Department of Energy, to help evaluate current hydrogeologic conditions and to assess the potential effects of changes in the hydrogeologic systems, either natural or human induced (D'Agnese and others, 1997, 2002). Ground-water flow models of the DVRFS require input data on the quantity and spatial distribution of recharge and on the variability of recharge in response to potential future climatic conditions (D'Agnese and others, 1999). Although previous estimates of recharge for the DVRFS were used to develop the upper boundary conditions for ground-water flow models, the spatial and temporal distributions of the recharge were not well defined, and the methods used to develop the previous estimates could not be used directly to evaluate changes in the hydrogeologic system, such as changes in climate, vegetation, or land use. Identifying localized zones with high potential recharge rates is necessary for predicting ground-water flow paths and travel times. A spatially detailed map of current climate recharge would help reduce uncertainties in calibrating ground-water flow models of the Death Valley region. In addition, a characterization of the temporal distribution of recharge, in

response to climate variability, is needed to develop transient ground-water flow models. The transient flow models can be used to predict the hydrologic response of the Death Valley region to potential future climate conditions (D'Agnese and others, 1999).

Conceptual and numerical models of net infiltration were first developed for Yucca Mountain, Nevada (located in the central part of the Death Valley region) in 1996. The net infiltration models were used to help define the upper boundary conditions for unsaturated zone flow and transport models (Flint and others, 2000, 2001a, b; Hevesi, 2001). A version of the net-infiltration model for Yucca Mountain (INFIL) was extended to include the area of the Death Valley region to develop preliminary estimates of net infiltration and potential recharge for a regional ground-water flow model (D'Agnese and others, 2002; Hevesi and others, 2002). A comparison of previous estimates of recharge (Hevesi and others, 2002) indicated that the preliminary estimates of net infiltration likely were overestimates of potential recharge for current climate conditions. This conclusion is supported by the calibration results of the ground-water flow model by D'Agnese and others (2002), which included updated estimates of ground-water discharge from the regional flow system. For the study reported here, an enhanced version of the net-infiltration model, INFILv3, was developed with the objective of addressing the limitations identified during the initial application of the INFIL model to the Death Valley region. The INFILv3 model provides a detailed representation of spatially distributed basin characteristics and hydrologic processes that control net infiltration and potential recharge in the Death Valley region. The INFILv3 model provides a detailed representation of spatially distributed basin characteristics and hydrologic processes that control net infiltration and potential recharge in the Death Valley region. The INFILv3 model provides a toll for evaluating the effects of climate variability and potential changes in drainage basin characteristics (such as changes in vegetation) on the temporal and spatial distribution of net infiltration and potential recharge.

Description of Study Area

Geographic Setting and Physiography

The study area for developing, calibrating, and applying the INFILv3 model is located between lat 35°N., long 115°W., and lat 38.25°N., long 118°W., and is referred to as the Death Valley region (fig. 1) (D'Agnese and others, 2002). The primary area of interest for estimating net infiltration is defined by the boundary of the Death Valley regional flow system (DVRFS) ground-water model by D'Agnese and others (2002). The DVRFS model boundary is similar, but not identical, to earlier boundaries (D'Agnese and others, 1997) used to define the Death Valley regional flow system (fig. 2). The DVRFS boundary generally approximates the area defined by Bedinger and others (1989) as the Death Valley ground-water region. The northern part of the DVRFS is in the southern section of the Great Basin of the Basin and Range physiographic province (Grayson, 1993) and extends into the Great Basin Desert (fig. 1). The Basin and Range is characterized by linear mountains and broad valleys with a distinct north-to-northwest trend. This physiography is primarily the result of normal faulting in response to east–west extensional tectonics. The southern and central parts of the DVRFS are in the northern Mojave Desert. The physiography of the southern part of the DVRFS is primarily the result of a combination of strike-slip faulting and downdrop block faults. Elevations range from 86 m below sea level at Death Valley to 3,600 m above sea level in the Spring Mountains. The relief between valleys and adjoining mountains exceeds 1,500 m at many locations (Bedinger and others, 1989). About 25 percent of the landscape in the study area is rugged mountainous terrain; the remainder is broad intermountain basins filled with alluvium and some interbedded volcanic deposits (Peterson, 1981).

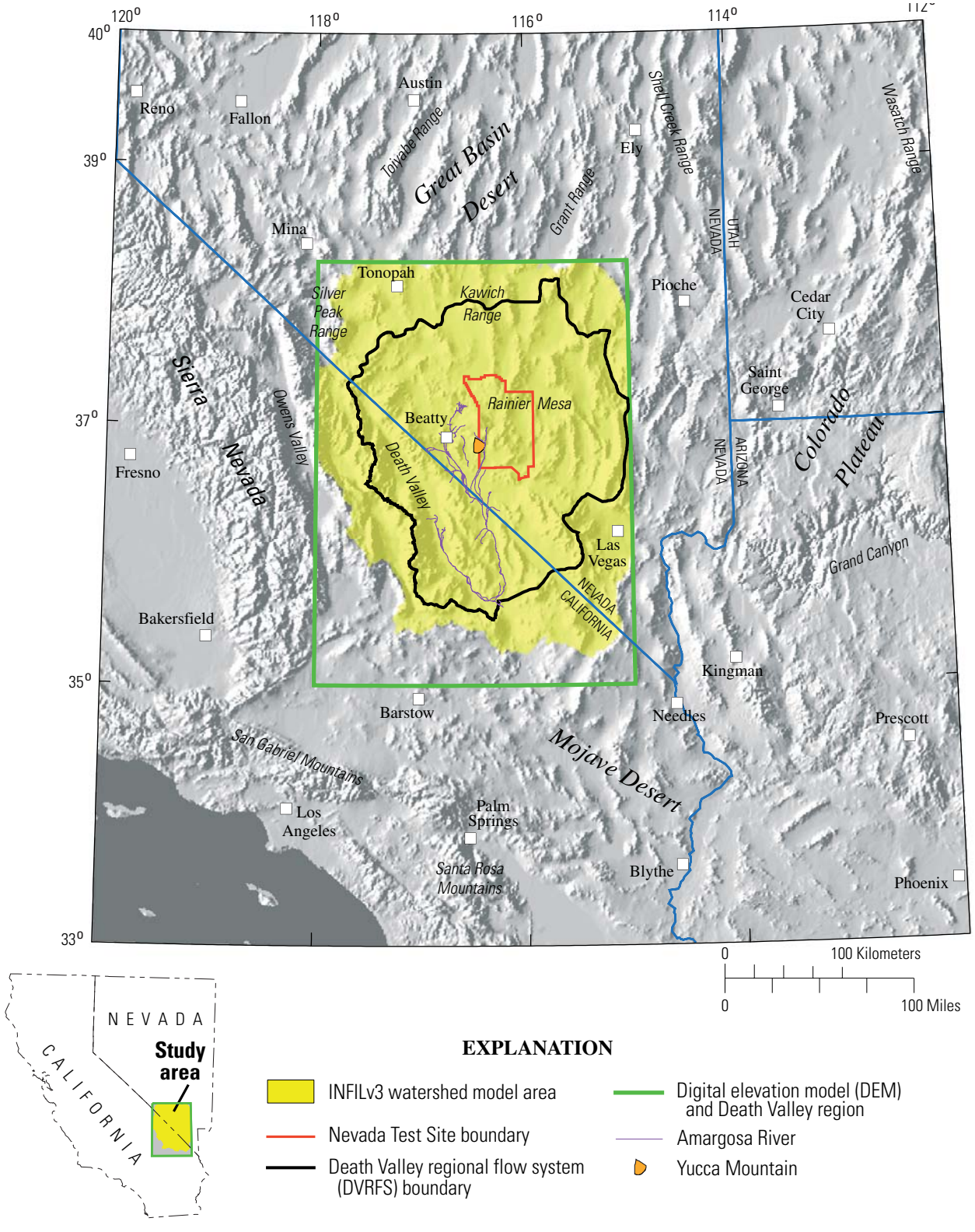

Figure 1. Map showing Geographic setting of the Death Valley region, Nevada and California.

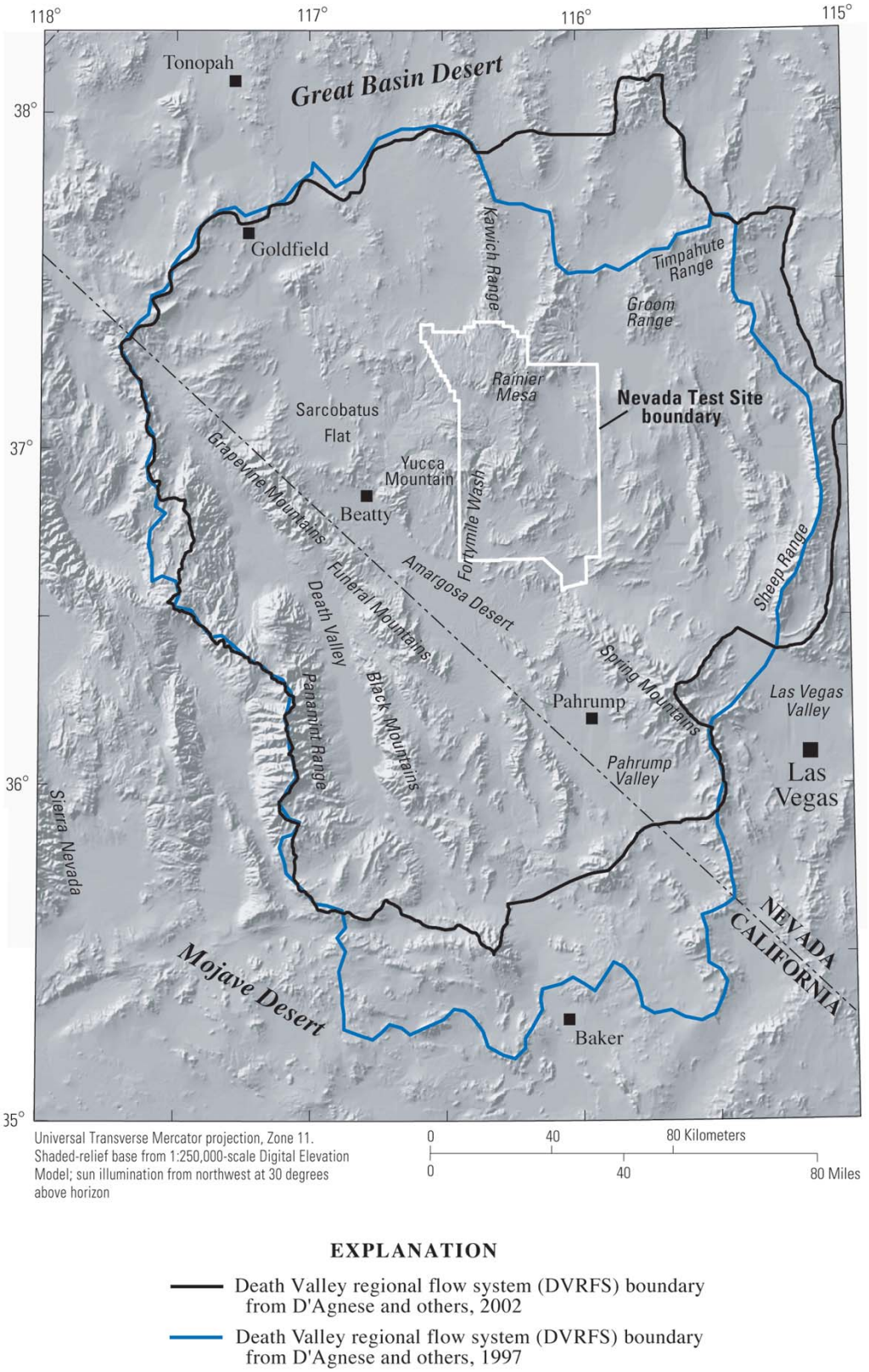

Figure 2. Death Valley regional flow system boundary and physiographic features of the Death Valley region, Nevada and California.

The Death Valley region includes many topographically closed basins and surface-water drainage basins. The Amargosa River (fig. 3), an intermittent stream in the Amargosa Desert, is the main stream in the largest surface-water drainage basin in the Death Valley region, with a area of approximately 15,000 km^2. The Amargosa River discharges into the southern part of the Death Valley saltpan, the largest playa lake in the Death Valley region (Hunt and others, 1966). The north Salt Creek drainage basin discharges into the northern part of the Death Valley saltpan. The south Salt Creek drainage basin is the main tributary basin to the Amargosa River in the lower Amargosa River drainage basin (Grasso, 1996). The Fortymile Wash drainage basin, a tributary drainage basin to the upper Amargosa River drainage basin, covers a large part of the Nevada Test Site (NTS), including much of the Yucca Mountain area (fig. 2).

The floors of the basins and the valleys tend to be broad and have nearly flat surfaces. Playas, common to arid environments, generally are at the lowest elevations of the closed basins in the DVRFS (fig. 3). The playas act as catchments for surface-water runoff (Grose and Smith, 1989). The playa lakebeds generally are dry but become shallow temporary lakes during wetter-than-average years (Grasso, 1996). Playas in Sarcobatus Flat, the Amargosa Desert, Pahrump Valley, and Death Valley are coincident with areas of ground-water discharge in the DVRFS, referred to in this report as ground-water discharge zones, (fig. 2) (D'Agnese and others, 2002). Other ground-water discharge zones include springs in the Oasis Valley (northwest of Yucca Mountain, near Beatty, Nev.), in the Amargosa Desert (Ash Meadows), and along the lower section of the Amargosa River.

The area within and adjacent to the DVRFS includes 42 hydrographic areas and subareas (fig. 4; table 1) that are a subset of the hydrographic areas delineating the topographically defined basins and subbasins in the Great Basin (Harrill and Prudic, 1998). Most of the hydrographic areas and subareas, herein referred to as hydrographic areas, were used in previous water-balance studies of the Death Valley regional hydrologic system (Avon and Durbin, 1994; D'Agnese and others, 1997; Harrill and Prudic, 1998; Hevesi and others, 2002). Estimates of average annual recharge have been made for each of the 42 areas; for some areas, estimates of recharge were made using several approaches (fig. 5; table 1).

Although most of the hydrographic areas, such as Sarcobatus Flat (area 146) and Pahrump Valley (area 162), represent topographically closed basins, the topographic divides are not well defined in some areas of the Death Valley region, such as those along the southern boundary of the lower Amargosa River drainage basin (Grasso, 1996). In some cases, the hydrographic areas represent tributary drainage basins of the larger drainage basins. Examples of hydrographic areas representing tributary drainage basins include Fortymile Canyon (area 227) and Oasis Valley (area 228). Most of the 42 hydrographic areas are part of the Death Valley hydrologic region, which is generally a closed system in terms of surface-water flow. Several of the hydrographic areas along the eastern edge of the Death Valley region are part of the Colorado River hydrologic region. Two areas adjacent to the northwestern boundary of the Death Valley region, Alkali Spring Valley (area 142) and Clayton Valley (area 143), are part of the South–Central Marshes hydrologic region.

Climate

The climate in the Death Valley region is arid to semiarid. The northern part of the region, which is in the Great Basin Desert, is characterized by warm, dry summers, and cold, dry winters. The southern part of the region, which is in the Mojave Desert, is characterized by hot, dry summers and warm, dry winters. The central part of the region includes the area around Yucca Mountain and the NTS (fig. 2). This area has been called the Transition Desert (Beatley, 1976) and represents a gradational zone between the Great Basin and Mojave Desert climates. For most locations throughout the region, the average annual potential evapotranspiration greatly exceeds the average annual precipitation. The mean annual open-water surface evaporation for the region ranges from 1,250 mm/yr in the mountains to greater than 2,500 mm/yr in the playas (Bedinger and others, 1989).

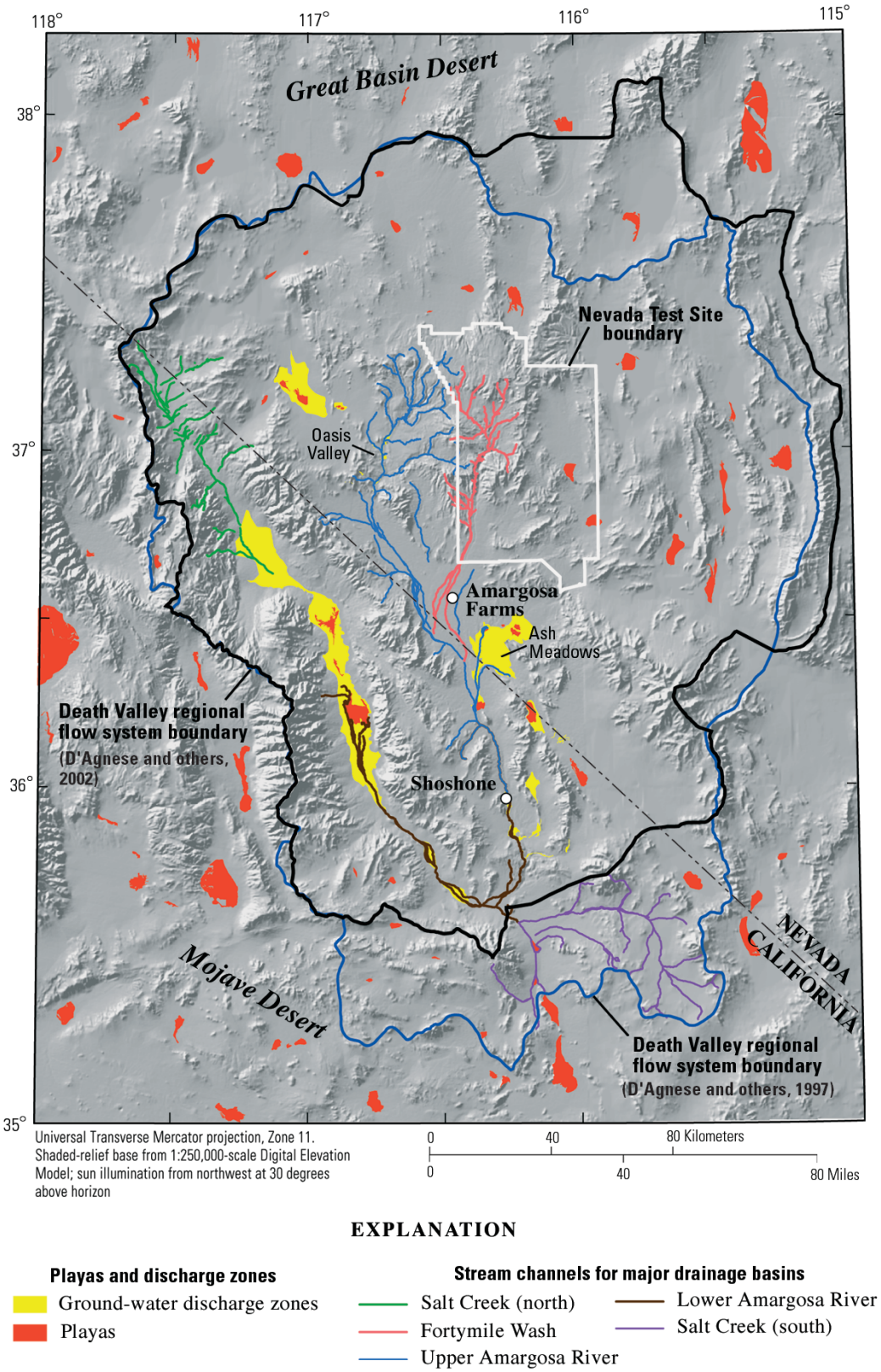

Figure 3. Hydrographic features of the Death Valley region, Nevada and California.

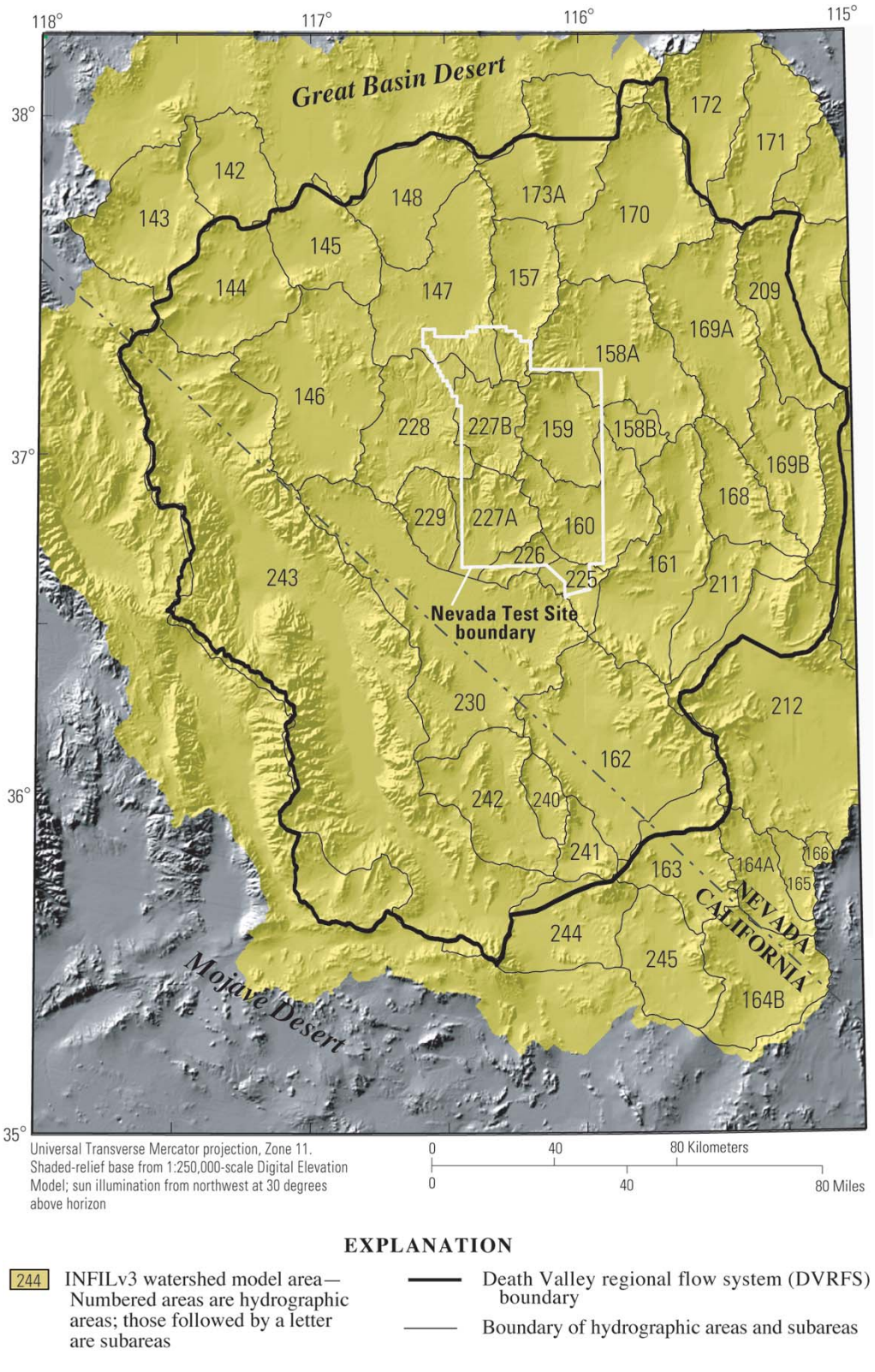

Figure 4. Area of the INFILv3 model and the 42 hydrographic areas and subareas within or adjacent to the Death Valley regional flow system, Nevada and California.

Table 1. Estimated recharge, methods for estimating recharge, and source of recharge estimates for the hydrographic areas and subareas in the Death Valley region and for the Death Valley regional flow system model area, Nevada and California

[Location of hydrologic areas and subareas shown in figure 4. Hydrologic region number: 34, Colorado System; 28, Death Valley System; 31, Penoyer Valley; 24, South-Central Marshes; 36, Mesquite Valley. km^2, square kilometer; mm/yr, millimeter per year; m^3/d, cubic meter per day; na, not applicable]

Hydrographic areas and subareas		Hydrologic region	Area (km^2)	Previous estimates of recharge		Source of recharge estimate	Estimation method
Name	Identifier			(mm/yr)	(m^3/d)		
Alkali Spring Valley	142	24	830	0.15	338	Scott and others, 1971	Maxey–Eakin empirical method
Amargosa Desert	230	28	3,445	.54	5,066	Walker and Eakin, 1963	Maxey–Eakin empirical method
Cactus Flat	148	28	1,023	.72	2,026	Rush, 1971	Maxey–Eakin empirical method
California Valley	241	28	347	.85	814	Harrill and others, 1988	Maxey–Eakin empirical method
California and Chicago Valleys	240 and 241	28	629	.58	1,000	D'Agnese and others, 1997	Ground-water flow model
Chicago Valley	240	28	281	.22	169	Harrill and others, 1988	Maxey–Eakin empirical method
Clayton Valley	143	24	1,438	1.29	5,066	Rush, 1968	Maxey–Eakin empirical method
Coal Valley	171	34	1,181	2.09	6,754	Eakin, 1963	Maxey–Eakin empirical method
Crater Flat	229	28	473	.57	743	Rush, 1971	Maxey–Eakin empirical method
Death Valley	243	28	9,518	1.04	27,017	Miller, 1977	Maxey–Eakin empirical method
Emigrant Valley[1]	158	28	1,993	8.04	43,900	D'Agnese and others, 1997	Ground-water flow model
Emigrant Valley (Groom Lake)	158A	28	1,711	2.31	10,807	Rush, 1971	Maxey–Eakin empirical method
Emigrant Valley (Papoose Lake)	158B	28	283	.02	14	Rush, 1971	Maxey–Eakin empirical method
Fortymile Canyon[2]	227	28	1,331	.63	2,300	D'Agnese and others, 1997	Ground-water flow model
Fortymile Canyon (Buckboard Mesa)	227B	28	598	2.89	4,728	Rush, 1971	Maxey–Eakin empirical method
Fortymile Canyon (Jackass Flats)	227A	28	733	1.51	3,039	Rush, 1971	Maxey–Eakin empirical method
Frenchman Flat	160	28	1,184	.10	338	Rush, 1971	Maxey–Eakin empirical method
Garden Valley	172	34	1,182	9.97	33,771	Eakin, 1963	Maxey–Eakin empirical method
Garden and Coal Valleys	172 and 171	34	2,362	5.61	37,148	Kirk and Campana, 1990	Deuterium model
Gold Flat	147	28	1,764	2.66	12,833	Rush, 1971	Maxey–Eakin empirical method

See footnote at end of table.

Table 1. Estimated recharge, methods for estimating recharge, and source of recharge estimates for the hydrographic areas and subareas in the Death Valley region and for the Death Valley regional flow system model area, Nevada and California—*Continued*

Hydrographic areas and subareas		Hydrologic region	Area (km^2)	Previous estimates of recharge		Source of recharge estimate	Estimation method
Name	Identifier			(mm/yr)	(m^3/d)		
Hidden Valley (south)	166	34	86	0.14	34	Scott and others, 1971	Maxey–Eakin empirical method
Indian Springs Valley	161	28	1,730	7.13	33,771	Rush, 1971	Maxey–Eakin empirical method
Ivanpah Valley (north)	164A	34	633	2.92	5,066	Scott and others, 1971	Maxey–Eakin empirical method
Ivanpah Valley (south)	164B	34	1,317	.47	1,689	Harrill and others, 1988	Maxey–Eakin empirical method
Jean Lake Valley	165	34	255	.48	338	Glancy, 1968b	Maxey–Eakin empirical method
Kawich Valley	157	28	930	4.64	11,820	Rush, 1971	Maxey–Eakin empirical method
Las Vegas Valley	212	34	3,855	9.18	101,313	Avon and Durbin, 1994[3]	Maxey–Eakin empirical method
	212	34	3,855	8.57	94,559	Dettinger, 1989	Chloride mass-balance model
	212	34	3,855	9.18	101,313	Harrill, 1976	Ground-water flow model
Lida Valley	144	28	1,390	.42	1,600	D'Agnese and others, 1997	Ground-water flow model
Lower Amargosa Valley	242	28	1,199	.09	300	D'Agnese and others, 1997	Ground-water flow model
Mercury Valley	225	28	287	1.07	844	Rush, 1971	Maxey–Eakin empirical method
Mercury and Rock Valleys	225 and 226	28	505	.94	1,300	D'Agnese and others, 1997	Ground-water flow model
Mesquite Valley	163	36	1,135	1.63	5,066	Glancy, 1968	Maxey–Eakin empirical method
	163	36	1,135	1.74	5,403	Dettinger, 1989	Chloride mass-balance
Oasis Valley	228	28	1,218	1.01	3,377	Rush, 1971	Maxey–Eakin empirical method
Pahranagat Valley	209	34	1,986	1.11	6,079	Eakin, 1963	Maxey–Eakin empirical method
	209	34	1,986	.92	5,066	Kirk and Campana, 1990	Deuterium model
Pahrump Valley	162	28	2,562	12.52	87,804	Avon and Durbin, 1994[3]	Maxey–Eakin empirical method
	162	28	2,562	17.81	124,952	Harrill, 1986	Ground-water flow model
Penoyer Valley	170	31	1,791	2.96	14,521	Avon and Durbin, 1994[3]	Maxey–Eakin empirical method
	170	31	1,791	2.20	10,807	Dettinger, 1989	Chloride mass-balance model
	170	31	1,791	2.62	12,833	Van Denburgh and Rush, 1974	Water-budget discharge
Railroad Valley (south)	173A	28	1,536	4.42	18,574	Avon and Durbin, 1994[3]	Maxey–Eakin empirical method

See footnote at end of table.

Table 1. Estimated recharge, methods for estimating recharge, and source of recharge estimates for the hydrographic areas and subareas in the Death Valley region and for the Death Valley regional flow system model area, Nevada and California—*Continued*

Hydrographic areas and subareas		Hydrologic region	Area (km^2)	Previous estimates of recharge		Source of recharge estimate	Estimation method
Name	Identifier			(mm/yr)	(m^3/d)		
	173A	28	1,536	3.94	16,548	Dettinger, 1989	Chloride mass-balance model
Rock Valley	226	28	218	0.17	101	Rush, 1971	Maxey–Eakin empirical method
Sarcobatus Flat	146	28	2,122	.70	4,053	Malmberg and Eakin, 1962	Maxey–Eakin empirical method
Shadow Valley	245	28	1,013	1.46	4,053	Harrill and others, 1988	Maxey–Eakin empirical method
Stonewall Flat	145	28	979	.13	338	Rush, 1968	Maxey–Eakin empirical method
Three Lakes Valley (north)	168	28	780	3.16	6,754	Rush, 1971	Maxey–Eakin empirical method
Three Lakes Valley (south)	211	28	782	9.48	20,263	Rush, 1971	Maxey–Eakin empirical method
Tikapoo Valley (north)	169A	28	1,596	2.01	8,780	Scott and others, 1971	Maxey–Eakin empirical method
Tikapoo Valley (south)	169B	28	958	4.37	11,482	Scott and others, 1971	Maxey–Eakin empirical method
Valjean Valley	244	28	1,082	.46	1,351	Harrill and others, 1988	Maxey–Eakin empirical method
Yucca Flat	159	28	776	1.11	2,364	Rush, 1971	Maxey–Eakin empirical method
Death Valley regional flow system model area	na	na	45,288	2.15	266,800	D'Agnese and others, 2002	Ground-water flow model

[1]Emigrant Valley (158), not shown in figure 4, is the combined area of Groom Lake (158A) and Papoose Lake (158B).
[2]Fortymile Canyon (227) not shown in figure 4, is the combined area of Jackass Flats (227A) and Buckboard Mesa (227B).
[3]Reference provides a summary of results from previous studies, but is not the original reference for the indicated recharge estimate.

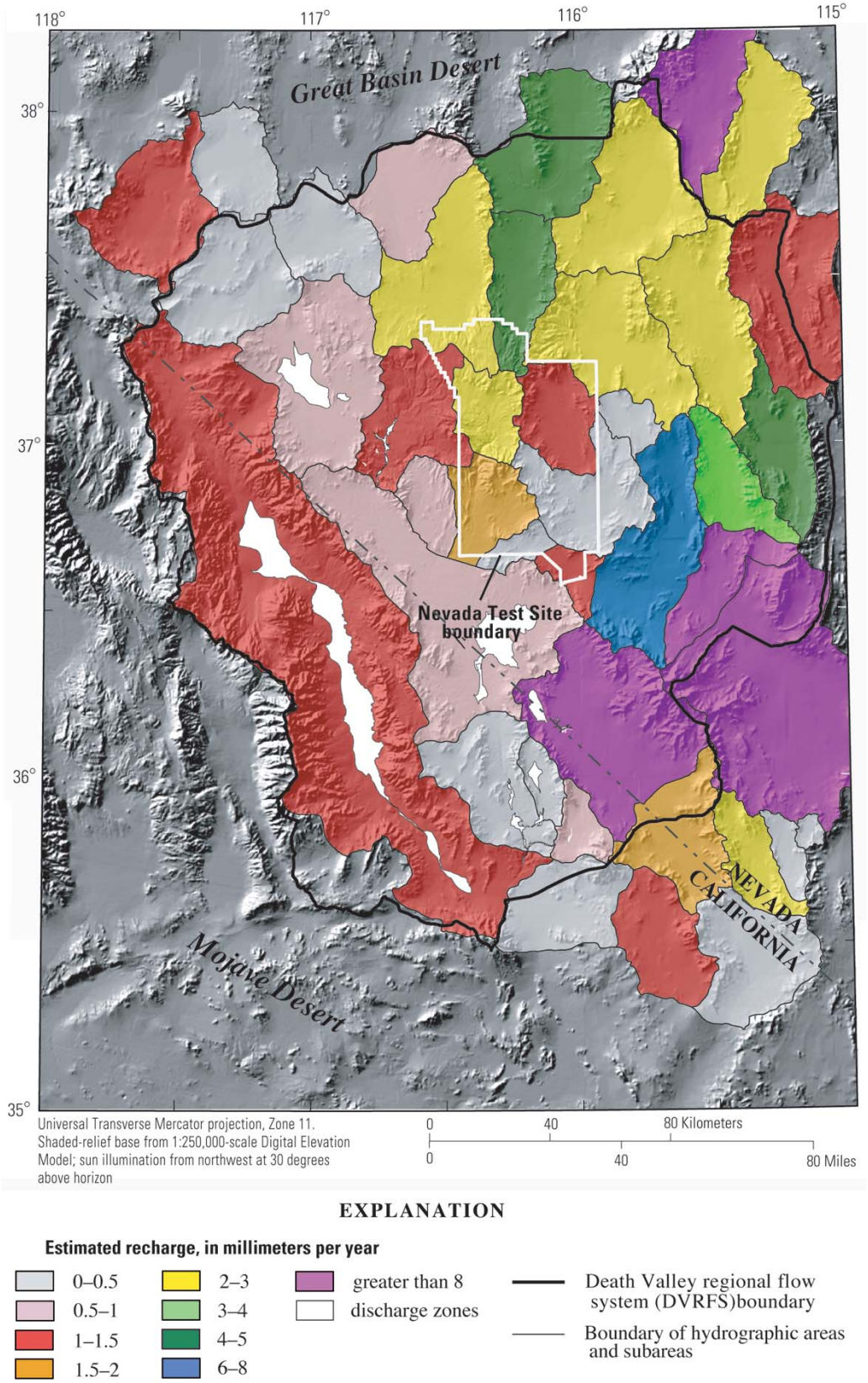

Figure 5. Estimated recharge for the hydrographic areas and subareas in the Death Valley region, Nevada and California. Estimates of basinwide recharge are from previous studies and are listed in table 1.

Weather patterns in the Death Valley region vary seasonally, having a bimodal annual distribution in precipitation that is characterized by widespread precipitation from cyclonic fronts that occur during October through June, and by isolated convective storm cells or storm-cell clusters from the southwestern summer monsoon that occurs during July through August (Grasso, 1996). For most years, precipitation during the winter contributes the greater part of the total annual precipitation in the Death Valley region (French, 1983; Hevesi and Flint, 1998). In the southern Great Basin and Mojave Deserts, winter precipitation generally is from low-intensity, long-duration (several hours to several days) storms produced by synoptic-scale weather patterns. Winter precipitation usually comes from the west and results in a regional rain shadow east of the Sierra Nevada; precipitation often is in the form of snow, especially at the higher elevations (more than 2,000 m). Precipitation tends to be more consistent in the winter, resulting in greater total seasonal accumulation relative to summer precipitation.

Summer precipitation is produced primarily by mesoscale weather patterns during the southwestern summer monsoon (Houghton, 1969; Pyke, 1972). Storms from the southwestern summer monsoon move into the Death Valley region from the south and southeast (French, 1983; Grasso, 1996). In contrast to winter precipitation, summer precipitation tends to come from isolated high-intensity, short-duration (1 to 2 hours) convective storms that affect small areas. The convective storms often include lightening and hail. Precipitation that occurs from August through September also can be caused by tropical storms moving north and northeast from the Gulf of California and the Pacific Ocean (Grasso, 1996), but the occurrence of tropical storms is not as consistent as the occurrence of convective storms from southwest summer monsoon.

Average annual precipitation in the central part of the Death Valley region has been estimated to be about is 180 mm/yr (Hevesi and others, 1991). Spatial variability in precipitation, caused primarily by the orographic effects of mountains and higher elevation terrain, is substantial. Orographic influences on summer and winter precipitation result in an increase in the frequency and amount of precipitation associated with increased elevation (Quiring, 1965; French, 1983; Hevesi and others, 1991; Hevesi and Flint, 1998). For a given elevation, precipitation tends to increase eastward across the Death Valley region owing to a corresponding increase in summer moisture from the southwestern summer monsoon combined with increasing distance from the Sierra Nevada rain shadow (Quiring, 1965; French, 1983).

The spatially distributed average annual precipitation for the Death Valley region (fig. 6) was estimated using a parameter-elevation regressions on independent slopes model (PRISM) that accounts for orographic effects on precipitation (Daly and others, 1994). The PRISM estimates indicate that the maximum precipitation in the region is about 500 to 600 mm/yr in the higher mountain ranges (such as the Spring Mountains), and the minimum precipitation is less than 50 mm/yr on the floor of Death Valley. Precipitation averages 100 to 150 mm/yr or less on the valley floors of the Amargosa Desert and at the lower elevations in the southern part of the region. Average annual precipitation at higher elevations in the mountains generally is greater than 250 mm/yr.

For most locations, the PRISM estimates of average annual precipitation are consistent with the estimates from elevation-correlation models used to estimate precipitation in the Death Valley region (French, 1983; Hevesi and others, 1991). However, there is a high degree of uncertainty in these estimates because the data used for spatial interpolation is sparse for much of the region. Uncertainty in the precipitation estimates generally is greatest for the more remote higher elevations of the mountain ranges owing to a decrease in the number and length of precipitation records for those elevations and to an increase in measurement error owing to an increase in the percentage of precipitation as snow. A multivariate geostatistical model developed for estimating precipitation in the Death Valley region (Hevesi and others, 1991) provides a higher estimate of average annual precipitation for the summit area of the Spring Mountains (approximately 700 mm/yr) than does the PRISM model (approximately 600 mm/yr). For Rainier Mesa on the NTS, the PRISM estimates are about 400 mm/yr, which is about 100 mm/yr higher than the estimates from the geostatistical model, which incorporates additional precipitation data from stations located within and adjacent to the NTS. For lower elevations, average annual precipitation estimates generally are more consistent between PRISM and other estimation methods.

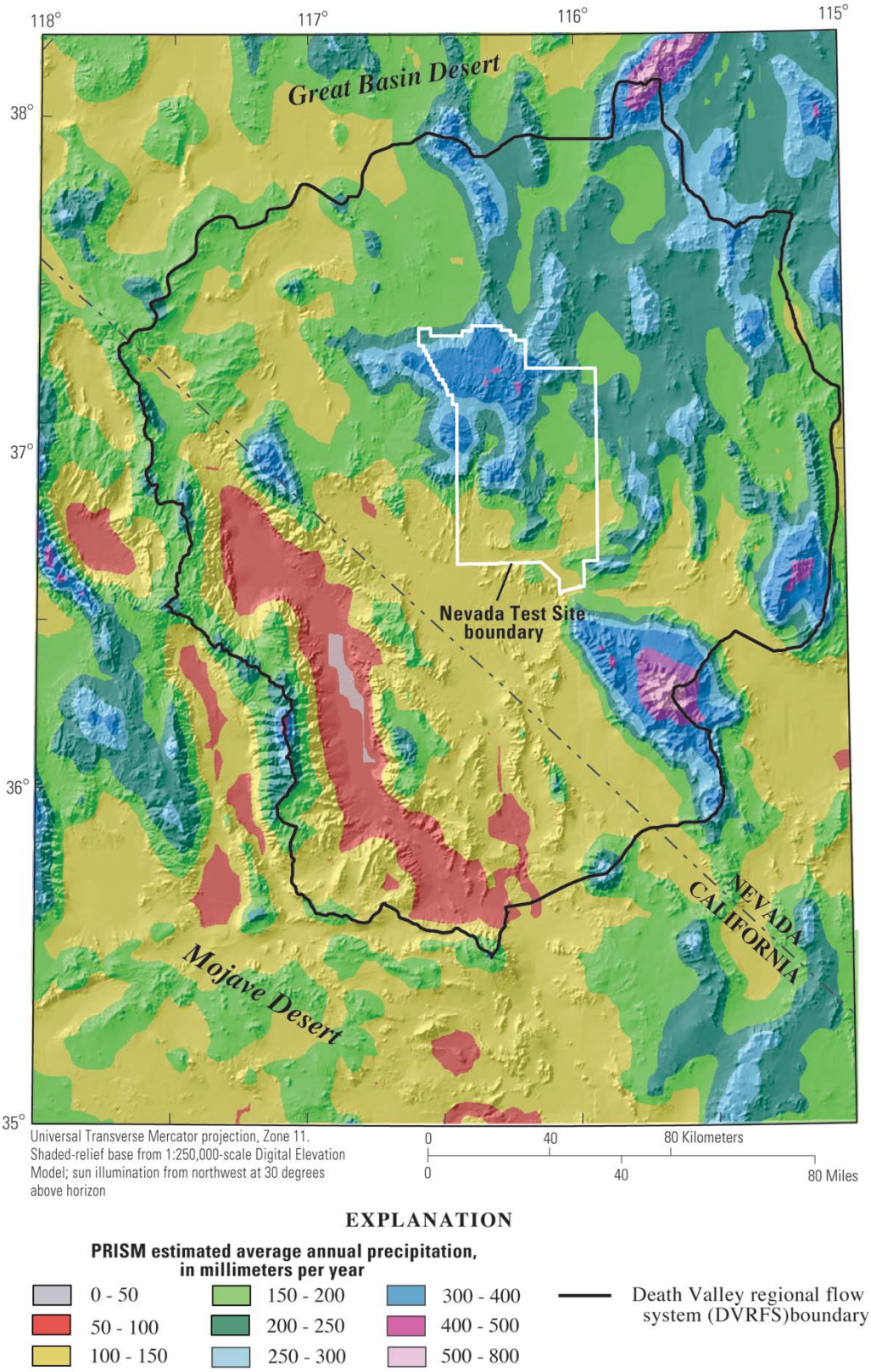

Figure 6. Average annual precipitation estimated using the parameter-elevation regressions on independent slopes model (PRISM) Daly and others, 1994 for the Death Valley region, Nevada and California.

Surface Water

Perennial surface water is sparse in the Death Valley region. Several perennial streams, however, originate as springs from shallow perched systems in the high elevations of the Spring Mountains. These mountain streams have highly variable flows during wet years and almost imperceptible flows during dry years. Streams fed from springs along the middle section of the Amargosa River in the Amargosa Desert (figs. 2 and 3) have the most consistent perennial flow. Most of the stream channels in the Death Valley region experience only intermittent flow in response to high-intensity storms (Grasso, 1996). Infrequent severe summer storms and regional winter storms occurring during wetter-than-average antecedent conditions can sometimes result in high volume surface-water flow of relatively short duration (flash flooding) in normally dry stream channels. Potential hazards from localized flash flooding in Death Valley were studied by Crippen (1981) for an intermittent stream in the Panamint Range and by Bowers (1990) for a drainage basin in the Grapevine Mountains. Potential hazards from flash flooding at Yucca Mountain (from a small tributary of the Fortymile Wash drainage basin) was studied by Glancy (1994). Temporary playa lakes form in some basins in response to storm runoff and spring discharge during wetter-than-average years but are depleted by evaporation during average and drier-than-average years. Periodic flooding along the Amargosa River, in response to above-average precipitation during the El Niño–Southern Oscillation, was the primary source of water that formed the ephemeral playa lakes on the floor of Death Valley during 1969 and 1993 (Grasso, 1996).

Ground Water

The predominant direction of ground-water flow in the DVRFS is from north to south, the direction of average elevation loss in the southern Basin and Range physiographic province. In contrast to surface-water flow patterns, regional ground-water flow patterns do not always coincide with topographic basins (Winograd and Thordarson, 1975). The regional ground-water flow system is compartmentalized into subregional flow systems because of the integrated effect of the regional carbonate rock aquifer, the complex geologic structure, and the shallow local flow systems controlled by recharge and discharge (D'Agnese and others, 2002). Most of the ground-water recharge in the region occurs at higher elevations and by direct infiltration of precipitation or snowmelt or by infiltration of surface water originating as runoff from precipitation or snowmelt (Winograd and others, 1998). Precipitation and runoff at the lower elevations generally do not recharge the system because of lower amounts of precipitation, higher potential evapotranspiration, and a decrease in runoff frequency. Discharge from the ground-water system, as flow from springs or as evapotranspiration from shallow water tables, occurs in several areas of the subregional flow systems in response to topographic, stratigraphic, and structural controls. Examples of ground-water discharge from the subregional flow systems include the springs at Oasis Valley north of Beatty, Nev., and the springs at Ash Meadows in the central part of the Amargosa Desert. Ground water that is not discharged from the subregional flow systems ultimately is discharged in Death Valley.

Vegetation

A detailed analysis of the spatial distribution of vegetation types and associations in the western United States is being developed as part of the USGS's Biological Resources (BR) National Gap Analysis Program (GAP). A digital vegetation map was developed using satellite imagery and other records based on the National Vegetation Classification System (http://www.gap.uidaho.edu/RegionalGAP/regional.htm). A western region vegetation map (WESTVEG), compiled using state-based GAP source data, indicates the general spatial distribution of vegetation types and land-surface characteristics in the Death Valley region (fig. 7). The WESTVEG plant associations in this region include Creosote–Bursage, Salt Desert shrubs, and sagebrush associations. The Creosote–Bursage association is prevalent in the southern part of the region, and the Salt Desert shrub and sagebrush associations are prevalent in the northern part of the region. The Creosote–Bursage association occupies the largest area relative to other vegetation associations in the region. In general, natural vegetation cover is sparse throughout most of the region, especially at the lower elevations except for zones of riparian vegetation in a few isolated locations that have spring discharge and areas of coniferous forests and Pinyon–Juniper woodlands at higher elevations where

precipitation is greater and air temperature is lower. The Pinyon–Juniper vegetation type generally occurs at elevations of approximately 2,000 m and higher, and denser forests of Ponderosa Pine and White Fir occur at higher elevations (2,500–3,500 m), such as the Spring Mountains.

Soils

Soils in the Death Valley region can be grouped into four types: (1) upland soils on the mountains and in areas characterized by rugged topography, (2) valley-fill soils on alluvial fans and terraces, (3) playa soils on the valley floors and playa basins, and (4) channel soils in active stream channels (Hevesi and others, 2002). Upland soils are usually less than 1-m thick, have a coarse texture with little moisture-holding capacity, and have high permeability. The valley-fill and playa soils are much thicker than the upland soils and tend to be medium- to coarse-textured; they also tend to be highly permeable. Playa soils are fine-grained, are characterized by a high percentage of clays or evaporites including silicified hardpans (Beatley, 1976), and have much lower permeability than valley-fill and upland soils. Soils in active channels tend to be coarse textured and more permeable than the soils of the surrounding terraces and interchannel areas of alluvial fans.

A regional-scale map of soil types in the Death Valley region was obtained from the State Soil Geographic database (STATSGO), a state-compiled geospatial database of soil properties that generally are consistent across state boundaries (U.S. Department of Agriculture, 1994). Mapped soil types are identified in the STATSGO database using a unique map unit identifier (MUID). A single MUID represents a group of similar soil types. Although the location of a given soil component within a mapped MUID area is not known, the percentage of MUID area covered by each component is defined, and the maximum and minimum thickness of all layers in each component is provided. The spatial distribution of the STATSGO MUIDs for the Death Valley region is shown in figure 8 using soil type map codes (assigned for the purpose of this report to link MUID locations with the soil properties input used in the INFILv3 model). The MUID map code locations in figure 8 are shown in groups of 10; the 149 STATSGO MUIDs mapped for the Death Valley region (and the corresponding map codes used for this study) are given in table 2, at back of report. The number of soil components for MUIDs in the Death Valley region range from 2 to 21 (fig. 9; table 2, at back of report). Soil attributes associated with each MUID, averaged using the combined weight of layer thickness and area for the soil components in each MUID, include the percentage of clay in the soil grain-size fraction less than 2 mm (sand and finer). For the Death Valley region, most locations consist of soils that have less than 10 to 15 percent clay in the fraction of soil material with grain sizes of 2 mm and finer (fig. 10). Many locations in this region consist of relatively coarse surficial material, exceeding 50 percent grain sizes larger than 2 mm (coarse sand, gravel, cobbles, and boulders) (table 2, at back of report), and the percentage of clay is fairly small. Exceptions to the areas with low clay content are the playa lakebeds where the percentage of clay can be as high as 50 percent. Higher clay contents also occur at the higher elevations in the Spring Mountains and the Sheep Range.

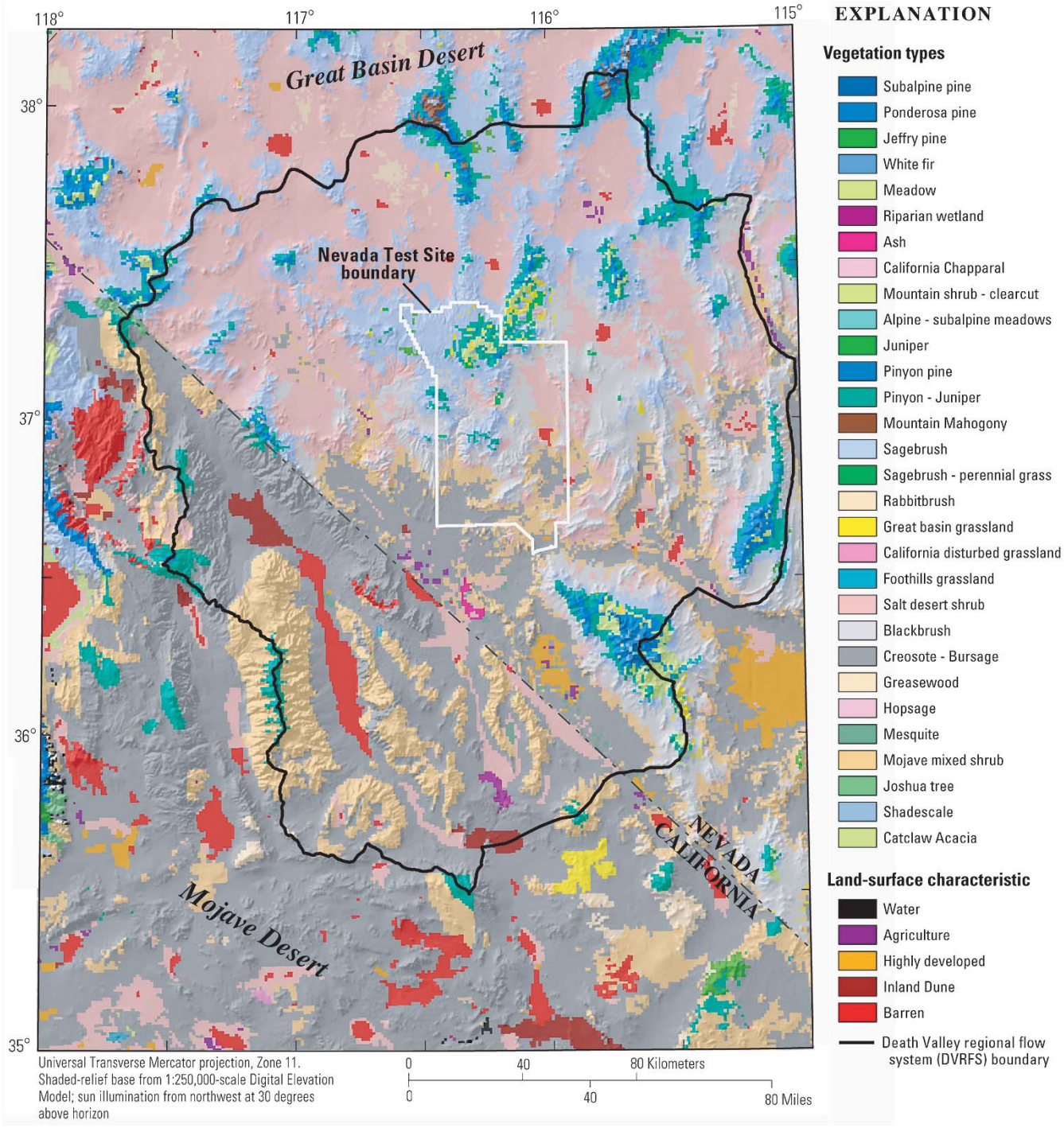

Figure 7. Vegetation types and land-surface characteristics in the Death Valley region, Nevada and California.
Vegetation types defined using western region vegetation (WESTVEG) Gap Analysis Program (GAP) data (Murray, 1997, accessed August 16, 2000)

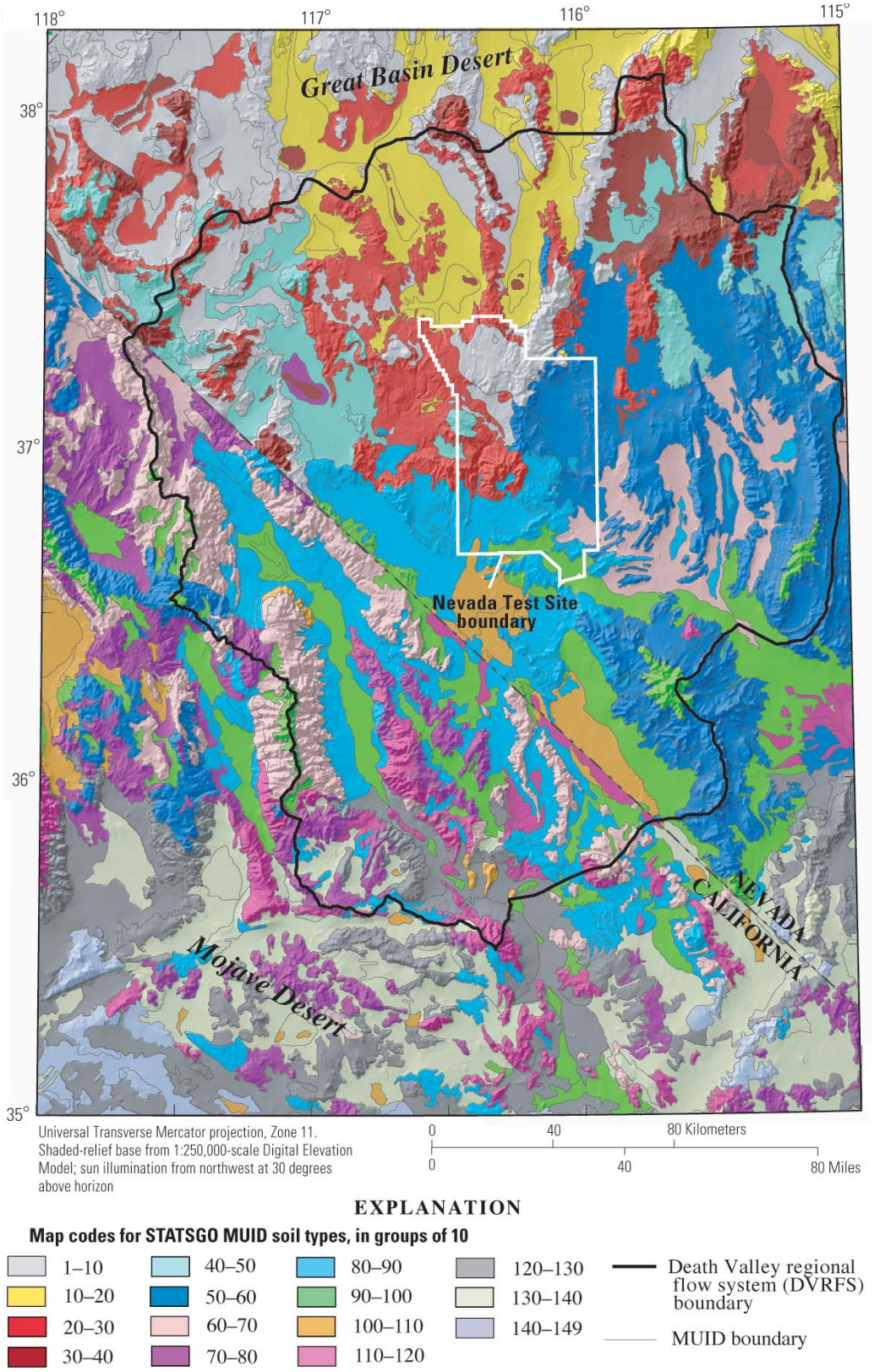

Figure 8. Spatial distribution of STATSGO MUID soil types in the Death Valley region, Nevada and California.
STATSGO, State Soil Geographic Database; MUID, map unit identifier (for STATSGO map units). (See table 2 for soil texture attributes.)

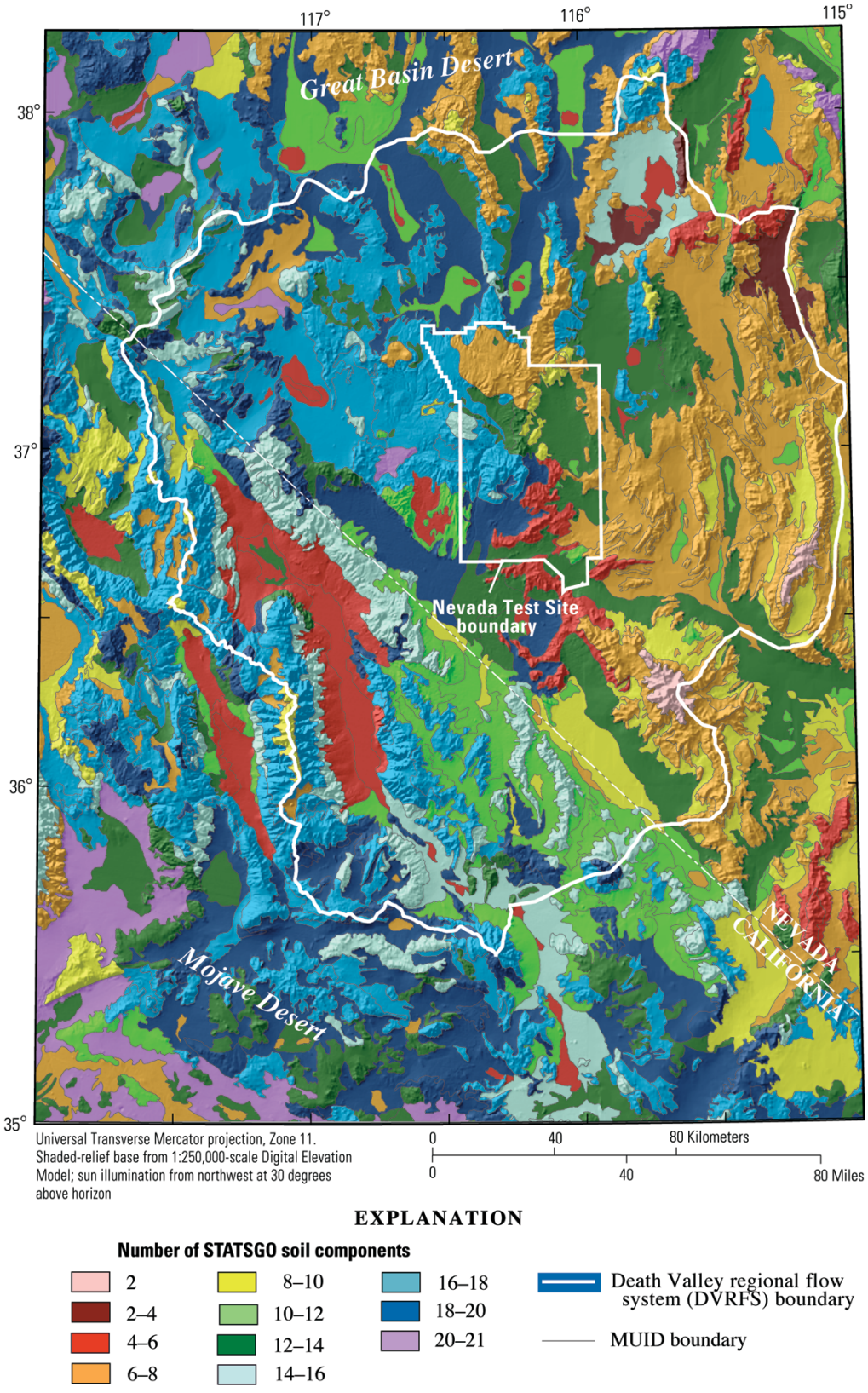

Figure 9. Number of STATSGO soil components for the MUIDs in the Death Valley region, Nevada and California.
STATSGO, State Soil Geographic Database; MUID, map unit identifier (for STATSGO map units).

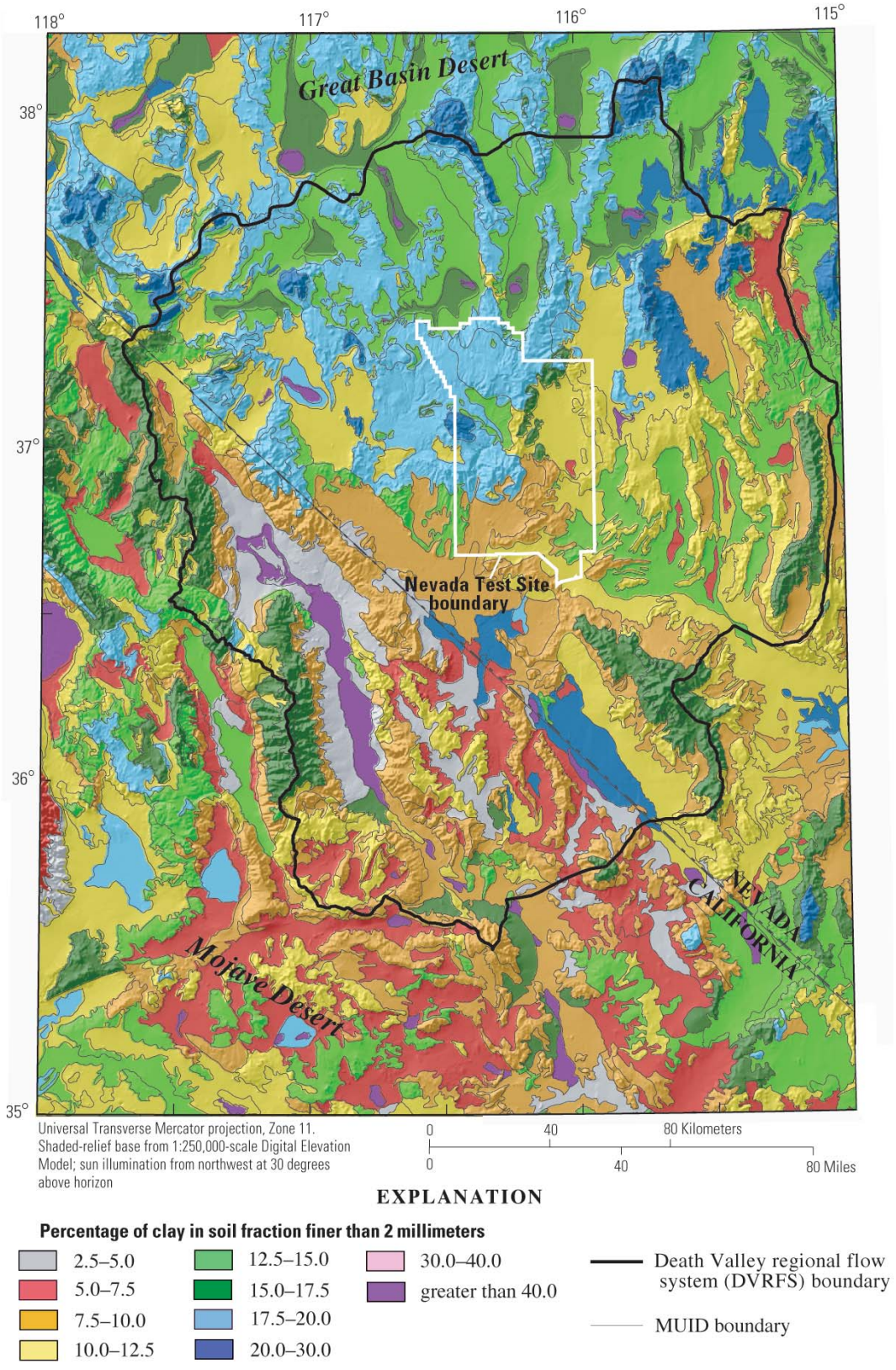

Figure 10. Percentage of clay in soil fraction finer than 2 millimeters in the Death Valley region, Nevada and California.

Hydrogeology

A detailed description of the hydrogeology of the Death Valley region is presented in Bedinger and others (1989), D'Agnese and others (1997), Faunt (1997), and Faunt and others (1997). The complex geology of the region was generalized by Turner and others (1996), D'Agnese and others (1997), and Faunt and others (1997) into hydrogeologic units that have considerable lateral extent and reasonably distinct hydrologic properties, particularly with respect to average differences in saturated hydraulic conductivities. The primary hydrogeologic units that have been identified in the Death Valley region (modified from Faunt and others [1997]) include (1) Quaternary and Tertiary valley fill, (2) Quaternary and Tertiary lava flows, (3) Tertiary volcanic rocks, (4) Tertiary volcaniclastic rocks, (5) Tertiary and Jurassic granitic rocks, (6) Mesozoic sedimentary and metavolcanic rocks, (7) Paleozoic carbonates rocks, (8) Paleozoic and Precambrian clastic rocks, (9) Precambrian igneous and metamorphic rocks, (10) Quaternary playa deposits, and (11) Paleozoic clastic rocks. The location of these units is given in figure 11. The relatively broad generalization of the hydrogeologic system has provided a useful starting point for the development of flow models and for modeling net infiltration (Flint and others, 2000; Hevesi and others, 2002). Estimates of saturated hydraulic conductivity used in the preliminary net-infiltration model for the Death Valley region ranged from 0.4 mm/yr (0.001 mm/d) for granitic rocks to 700,000 mm/yr (2,000 mm/d) for valley-fill deposits (Hevesi and others, 2002). Consolidated hydrogeologic units that have a high saturated hydraulic conductivity include the Paleozoic carbonate rocks and the Mesozoic sedimentary and metavolcanic rocks; units that have a low saturated hydraulic conductivity include the Precambrian igneous and metamorphic rocks. Units that have an intermediate saturated hydraulic conductivity include the Tertiary volcanic rocks.

Net Infiltration and Recharge

Net infiltration is the drainage of rain, snowmelt, and infiltrated surface water across the lower boundary of the root zone (Flint and others, 2001c; Hevesi and others, 2002). Ground-water recharge to a basin or saturated-zone ground-water system includes the percolation flux across the water table (flow from the unsaturated zone to the saturated zone) and lateral inflow through the saturated zone (interbasin transfer) across the basin or the regional saturated-zone boundary. Net infiltration is not necessarily equivalent to recharge because of interbasin transfer and processes affecting deep percolation through thick unsaturated zones.

Net infiltration can be an indicator of potential recharge due to downward percolation through the unsaturated zone to the saturated zone in response to the infiltration of rain, snowmelt, and overland flow. However, in many locations in the Death Valley region, the unsaturated zone has a thickness of more than 500 m, and net infiltration may be considerably different than recharge at the water table. The potential for differences between net infiltration and recharge increases with increased unsaturated zone thickness, ground-water travel time through the unsaturated zone, climate variability, and geologic heterogeneity in the unsaturated zone.

Field studies indicate that net infiltration in the Death Valley region usually is episodic and infrequent at most locations, typically occurring during and after periods of high-volume winter precipitation when evapotranspiration is low (Flint and others, 2001c). An indication of episodic infiltration into fractured bedrock in response to winter precipitation has been shown with field studies using water-potential measurements for Yucca Mountain. For lower elevations (less than 1,500 m) in the Death Valley region, net infiltration occurs only during wetter-than-average winters or in response to surface-water runoff during infrequent, large (high intensity) storms.

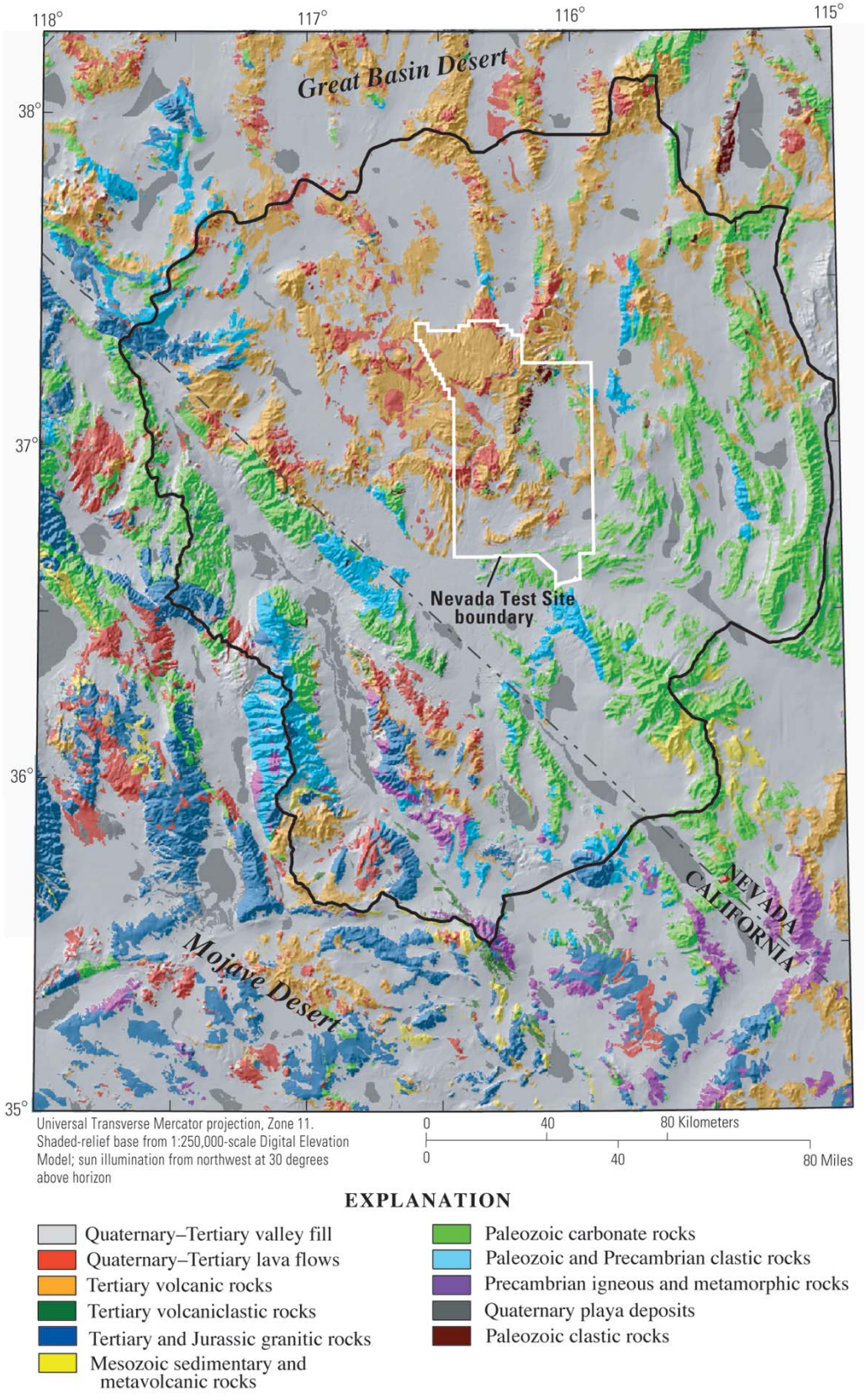

Figure 11. Hydrogeologic units in the Death Valley region, Nevada and California. Modified from Faunt and others (1997) and D'Agnese and others (2002).

Studies of streamflow and of water-table elevations (Savard, 1995, 1998) provide evidence of deep (more than 10 m) percolation through the unsaturated zone beneath the active channel of the Fortymile Wash, east and northeast of Yucca Mountain, in response to streamflows in 1993 and 1995. Savard (1995, 1998) showed that deep percolation coincided with a rising water table beneath the channel. Using a combination of temperature and water potential measurements at various depths along a vertical borehole located at Yucca Mountain in the stream channel of a small tributary to Fortymile Wash, LeCain and others (2002) showed evidence of deep percolation in response to a brief (1-day) occurrence of streamflow during the wetter-than-average winter of 1998. For higher elevation locations (more than 2,000 m), net infiltration resulting from snowmelt is likely a more consistent, seasonal process (Winograd and others, 1998). For the Death Valley region as a whole, net infiltration in direct response to infiltrating rain and snowmelt is considered the primary component of total recharge (D'Agnese and others, 2002). Net infiltration along stream channels in response to streamflow is considered a secondary component owing to the much smaller area affected (Hevesi and others, 2002).

Previous Studies

Net infiltration and recharge previously were estimated for locations and basins within the Death Valley region using various methods including empirical equations that were based on variables such as precipitation, geochemistry methods, water-balance methods (for example, basinwide estimates of discharge or numerical models accounting for all significant components of the water balance), and soil-physics techniques. Using the water-balance method, Winograd and Thordarson (1975) estimated that 3 percent of precipitation becomes recharge; their estimate was based on discharge measurements from springs south of Yucca Mountain near the Nevada–California border. The Maxey–Eakin method (Maxey and Eakin, 1950) was used in several previous water-balance studies of basins in the Death Valley region to estimate recharge to ground-water basins in Nevada (Watson and others, 1976; Dettinger, 1989; Avon and Durbin, 1994; Harrill and Prudic, 1998; Donovan and Katzer, 2000). Depending on the range in average annual precipitation for a given basin, the Maxey–Eakin method classifies areas of a basin into five recharge zones: (1) 0 percent is recharged when precipitation is less than 203 mm/yr, (2) 3 percent is recharged when precipitation is 203 to 304 mm/yr precipitation, (3) 7 percent is recharged when precipitation is 305 to 380 mm/yr precipitation, (4) 15 percent is recharged when precipitation is 381 to 507 mm/yr precipitation, and (5) 25 percent of precipitation is recharge for 508 mm/yr or greater precipitation (Maxey and Eakin, 1950). By comparing the Maxey–Eakin estimates with 40 estimates of recharge obtained using a basinwide water-budget analysis and 27 estimates of recharge obtained using geochemical and numerical modeling approaches, Avon and Durbin (1994) concluded that the Maxey–Eakin method provides a reasonable method of estimating recharge for basins in Nevada. Harrill and Prudic (1998) reached a similar conclusion regarding the applicability of the Maxey–Eakin method for estimating recharge to ground-water basins in Nevada.

Several studies have presented modified and updated versions of the Maxey–Eakin method; these versions use more recent precipitation, geochemical, and basinwide water-balance data. Avon and Durbin (1994) developed a new set of scaling factors (recharge as a percentage of average annual precipitation) for the five recharge zones by fitting the recharge-precipitation model to more recent estimates of ground-water discharge data. D'Agnese and others (1997) developed a modified version of the recharge-precipitation relation using additional scaling factors, or ranking criteria, qualitatively related to geology, vegetation, and slope and aspect. Donovan and Katzer (2000) developed a refined form of the Maxey–Eakin relation to estimate recharge volumes for the Las Vegas Valley (area 212) using precipitation data from a localized network of high-elevation monitoring sites in the Spring Mountains and the Sheep Range. Hevesi and Flint (1998) substituted a continuous curve, fitted to the Maxey–Eakin step function, to estimate recharge using a spatially detailed precipitation map based on a geostatistical model.

Although the Maxey–Eakin transfer method has been used extensively to estimate recharge in Nevada, limitations have been identified in the application of this method. The original Maxey–Eakin model was calibrated to basinwide water-balance estimates; therefore, application of the model using more recent precipitation data but without recalibrating the model using more recent discharge data likely would decrease the accuracy of results (Charles Russell, Desert Research Institute, written commun., 2000). In addition to average annual precipitation, other factors also can affect recharge (D'Agnese and others, 1997). Crippen (1965) combined an evaporation-transfer function with a precipitation-transfer function to develop an empirical method of estimating recharge, or recoverable water, for mountain basins of southern California; his method also accounts for regional differences in climate by using curves fitted to specific climate zones.

Geochemical methods used to obtain estimates of net infiltration and recharge for basins in Nevada include the chloride mass-balance (CMB) method and a deuterium-calibrated, mixing-cell flow model (Avon and Durbin, 1994). Kirk and Campana (1990) applied the deuterium model to obtain 11 estimates of recharge for the White River ground-water flow system in southeastern Nevada, which include three of the hydrographic areas analyzed in this current study (Pahranagat Valley [area 209], Coal Valley [area 171], and Garden Valley [area 172]). Dettinger (1989) applied the CMB method to 16 basins in Nevada; his estimates of chloride-balance were similar to those obtained using the Maxey–Eakin method and the water-balance calculations. The CMB method equates chloride in recharge water and runoff to chloride deposited in source areas by precipitation and dry fallout. Dettinger (1989) concluded that the CMB method is applicable for estimating approximate average rates of recharge for many desert basins of the western United States, but it may not be applicable for fractured rock under shallow soils because the method assumes piston flow in porous media.

Lichty and McKinley (1995) analyzed recharge, using both the CMB and the water-balance modeling approaches, for two analogue basins in central Nevada where field measurements were collected for a 6-year study. Results of their study indicate recharge rates of 10 to 30 mm/yr for a drainage basin that has an average annual precipitation of 270 mm and 300 to 320 mm/yr for a drainage basin that has an average annual precipitation of 640 mm. They determined that the CMB method is the more robust method of estimating basinwide recharge for the two study basins. The higher degree of uncertainty associated with the estimates obtained using the water-balance model primarily is associated with the uncertainty in the spatially varying model inputs, such as the spatial distribution of precipitation and snow depth.

Soil-physics techniques have been applied for estimating net-infiltration rates in the Death Valley region at locations with thick soil cover. These methods require a knowledge of the soil properties and ambient soil moisture conditions in this region and an assumption of steady-state conditions. Winograd (1981) estimated that the net-infiltration rate at Yucca Flat in the northeastern part of the NTS (fig. 2) is about 2 mm/yr. Nichols (1987) used water-potential measurements and a numerical model to estimate net-infiltration rates at the Amargosa Desert Research Site (ADRS) near Beatty, Nev., about 30 km west of Yucca Mountain. Nichols (1987) estimated a rate of net infiltration of 0.04 mm/yr at the ADRS; measured precipitation rates are substantially lower at this site than the rates measured at the northeastern part of the NTS.

For the study reported here, previous estimates of basinwide recharge for the 42 hydrographic areas in the Death Valley region (figs. 4 and 5; table 1) were used to evaluate estimates of net infiltration. A summary of the results of the previous studies is provided by Avon and Durbin (1994), D'Agnese and others (1997), and Harrill and Prudic (1998). Most of the basinwide recharge estimates were obtained using the Maxey–Eakin method. For some of the hydrographic areas, recharge estimates were based on estimates from the chloride mass-balance model, a deuterium mixing-cell model, or calibration results for ground-water flow models. In addition to the recharge estimates from these methods, table 1 includes a recharge estimate of 266,800 m^3/d obtained by D'Agnese and others (2002) for the area of the DVRFS model; this estimate is based on the calibration results of a steady-state ground-water flow model.

MODEL DEVELOPMENT

Conceptual Model of Net Infiltration

A conceptual model of net infiltration, developed from field studies at Yucca Mountain during 1980 through 1995, was used to develop numerical models of net infiltration for Yucca Mountain and the surrounding Death Valley region. The numerical models of net infiltration (INFIL and INFILv2) were used to define the upper boundary condition of a three-dimensional unsaturated-zone ground-water flow model for Yucca Mountain and to develop net-infiltration estimates for a range of different climate scenarios. Detailed descriptions of the conceptual and numerical models of net infiltration for Yucca Mountain are given in reports by Flint and others (2001a,b,c) and Hevesi (2001). Extension of the conceptual and numerical models of net infiltration to the surrounding Death Valley region is described in Flint and others (2000) and Hevesi and others (2002).

The conceptual model of net infiltration in the Death Valley region is represented by the major components of the water balance for arid to semiarid environments; these components include precipitation; infiltration of rain, snowmelt, and surface water into soil or bedrock; runoff; surface-water run-on (overland flow and streamflow); bare-soil evaporation; transpiration from the root zone; redistribution or changes in water content in the root zone; and net infiltration across the lower boundary of the root zone. The conceptual model defines net infiltration as downward drainage, or flux, across the lower boundary of the root zone, or the depth at which the seasonal effects of evapotranspiration become insignificant. The conceptual model provides a framework for applying the water-balance modeling approach to develop a numerical model of net infiltration using a horizontal grid of model nodes, or cells, with a vertical discretization representing the root zone as a series of layers (fig. 12).

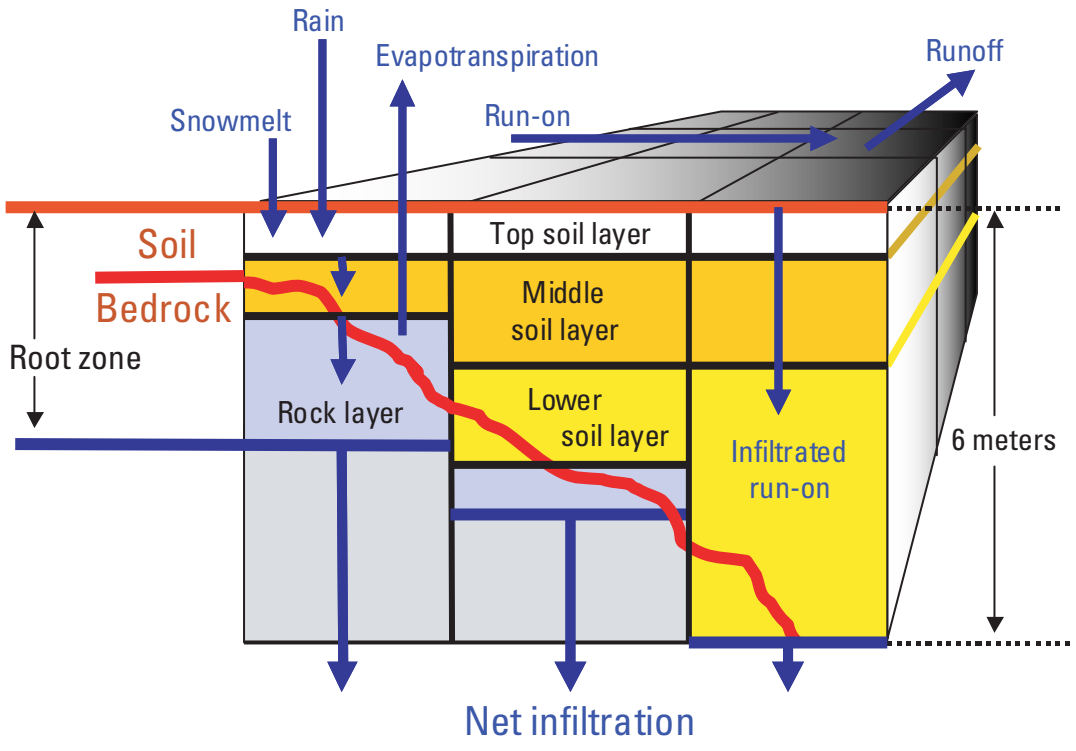

Figure 12. Conceptual model of net inflation illustrating the layered root-zone water-balance model of the Death Valley region, Nevada and California.

The conceptual model defines rain, snowmelt, and surface-water run-on as inputs to a layered root-zone water-balance model with 1 to 5 soil layers and a lower bedrock or deep alluvium layer. For each model cell, the number and thickness of layers is dependent on soil thickness, with the thickness of the lower bedrock layer increasing with decreasing soil thickness. The layers define storage components for the root zone where root density decreases from the top to the bottom layer, and the processes of evapotranspiration and downward drainage are dependent on the amount of water stored in each layer. Evapotranspiration, the main output component of the conceptual root-zone water-balance model, is dependent on both the water content of the root zone and potential evapotranspiration. Downward drainage is constrained by the hydraulic conductivity of the layers and the available storage capacity of the underlying layer. When the input of water to the root zone exceeds either the available storage capacity or the hydraulic conductivity of the surface layer, runoff is generated as an output component of the root-zone water balance and is routed to downstream grid cells as surface-water run-on. During the surface-water routing process, run-on is allowed to infiltrate back into the root zone and thus becomes an input component to the root-zone water balance. In the conceptual model, all runoff originates as excess rain or snowmelt, and all run-on to downstream grid cells originates as overland flow. Streamflow occurs as overland flow that is routed downstream from the sideslopes and inter-channel areas and concentrated into the channels defined by the topography. Streamflow originating as discharge from springs or as streambank seepage along gaining streams is limited to a few locations in the Death Valley region and is not included in the conceptual model of net infiltration used in this study. For the higher elevations in the Death Valley region, the processes of snowfall, snow accumulation, sublimation, and snowmelt are important components of the water-balance processes affecting net infiltration and are included in the conceptual model. Downward drainage through the root-zone layers can eventually result in drainage through the bottom layer (either bedrock or soil); drainage through the bottom layer is the net infiltration output component from the root-zone water balance.

For the Death Valley region, precipitation and evapotranspiration are the primary components of the water-balance processes controlling net infiltration. Rain, snowmelt, or surface-water runoff infiltrates the soil or bedrock across the air-soil or air-bedrock interface and then drains downward through the root zone (Flint and others 2001c; Hevesi and others, 2002). Redistribution of water in the root zone occurs owing to the combined effects of downward drainage through soil or rock and evapotranspiration after water has stopped infiltrating at the ground surface. In the conceptual model, redistribution owing to lateral flow in the root zone is assumed to be negligible. Net infiltration is the drainage flux, or flow rate, at the shallowest depth beneath the ground surface where evapotranspiration no longer affects the downward drainage of infiltrated water (Flint and others 2001c; Hevesi and others, 2002). The approximate depth of net infiltration is variable in both space and time. For the thick unsaturated zone that exists at most locations in the Death Valley region, net infiltration becomes deep percolation and is represented in the conceptual model as potential recharge. Most of the deep percolation originating as net infiltration eventually becomes actual recharge at the water table. For some locations in the unsaturated zone, however, part of the deep percolation may be captured and diverted laterally above relatively impervious rock units. The diverted water may then return to the root zone as spring discharge that eventually contributes more to evapotranspiration then to recharge.

INFILv3 Model

The conceptual model of root-zone water-balance processes and net infiltration in the Death Valley region was based on components of a mass-balance (also referred to as water balance) equation and is represented by the INFILv3 model. The governing equations in the INFILv3 model are used to perform a daily water-balance simulation of the root zone. The primary governing equation used for the daily root-zone water-balance simulation is

$$NI_d^i = SM_d^i + RAIN_d^i + RI_d^i - D_d^i - \sum_{j=1}^{6} \left(\Delta W_d^i\right)_j - \sum_{j=1}^{6} \left(ET_d^i\right)_j , \quad (1)$$

where

NI_d^i is total net infiltration from the bottom of the root zone for day [d], grid location i,
SM_d^i is snowmelt,
$RAIN_d^i$ is precipitation occurring as rain,
RI_d^i is water that infiltrated the root zone from surface-water run-on,
D_d^i is surface-water discharge (outflow),
$(\Delta W_d^i)_j$ is the change in the root-zone water storage for layer j, and
$(ET_d^i)_j$ is evapotranspiration from layer j.

The total change in root-zone water storage for all six root-zone layers is $\sum(\Delta W_d^i)_j$, and the total root-zone evapotranspiration is $\sum(ET_d^i)_j$.

Secondary governing equations are used to represent other components of the daily water balance that are not directly defined by equation 1. For example, snowmelt (SM_d^i) is equal to snowfall (SF_d^i) minus sublimation (SUB_d^i); $RAIN_d^i$ is equal to total precipitation (PPT_d^i) minus snowfall (SF_d^i); and surface-water runoff (RO_d^i) is equal to RI_d^i plus discharge (D_d^i). For each daily time step, SM_d^i, $RAIN_d^i$, and RI_d^i are simulated as input terms; SF_d^i, RO_d^i, and ΔW_d^i are simulated as storage terms; and SUB_d^i, NI_d^i, ET_d^j, and D_d^i are simulated as output terms. Also included in the daily water balance are deterministic and empirical equations for the simulation of (1) evapotranspiration as a function of potential evapotranspiration and root-zone water content, (2) snowmelt as a function of air temperature and snow pack depth, and (3) sublimation and potential evapotranspiration as a functions of simulated net radiation and air temperature. Net radiation is simulated using an hourly solar radiation model (Flint and Childs, 1987).

The simulation is run as a continuous time series of daily water-balance calculations, where daily snowfall, SF_d, is added to the snowpack storage component, and the root-zone water contents are updated and used as the initial conditions for the following day. The daily water-balance calculation uses a two-step algorithm to include surface-water runoff and run-on, where runoff, RO_d, is generated during the first part of the daily time step and the runoff volume is then routed downstream as surface-water run-on during the second part of the daily step. During the routing process, run-on can infiltrate back into the root zone and contribute to the total daily net-infiltration amount. Increases in the root-zone water contents are used the following day as the new initial conditions for the root-zone water balance.

Calculations in the INFILv3 model are done using a grid-based representation of the drainage basin being simulated, where all grid cells have equal areas. Although the mass-balance calculations are based on water volumes (temperature effects on water density are assumed to be negligible in the volume balance form of the continuity equation, which is based on the conservation of mass), the actual calculations are performed using water-equivalent depths. To perform simulations, the INFILv3 model requires an estimate of initial root-zone water contents; a daily time-series input consisting of total daily precipitation and maximum and minimum air temperature; and a set of model input parameters defining drainage basin characteristics, model coefficients for simulating evapotranspiration, drainage, and the spatial distribution of daily precipitation and air temperature, average monthly atmospheric conditions, and user-defined run-time options. For a multiyear simulation period, the simulated components of the daily water balance are summed through time to calculate total annual amounts and average annual rates.

Model Parameters

Inputs to the INFILv3 model consists of four main input groups: (1) climate and meteorological data, (2) digital map files from GIS and preprocessing routines, (3) attribute tables, and (4) model control options (fig. 13). Climate and meteorological data consist of daily climate records, climate station locations and elevations, model coefficients from monthly climate models and monthly atmospheric properties. Digital map files include a DEM and digitized maps of the spatial distribution of bedrock geology, soil types, and vegetation types. The digital map files are preprocessed and combined into a single watershed-input file containing all spatially distributed drainage basin characteristics. The watershed-input file includes a set of topographic parameters that were developed from the DEM using several different preprocessing routines. The attribute tables define bedrock and deep alluvium properties, soil properties, and vegetation properties representing the hydrologic characteristics of the root zone. For the study reported here, bedrock refers to the hydrogeologic units underlying the root zone and includes both consolidated and unconsolidated geologic rock types. Model outputs include (1) time-series results including the annual, monthly, and daily time series for simulated components of the water balance, expressed as the mean simulation result for all grid cells and also as the simulation result for specified grid locations, (2) spatially distributed simulation results for all components of the water balance indicating the daily, annual, and average annual results at all grid cells, and (3) summary statistics for model inputs and outputs, including the mean, maximum, and minimum values for all grid cells in the model domain.

Table 3 (at back of report) lists the input parameters required by the INFILv3 model, including source data, preprocessing routines used to developed input parameters from the source data, input files, parameter names, parameter descriptions, parameter use, parameter units, and a qualitative measure of parameter accuracy. Seven primary sources of data were used either directly as input or to develop parameters using preprocessing routines: (1) the DEM and topographic parameters developed using the DEM, (2) soil properties associated with the STATSGO database, (3) bedrock and deep alluvium properties associated with the digital map of hydrogeologic units, (4) vegetation and root-zone properties associated with the GAP database, (5) daily climate inputs developed from National Oceanic and Atmospheric Administration/National Climatic Data Center (NOAA/NCDC) climate records, (6) monthly atmospheric parameters, and (7) user-defined model coefficients and simulation options included in the model control file, including snowmelt and sublimation parameters, simulation time parameters, storm duration parameters, evapotranspiration parameters, and stream-channel parameters.

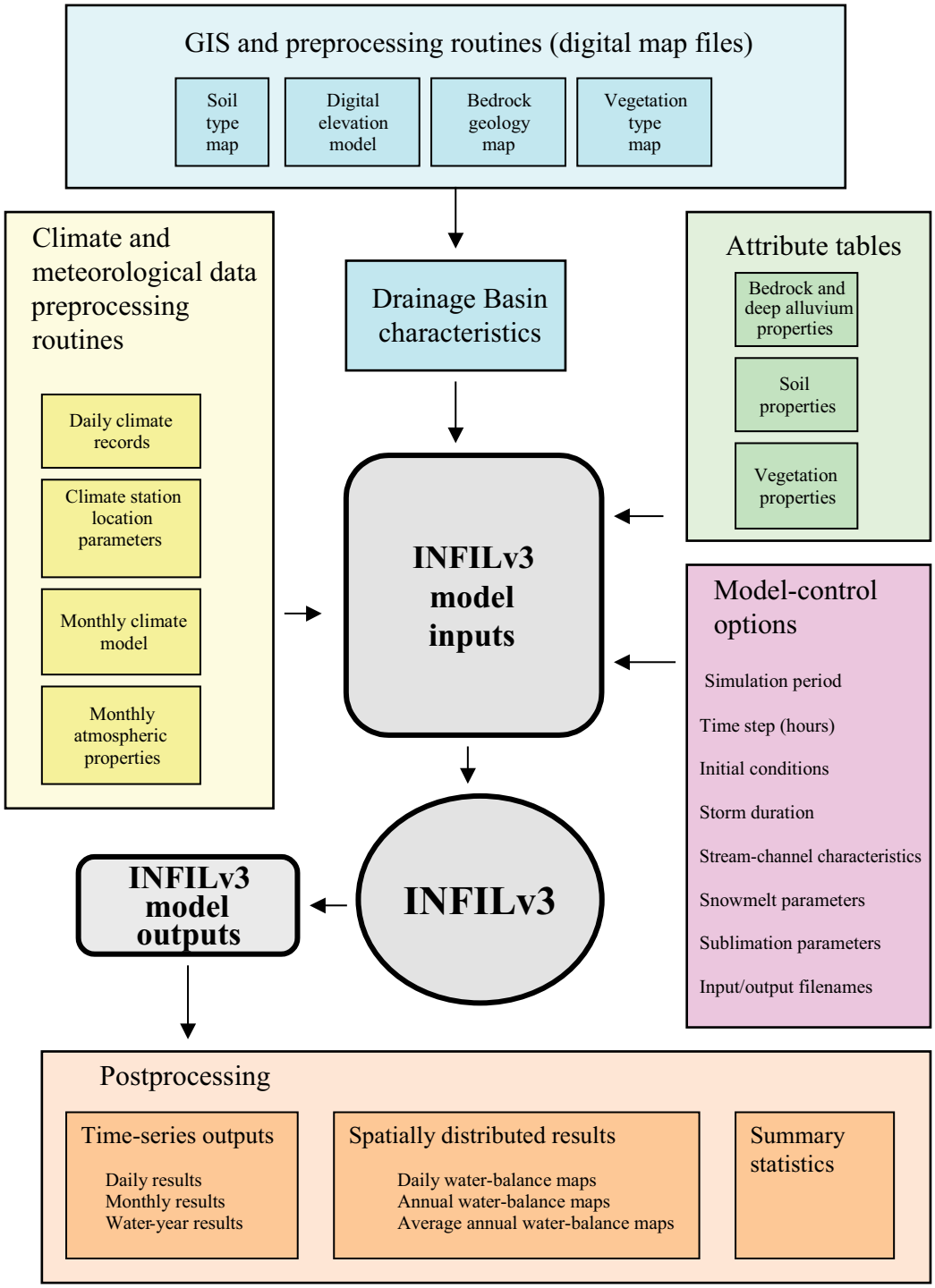

Figure 13. Inputs and outputs in the program structure of the INFILv3 model of the Death Valley region, Nevada and California.

Model inputs defining the physical characteristics of the drainage basins were developed from available data sources using a combination of GIS applications and FORTRAN routines. These model inputs include topographic parameters, soil properties (SOILTYPE and the associated soil properties SOILTHCK, SPOR, SWP, SOILB, and SKS in table 3, at back of report), properties of the bedrock underlying the soil (ROCKTYPE and the associated bedrock properties RKPOR, RK_{LO}, and RK_{HI} [see table 4 at back of report]), and vegetation properties (VEGTYPE and the associated vegetation properties VEGCOV, RZDEN, and RZTHCK, (see tables 5 and 6, at back of report). The topographic parameters were calculated using the DEM; these include slope (SLP), aspect (ASP), blocking ridge angles (RIDGE), skyview factor (SKYVIEW), and surface-water flow-routing parameters (LOCID, IROUT, and UPCELLS). Daily climate inputs include total daily precipitation (PPT) and maximum and minimum daily air temperature (TMAX and TMIN). Additional model inputs include parameters defining monthly climate models, model coefficients used to estimate snowmelt and sublimation, monthly atmospheric characteristics used for simulating incoming solar radiation, initial root-zone water contents, and various run-time options.

Model Geometry and Discretization

The INFILv3 model area and grid were defined using a composite DEM originally developed by Turner and others (1996) for the Death Valley region; the area was extended 0.25 degrees northward to cover the modified boundary of the DVRFS (Claudia Faunt, U.S. Geological Survey, written commun., 2000; D'Agnese and others, 2002). The DEM encompasses an area of 97,136 km^2; this area, referred to in this study as the Death Valley region, includes the entire area of the DVRFS (fig. 2). The DEM grid consists of 1,300 rows (from north to south) and 983 columns (from east to west), with an equivalent grid spacing of 278.5 m in the north–south and east–west directions. The DEM grid includes a total of 1,252,418 elevations. The grid locations are defined by the projection Universal Transverse Mercator (UTM), zone 11, and all horizontal coordinate information is referenced to the North American Datum of 1927.

The INFILv3 model grid cell input was developed by compiling a set of separate input grids for all spatially distributed drainage basin characteristics, including soil type, soil depth, hydrogeologic unit, vegetation type, elevation, slope, aspect, flow routing parameters, skyview parameter, geographic coordinates, and 36 blocking ridge parameters. The base grids were developed using the DEM as the template grid. GIS applications were used to transfer, or rasterize, the vector-based data sources (including the STATSGO MUID map and the hydrogeologic units map) and also the raster-based data source (the WESTVEG map used to identify vegetation types is raster-based GAP data) to the template grid.

Vertical discretization of each grid cell was defined using six root-zone layers with variable thicknesses, where layer thickness is a function of soil thickness. The upper five layers of the model were used to define root-zone characteristics in soil, and the bottom layer (layer 6) was used to define root-zone characteristics in consolidated bedrock where roots were assumed to extend into fractures. The thickness of the lowermost soil layer was decreased and the thickness of the bedrock layer was increased as a linear function of the total soil thickness, which was estimated for all model nodes. If the thickness of the lowermost soil layer was reduced to 0 (as a function of decreased total soil thickness), the thickness of the overlying soil layer was reduced with a continued decrease in soil thickness. For locations with thin soils (a total soil thickness of less than 1 m), the thickness of the bedrock layer (layer 6) generally exceeded the total thickness of the soil layers, depending on the vegetation type and the corresponding RZTHCK parameter. Locations with thicker soils (a soil thickness of greater than 1 m) generally consisted of all five soil layers; the bottom bedrock layer (layer 6) had a thickness of 0, indicating that consolidate rock was estimated to be deeper than the assumed root-zone depth. For these locations, the root zone was simulated as being underlain by deep alluvium rather than by consolidated bedrock.

INFILv3 Model Algorithm

The general algorithm for the INFILv3 model consists of a set of preprocessing steps for developing model inputs, model initialization, a daily water-balance loop, and postprocessing of the daily results for developing monthly, annual, and average annual values for all water-balance terms (fig. 14). The daily water-balance loop includes several different subroutines that provide estimates of the various components of the water balance, such as potential evapotranspiration, snowmelt, and sublimation. The primary subroutines are (1) DAYDIST, a spatial interpolation algorithm for estimating daily precipitation and air temperature at each grid cell; (2) POTEVAP, a potential evapotranspiration model based on simulated incoming solar radiation; (3) SNOW, a snowfall, snowmelt, and sublimation model; (4) ETINFIL, a root-zone infiltration and evapotranspiration routine; and (5) SWINFIL, a surface-water flow routing algorithm. Infiltration and drainage through the root zone is simulated during the routing algorithm, but evapotranspiration is not calculated. Net infiltration is based on a root-zone drainage function and is calculated during both the ETINFIL and SWINFIL routines. Total daily net infiltration is the sum of net infiltration calculated during the ETINFIL and SWINFIL routines. Using spatially distributed estimates of daily precipitation and air temperature as input, the daily water balance is simulated as a continuous time series for multiyear periods, and an average net-infiltration rate is calculated using the daily results.

For each daily time step, the application of the SWINFIL routine is dependent on whether runoff is generated at any model grid location following an initial water-balance calculation for the root zone by the ETINFIL routine. For the initial calculation, infiltration into the root zone, evapotranspiration, changes in the root-zone water content, and net infiltration in direct response to rainfall and snowmelt are calculated by ETINFIL to determine runoff generation. If runoff is not generated, the simulation is continued the next day. If runoff is generated (as excess rainfall or snowmelt), the surface-water routing algorithm is activated. During the routing process, surface-water run-on infiltrates into the root zone depending on the soil and bedrock hydraulic conductivity and the available storage capacity of the root zone. The new value for root-zone water content is then used as the initial condition for the next day's water-balance calculation. Surface-water flow that does not infiltrate into the root zone becomes surface-water discharge from the drainage basin (watershed) being modeled. In closed basins, surface water discharges to playas and is assumed to evaporate.

Within each daily time step, the potential evapotranspiration routine, POTEVAP, uses an hourly time step to simulate net radiation based on calculated solar position and simulated incoming solar radiation. The hourly time step is used to calculate solar position, as a function of geographic position and the day of year and to account for shading effects from surrounding terrain as a function of solar position. The remaining components of the water balance, including snowmelt, sublimation, evapotranspiration, infiltration, drainage, runoff generation, and surface-water flow routing, are based on a daily time step.

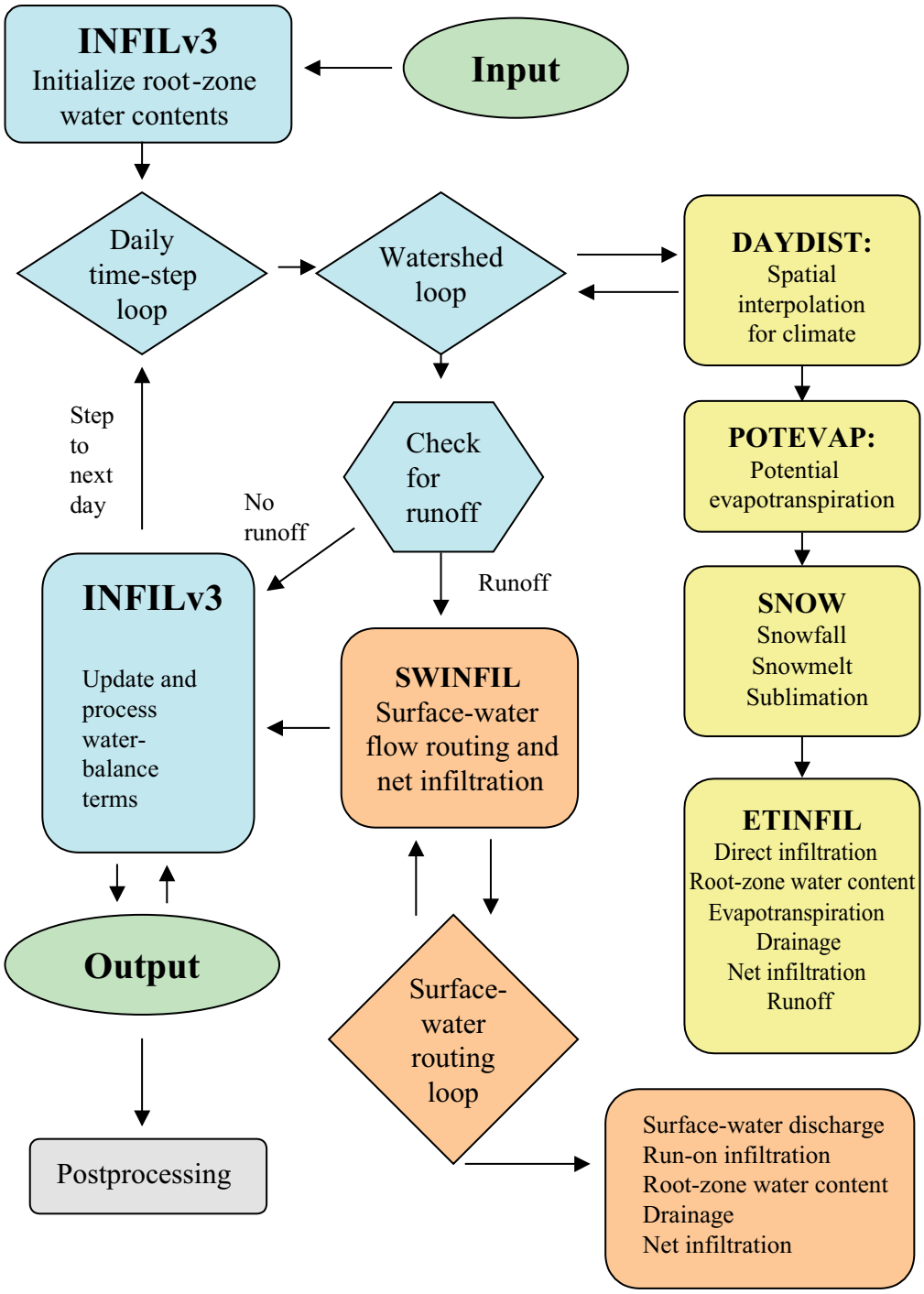

Figure 14. Main subroutines of the INFILv3 model of the Death Valley region, Nevada and California.

Subroutines

DAYDIST: Spatial Distribution of Daily Climate Parameters

Daily precipitation and air temperature are spatially distributed across the model domain by the DAYDIST routine using monthly precipitation-elevation and air temperature-elevation regression models combined with an inverse-distance squared interpolation algorithm (fig. 15). The regression models were developed using monthly data compiled from the daily climate records. Monthly regression models for precipitation define total monthly precipitation as a function of elevation, and monthly regression models for maximum and minimum air temperature define average monthly maximum and minimum air temperature as functions of elevation. The regression equations for precipitation and air temperature are applied in the spatial interpolation algorithm if the r-squared regression statistic (also referred to as the coefficient of determination) is greater than 0.25. The regression model types include the linear model (regression model type 1)

$$E_m^{\,i} = A_m(\mathrm{ELEV}^i) + C_m, \tag{2}$$

and the quadratic model (regression model type 3)

$$E_m^{\,i} = A_m(\mathrm{ELEV}^i)^2 + B_m(\mathrm{ELEV}^i) + C_m, \tag{3}$$

where

$E_m^{\,i}$ is the estimated monthly climate parameter (daily precipitation [PPT], maximum daily air temperature [TMAX], or minimum daily air temperature [TMIN]) for grid location i and month m,

A_m, B_m, and C_m are the regression model coefficients for each month m, and

ELEV^i is the elevation for grid location i.

In the first step of the spatial interpolation routine, daily precipitation data (PPT) or air temperature data (TMAX, or TMIN) are scaled using the ratio of the estimated average monthly precipitation (or air temperature) at each active precipitation station and the estimated monthly precipitation (or air temperature) at the grid location being interpolated. The monthly estimate for the grid location is obtained using the developed monthly regression models for each climate parameter and the estimated elevation of the location being interpolated, as specified by the DEM. In the second part of the routine, the interpolated daily value is calculated for the grid location using a modified inverse-distance-squared interpolation:

$$E_d^{\,i} = \sum_{k=1}^{132} \left\{ \left[\left(1/(\mathrm{DIST}^k)^2\right) / \left(\sum_{k=1}^{132} (1/\mathrm{DIST}^k)^2 \right) \right] \frac{(E_m^{\,i})}{(E_m^{\,k})} (X_d^{\,k}) \right\} \tag{4}$$

where

$E_{d_k}^{\,i}$ is the estimated daily value of PPT, TMAX, or TMIN for day [d] at model grid location i,

DIST^k is the distance between grid location i and climate station k,

$E_m^{\,i}$ is the monthly estimate for grid location i,

$E_{m_k}^{\,k}$ is the monthly estimate for climate station k, and

$X_d^{\,k}$ is the daily climate parameter value of PPT, TMAX, or TMIN at climate station k for day [d].

The summation in equation 4 is applied to all 132 climate stations (k=1, 132). Equation 4 is used for all grid locations i and for all three climate parameters (PPT, TMAX, and TMIN). Average daily air temperature is calculated as the average of the estimated TMAX and TMIN values (Flint and Childs, 1987).

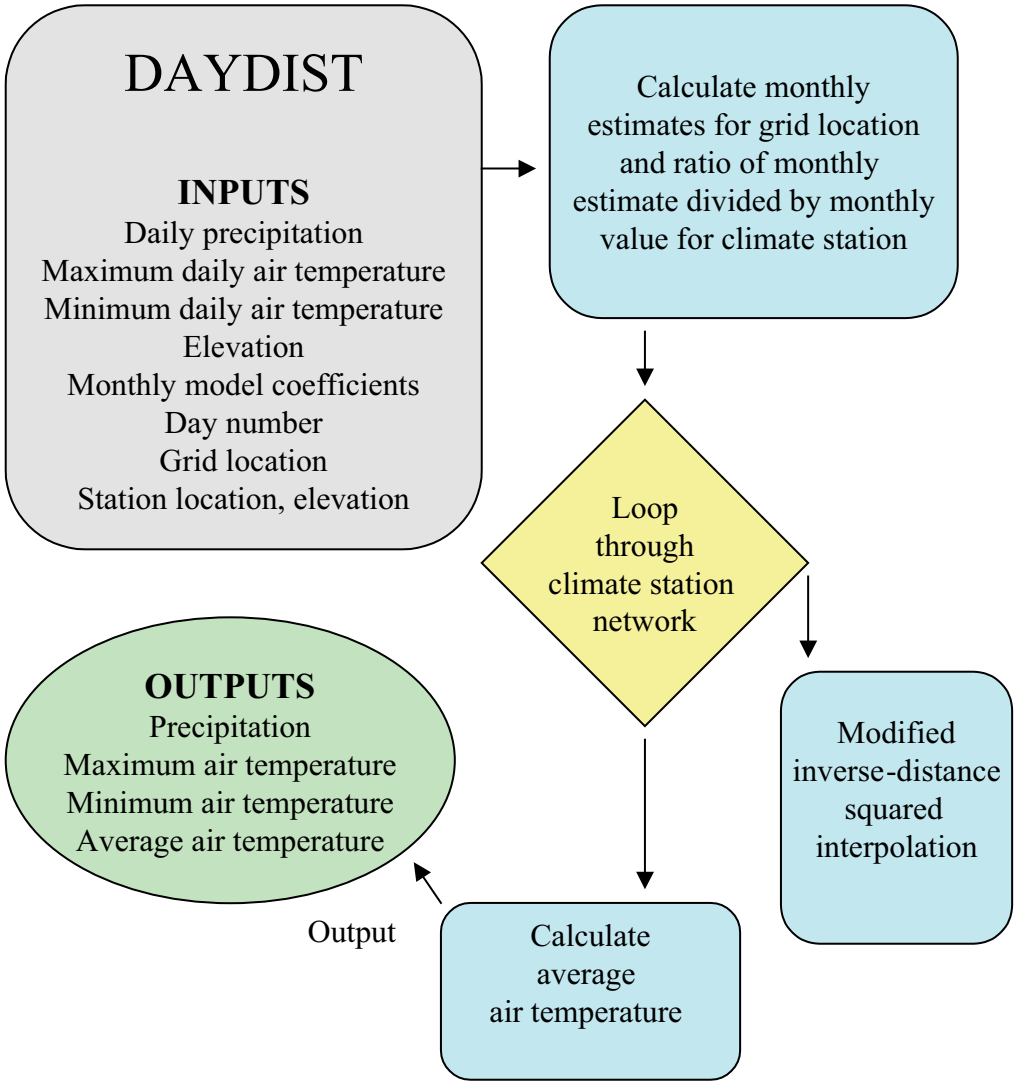

Figure 15. Subroutine DAYDIST in the INFILv3 model of the Death Valley region, Nevada and California.
DAYDIST, spatial distribution of daily climate parameters

POTEVAP: Potential Evapotranspiration

Potential evapotranspiration is simulated using the subroutine POTEVAP (fig. 16). Input parameters for the subroutine include (1) average air temperature, (2) elevation (ELEV), (3) atmospheric parameters ozone [OZONE], precipitable water [WP], atmospheric turbidity [BETA], circumsolar-diffuse radiation [CSR], surface reflectivity [PG]), (4) blocking ridge angles (RIDGE), (5) skyview reduction factor (SKYVIEW), (6) day number, (7) grid location (LAT, LON), (8) slope (SLP), and (9) aspect (ASP). The subroutine contains an hourly time-step loop to simulate incoming solar radiation.

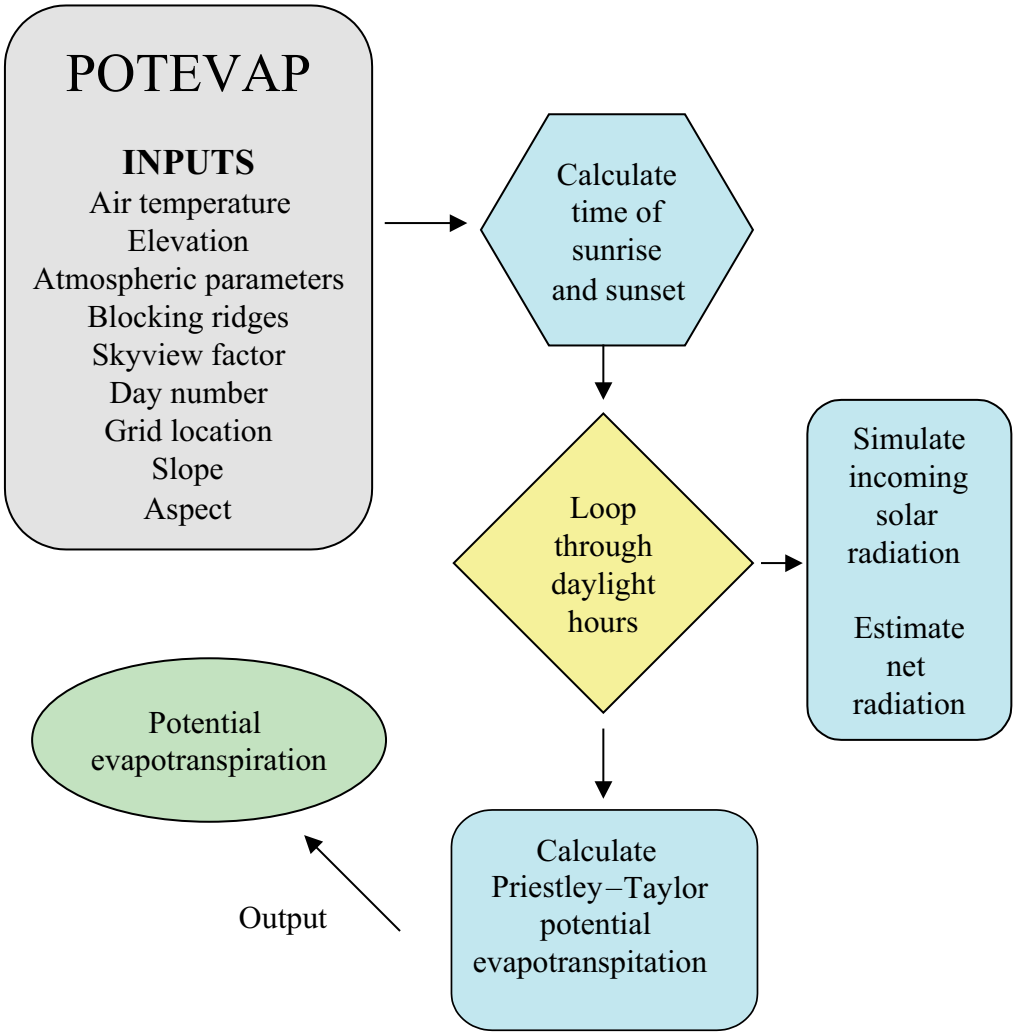

Figure 16. Subroutine POTEVAP in the INFILv3 model of the Death Valley region, Nevada and California.
POTEVAP, potential evapotranspiration

In the INFILv3 model, daily evapotranspiration from each root-zone layer is simulated as an empirical function of potential evapotranspiration and water content on the basis of a modified form of the Priestley–Taylor equation (Flint and Childs, 1991). In the POTEVAP subroutine, the Priestley–Taylor equation (Priestley and Taylor, 1972) is used to calculate potential evapotranspiration:

$$\lambda(\mathrm{PET}_d^{\,i}) = \alpha\left(\frac{S}{S+\gamma}\right)_d^{i}((R_n)_d^{\,i} - G_d^{\,i}), \tag{5}$$

where $\lambda(\mathrm{PET}_d^{\,i})$ is the latent heat flux, with λ the latent heat of vaporization, and $(\mathrm{PET}_d^{\,i})$ is the rate of potential evaporation at grid location i for day d; and α, an empirical coefficient, is determined to be 1.26 for freely evaporating surfaces (Priestley and Taylor, 1972; Stewart and Rouse, 1977; Eichinger and others, 1996). The available energy is $(R_n)_d^{\,i} - G_d^{\,i}$, where $(R_n)_d^{\,i}$ is net radiation, and $G_d^{\,i}$ is the soil-heat flux. The slope of the vapor density deficit curve, $S/(S+\gamma)_d^{\,i}$, is derived from the temperature used to convert available energy into potential evapotranspiration (Campbell, 1977, table A.3).

To apply the Priestley–Taylor equation (eq. 5), net radiation (R_n) and soil-heat flux (G) were estimated on the basis of calculations of solar radiation and soil temperature at Yucca Mountain (Flint and others, 2001a) made using a modified form of the solar radiation (SOLRAD) model of Flint and Childs (1987). Potential evapotranspiration was calculated on an hourly basis and summed over the period of 1 day to obtain an estimate of total daily potential evapotranspiration, which was then used as input for calculating actual evapotranspiration in the root zone.

The SOLRAD model uses detailed site geometry and monthly regional atmospheric properties from the National Weather Service (NWS) to calculate daily solar radiation. The atmospheric properties are monthly averages for ozone, precipitable water, atmospheric turbidity, circumsolar-diffuse radiation, and surface reflectivity (table 3 at back of report). The site geometry includes latitude (LAT), longitude (LON), slope (SLP), aspect (ASP), elevation (ELEV), and a set of 36 angles above horizontal used to account for shading effects from surrounding ridges that block the sky (blocking ridge angles, RIDGE, and skyview reduction, SKYVIEW) from direct-beam and diffuse sky radiation. To model solar radiation, the position of the sun is calculated every hour, starting at sunrise each day, using the site location inputs (LAT and LON) and the simulation day number (Flint and Childs, 1987). Direct-beam and diffuse sky radiation are calculated using the atmospheric properties and applied to the surface on the basis of slope, aspect, and the amount of sky and sun that would be blocked by the surrounding topography. Ground-reflected radiation is added to the solar radiation term and is simulated on the basis of the area of the surrounding topography, the surface reflectivity, and the direct-beam and diffuse sky radiation that reflects from the surrounding topography.

SNOW: Snowfall, Snowmelt, and Sublimation

The occurrence of precipitation as snow is simulated as a simple step-function using average daily air temperature, where all precipitation is assumed to be snow when the average daily air temperature is equal to or less than 0°C. Daily snowfall is added to the snowpack storage term in the daily water balance. The snowpack storage accounts for the amount of water stored in the snowpack and is based on snowfall accumulation and losses from sublimation and snowmelt. Snowpack storage is carried over as an antecedent condition for the following day's water-balance calculation. When the average daily air temperature is less than or equal to freezing, the snow cover term is reduced by a fraction defined using an assumed sublimation model that calculates sublimation as a percentage of potential evapotranspiration and the available water in the snowpack. When the daily maximum air temperature is greater than freezing, an empirical temperature-index model is applied using parameters calibrated for the Sierra Nevada (Maidment, 1993) to calculate the daily snowmelt, and the snowpack is reduced by this amount. Snowmelt for November through April was estimated using

$$M_d^i = 0.96(\mathrm{TMAX}_d^i), \qquad \mathrm{TMAX}_d^i > 0$$

$$M_d^i = 0, \qquad \mathrm{TMAX}_d^i \le 0\,, \tag{6}$$

where TMAX_d^i is the maximum daily air temperature for day d and M is the daily snowmelt amount. Snowmelt for May through October was estimated using

$$M_d^i = 1.14(\mathrm{TMAX}^i{}_d), \qquad \mathrm{TMAX}_d^i > 0$$

$$M_d^i = 0, \qquad \mathrm{TMAX}_d^i \le 0\ . \tag{7}$$

ETINFIL: Infiltration, Drainage, Evaporation, and Runoff

The root-zone water-balance calculation incorporates a two-step process to couple surface-water flow with the processes of infiltration, drainage, and evapotranspiration. The first step of the root-zone water-balance simulation is performed by the ETINFIL subroutine (fig. 17), which consists of (in order of application) the following: (1) Initial runoff (runoff and infiltration into the root zone from snowmelt and rainfall [runoff-1]); (2) downward drainage and an initial change in storage in all the root-zone layers; (3) evapotranspiration from root-zone layers; and (4) net infiltration, total runoff (runoff-2), and final change in storage for all root-zone layers.

Depending on soil depth, either soil or bedrock saturated hydraulic conductivity is used to calculate an initial runoff amount in response to total water inflow from rain and snowmelt. The initial runoff amount represents the fraction of water inflow exceeding the soil or bedrock infiltration capacity. An estimate of storm duration is used to determine rainfall intensity, with separate estimates used for winter and summer storms (STORMWIN and STORMSUM, respectively) (table 3 at back of report). An assumed daily snowmelt duration is used to determine snowmelt intensity. The total water inflow rate is compared with the soil or bedrock saturated hydraulic conductivity, adjusted for storm duration, to determine the occurrence and magnitude of the initial runoff amount.

Infiltration and Drainage

The governing water balance for the root zone is solved by updating the initial water content of each root-zone layer j using the final water content of the previous day, plus infiltrated run-on, RI_j^i, and then calculating a new water content for each root-zone layer based on infiltration across the top of each layer, evapotranspiration losses from each layer, downward drainage and drainage out from the bottom of each layer, and contributions to runoff from each layer using

$$\Delta W_j^i = RI_j^i + I_j^i - DR_j^i - ET_j^i - RO_j^i, \tag{8}$$

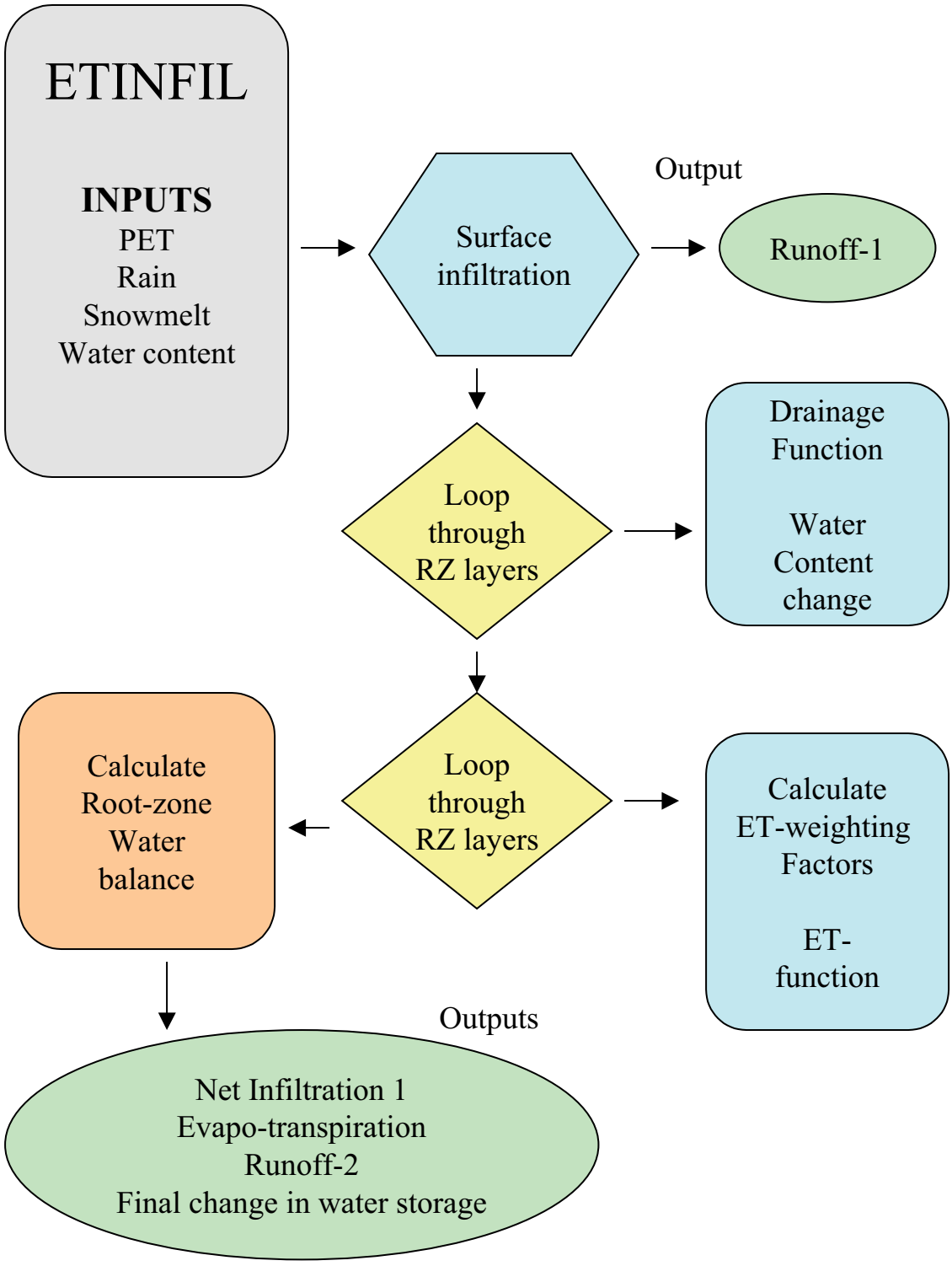

Figure 17. Subroutine ETINFIL in the INFILv3 model of the Death Valley region, Nevada an California.

where

ΔW_j^i is the change in the layer water content for layer *j*, grid location *i*;

RI_j^i is infiltrated surface-water run-on from the previous day,

I_j^i is infiltration into layer *j* from the layer above,

DR_j^i is drainage through layer *j* into layer *j* + 1,

ET_j^i is evapotranspiration from the layer *j* based on water content, root-zone parameters and a weighting function applied to potential evapotranspiration, and

RO_j^i is the contribution to runoff from layer *j*.

ET_j^i is simulated after drainage through all layers has been simulated, and ΔW_j^i is updated. The final ΔW_j^i is calculated by checking the temporary storage terms for each layer used to redistribute excess water upward to the overlying layers. The upward redistribution of the temporary storage terms results in the generation of surface-water runoff RO_j^i when the available storage capacity of overlying layers in the root zone is not sufficient.

Equation 8 is applied successively downward through all the root-zone layers, with net infiltration, NI^i, equal to drainage for the bottom layer (layer 6), DR_6^i, in equation 8. Downward drainage, DR_j^i, is calculated using a modified form of an empirical drainage model presented in Jury and others (1991) for approximating water contents in a draining soil profile. In the ETINFIL subroutine, the modified drainage model is applied successively to each layer, starting with the top layer and moving down through all soil layers, using the following set of equations:

$$DR_j^i = (VWCA_j^i - VWCB_j^i) \times THCK_j^i \times 1,000, \tag{9}$$

where $VWCA_j^i$ is the initial volumetric water content calculated using

$$VWCA_j^i = GA2_j^i \times (GT_j^i + GC2_j^i)^{(-GB^i)} \tag{10}$$

and $VWCB_j^i$ is the final volumetric water content calculated using

$$VWCB_j^i = GA2_j^i \times [(GT_j^i + 1) + GC2_j^i]^{(-GB^i)}, \tag{11}$$

where

$$GA2_j^i = \left\{ SPOR_j^{i(GN^i + 1)} \times \ [(THCK_j^i \times 1,000)/(GN^i \times SKS_j^i)] \right\}^{(1/GB^i)} \tag{12}$$

$$GT_j^i = \left[(VWCC_j^i/(GA2_j^i))^{(1/-GB^i)} \right] - GC2_j \tag{13}$$

$$VWCC_j = SOILMM_j^i/THCK_j^i/1,000 \tag{14}$$

$$GC2_j^i = (THCK_j^i \times 1,000 \times SPOR_j^i)/(GN^i \times SKS_j^i) \tag{15}$$

$$GB^i = 1/GN^i \tag{16}$$

$$GN^i = 2.0 \times SOILB^i + 3 \tag{17}$$

In equations 9 through 17, $SOILB^i$ is an input parameter calculated using STATSGO soil texture (tables 2 and 3 at back of report) for the soil type at grid location *i*; $THCK_j^i$ is layer *j* thickness at grid location *i*; SKS_j^i is the soil saturated hydraulic conductivity for the soil type at grid location *i*, layer *j*, (also calculated using STATSGO soil texture); $SPOR_j^i$ is soil porosity for location *i* (calculated using bulk density data provided by STATSGO and an assumed particle density); and $SOILMM_j^i$ is the simulated soil layer water content, expressed as an equivalent water depth (in millimeters) for grid location *i* and layer *j*. The input parameters $SOILB^i$ and SKS_j^i are calculated based on the average percentage of sand and clay for each STATSGO MUID and empirical equations from Campbell (1985).

For each soil layer *j* having a thickness greater than 0, equations 9 through 17 define DR_j^i as a potential drainage term. Actual drainage is calculated by comparing DR_j^i to the saturated hydraulic conductivity of the underlying layer. If DR_j^i is greater than the saturated hydraulic conductivity of the underlying layer, DR_j^i is set equal to the saturated hydraulic conductivity of the underlying layer, and the "excess water" is added back to the layer *j* water content. For infiltration and drainage during saturated conditions, the excess water that cannot drain is added to a temporary storage term that is used to calculate runoff and the final distribution of water in the root zone (following the simulation of evapotranspiration).

For locations that have deep soils (the root zone is underlain by an unconsolidated hydrogeologic unit), the thickness of the bedrock layer (root-zone layer 6) is set to 0, and potential drainage through soil layer 5 (DR_5^i, calculated by applying equations 9 through 17) is compared with the saturated hydraulic conductivity of the underlying unconsolidated hydrogeologic unit (Quaternary and Tertiary valley fill, Quaternary playa deposits) (fig. 11). If the potential drainage for layer 5, DR_5^i, exceeds the saturated hydraulic conductivity of the underlying layer, then the actual drainage, net infiltration, is set equal to the saturated hydraulic conductivity, and the excess drainage amount is added back to the temporary storage component for layer 5.

For locations that have thin soils, the bottom of the root zone is extended down into the underlying consolidated bedrock layer, assuming that roots extend into rock fractures. The thickness of layer 6, the bedrock layer for the root zone, is calculated as a function of the overlying soil thickness using

$$THCK_6^i = RZDPTH^i - (SOILTHCK^i / THCKC), \tag{18}$$

where

$THCK_6^i$ is the thickness of layer 6, in meters, for location *i*,

$RZDPTH^i$ is the maximum thickness for the bedrock layer,

$SOILTHCK^i$ is the estimated soil thickness, (in meters, and

$THCKC$ is a model coefficient (usually set to 1 or 2).

Net infiltration is drainage through layer 6 and is calculated using

$$DR_6^i = RK^i_{LO}, \qquad (WC_6^i \times THCK_6^i \times 1,000) < (RPOR^i \times THCK_6^i \times 1,000)$$

$$DR_6^i = RK^i_{HI}, \qquad (WC_6^i \times THCK_j^i \times 1,000) \geq (RPOR^i \times THCK_6^i \times 1,000) + RK^i_{HI}, \tag{19}$$

where

RK^i_{LO} is the effective bedrock hydraulic conductivity used to represent unsaturated conditions,

WC_6^i is the water content for the bedrock layer at location *j*,

$THCK_6^i$ is the layer thickness,

$RPOR^i$ is the effective root-zone porosity for the bedrock layer, and

RK^i_{HI} is the effective bedrock hydraulic conductivity used to represent saturated conditions.

Evapotranspiration

Evapotranspiration from each layer is simulated using a modified form of the Priestley–Taylor equation and the updated water contents for each layer calculated by the downward drainage function. The modified Priestley–Taylor equation relates the empirical coefficient in equation 5, α, to seasonal changes in soil-water content (Davies and Allen, 1973; Flint and Childs, 1991). This modified version has been successfully used in arid and semiarid environments (de Bruin, 1988; Stannard, 1993). When expressed as a function of soil-water content, α is replaced with α'

$$\alpha' = \alpha(1 - e^{\beta\Theta}), \tag{20}$$

where α, usually set to 1.26, was allowed to vary between 1 and 1.5; β was set to –10.0; and Θ is relative saturation defined as

$$\Theta = \frac{(\theta - \theta_r)}{(\theta_s - \theta_r)}, \tag{21}$$

where

θ is soil-water content,

θ_r is residual soil-water content SWP for plant transpiration (soil-water content at –60 bars water potential), and

θ_s is porosity (*SPOR* for layers 1 through 5, *RPOR* for layer 6).

θ_r is the approximate potential at which desert plants no longer transpire (also referred to as the wilting point, SWP).

In the ETINFIL subroutine, the modified form of the Priestley–Taylor equation is used to simulate both bare-soil evaporation and plant transpiration. Bare-soil evaporation is simulated from the top two layers of the root zone having a non-zero thickness (usually layers 1 and 2) using

$$BSE_j^{\,i} = \left\{ BSEA \times \left[1 - e^{(BSEB \times \Theta_j^{\,i})} \right] \right\} \times (1 - VEGCOV^i) \times PETE_j^{\,i} \ , \tag{22}$$

where $BSE_j^{\,i}$ is the daily bare-soil evaporation, in millimeters; *BSEA* (α in eq. 20) was set to 1.04 on the basis of the standard value used for bare-soil surfaces; and *BSEB* (β in eq. 20) was set to –10.0 (Flint and Childs, 1987); $VEGCOV^i$ is the estimated vegetation cover for location *i*; $\Theta_j^{\,i}$ is relative saturation calculated using equation 21; and $PETE_j^{\,i}$ is the potential evapotranspiration rate (in mm/day) simulated for location *i,* layer *j*. Equation 22 is applied to the top layer first, and is $PETE_1^{\,i}$ set equal to $PET_d^{\,i}$ (from eq. 5). For the second layer, $PETE_2^{\,i}$ is calculated by subtracting $BSE_1^{\,i}$ from $PET_d^{\,i}$. Total bare-soil evaporation $(BSE_1^{\,i} + BSE_2^{\,i})$ cannot exceed $(1 - VEGCOV^i) \times PET^i$.

Bare-soil evaporation is simulated before transpiration, and thus the total energy available for transpiration, $PETT_0^{\,i}$, is calculated using

$$PETT_0^{\,i} = (VEGCOV^i \times PET^i) - (BSE_1^{\,i} + BSE_2^{\,i}) \ . \tag{23}$$

The simulation of transpiration takes into account the root-density weighting factors for each layer, as well as the distribution of available water in all the root-zone layers. Starting with the top layer and stepping down through the root zone, transpiration from each layer, $ET_j^{\,i}$, is simulated using

$$ET_j^{\,i} = WGT_j^{\,i} \times \{ ETA \times [1 - e\ (ETB \times \Theta_j^{\,i})] \} \times PETT_j^{\,i} \ , \tag{24}$$

where *ETA* is set to 1.5, *ETB* is set to –10.0, and the weights WGT_j^i are calculated using

$$WGT_j^i = (\Theta_j^i \times RZDEN_j^i) / \sum_{j=1}^{6} (\Theta_j^i \times RZDEN_j^i), \qquad WGT_j^i \le RZDEN_j^i$$

$$WGT_j^i = RZDEN_j^i \ , WGT_j^i > RZDEN_j^i \tag{25}$$

with $RZDEN_j^i$ being the estimated root density terms for the six root-zone layers. In equation 25, the root-density terms and the simulated relative saturations are both used to dynamically condition the weighting factors. The root-density terms also are used to limit the magnitude of each weighting factor. For the top root-zone layer, $PETT_j^i$ is set equal to $PETT_0^i$. As equation 25 is applied sequentially down through each layer, the $PETT_j^i$ term is adjusted using

$$PETT_j^i = PETT_{j-1}^i - ET_{j-1}^i \quad . \tag{26}$$

In applying equation 26 to the simulation of transpiration, the transpiration demand is satisfied by first using the top root-zone layers. Thus, for a fully saturated root-zone profile, transpiration losses are higher for the top layers. As the top layers start drying faster relative to the lower layers, the transpiration rates increase for the lower root-zone layers. When the top layers reach the water content defined as the wilting-point (SWP [table 3 at back of report]), the total available energy for transpiration is shifted to the lower part of the root zone.

Runoff Generation

During the first step of the ETINFIL algorithm, an initial runoff amount $RO1^i$ is generated at grid location *i* if the snowmelt or rain intensity exceeds a threshold infiltration capacity. The threshold infiltration capacity for soil and bedrock is defined using

$$ASKS^i = SKS^i / (24 / STORM)$$

$$ARK_{HI}^i = (RK_{HI}^i) / (24 / STORM) \tag{27}$$

where *STORM* is the assumed duration of precipitation or snowmelt, in hours. If the rain and (or) snowmelt intensity exceeds the infiltration capacity $ASKS^i$ or ARK_{HI}^i, infiltration into the root zone is set equal to $ASKS^i$ or ARK_{HI}^i (depending on soil thickness), and the excess rain and (or) snowmelt is added to the initial runoff amount $RO1^i$.

The final runoff amount, $RO2_j^i$, is calculated using a redistribution algorithm that steps sequentially through all root-zone layers, starting at the bottom and moving up to the top layer. To simulate $RO2_j^i$ and the final water content of each layer ($SOILMM^j$ and $ROCKMM^i$), the storage capacity of each layer is checked against the amount of water held in a temporary storage variable for each layer. If the temporary storage variable exceeds the storage capacity of the layer, the excess water $RO2_j^i$ is added to the overlying layer. The algorithm moves sequentially up through the root-zone layers until all excess water held in temporary storage has been redistributed to overlying layers that have available storage capacity. If excess water remains after the upward redistribution has reached the top soil layer, the excess water is added to the runoff term. The runoff generated by the upward redistribution process represents the fraction of in-flowing water that exceeds the storage capacity of the root zone. Total runoff RO_j^i is the sum of the excess root-zone water $RO2_j^i$ and the initial runoff $RO1_j^i$ calculated as excess rainfall and (or) snowmelt.

SWINFIL: Surface-Water Flow Routing

Using the surface-water routing routine, SWINFIL, the INFILv3 model incorporates the downstream routing of runoff and the simulation of surface-water discharge (as total daily discharge) for all days when runoff is generated by the ETINFIL routine. During the routing process, surface water is allowed to infiltrate back into the root zone (in both soil and bedrock). Surface-water flow is thus coupled to the root-zone water balance by the infiltrated run-on component. At each grid cell in the INFILv3 model domain, the surface-water discharge depth is equal to the runoff generated at that grid cell, plus run-on routed from upstream grid cells, minus infiltrated run-on. The simulated surface-water discharge volume, which can be compared with streamflow records for model calibration, is calculated using the discharge depth and the grid cell area of 77,559 m^2.

If runoff is generated at any location in the drainage basin grid, SWINFIL is activated; otherwise, the simulation steps forward to the next day. The surface-water routing algorithm loops through the drainage basin grid, starting with the highest elevation and moving down through the drainage basin grid until the lowest elevation in the drainage basin is reached. Using a standard eight-directional (D-8) routine algorithm, runoff from the grid cell identified by LOCID is routed as run-on to the grid cell identified by IROUT, with LOCID and IROUT acting as pointers to connect upstream and downstream cells. The D-8 routing algorithm represents convergent flow only; each grid cell can have only one downstream cell but may have multiple upstream cells. Infiltration losses into the root zone are subtracted from the runoff being routed as run-on to the downstream grid cell.

The SWINFIL subroutine (fig. 18) uses a simplified form of the downward drainage algorithm, where drainage into the root zone and the underlying layers occurs only when the overlying layer has become fully saturated. Drainage from unsaturated layers, which is simulated in ETINFIL, is not simulated in SWINFIL. The drainage amount is limited by the saturated hydraulic conductivity of the underlying layer. Evapotranspiration is not calculated during surface-water routing, but the change in the water content of each layer j is stored and added to the next day's water-balance calculation as the infiltrated run-on component (RI_j^i in equation 8 of the ETINFIL subroutine). Net infiltration in direct response to the infiltration of surface-water run-on is defined as run-on net infiltration and is added to the total daily net-infiltration term. Total infiltration during surface-water routing is equal to the sum of infiltrated run-on and run-on net infiltration.

Input parameters used in the surface-water flow-routing algorithm include the upstream and downstream cell location identifier, the number of upstream cells, four coefficients used to model the fraction of each grid cell area wetted by surface-water run-on, and two coefficients used to scale the soil saturated hydraulic conductivity for grid cells in larger stream channels. The fraction of each grid cell area wetted by surface-water run-on is defined by

$$FLAREA^i = CHAN1 + \left[\left(UPCELLS^i \times FLOWIN^i\right)^{((1-SL2^i)/2)}\right]/CHAN2$$
$$+ CHAN3 - UPCELLS^i/4, \qquad FLAREA^i \le CHAN4 \tag{28}$$
$$FLAREA^i = CHAN4, \qquad FLAREA^i > CHAN4,$$

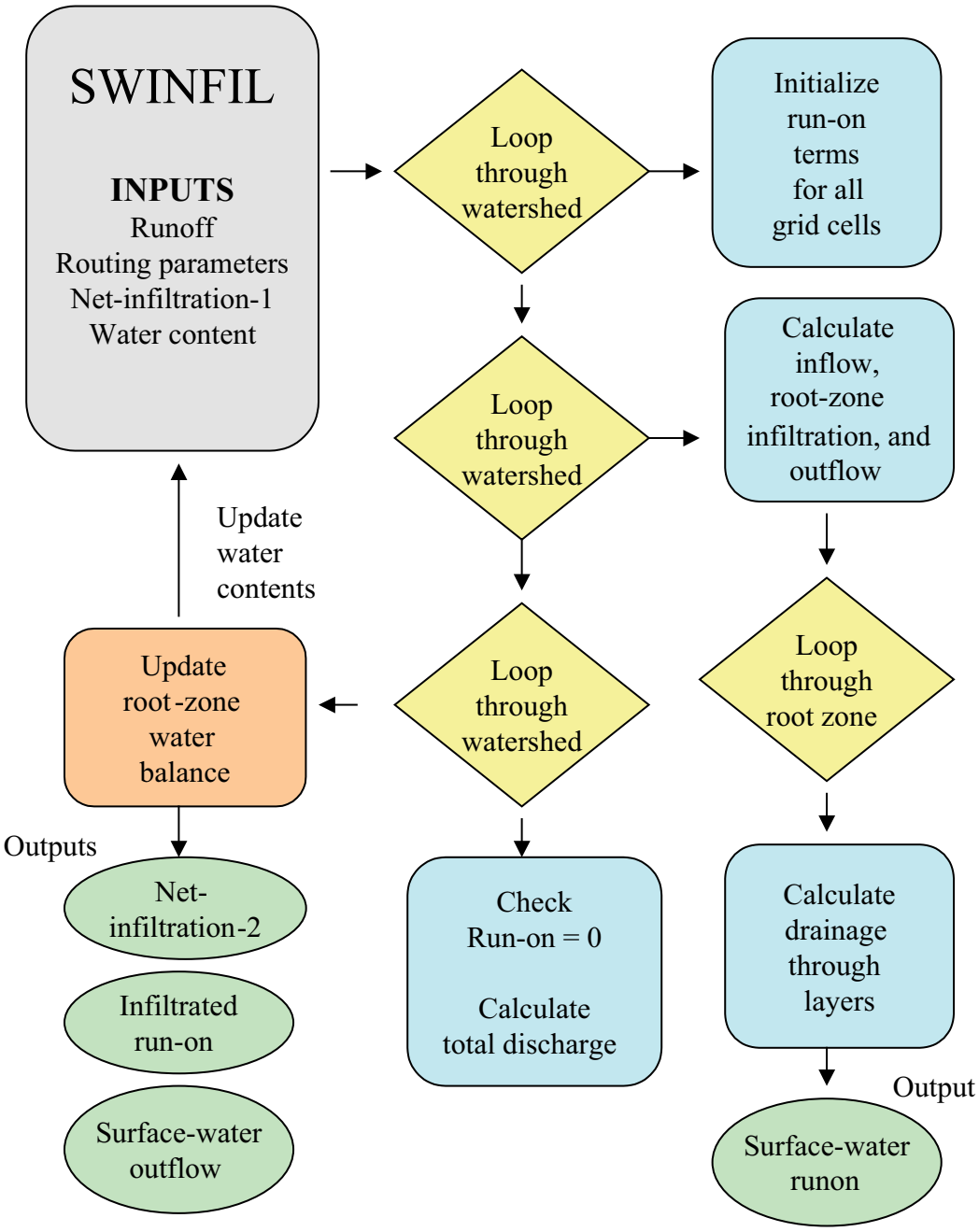

Figure 18. Subroutine SWINFIL in the INFILv3 model of the Death Valley region, Nevada and California.
SWINFIL, surface-water flow routing.

where

$FLAREA^i$	is the effective flow area for grid location *i,*
*CHAN*1	is a model coefficient,
*CHAN*2	is a model coefficient,
*CHAN*3	is a model coefficient,
*CHAN*4	is a model coefficient,
$UPCELLS^i$	is the number of upstream cells for grid location *i*,
$FLOWIN^i$	is the simulated surface-water run-on for grid location *i*, and
$SL2^i$	is the ground-surface slope for grid location *i*.

Using this model, *CHAN*1 defines the minimum effective flow area, *CHAN*3 defines the maximum headwater flow area, and *CHAN*4 defines the maximum stream-channel flow area. The headwater flow area is used to represent upland areas where overland flow processes are more significant compared with channel flow. For low-flow conditions, steep channels, and small upstream areas, the effective flow area is defined by the *CHAN*1 coefficient. The effective flow area increases as a continuous function and approaches or equals the *CHAN*4 coefficient as the surface-water run-on depth increases, the channel gradient decreases, and the number of upstream cells (and thus upstream area) increases. To help account for dispersive flow across alluvial fans in the lower sections of the drainage basins, the *CHAN*4 coefficient can be set to a value greater than 1, allowing the effective flow area to be greater then the grid cell area.

The soil saturated hydraulic conductivity for grid location ^{i}, SKS^i is scaled for stream-channel locations using

$$KSCHN^i = SKS^i \times [(UPCELLS^i - KSCHN1)/KSCHN2 + 1] \quad , \quad KSCHN^i/SKS^i \le KSCHN3$$

$$KSCHN^i = SKS^i \times KSCHN3, \quad KSCHN^i/SKS^i > KSCHN3 \tag{29}$$

where $KSCHN^i$ is the scaled soil saturated hydraulic conductivity. The maximum value for $KSCHN^i$ is defined by *KSCHN*3.

The final adjustment to the saturated hydraulic conductivity for soil and bedrock is used to account for the simulated wetted area and the estimated flow duration

$$KSCHNF^i = (KSCHN^i \times FLAREA^i)/(24/\mathrm{STORM})$$

$$= (RK^i{}_{HI} \times FLAREA^i)/(24/\mathrm{STORM}) \ , \tag{30}$$

where

$KSCHNF^i$	is the final adjusted saturated hydraulic conductivity of the soil, and
RKS^i	is the final adjusted saturated hydraulic conductivity of bedrock.

The parameter STORM, which is the flow duration in hours, is set equal to the duration of the precipitation (STORMSUM for summer precipitation and STORMWIN for winter precipitation). Using equations 28 through 30, flow duration, wetted area, and channel characteristics are represented in the INFILv3 model by scaling the saturated hydraulic conductivity that controls the total amount of infiltration into the root zone. For example, as the wetted area increases, the potential channel losses for streamflow increases because the $KSCHN^i$ term increases. As storm duration decreases, the potential channel losses for streamflow decreases because the effective streamflow intensity increases relative to the infiltration capacity of the channel. The RKS^i term is used to control infiltration capacity into the root zone only when soil thickness is less than or equal to 0.1 m, otherwise the infiltration capacity into the root zone is controlled by $KSCHNF^i$ (from eq. 30).

Simulation of Net Infiltration

Application of the INFILv3 model consists of running the daily simulation through a continuous multiyear period to develop relatively stable estimates of time-averaged net infiltration and potential recharge. Total net infiltration is the sum of the direct net infiltration simulated in the ETINFIL subroutine and the surface-water run-on net infiltration simulated in the SWINFIL subroutine. The average infiltrated surface-water run-on rate, which is the component of runoff that infiltrated back into the root zone during the surface-water flow routing, is also calculated from the daily results. The average annual runoff rate minus the average annual infiltrated run-on rate equals the average annual outflow rate. The average annual change in the root-zone water content indicates the difference between the water content at the beginning of the simulation period (after a specified start-up period) and the water content simulated for the last day of the simulation period. The mass-balance check for the simulated average-annual water balance terms is given by

$$MB^i = RAIN^i + MELT^i + IR^i - ET^i - \Delta WC^i - RO^i - NI^i = 0, \quad (31)$$

where

MB^i is the mass-balance result at grid location i,
$RAIN^i$ is rainfall at grid location i,
$MELT^i$ is snowmelt,
IR^i is infiltrated run-on,
ET^i is evapotranspiration,
ΔWC^i is the change in water content,
RO^i is runoff, and
NI^i is net infiltration.

The mass-balance result should be 0.

Drainage Basin Parameters

Topographic Parameters

Parameters developed from the DEM, referred to as topographic parameters (table 3 at back of report), are used in the potential evapotranspiration and the surface-water flow-routing subroutines. Topographic parameters include slope, aspect, streamflow routing parameters, the skyview parameter, and the 36 blocking ridge parameters. Slope and aspect, along with geographic location attributes for the UTM base grid, are calculated using standard GIS operations. FORTRAN routines are used to develop routing parameters (Hevesi, 2001), define the stream-channel network, and develop the skyview and blocking ridge parameters (Flint and Childs, 1987). The routing parameters consist of upstream and downstream cell identifiers. The upstream cell identifier (LOCID) is defined using a sorting routine GRDSORT01, where the DEM is sorted in descending order according to elevation. The downstream cell identifier (IROUT) is defined using a modified D-8 flow-routing algorithm, ROUTER03, where flow directions are based on the elevations of the eight grid cells adjacent to the grid cell the flow is being routed from. The modified D-8 routing algorithm was developed to route flow through depressions in the DEM by expanding the D-8 method to laterally scan 20 grid cell layers (rows and columns) beyond the cell being routed from when a depression is encountered. Most DEM depressions in the Death Valley region are unwanted artifacts of the 278.5 m grid spacing and the DEM resolution, which fails to represent all linear channel features. In addition to the flow routing parameters LOCID and IROUT, the input parameter UPCELLS, which indicates the total number of upstream cells for all model grid cells (used in equation 28), is also calculated by ROUTER03.

The 36 blocking ridge angles (RIDGE) are calculated using the SKYVIEW pre-processing routine, where SKYVIEW is a modified version of the original algorithm provided in Flint and Childs (1987). The blocking ridge angles define the inclination above horizontal for the higher topography surrounding a given grid cell, and are used to simulate the effects of shading caused by rugged topography, which can have a significant effect on potential evapotranspiration. The blocking ridge angles are calculated for thirty-six 10-degree horizontal arcs (starting with north as the 0-degrees azimuth direction), and the cumulative effect of all 36 blocking ridge angles is the reduction-in-skyview parameter (SKYVIEW). The SKYVIEW parameter is used to define the total incoming solar radiation component in the net-radiation simulation. Calculations in the SKYVIEW preprocessing routine are made using the DEM as input and a technique for approximating the 10-degree horizontal angles based on northing and easting grid cell distances.

Hydrogeologic Parameters

A generalized hydrogeologic map was used to define the spatial distribution of different rock types (fig. 11) over the model grid. The hydrogeologic map is a modified version (Claudia Faunt, U.S. Geological Survey, written commun., 2001) of the original hydrogeologic map of the Death Valley region compiled by Faunt and others (1997). The spatial distribution of the hydrogeologic units determines the values for saturated hydraulic conductivity and root-zone storage capacities assigned to the bottom root-zone layer (layer 6) for all model nodes. In the INFILv3 model, the hydraulic conductivities for the consolidated hydrogeologic units are defined using a set of high and low values, whereas the hydraulic conductivities for the unconsolidated hydrogeologic units are defined using a single value (the high and low values are equivalent). A low value is used to represent matrix permeability, and a high value is used to represent the saturated bulk permeability of the fractures and the matrix combined. For the INFILv3 models used in this study, the lower conductivities were assumed to be 2 orders of magnitude lower than the high conductivity values for model version A, and 3 orders of magnitude lower than the high conductivity values for model version B (table 4, at back of report). The higher conductivities were assigned initial values that generally were consistent with the values of saturated hydraulic conductivity provided in Bedinger and others (1989), D'Agnese and others (1997), and Faunt and others (1997).

Soil Parameters

A major limitation in the preliminary application of INFIL to the Death Valley region was the uncertainty in estimates of the soil input parameters required by the model (Hevesi and others, 2002). A primary objective in the application of INFILv3 to the Death Valley region was to use existing soil data provided by STATSGO to develop an improved set of soil input parameters. STATSGO, a state soils geographic database developed by the Soil Conservation Service (U.S. Department of Agriculture, 1994), provides a set of attributes for each MUID mapped for each state. In the STATSGO database, each MUID consists of one or more soil components, and each soil component consists of one or more soil layers. The database defines the percentage of an area covered by each soil component that constitutes a given MUID and the thickness of each layer associated with a given soil component. The layer-attribute data available in STATSGO includes layer depth, permeability, bulk density, and soil textural data for each of several layers associated with each soil component.

STATSGO GIS files for Nevada and California were compiled into a single continuous GIS coverage for the area of the Death Valley DEM. The combined STATSGO coverage provided 149 separate MUIDs for the area of the DEM (table 2, at back of report). Soil input parameters required by INFILv3 include soil thickness (SOILTHCK), soil porosity (SPOR), wilting-point water content (SWP), saturated hydraulic conductivity (SKS), and a drainage curve coefficient (SOILB) representing the relation between water content and unsaturated hydraulic conductivity. The soil parameters were estimated for each STATSGO MUID using a weighted averaging procedure applied to the layer-attribute data from STATSGO. The calculation uses an area-weighting method for averaging the data provided for soil components into a single average value for each MUID. The area-weighting calculation was combined with a layer-thickness averaging calculation to process the soil-texture data provided for each soil component layer. The calculation allowed for the development of average soil properties for each MUID.

The developed soil parameters obtained for each MUID using the STATSGO data processing procedure are given in table 2 (at back of report). The table includes the average soil texture attributes calculated for each MUID. The soil texture illustrates the relatively high percentage of coarse material (gravel, cobbles, and, in some cases, rock) along with a very low percentage of clays, which is characteristic of most of the soils in the Death Valley region. The soil texture data were used with equations from Campbell (1985) to estimate the drainage curve coefficient (SOILB), the wilting-point water content (SWP) for transpiration, and the saturated hydraulic conductivity (SKS). Soil porosity (SPOR) was estimated using bulk density data from STATSGO and an estimated value of 2.5 for particle density (fig. 19).

Soil thickness (SOILTHCK) was estimated using a combination of data from STATSGO and the hydrogeologic map from D'Agnese and others (1997). Average soil depth for the 149 STATSGO MUIDs was calculated using the area-weighting averaging of the average soil thickness for each soil component (fig. 20), which was calculated by summing the average layer thickness of each layer in the soil component. Soil thickness estimates are given in table 2 (at back of report). The location of thick soils (greater than 6 m) was defined by identifying all grid cells assigned to the valley fill or playa rock types from the hydrogeology map. The maximum depth of the root zone was set equal to 6 m for all locations with thick soils, and the root zone was assumed to be underlain by deep alluvium (unconsolidated rock types).

Vegetation and Root-Zone Parameters

The WESTVEG GAP regional map of vegetation types was used to develop estimates of vegetation cover and root density. Vegetation types were grouped into estimated vegetation associations that have similar root-zone depths and densities (fig. 21). For example, vegetation types such as subalpine pine, Ponderosa pine, White Fir, Juniper, and Pinyon pine were grouped into the coniferous forest association and with a maximum root-zone depth of 6 m in soils and 2.5 to 3 m in fractured bedrock (tables 5 and 6, at back of report). Vegetation cover estimated using the GAP vegetation type, varied from 0 to 90 percent (fig. 22). For example, Ponderosa pine was estimated to have an average vegetation cover of 60 percent whereas Juniper was estimated to have an average vegetation cover of 40 percent. The vegetation cover estimate, combined with the maximum root-zone depth estimate, was used to estimate root density as a function of depth (tables 5 and 6, at back of report). Vegetation associations with shallow root-zone depths, such as grasslands and desert shrubs, were assumed to include some plant types with deeper root depths (the mapped vegetation types represent the dominant vegetation types). Root densities of 5 to 10 percent were estimated for the deepest soil layer (3 to 6 m deep) and the consolidated rock layer (maximum depth of 0 to 3.0 m). The root densities for the deepest soil layer and the consolidated rock layer were used to account for the contributions of vapor flow and upward gradients to evapotranspiration, and are assumed to be higher than actual root densities.

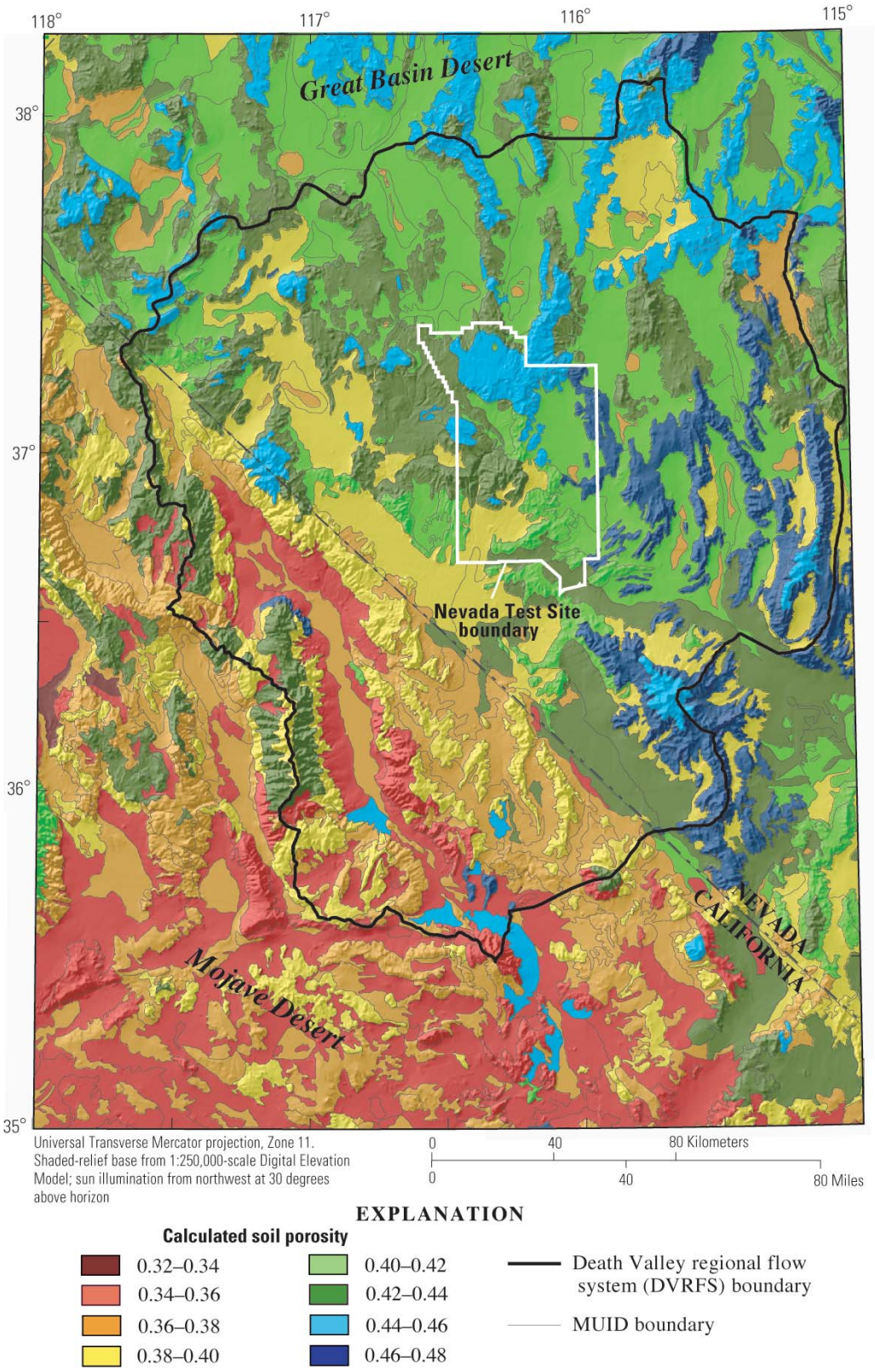

Figure 19. Soil porosity in the Death Valley region, Nevada and California.
Estimated using bulk density data from STATSGO (State Soil Geographic database).

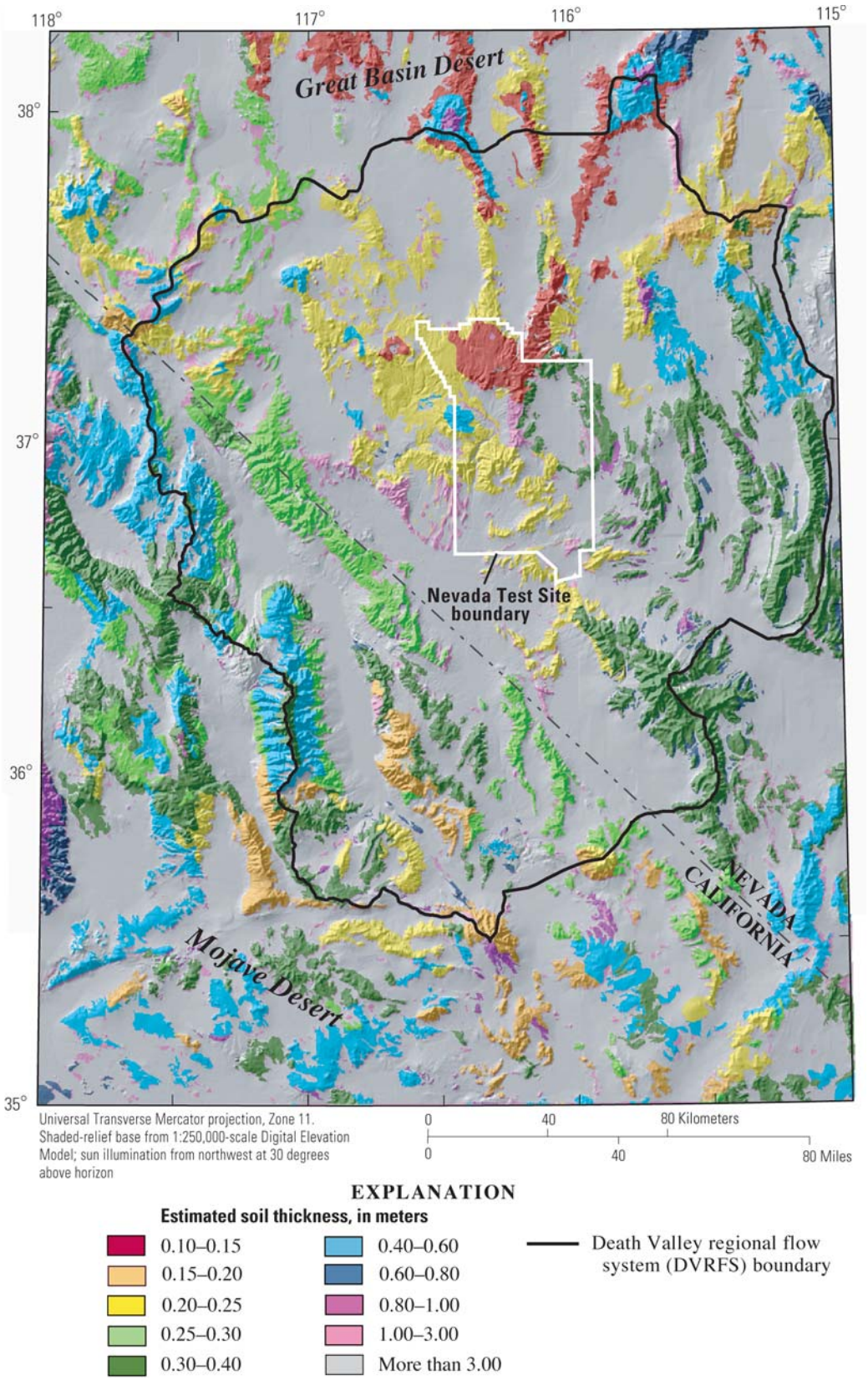

Figure 20. Soil thickness in the Death Valley region, Nevada and California.
Soil thickness estimated using a combination of data from STATSGO (State Soil Geographic database) and a hydrogeologic map from D'Agnese and others (1997).

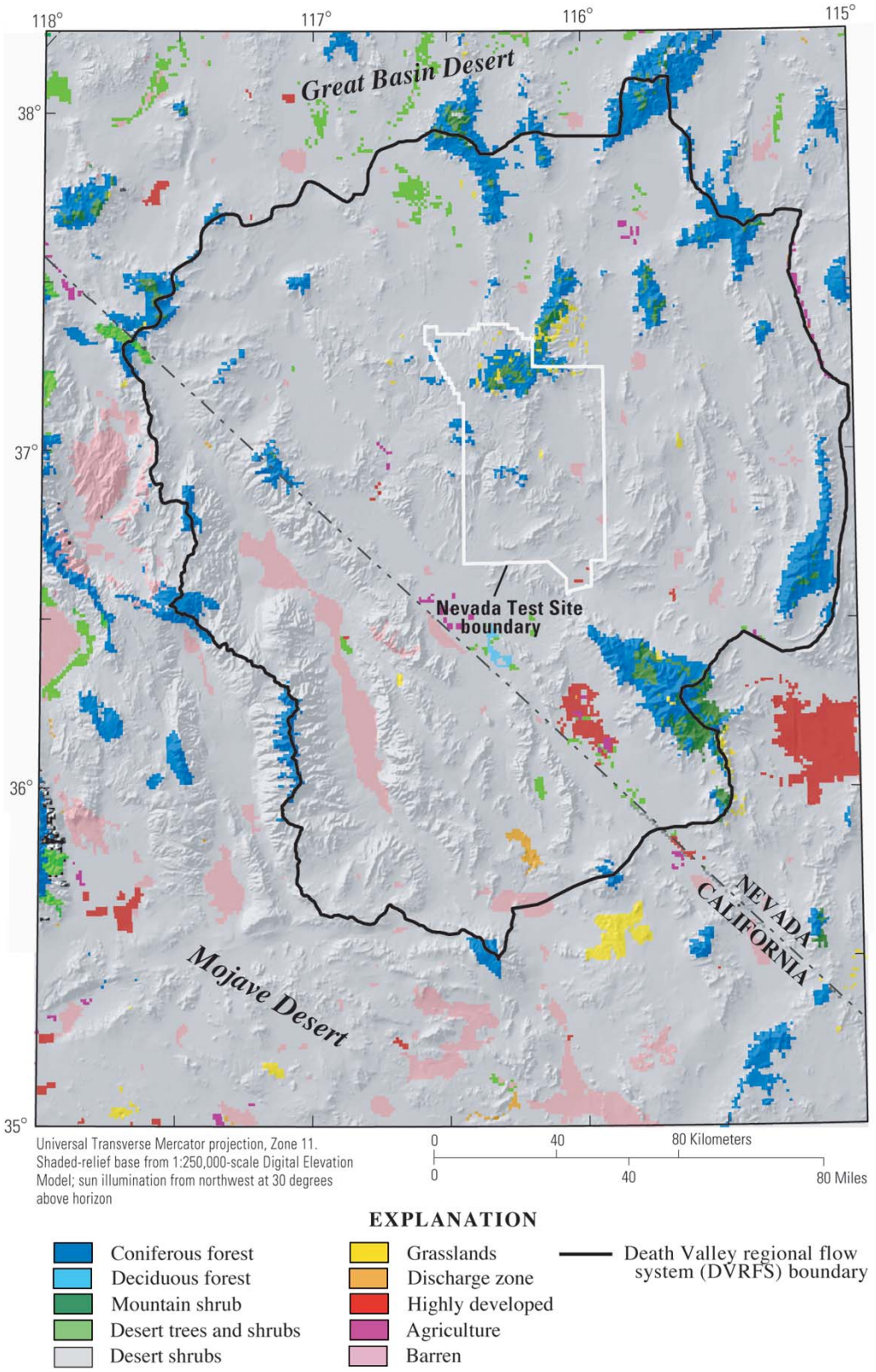

Figure 21. Estimated vegetation associations in the Death Valley region, Nevada and California.
Estimated from a western region vegetation map developed by the U.S. Geological Survey Gap Analysis Program (WESTVEG GAP).

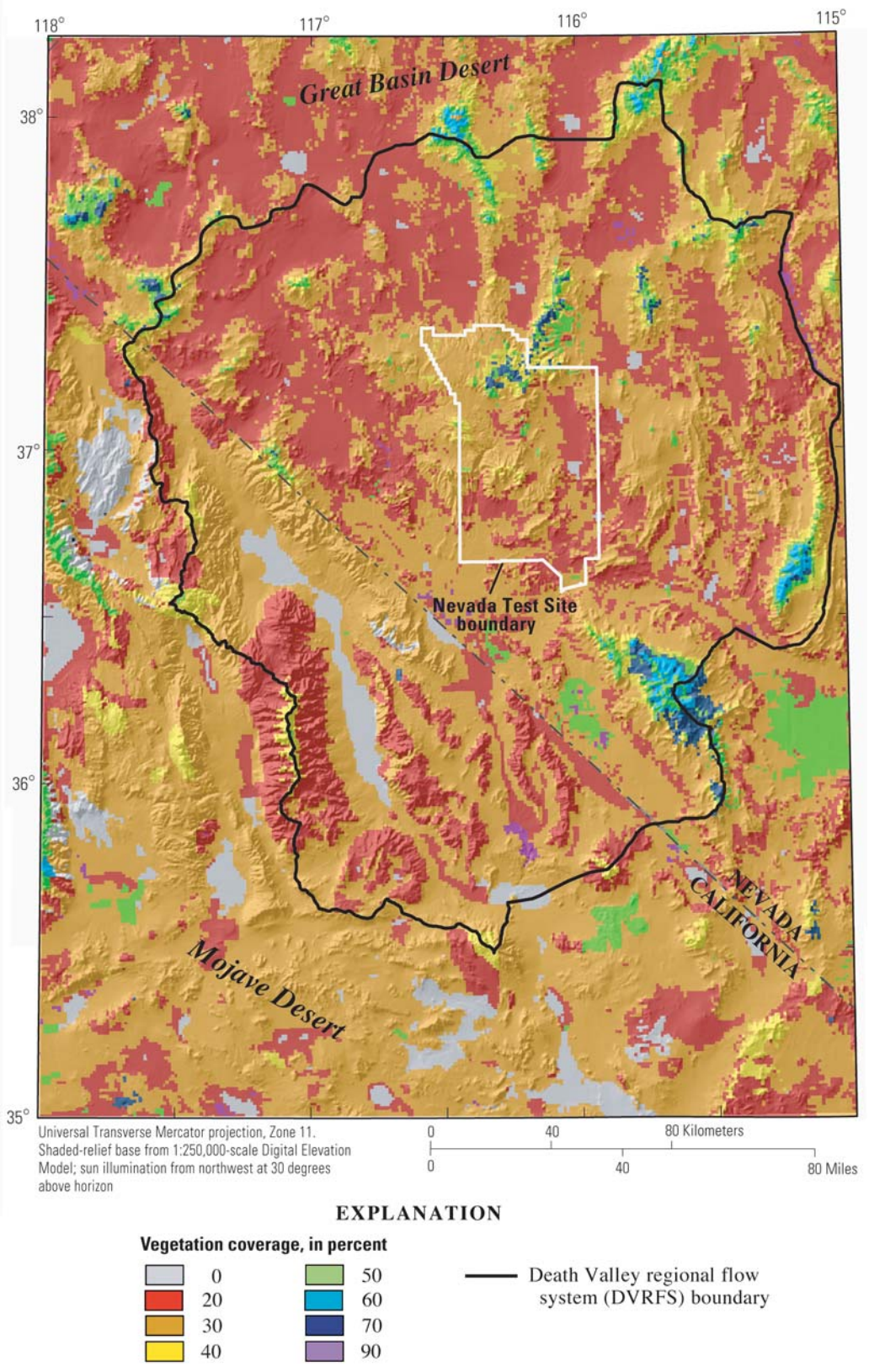

Figure 22. Estimated vegetation cover in the Death Valley region, Nevada and California.
Estimated from a western region vegetation map developed by the U.S. Geological Survey Gap Analysis Program (WESTVEG GAP).

Climate Parameters

Daily Precipitation and Air Temperature

Daily precipitation and air-temperature records for 1900 through 1999 were obtained from NOAA/NCDC and NOAA Air Resources Laboratory (NTS stations) for a regional network of 132 stations in the southern Nevada, Arizona, Utah and southeastern California (fig. 23). All stations used had 9 or more years of record for precipitation. Air temperature records were not available for all stations. Station locations and a summary of the climate records are given in table 7 (at back of report). The wettest record is for station 75 (Mount San Jacinto WS) at an elevation of 2,568 m above sea level, which has an average annual precipitation of 632 mm for 47 years of record. The driest record is for station 48 (Greenland Ranch in Death Valley) at an elevation of –51 m above sea level (the lowest elevation station), which has an average annual precipitation of 37 mm for 12 years of record. Station 101 (South Lake), located at 2,920 m above sea level along the eastern slope of the Sierra Nevada, has the highest elevation providing a total elevation range of 2,979 m for the network. The longest record in the network, 97 years, is for station 87 (Parker). A total of 30 stations have records of at least 50 years, including station 102 (St. George) with 70 years, station 86 (Palm Springs) with 70 years, and station 21 (Boulder City) with 66 years.

Monthly Regression Models for Climate

Average monthly precipitation and monthly average maximum and minimum daily air temperature were calculated from the daily climate records for each station. Using equations 2 and 3 and the calculated monthly averages (for precipitation and maximum and minimum daily air temperature) and station elevations, regression models were developed for the three monthly climate parameters: average monthly precipitation, monthly average maximum daily air temperature, and monthly- average minimum daily air temperature (table 8, at back of report). An example of the data and the regression results for April is given (fig. 24). The monthly air temperature data show the expected negative correlations with elevation, whereas the monthly precipitation data show fair to marginal positive correlations with elevation. Average monthly precipitation for August did not indicate a significant correlation with elevation; a regression model for August was not used in the spatial interpolation of daily precipitation data (August precipitation was estimated using the standard inverse-distance-squared algorithm). The 11 regression models for monthly precipitation and the 12 models for maximum daily air temperature used in the spatial interpolation of the daily climate data are given in figure 25.

Precipitation estimates obtained using the INFILv3 spatial interpolation subroutine and estimates from PRISM were evaluated by comparing the estimates with measured precipitation (fig. 26). The INFILv3 estimates provided an improved fit to the measured precipitation values, particularly for the higher elevation locations. The improved performance of the INFILv3 model probably is the result of the additional precipitation records used for INFILv3 (for example, the PRISM model does not incorporate the NTS stations). Although it was determined that the INFILv3 spatial interpolation model may provide better estimation accuracy relative to PRISM in terms of monthly and annual precipitation amounts in the Death Valley region, the accuracy of the daily precipitation estimates was not analyzed. The monthly regression models using the INFILv3 spatial interpolation are not necessarily optimized for estimation accuracy because possible outliers were not eliminated, single sample populations were assumed, and multiple regressions and data transformations were not explored in developing the monthly models.

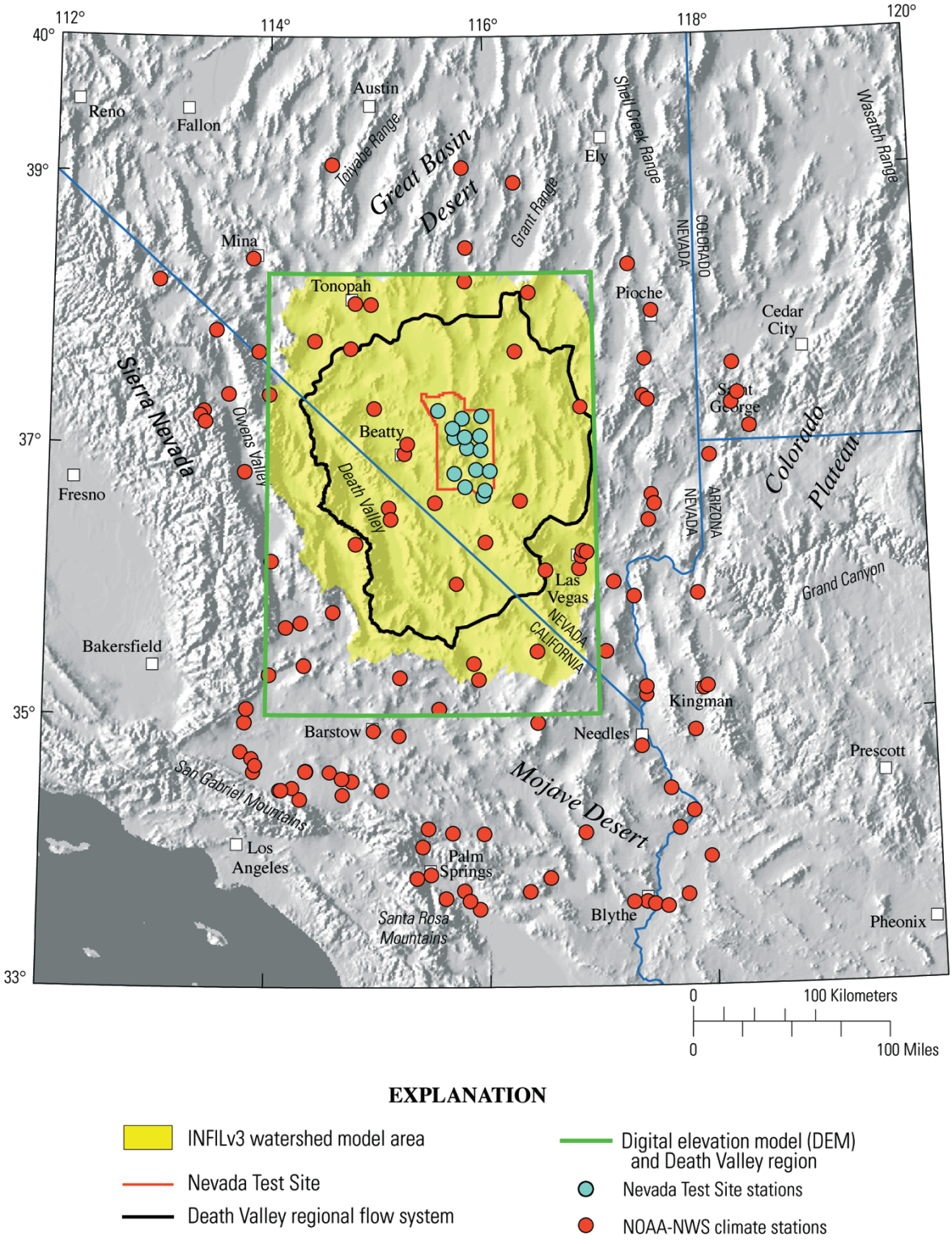

Figure 23. Location of daily climate stations in parts of Arizona, California, Nevada, and Utah.

NOAA NWS, National Oceanic and Atmospheric Administration Nation Weather Service

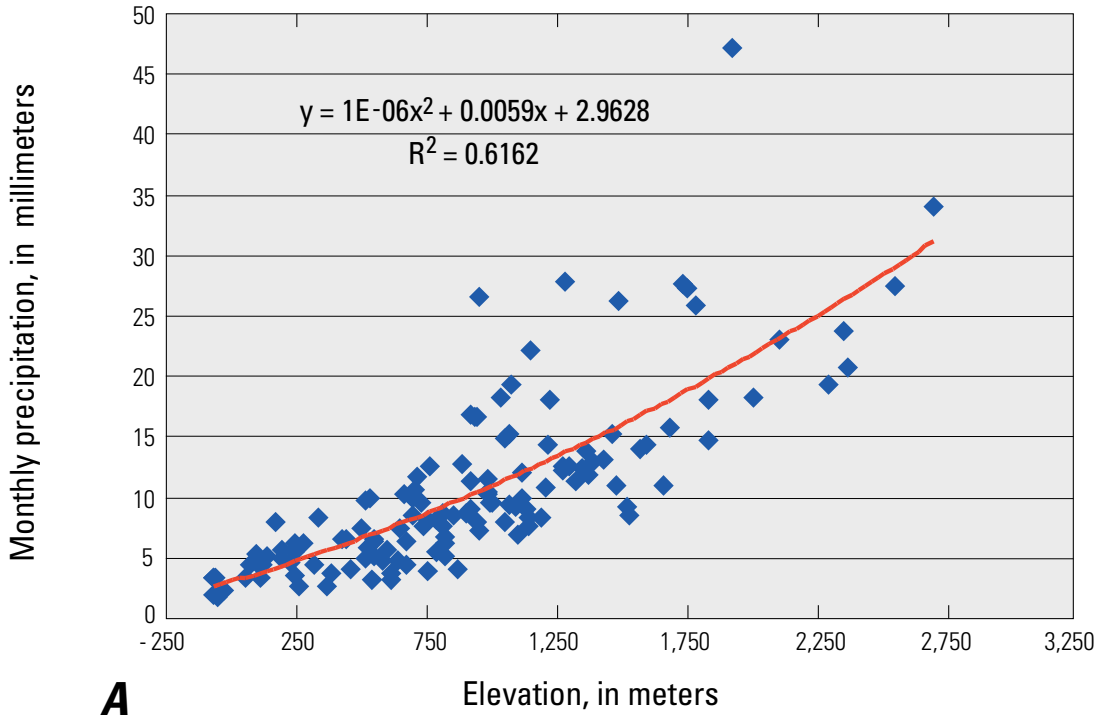

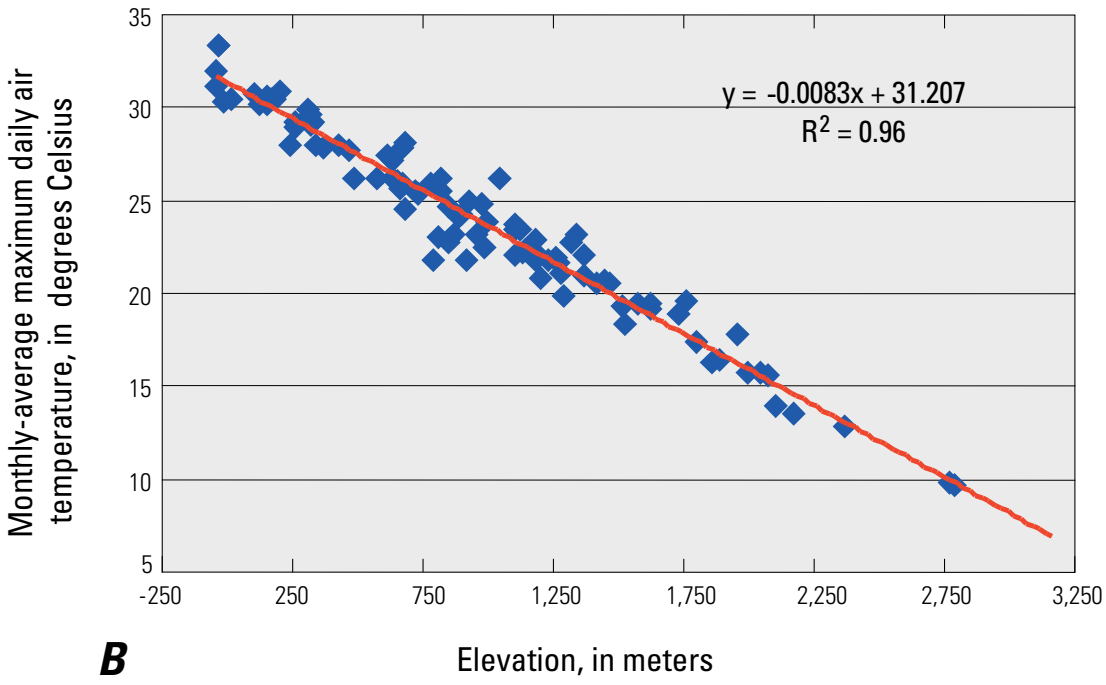

Figure 24. Fitted regression models defining precipitation and daily air temperature for April as functions of elevation in the Death Valley region, Nevada and California.

A. Average monthly precipitation. *B*. Monthly average maximum daily air temperature.

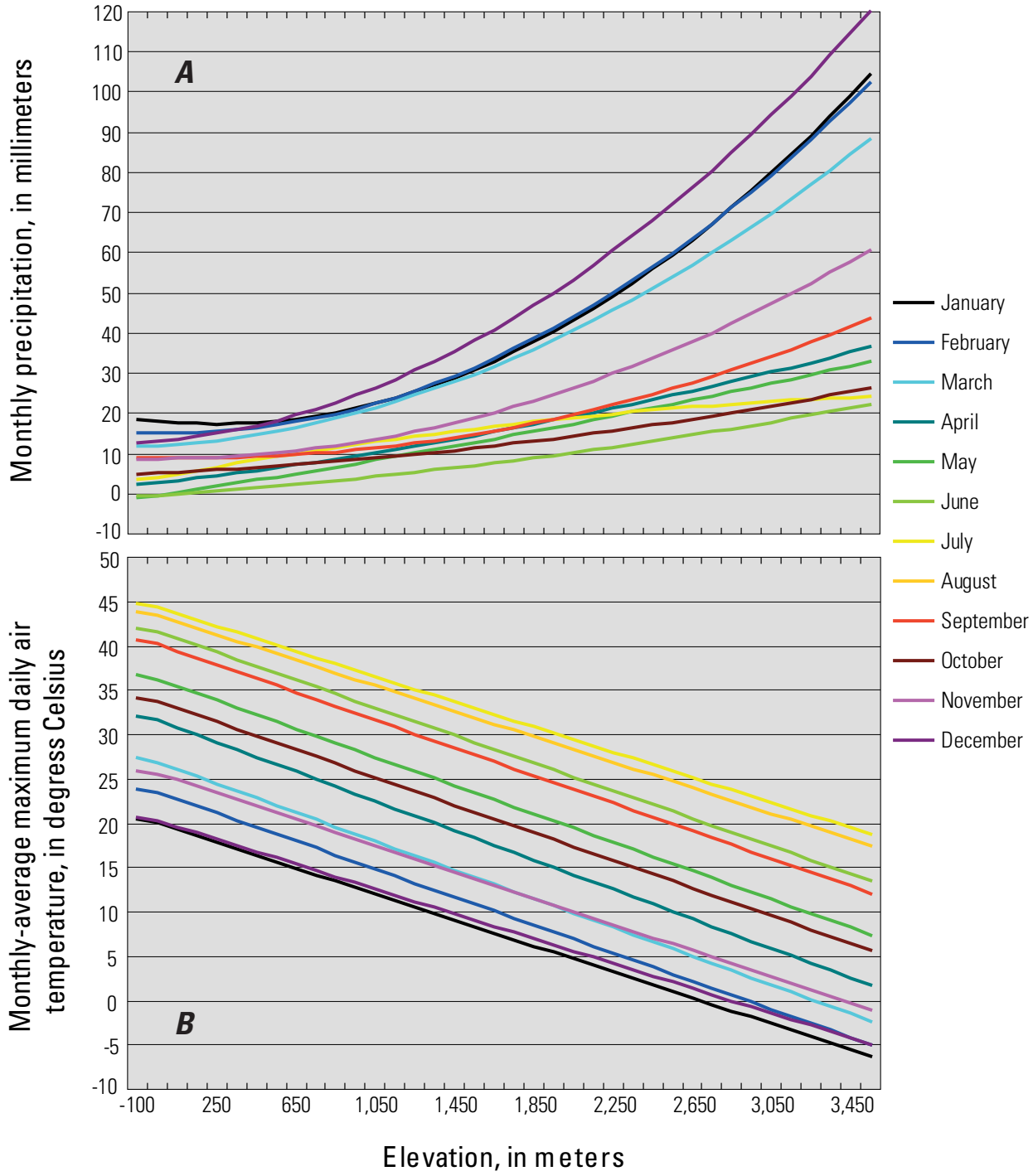

Figure 25. Fitted regression models defining monthly precipitation and daily air temperature as functions of elevation in the Death Valley region, Nevada and California.

A. Average monthly precipitation. *B*. Monthly average maximum daily air temperature.

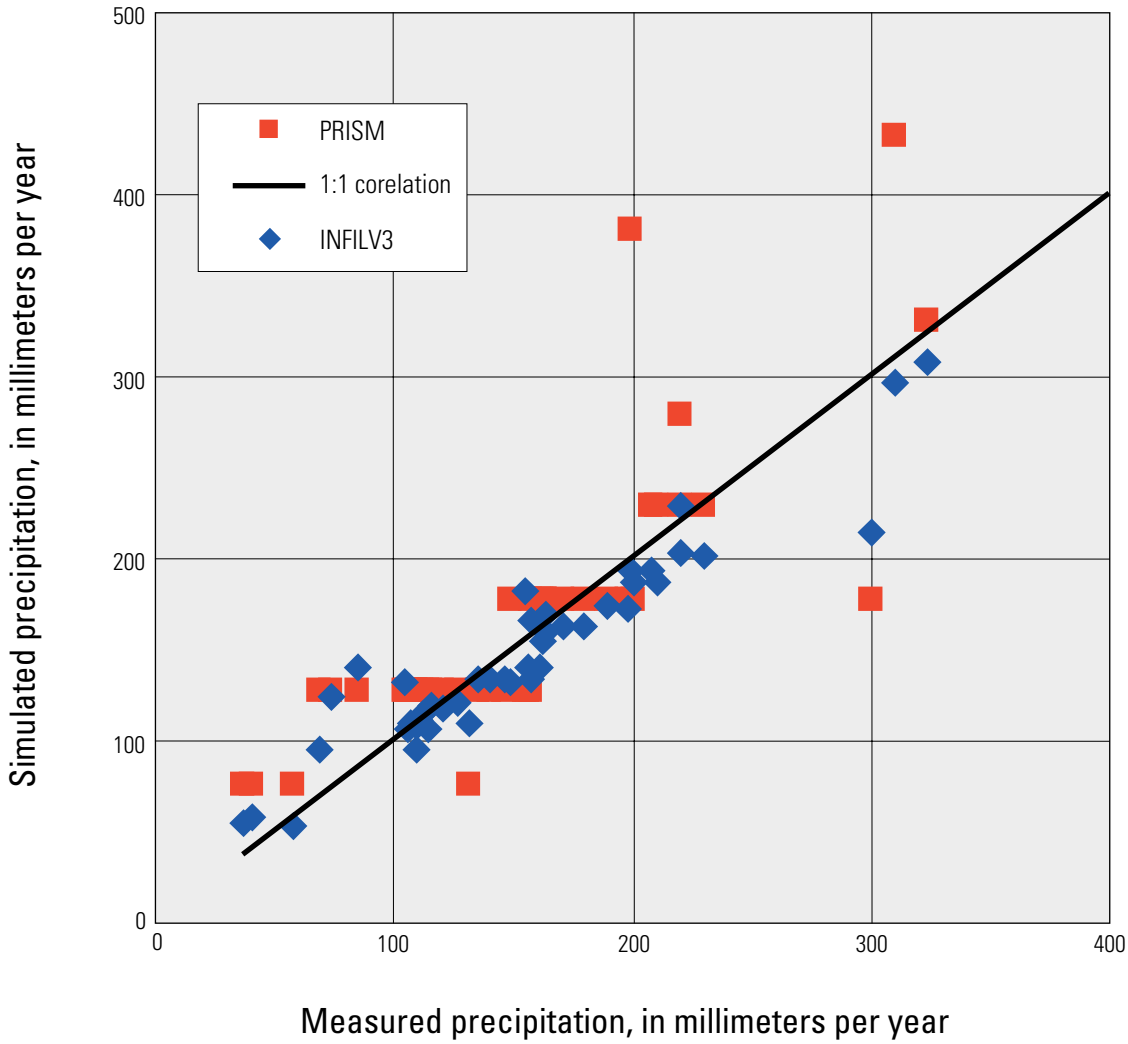

Figure 26. INFILv3 and PRISM estimates of average annual precipitation with measured precipitation for the Death Valley region, Nevada and California. INFILv3, net-infiltration watershed model; PRISM, parameter-elevation regressions on independent slopes model. (Modified from Daly and others, 1994)

Monthly Atmospheric Conditions

Parameters defining average monthly atmospheric conditions are required inputs for the simulation of net radiation in the SOLRAD routine. The required inputs are estimated monthly values of (1) OZONE, ozone layer thickness; (2) WP, precipitable atmospheric water; (3) BETA, mean atmospheric turbidity; (4) CSR, circumsolar radiation; and (5) PG, surface reflectivity. The model inputs used for this study are given in table 9 (at back of report). These parameter values are the same values used in previous applications of INFIL for Yucca Mountain and the Death Valley region (Flint and others, 2001a,b; Hevesi, 2002).

Assumptions and Model Limitations

A general assumption applied in this study was that the use of a distributed-parameter watershed model is appropriate for estimating net infiltration and potential recharge for the Death Valley region. Although the water-balance method used in the model required many simplifying assumptions concerning the physics of unsaturated

ground-water flow, this approach allowed for the use of a relatively dense model grid (1,300 rows and 983 columns). For the scale of the Death Valley region, the grid spacing of 278.5 m provided a detailed representation of the spatial distribution of the parameters controlling net infiltration, such as topography, soils, vegetation, and bedrock geology. Examples of previous applications of distributed-parameter water-balance models requiring similar assumptions for unsaturated flow are documented in Hatton (1998).

Additional assumptions applied to the water-balance calculations were that the process of vapor flow and the effects of temperature on water density are negligible relative to other processes and conditions affecting net infiltration. Water density was assumed constant so that the governing equations in the water-balance model used to calculate net infiltration could be applied as a volume balance rather than as a mass balance. In each grid cell of the model domain, water was assumed to drain vertically downward in soil and bedrock; lateral inflow or outflow between grid cells was assumed to be 0. Net infiltration was assumed to occur as gravity drainage under a unit gradient. The effect of capillary forces on unsaturated flow in the root zone was not included in the model.

The INFILv3 model simulates streamflow originating as runoff and as subsequent overland flow, but it does not simulate streamflow originating as baseflow from deep ground-water discharge or as through-flow from perched saturated zones that may exist at some locations, such as the alluvium-bedrock contact in washes. Thus, a major assumption applied in this method of calibration is that overland flow, generated in response to rainfall or snowmelt, is the primary component of streamflow measured in the Death Valley region. Simulation of daily streamflow in the INFILv3 model is based on a daily routing algorithm that assumes episodic streamflows with durations less than 24 hours. Simulated streamflow either discharges from the drainage basin or infiltrates into the root zone in the daily time step. Temporary perched ground-water systems, which may be an important component of streamflow and spring discharge in high mountain drainage basins, is not represented by the INFILv3 model. In addition, dispersive streamflow, which can be an important characteristic of streamflow and overland flow across alluvial fans and basins, is not directly represented in the surface-water flow-routing algorithm. All surface-water flow is simulated as convergent streamflow.

Sources of model uncertainty include input parameters such as the hydraulic conductivity of bedrock, soil thickness, soil hydrologic properties, parameters used to define stream-channel characteristics, and root density as a function of depth. Another source of model uncertainty is the limitations of the model in representing the spatial and temporal distribution of precipitation and air temperature using available climate records and in the assumptions of storm duration, snowmelt duration, and flow duration.

MODEL CALIBRATION AND EVALUATION

Model calibration was done using an iterative trial-and-error process of fitting simulated streamflow to measured streamflow obtained from available records in the Death Valley region. Model evaluation consisted of comparing basinwide net-infiltration estimates with previous estimates of basinwide recharge. Overall model calibration consisted of an integrated process of fitting simulated streamflow to measured streamflow, evaluating the selected model on the basis of basinwide recharge estimates, and then repeating the process of fitting simulated streamflow to measured streamflow using the constraints imposed by the model evaluation results. For model calibration, historical streamflow records were compiled for 31 stream-gaging sites in the Death Valley region (figs. 27 and 28; table 10 at back of report). Most of the gaging sites are within the boundary of the DVRFS. Several sites located well outside of the DVRFS, such as the Darwin Creek near Darwin (map code DC, gage 10250800) and the Caruthers Creek near Ivanpah, Calif. (map code CC, gage 10252550) sites, were also included in the model calibration to increase the number of records used and the range of soil, bedrock, and vegetation types represented in the calibration. For the model evaluation, estimates of basinwide net infiltration were developed and compared with previous estimates of basinwide recharge for 42 selected hydrographic areas and subareas in the Death Valley region (fig. 4; table 1), and with a previous estimate of total recharge for the DVRFS obtained by calibrating a ground-water flow model to measured water levels and estimated discharge (D'Agnese and others, 2002).

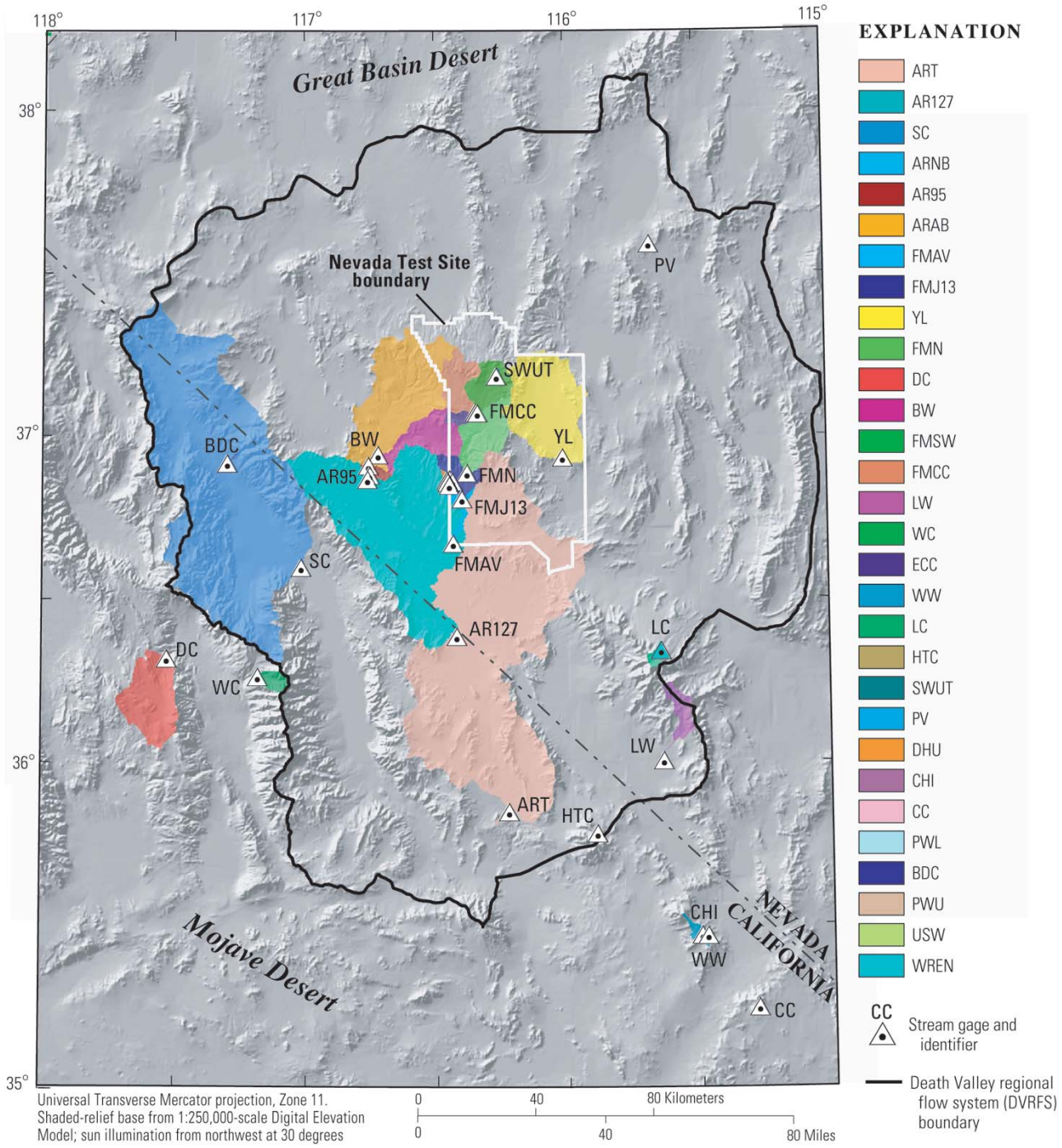

Figure 27. Location of stream gaging sites and drainage basin areas used in the calibration of the INFILv3 model of the Death Valley region, Nevada and California.

Only partial listing of gages is provided in legend.

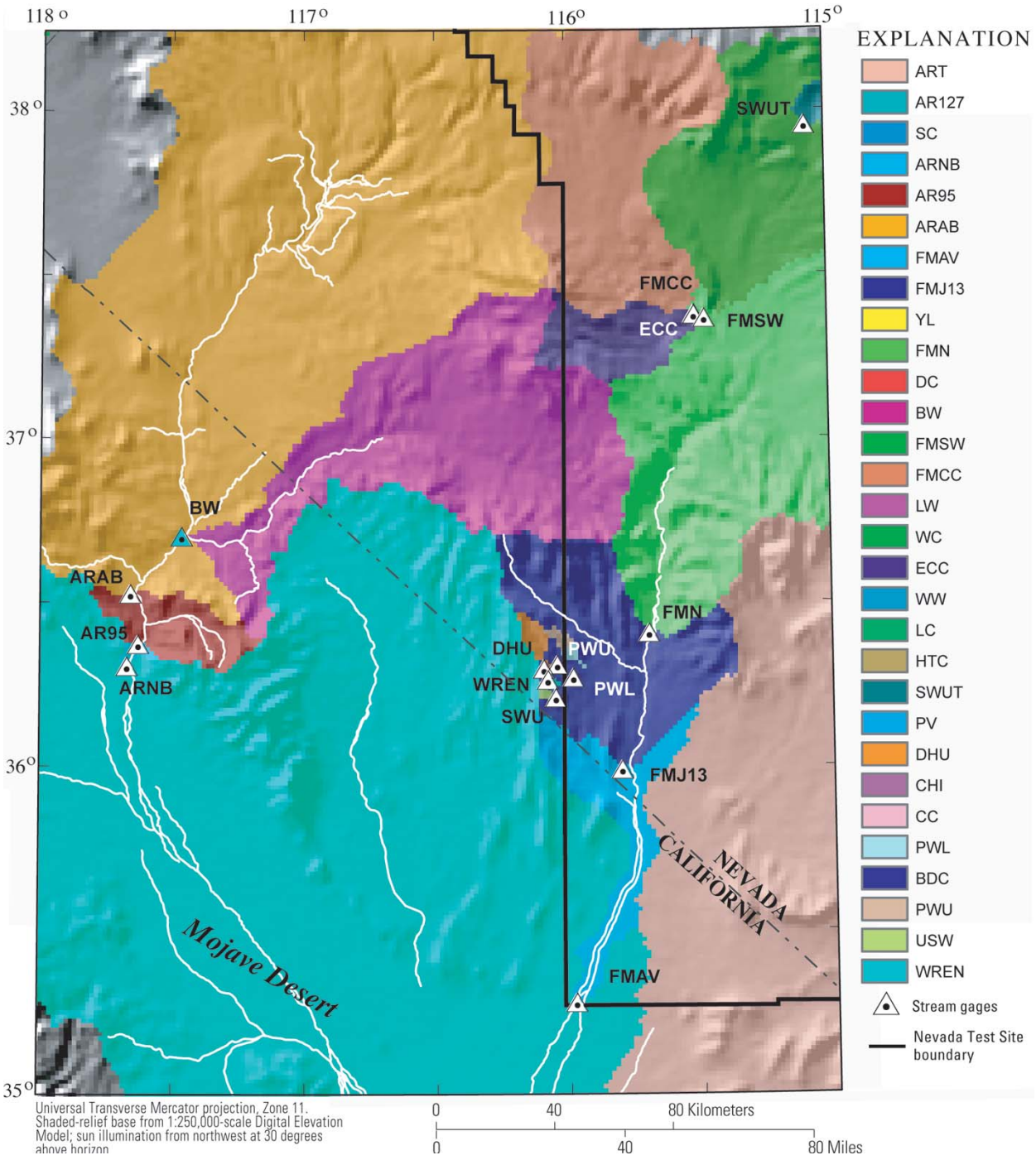

Figure 28. Location of stream gaging sites and drainage basin areas in the upper Amargosa River drainage basin and the area of the Nevada Test Site, Death Valley region, Nevada and California.

Both the calibration and the evaluation procedures consisted of calculating goodness-of-fit values for the average estimation error, the standardized mean square error, and the Pearson correlation coefficient, and then qualitatively comparing results for different sets of model input parameters. The criteria used for evaluating the results using the goodness-of-fit statistics were subjective and based on minimizing the values for the average estimation error and the standardized mean square error, while maximizing the value of the correlation coefficient. Quantitative statistical tests were not applied to accept or reject models. The average estimation error (AEE) was calculated using

$$\mathrm{AEE} = \left[\sum_{l=1}^{n} ((Z_l)^* - Z_l) \right] / n \quad , \tag{32}$$

where

Z_l^* is the estimated parameter,

Z_l is the measured parameter,

l is the index for 1 to n pairs of estimated and measured values, and

n is the number of measured values.

The average estimation error was used to indicate bias in estimated values, with higher absolute values indicating greater bias.

The standardized mean square error (SMSE) was calculated using

$$\mathrm{SMSE} = \left[\sum_{l=1}^{n} (Z_l^* - Z_l) \right]^2 / Z_{VAR} \quad , \tag{33}$$

(34)

where the parameters Z_l* and Z_l are the same as for the average estimation error, and Z_{VAR} is the sample variance for the measured parameter. The standardized mean square error provides an indication of the goodness-of-fit between the estimated and the measured values, with smaller values indicating better results. Values of less than 1 indicate that the estimates provide an improved fit to measured values relative to the sample mean.

The Pearson correlation coefficient (CC) is a measure of linear association (Maidment, 1993). The Pearson correlation coefficient was calculated using

$$\mathrm{CC} = \left[\sum_{l=1}^{n} (Z_l^* - \hat{Z}^*)(Z_l - \hat{Z}) \right] / [(Z_l^* - \hat{Z}^*)^2 (Z_l - \hat{Z})^2]^{0.5} \quad , \tag{35}$$

where

$\hat{Z}^*$ is the sample mean for the simulated parameter (total discharge, maximum discharge, or number of days with streamflow), and

$\hat{Z}$ is the sample mean for the measured parameter.

Positive values for CC indicate a positive correlation between estimated and measured pairs. Absolute values for CC range from 0.0 to 1.0, with a value of 0.0 indicating no correlation and a value of 1.0 indicating perfect correlation. For sample sizes greater than 30, a CC value of 0.50 or higher indicates a fair to strong positive correlation. The closer the value of CC to 1.0, the better the correlation between the simulated and measured parameter.

Model Fitting

Model parameters adjusted in the process of fitting models to streamflow measurements and estimates of basinwide recharge included bedrock hydraulic conductivity, root densities, winter and summer storm duration, wetted area for stream channels, and the hydraulic conductivity of soils for stream channels. Adjustments to these parameters were done manually using a trial-and-error process of model fitting. Additional parameters that were adjusted during model calibration and evaluation included coefficients affecting sublimation and snowmelt rates and factors affecting potential evapotranspiration, such as the time step in the solar radiation model (either a 1- or 2-hour time step was used). Simulation results were less sensitive to these parameters.

Differences in the input parameters used for four models selected to help illustrate results for model calibration and evaluation are given in table 11 at back of report. With the exception of the model differences, all other model inputs were identical for the four selected models. Calibration and evaluation results for these models illustrate model sensitivity to stream-channel characteristics, bedrock hydraulic conductivity, storm duration, and root densities. Model 2 is identical to model 1, except that streamflow was decoupled from the root-zone component, and all runoff was discharged to playas or to downstream drainage basins. The purpose of decoupling the streamflow component was to evaluate the effect of streamflow on basinwide net infiltration and to determine the maximum streamflow that could be simulated for a given set of model inputs.

Differences between model 1 and model 3 include a slight reduction in the sublimation rate parameter 1 SUBPAR1 (0.4 and 0.35, respectively), a decrease in storm duration (from 2 hours to 1 hour for summer storms and from 12 hours to 8 hours for winter storms, respectively), a decrease in bedrock saturated hydraulic conductivity (refer to table 4 for differences in bedrock properties rock parameters input file B, used in model 3, relative to bedrock properties input file A, used in model 1), a decrease in the stream-channel wetted area, and a decrease in stream-channel hydraulic conductivity for soils. The decrease in storm duration has the effect of increasing precipitation intensity because the total daily precipitation input is not changed. In general, the changes in parameters for model 3 results in an increased tendency to generate runoff, a decreased tendency for infiltration of surface water, and a decreased tendency for net infiltration.

The parameters used in model 4 are similar to those used for model 3, except storm duration is set back to 2 hours for summer storms and 12 hours for winter storms, the sublimation coefficient is set back to 0.4, and the solar radiation subroutine uses a 1-hour time step. An important difference in model 4 relative to all other models is the use of root-zone coefficients input file B (refer to tables 5 and 6 for differences between root-zone coefficients input files A and B), which uses higher root densities in the lower layers of the root zone.

Comparison of Simulated and Measured Streamflow

To simulate the daily streamflows used in model calibration, calibration watershed models were developed to represent the drainage basin upstream of each gaging site (figs. 27 and 28; table 10). The models were defined by the surface-water flow-routing parameters developed using the 278.5-meter DEM. The accuracy of these models in representing the true drainage basin upstream of a given gaging site was limited by the accuracy of the DEM in capturing the true stream-channel network. To assess that accuracy, the drainage basins of the calibration models were compared with the NWIS-documented drainage basins available for most of the gages (table 10). Except for the drainage basins of two gages, the basins in the model showed a good comparison with the NWIS-documented drainage basins. For example, the basin of the model upstream of the Amargosa River at Tecopa gaging site (map code ART, gage 10251300) is 8,185.9 km^2, which is in satisfactory agreement with the NWIS-documented basin area of 8,000 km^2. The two models with the greatest relative discrepancy between the drainage basin model area and the NWIS-documented drainage basin area were the Stockade Wash unnamed tributary site (map code SWUT, gage 10251248) and the Fortymile Wash above East Cat Canyon site (map code FMCC, gage 10251242). In general, the accuracy of the model in representing the drainage-basin characteristics upstream of a gaging site decreases with decreasing drainage-basin area.

The simulation periods used to develop the simulated daily streamflows included a model start-up period of at least 3 years prior to the beginning date of the streamflow record being used for calibration. The start-up period was needed to reduce the uncertainty in the estimated initial root-zone water contents required by the model. In all cases, the initial soil-water content was set to 20 percent greater than the wilting-point water content for all soil layers, and the initial rock-layer water content was set to 0.

Comparison of simulated and measured streamflow consisted of calculating a set of streamflow parameters from the simulated and recorded time series of daily streamflow, and then calculating the calibration statistics using the streamflow parameters. The parameters included (1) total discharge for the entire period of record, (2) the number of days having measured flow, (3) maximum daily discharge, (4) annual (water year) discharge, (5) monthly discharge, (6) streamflow discharge, and (7) daily discharge. Streamflow (or flow) discharge was defined in this study as any period of consecutive daily measured streamflow above an estimated baseflow. Flow discharge is the total measured or simulated discharge volume for the flow period. To calculate streamflow parameters considered representative of the overland flow component of the hydrograph, a uniform (constant) daily baseflow discharge volume was estimated for the daily discharge records having an identifiable baseflow component. To remove the baseflow component, daily discharge was set to 0 for all days in a given streamflow record having daily discharge volumes equal to or less than the estimated base flow. For all days having a discharge volume greater than the estimated base flow, the base flow volume was subtracted from the discharge volume.

Estimates of a uniform baseflow rate (or daily discharge volume) were based on a subjective visual analysis of hydrographs of daily mean discharge to identify the baseflow component of the hydrograph. For example, the hydrograph for the Salt Creek near Stovepipe Wells gaging site (map code SC, gage 10251100) indicates a well-defined seasonal baseflow component, with a mean total daily discharge ranging from about 100 to 3,000 m^3 (fig. 29). Superimposed on the baseflow component is an overland-flow component, with several larger flows having a total daily discharge in the range of 10,000 to 100,000 m^3. To use this record for model calibration, an estimated daily baseflow rate of 3,000 m^3/d was assumed. This baseflow component was subtracted from the streamflow record (negative results were set to 0), and only flows with a daily discharge greater than 3,000 m^3/d were considered in the comparison of simulated and measured streamflow.

The simulated daily streamflow for the Salt Creek gaging site obtained using model 1 is shown in figure 29. Although the general frequency of simulated streamflow seems reasonable compared with measured streamflow, the model overestimates daily streamflow by as much as 2 orders of magnitude for many of the streamflow estimates. For the Salt Creek drainage basin in the northern part of Death Valley, the spatial coverage of historical daily climate records is poor, and uncertainty in the estimated spatial distribution of daily climate inputs is high relative to that for other areas in the Death Valley region, such as the NTS. For this reason, application of a watershed model to predict daily streamflow at this gaging site was problematic. Although the Salt Creek streamflow record was more difficult to use owing to the baseflow component observed in the daily hydrograph, the primary model limitation for this drainage basin is the poor coverage of daily climate records. Other drainage basins for which calibration to daily streamflow records was difficult because of the sparsity in the coverage of climate stations include Darwin Creek near Darwin (map code DC, gage 10250800) and Wildrose Canyon near Wildrose station (map code WC, gage 10250600), both in Panamint Valley.

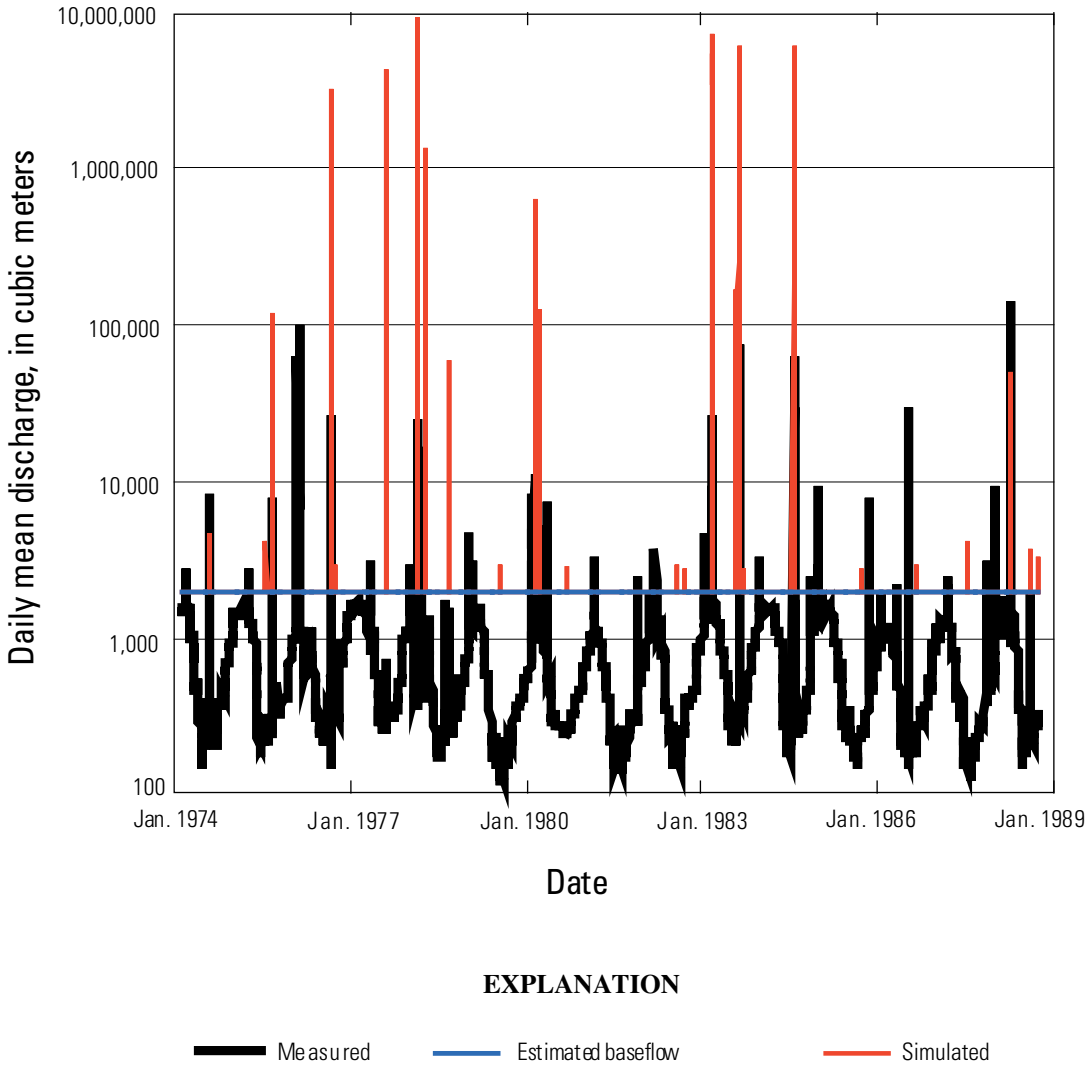

Figure 29. Measured and simulated daily discharge at the Salt Creek near Stovepipe Wells stream gage, Death Valley, California. Map code SC, gage 10251100.

Additional model limitations in simulating streamflow were taken into account when comparing simulated and measured streamflow. For the calibration basins representing the larger area drainage basins, such as the Salt Creek drainage basin upstream of the Salt Creek near Stovepipe Wells gaging site (map code SC, gage 10251100) in the northern part of Death Valley, and the Amargosa River drainage basin upstream from the Amargosa River at Tecopa gaging site (map code ART, gage 10251300), streamflow originating from storms in the headwater area of the drainage basins is likely to take longer than 24 hours to reach the gaging site. For smaller calibration basins representing the smaller area drainage basins, such as the drainage basins upstream of gages such as the Lee Canyon near Charleston Peak gage (map code LC, gage 09419610), the Wildrose Canyon near Wildrose Station gage (map code WC, gage 10250600), and Caruthers Creek near Ivanpah, Calif. gage (map code CC, gage 10252550), periods of streamflow may be attenuated by shallow perched systems that distribute precipitation from relatively short storms (1 to 2 days) as sustained streamflow over a much longer duration (30 to 60 days). For these drainage basins, differences in the timing and duration of simulated streamflow compared with measured streamflow was expected. For example, a 1- or 2-day difference in the timing between simulated and measured streamflow at gaging sites such as ART and SC was considered reasonable. Comparison of total storm discharge,

rather than daily discharge, was used to help account for model limitations in representing real-time streamflow as daily mean discharge for a diverse set of drainage systems. Although numerous streamflow records for peak flow are available for the Death Valley region, these data were not included in model calibration because of the limitations of the model in representing real-time peak streamflow using a simplified daily routing process.

Streamflow Frequency

Streamflow frequency was calculated as the number of days that had simulated or measured streamflow. Streamflow frequency was used to assess whether a given model overpredicted or underpredicted occurrences of streamflow. The results in table 12 (at back of report) indicate the total number of days that had measured streamflow for the 31 gages used in model calibration. Estimates of baseflow were subtracted from the records of 7 of the 31 gages (Amargosa River at Tecopa [map code ART, gage 10251300], Amargosa River at Highway 127 near California–Nevada line [map code AR127, gage 10251259], Salt Creek near Stovepipe Wells [map code SC, gage 10251100], Amargosa River at Beatty [map code ARAB, gage 10251217], Darwin Creek near Darwin [map code DC, gage 10250800], Lovell Wash near Blue Diamond [map code LW, gage 10251980], and Caruthers Creek near Ivanpah, Calif. [map code CC, gage 10252550]). For the adjusted records, Amargosa River at Tecopa [map code AR127, gage 10251259] and Caruthers Creek near Ivanpah, Calif. [map code CC, gage 10252550] have the highest frequency of daily streamflow.

Comparison of the calibration statistics for the four models indicates that models 1, 3, and 4 are similar in predicting streamflow and that model 3 provides slightly better results relative to models 1 and 4 based on lower AEE and SMSE values. All three models tend to underpredict streamflow frequency. This may indicate that, even though an attempt was made to remove the baseflow component from the streamflow records, baseflow may still be present in many of the records. In contrast, model 2, which does not allow runoff to infiltrate during routing, tends to overpredict streamflow frequency by an average of 107 days per gage.

Total Discharge

Simulated total discharge for 31 calibration drainage basins was compared with measured total discharge to assess whether a given model overpredicted or underpredicted the total discharge volume being routed downstream to playas (fig. 30; table 13, at back of report). Accuracy in predicting total discharge for multiyear periods was considered important for assessing the regional water balance and for increasing confidence in the estimates of long-term average basinwide net infiltration. A maximum total discharge of 71,543,027 m^3/d was recorded for the Amargosa River at Tecopa gage (map code ART, gage 10251300), and a minimum total discharge of 0 was recorded for the Wheaton Wash near Mountain Pass gage (map code WW, gage 10252330). Calibration statistics for total discharge indicate that model 4 provides the best match to measured streamflow in terms of SMSE, whereas model 1 provides the best match in terms of AEE. Model 1 tends to underpredict streamflow, as indicated by an AEE value of –470,271 m^3, and models 2, 3, and 4 tend to overpredict streamflow.

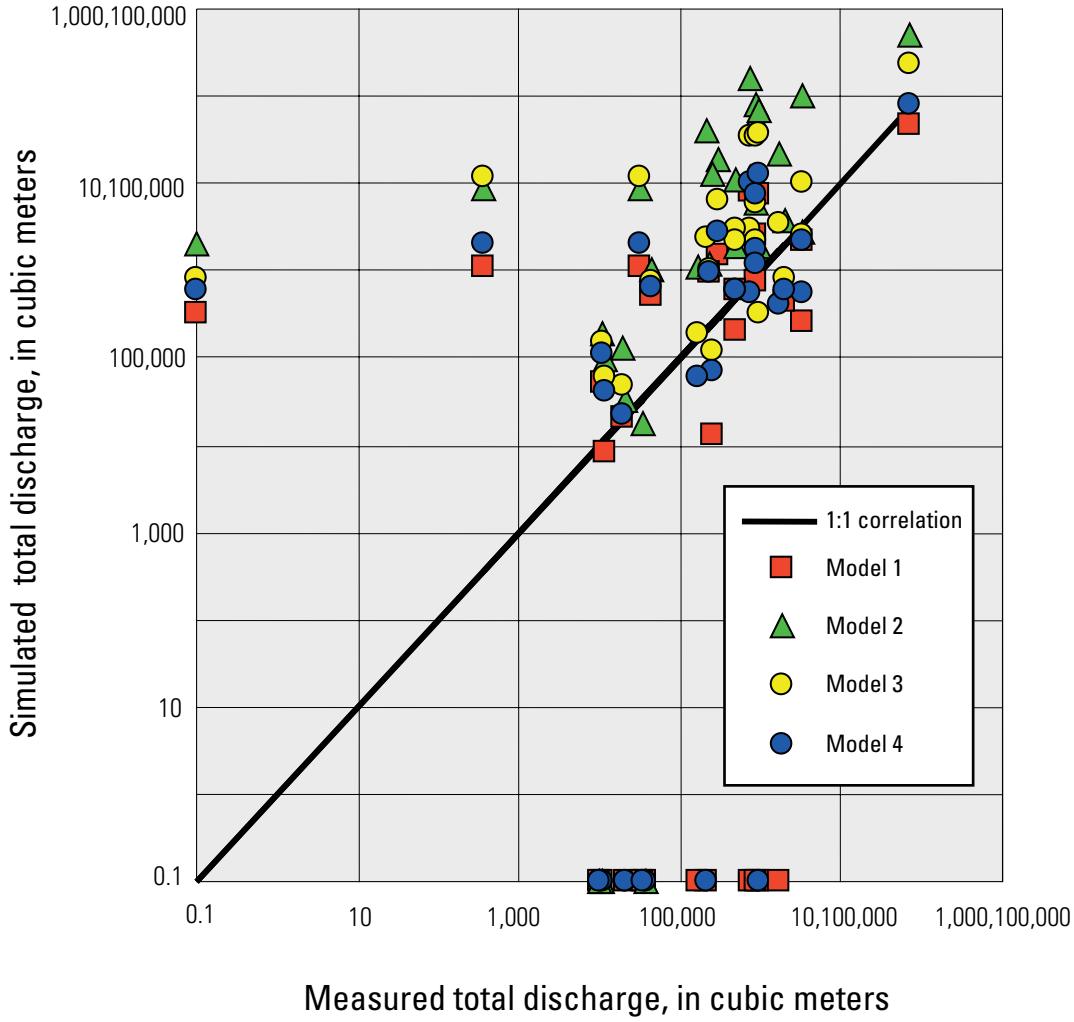

Figure 30. Measured and simulated total discharge at 31 stream gages using INFILv3 models 1–4 of the Death Valley region, Nevada and California.

Maximum and Average Daily Discharge

Comparison of simulated and measured maximum daily discharge provides a better indication of whether reasonable daily discharge magnitudes are being simulated, relative to comparisons made using total discharge. Maximum measured and simulated streamflow values are given in table 14 (at back of report). The maximum daily discharge values for measured streamflow range from 3,659,997 m^3 for the Amargosa River at Tecopa gage (map code ART, gage 10251300) and 1,338,326 m^3 for the Amargosa River at Highway 95 below Beatty gage (map code AR95, gage 10251218) to 196 m^3 for the Yucca Lake 02 2415 gage (map code YL (YL02), gage 10247902) and 6,361 m^3 for Wren Wash at Yucca Mountain (map code WREN, gage 102512536). The simulated streamflow shows a better comparison to the intermediate and smaller drainage basins in terms of predicting maximum daily streamflow, and models 1 and 4 perform better than models 2 and 3. For the larger drainage basins such as the Amargosa River at Tecopa gage drainage basin, the INFILv3 models overpredicted maximum daily discharge by at least 1 order of magnitude; model 1 provided the closest match with a simulated daily discharge of 37,389,028 m^3. The cause of this discrepancy partly can be attributed to limitations in simulating real-time streamflow (streamflows at the Amargosa River at Tecopa gage tend to have durations longer than 24 hours) because processes causing attenuation of flood waves moving downstream along the Amargosa River drainage basin are not represented by the

INFILv3 model. Overall, model 1 provides the lowest AEE and SMSE values relative to the other models. All models show a good positive correlation of 0.74 or 0.75 with measured maximum daily streamflow, following the expected trend of increasing discharge magnitudes with increasing drainage area.

Average daily storm discharge, calculated as total measured or total simulated discharge divided by the total number of days with measured or simulated discharge, also follows an expected trend of increasing average daily discharge with increasing drainage basin area, although the simulated discharge shows a stronger correlation to drainage basin area than measured discharge (fig. 31). All models show a somewhat better comparison to measured average daily storm discharge for the smaller drainage basins. The larger drainage basins seem to indicate a higher variability in average storm discharge. For example, the INFILv3 model representing the drainage basin for the Yucca Lake 02 2415 gage has a relatively large area, (approximately 788 km (table 10, at back of report), but the second lowest average storm discharge, 122 m^3/d. Complicating this analysis is the effect of record length; the Yucca Lake gages have the shortest records and thus may not provide a representative sample of streamflow for these drainage basins.

Annual Discharge

Comparison of simulated annual discharge for models 1 and 2 with measured annual discharge showed that both models predict streamflow when no streamflow was measured and fail to predict streamflow when streamflow was measured (fig. 32). Adjusting the model coefficients to decrease or increase the simulated streamflows did not necessarily improve model fit, as indicated by the comparison of simulated values for models 1 and 2 (model 1 tends to underpredict streamflow, whereas model 2 strongly overpredicts streamflow). Analysis of the simulated and measured annual discharge for the Salt Creek near Stovepipe Wells and the Amargosa River at Tecopa gaging sites indicates better performance by model 1 in predicting annual streamflow and in providing a general match between simulated and measured values for the Salt Creek near Stovepipe Wells record (fig. 33). Although model 2 overpredicted discharge for many of the water years at both stream gages, it predicted the occurrence of streamflow better than model 1 at the Amargosa River at Tecopa gage. A primary limitation of the INFILv3 models for simulating the streamflow record at both stream-gage sites is the uncertainty in channel characteristics. Additional limitations include a variable baseflow component in the daily hydrograph and limited coverage in daily climate data for the remote mountain ranges along the western side of the basin (the eastern side of Death Valley).

Monthly Discharge

The results of the calibration statistics indicate that model 1 provides the best fit between measured and simulated monthly streamflows on the basis of lower AEE and SMSE values relative to those for the other models (table 14 at back of report). The correlation between measured and simulated streamflow is stronger for models 2 and 3 compared with that for models 1 and 4 (table 15, at back of report). Model 2 had the highest correlation coefficient of 0.71, whereas model 1 had a marginal correlation of 0.50. Model 3 had the best results in terms of predicting streamflow frequency; it simulated an average of 0.24 days per month of streamflow compared with the measured average of 0.61 days per month. The scatter plot of simulated monthly discharge using INFILv3 model 1 in relation to measured monthly discharge indicates a fair correlation for those months during which streamflow was both measured and simulated (fig. 34). The comparison of monthly discharge with measured discharge showed that for many of the months, the model predicted streamflow when no streamflow was measured and failed to predict streamflow when streamflow was measured. Improving model performance to successfully predict the occurrence (or absence) of streamflow for all months at all gaging sites will likely require improvements in the accuracy of the daily climate inputs.

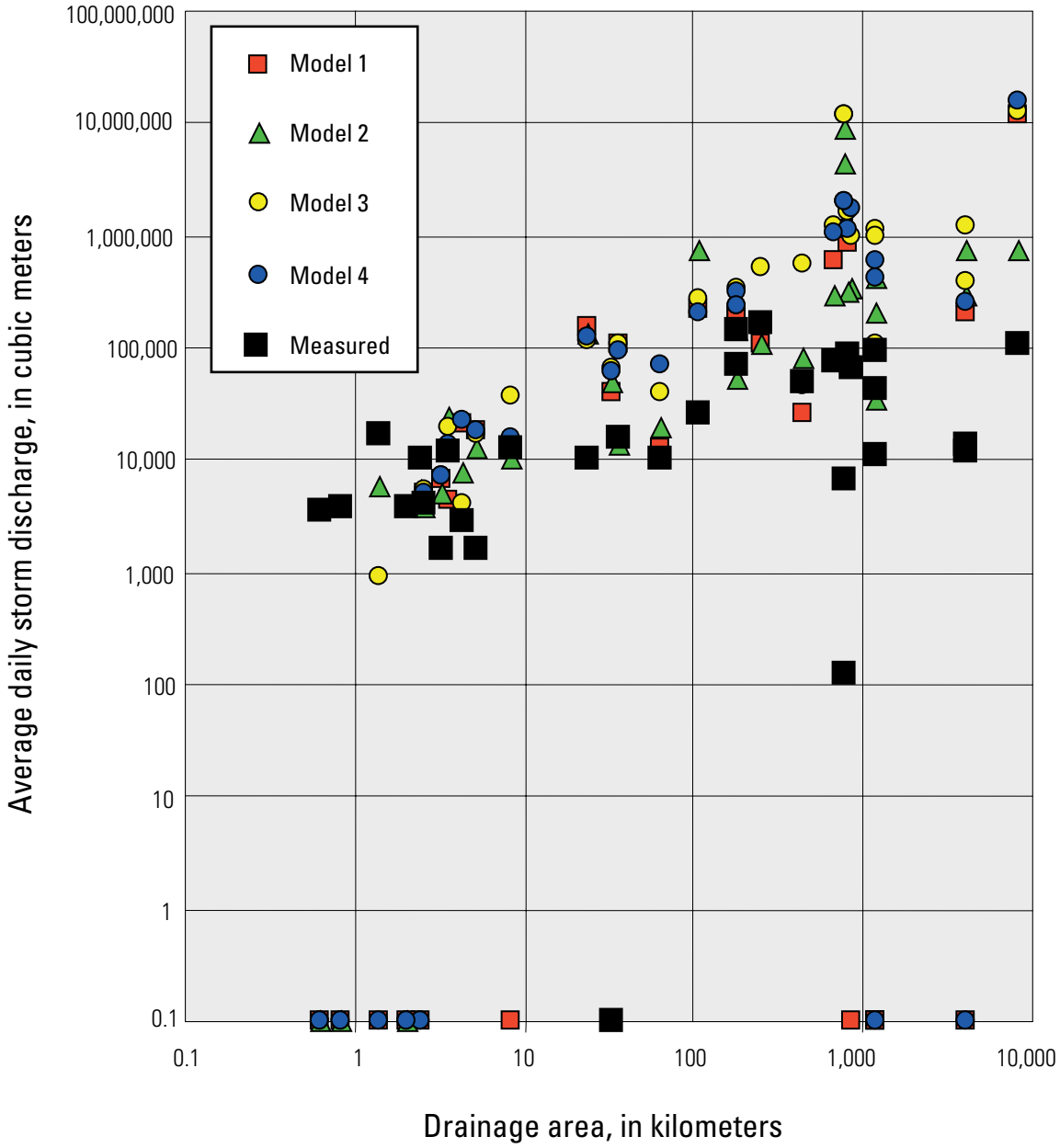

Figure 31. Measured and simulated average daily storm discharge in relation to drainage basin area for the Death Valley region, Nevada and California.

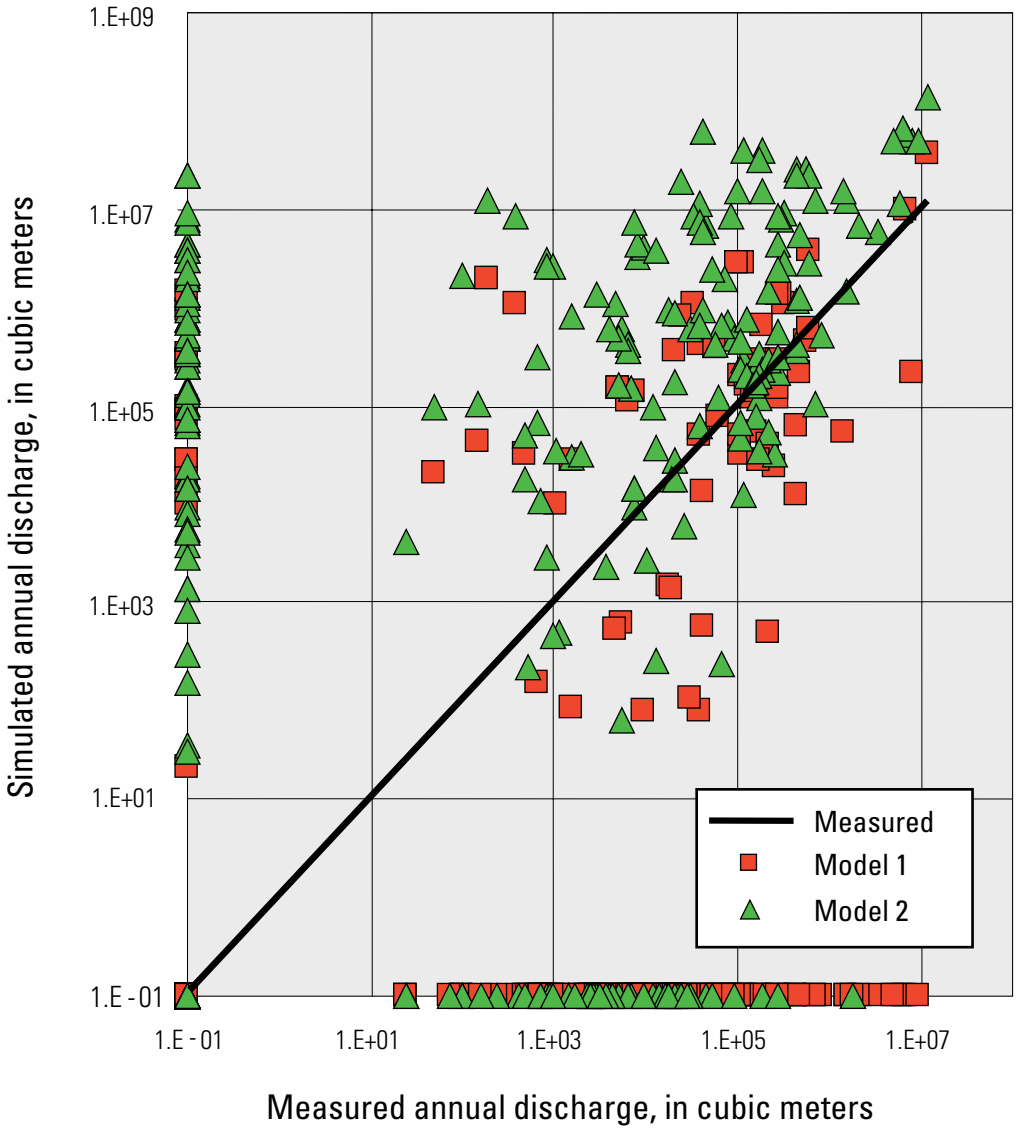

Figure 32. Measured and simulated annual discharge for INFILv3 models 1 and 2 for the Death Valley region, Nevada and California.

Flow Discharge

Flow discharge was defined as the accumulated discharge volume for a continuous sequence of measured and simulated daily discharge. The objective of comparing total flow discharge with measured streamflow was to help mitigate some of the difficulties encountered in the direct comparison of daily discharge, such as model limitations in representing real-time streamflow for larger drainages and in the attenuation of flood waves.

Out of a total of 108,229 days of record, 2,102 days had measured streamflow, which is approximately three times greater than the number of days with simulated streamflow (ranging from 624 days for model 1 to 847 days for model 3) using INFILv3 models that allow infiltration of run-on into the root zone (table 16, at back of report). As indicated by results for model 2, when run-on is not allowed to infiltrate into the root zone, the number of days having simulated streamflow increases to 5,508. This shows fairly high model sensitivity to parameters controlling infiltration along stream channels, such as the adjusted hydraulic conductivity that represents soils in channels and the wetted area factor that represents the area of each grid cell covered by the run-on volume.

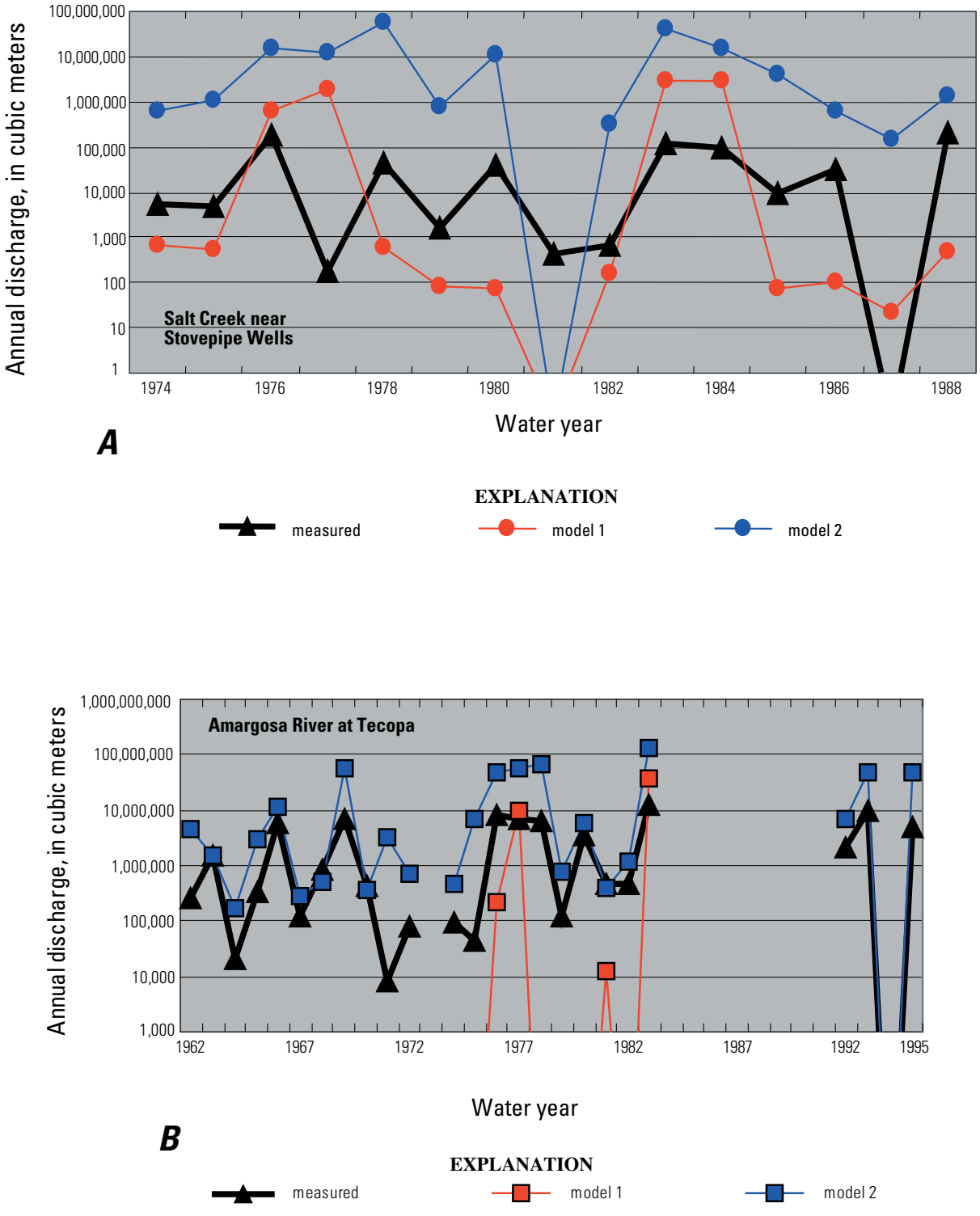

Figure 33. Measured and simulated annual discharge at selected stream gages in Death Valley, California. *A*, Salt Creek near Stovepipe Wells. *B*, Amargosa River at Tecopa.

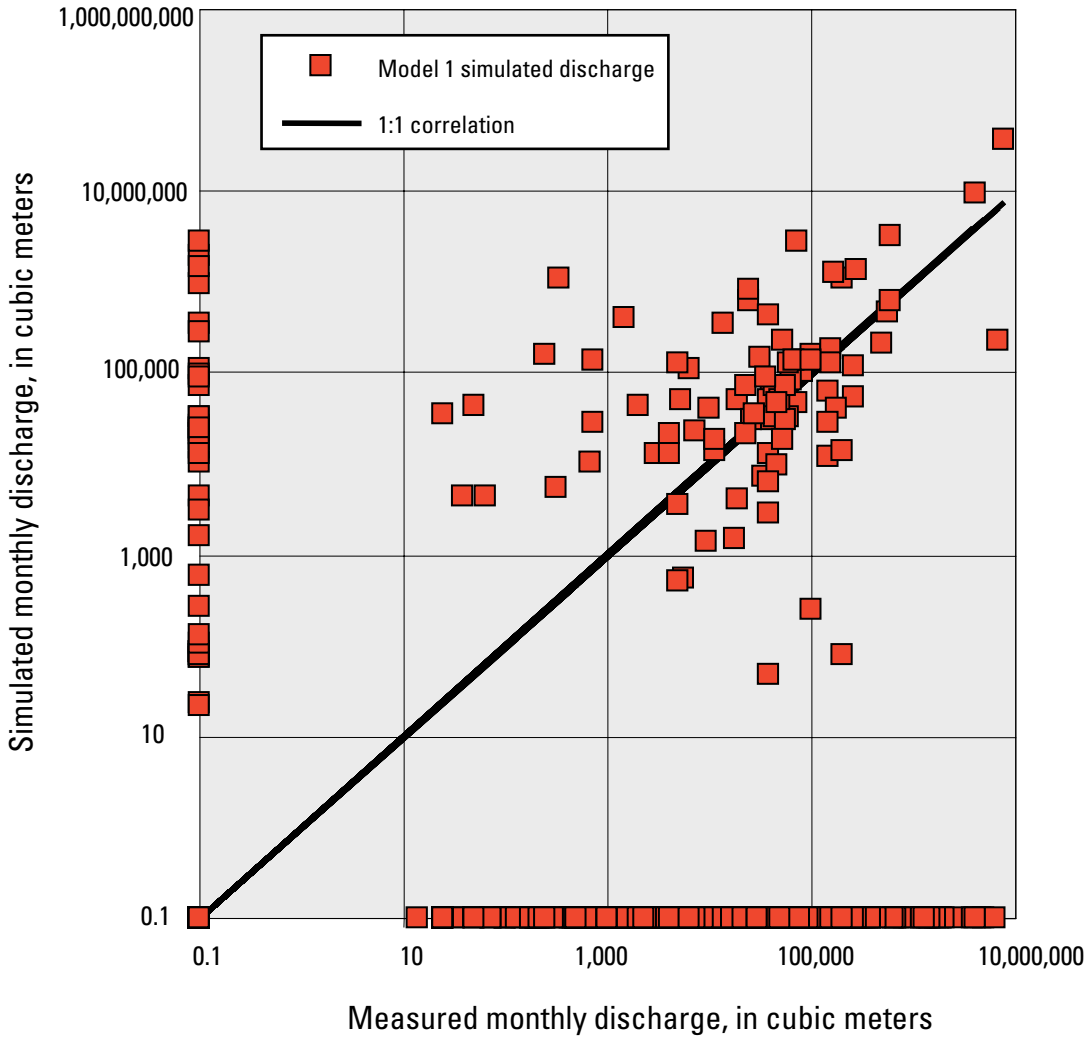

Figure 34. Monthly discharge simulated using INFILv3 model 1 and measured monthly discharge for the Death Valley region, Nevada and California.

Calibration based on total flow discharge showed many of the same limitations encountered when comparing simulated and measured monthly and daily streamflow. Calibration results for many of the smaller drainage basins, such as Lee Canyon near Mount Charleston (map code LC, gage 09419610), Wildrose Canyon near Wildrose Station (map code WC, gage 10250600), and Lovell Wash near Blue Diamond (map code LW, gage 10251980), were strongly dependent on the accuracy of the daily climate data in representing storms. In addition, model calibrations were more difficult for the smaller drainage basins in the more remote mountainous terrain because of the prevalence of streamflow from localized high-intensity summer storms. For many of these smaller drainage basins, streamflow from summer thunderstorms was the dominant component of the hydrograph record; therefore, a successful calibration was dependent on assumptions concerning precipitation intensity, as well as the limitations in the coverage and density of the daily climate records. Higher resolution precipitation data (such as hourly or 15-minute precipitation totals) are needed for a more successful calibration.

Because of the numerous limitations affecting model calibration based on streamflow records, the selection of a set of model parameters defining a calibrated model was based on a combination of qualitative and quantitative considerations. A primary consideration in the selection of an appropriate set of model parameters for estimating winter and summer storm durations, stream-channel characteristics, root-zone depths and densities, and bedrock properties was that the selected model did not consistently overestimate or underestimate the total discharge volume. The greatest general difficulty encountered in developing a simultaneous calibration to all 31 streamflow records using a consistent set of model parameters was that streamflow often was simulated during periods when no streamflow was measure or that no streamflow was simulated during periods when streamflow was measured.

Calibration results indicated that INFILv3 model 1 provides the best overall fit to the measured streamflow in the Death Valley region, and model 2 provides the poorest overall fit. Model 4 also provided a satisfactory calibration result and, in some cases, indicates improved model performance relative to model 1. For example, model 4 provides a reasonable fit (within a factor of 3) to measured total discharge for several gaging sites in the upper Amargosa drainage basin (AR95, ARAB, and FMAV), and a good fit for the ART gaging site in the lower Amargosa drainage basin (simulated total discharge of 78,525,258 m^3/d compared with a measured total discharge of 71,543,027 m^3/d) (table 13 at back of report). Model 2, which does not allow surface water run-on to infiltrate into soil or bedrock during the routing process, overestimates discharge by approximately 1 order of magnitude. In some cases, however, streamflow frequency is better predicted using model 2 relative to the other models. Model 3, which tends to overpredict streamflow by a factor of 3 to 5, also tends to provide improved predictions of the frequency and occurrence of streamflow relative to the predictions of models 1 and 4. For the purpose of estimating net infiltration and potential recharge and for simulating basinwide water balances, model performance based on predicting streamflow magnitude was considered more important than model performance based on streamflow frequency and occurrence.

Simulation of Net Infiltration, 1950–99

The INFILv3 model was used to simulate daily net infiltration for water years 1950 to 1999. The start date for the simulation was specified as October 1, 1947, using an assumed initial water content for soil layers 20 percent greater than the wilting-point water content for each soil type. The initial root-zone water content for the bedrock layer was set to 0. Results for water years 1947–49 were not included in the calculation of the average annual rates for the components of the water balance. The 3-year start-up period was assumed adequate for minimizing the effect of the assumed initial conditions on the calculated 50-year averages.

Watershed Model Domains for the Death Valley Region

Model simulations were done using a set of 61 separate INFILv3 model domains, or drainage basin modeling areas, referred to in this section as watershed model domains (fig. 35; table 17, at back of report). The separate watershed model domains are defined by the simulated surface-water drainage-basin network and generally coincide with the surface-water flow divides represented by the boundaries of the hydrographic areas (fig. 4; table 1). Most of the 61 watershed model domains represent closed systems in terms of surface-water flow. Surface-water outflow from these closed systems is contained within the model domain area and represents discharge to playas at the lowest elevation grid cell. Outflow is assumed to contribute to temporary playa lakes, and all water to these lakes is assumed to evaporate. For some model domains, such as Beatty Wash 1 (map no. 6) and Las Vegas Valley 1 (map no. 31), outflow is distributed to the downstream model domain. These smaller domains (Beatty Wash 1 consists of only 119 grid cells, and Las Vegas Valley 1 consists of only 8 grid cells) define subbasins and grid cell clusters that were isolated sections of larger drainage-basin systems and were not initially included with the larger system because of limitations in the automated procedure used to extract watershed domains from the numerically generated drainage network. For several larger closed basins, such as Death Valley, Panamint Valley, and Pahrump Valley, the multiple watershed model domains discharge into a single playa. The composite area of the 61 watershed model domains defines the INFILv3 model area for the Death Valley region and extends beyond the area of the DVRFS.

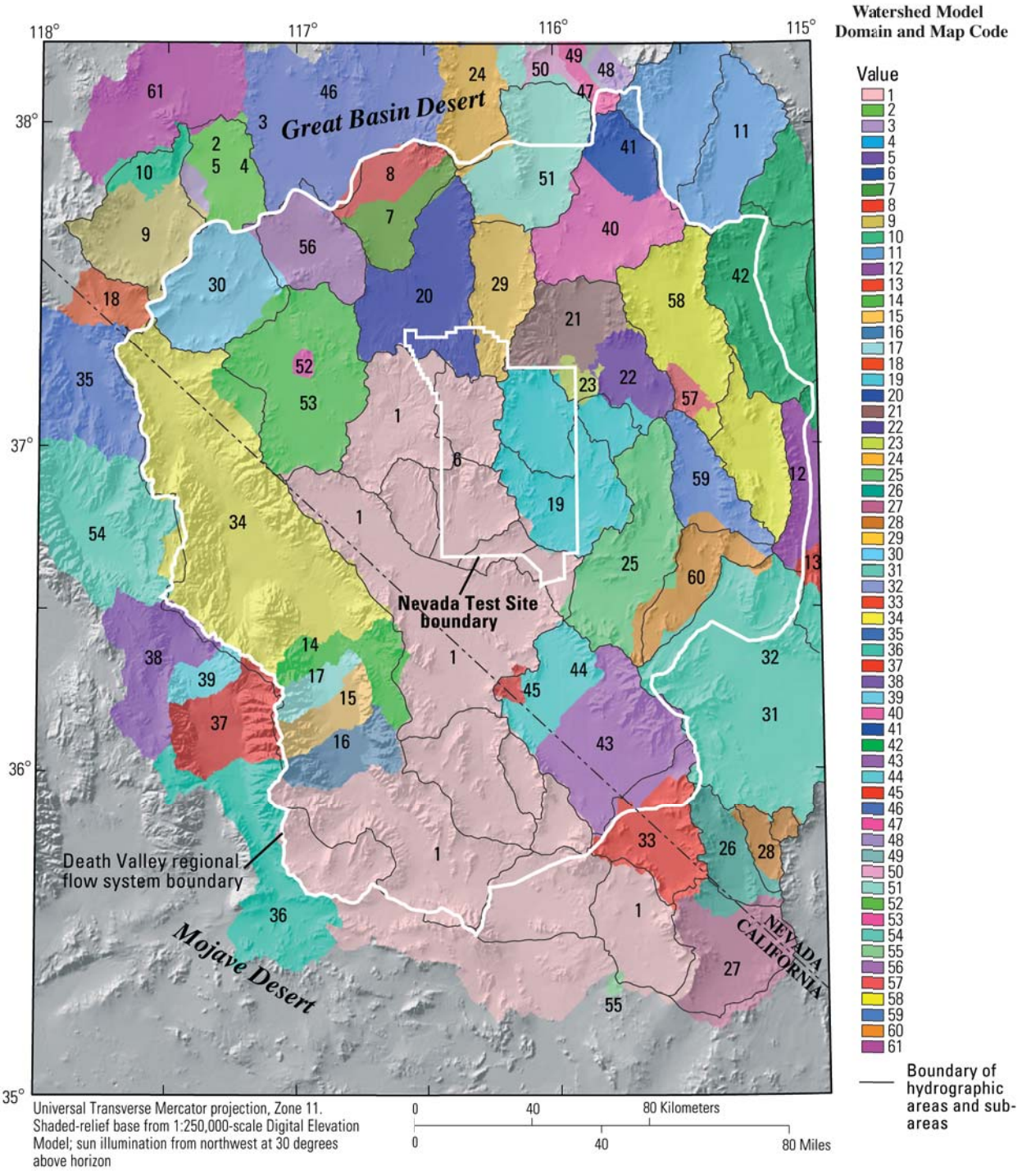

Figure 35. Watershed model domains used for 50-year simulations of the INFIILv3 model of the Death Valley region, Nevada and California.

Basin characteristics for the 61 watershed model domains (table 17) range from a maximum average elevation of 1,978 m for Fish Lake Valley 0 (map no. 18) to a minimum average elevation of 612 m for Death Valley 1 (map no. 15). The Saline Valley watershed model domain (map no. 54) is characterized by rugged topography which has an average slope of 10.9 degrees and maximum slope of 43.1 degrees, as compared with domains such as Cactus Flat 0 (map no. 7) which has an average slope of 2.0 degrees and a maximum slope of 20.1 degrees. The average soil thickness of all the soil layers ranges from a maximum of 6.0 m for small domains in the central part of basins, such as Alkali Springs Valley 2 (map no. 4) and Las Vegas Valley 1 (map no. 31), to a minimum thickness of 0.69 m for Beatty Wash (map no. 6), a small upland watershed model domain along the western boundary of the NTS.

Twenty nine of the watershed model domains consist of more than 10,000 grid cells. The largest watershed model domain is defined by the Amargosa River Basin; it consists of more than 200,000 cells. The total 77,065 km^2 area of the INFILv3 model (61 watershed model domains) used for the 50-year simulation consists of 993,635 model cells. Results of the 61 separate model runs were combined using a postprocessing routine to develop a composite set of model results for the entire INFILv3 model area. The combined results were further developed as raster-based map images using GIS applications; the results were used for evaluating spatial distributions.

Simulation Results for Watershed Modeling Domains

Results of the INFILv3 model simulations include the basinwide average annual water-balance components and the daily time series for all water-balance components. Results of the 1950–99 simulation for INFILv3 model 1 are given in table 18 (at back of report). Simulated average daily air temperatures range from 19.4°C for the Death Valley 1 watershed model domain (map no. 15) to 8.3 °C for Fish Lake Valley 0 (map no. 18). Simulated precipitation ranges from 289.6 mm/yr for Railroad Valley North 2 (map no. 48) to 120.3 mm/yr for Death Valley 1 (map no. 15). Railroad Valley North 2 also has the greatest simulated snowfall (102.4 mm/yr). Maximum total net infiltration rates include 6.35 mm/yr for Coyote Valley 0 (map no. 12), 7.51 mm/yr for Pahrump Valley 0 (map no. 43), 8.35 mm/yr for Railroad Valley North 2 (map no. 48), and 8.7 mm/yr for Saline Valley (map no. 54). Maximum runoff rates include 8.74 mm/yr for Beatty Wash 1 (map no. 6), 7.53 mm/yr for Death Valley 3 (map no. 17), 7.56 mm/yr for Groom Lake 0 (map no. 21), 9.52 mm/yr for Panamint Valley 1 (map no. 37), and 9.68 mm/yr for Railroad Valley North 2 (map no. 48) (fig. 35).

The infiltrated run-on results indicate the average annual rate of surface-water infiltration into the root zone during the downstream routing process. For a given drainage basin, this component of the water balance can equal but cannot exceed the runoff generation rate. Surface-water outflow is equal to runoff minus the sum of run-on net infiltration and infiltrated run-on. If infiltrated run-on plus run-on net infiltration equals runoff, then surface-water outflow from the watershed model domain is 0 (surface water does not reach the playa or the mouth of the drainage system). Some examples of watershed model domains with relatively high outflow rates (exceeding 0.1 mm/yr) include Beatty Wash 1 (6.245 mm/yr), Death Valley 0 through Death Valley 3, Pahrump Valley 0, Pahrump Valley 1, Railroad Valley North 2, and Panamint Valley 0 through Panamint Valley 2.

Infiltrated run-on is water added to the root-zone storage; it is either lost to evapotranspiration or contributes to total net infiltration. Higher values of infiltrated run-on indicate a greater potential for net infiltration; the maximum net infiltration rates tend to be well correlated to the maximum rates of infiltrated run-on. However, if the hydraulic conductivity of the underlying bedrock is low or the storage capacity of the soil is high, most of the infiltrated run-on can be lost to evapotranspiration, rather than contributing to net infiltration.

Run-on net infiltration is net infiltration that occurs during the downstream routing process. During streamflow, run-on net infiltration tends to occur only where the root zone is already close to being saturated and the available storage capacity of the root zone is low. As indicated by the results in table 18 (at back of report), net infiltration in direct response to run-on (run-on net infiltration) is less than 0.1 mm/yr for most drainage basins and, thus, is not a very significant component of the overall water balance. For the INFILv3 model used in this study, the total contribution of surface-water run-on to net infiltration could be quantified only by rerunning the model with surface-water flow decoupled (that is, run-on was not allowed to infiltrate during the routing process) and subtracting the two results.

Simulated 1950–99 precipitation results for four selected watershed model domains (fig. 36)—Amargosa River 0 (AR0), Saline Valley 0 (SV0), Kawich Valley 0 (KV0), and Pahrump Valley 0 (PV0)—indicates a high variability of annual precipitation in the Death Valley region and a strong similarity in annual precipitation patterns among the four areas (fig. 36*A*). Simulated annual precipitation ranges from about 480 mm for Kawich Valley 0 (KV0) to 50 mm for Amargosa River 0 (AR0). The pattern of annual variability shows some correspondence to the El Niño Southern Oscillation (ENSO), which is a naturally occurring sea surface temperature oscillation in the tropical Pacific Ocean that has been shown to be correlated to global climate patterns (Philander, 1990). Simulated above average precipitation generally corresponds to positive (El Niño) phases of ENSO in water years 1952, 1958, 1973, 1977–78, 1983, 1988, 1992–95, and 1998 (water years 1964 and 1970 do not follow this relation). The 5-year running mean annual precipitation calculated for the four model domains shows a good correspondence to the Pacific (inter) Decadal Oscillation (PDO), which is an interdecadal (10 to 50 year) index of climate variability based on the time series of the North Pacific sea-surface-temperature pattern (Mantua and others, 1997). This simulated trend of below average precipitation from water years 1950 through 1976 shows a good correspondence to the negative (cool) phase of the PDO, while the simulated trend of above average precipitation shows a good correspondence to the positive (warm) phase of the PDO from water years 1977 through 1998 (fig. 36*B*). All four model domains show a close similarity in the trends affecting the 5-year running mean, but the Pahrump Valley 0 domain (PV0), located in the southern part of the Death Valley region, shows the greatest relative increase in average annual precipitation following the onset of the positive PDO. Results for all watershed model domains show an overall trend of increasing precipitation.

Simulated annual net infiltration for 1950–99 for the 61 watershed model domains in the DVRFS indicates an even higher degree of annual variability than precipitation (fig. 36*C* and D). Maximum annual net infiltration of approximately 15 mm occurred in water years 1978 and 1993, both years are characterized by an extended El Niño. The 5- and 10-year running means follow the trend of increasing precipitation and, thus, also correspond to the positive PDO trend. For the first 14 years of the simulation (1950–64), the annual net infiltration did not exceed the mean net infiltration rate of 2.6 mm/yr. For the last half of the simulation period (1975–99), the 10-year running mean exceeds 4 mm/yr for several years. In general, the periods of high annual net infiltration are consistent with the El Niño phase of ENSO and wetter than average winter seasons, whereas the general trend of higher annual net-infiltration rates during the last half of the 1950–99 simulation period is correlated to the combined occurrence of increased El Niño frequency and a positive PDO (Schmidt and Webb, 2001). Possible biases caused by changes in the location and coverage of climate records also may have had an effect on the observed trends, but this was not investigated for this study.

Relative differences in the 5-year mean net-infiltration rates are similar for all locations throughout the Death Valley region, and are well correlated to the 5-year mean precipitation rates for each selected area (fig. 36*B* and *D*). The long-term (50-year) trend of increasing net infiltration is the result of an apparent trend of increasing precipitation. During the first 15 to 19 years of the simulation (from 1950 to 1968), conditions were drier than average in the Death Valley region (fig. 36*C*). Spatial variability in net infiltration across the Death Valley region is dependent partly on spatial variability in precipitation trends. For example, differences in the spatial distribution of annual precipitation may have caused the Saline Valley (SV0) area in the northwestern part of the model domain to have some of the highest annual net infiltration rates in the time series; these high rates occurred during the drier-than-average 1970–76 period. In contrast, annual net infiltration for the other locations (AR0, KVO, and PV0) were not as high during this period compared with the wetter-than-average periods of the early 1980s and the mid 1990s. Variability in the annual distribution of rainfall and snowfall across the Death Valley region may be dependent partly on regional differences in ENSO- and PDO-cycle effects on precipitation and air temperature; that is, wetter-than-average years in the extreme southern part of the region occurred during average or drier-than-average conditions in the northern part of the region.

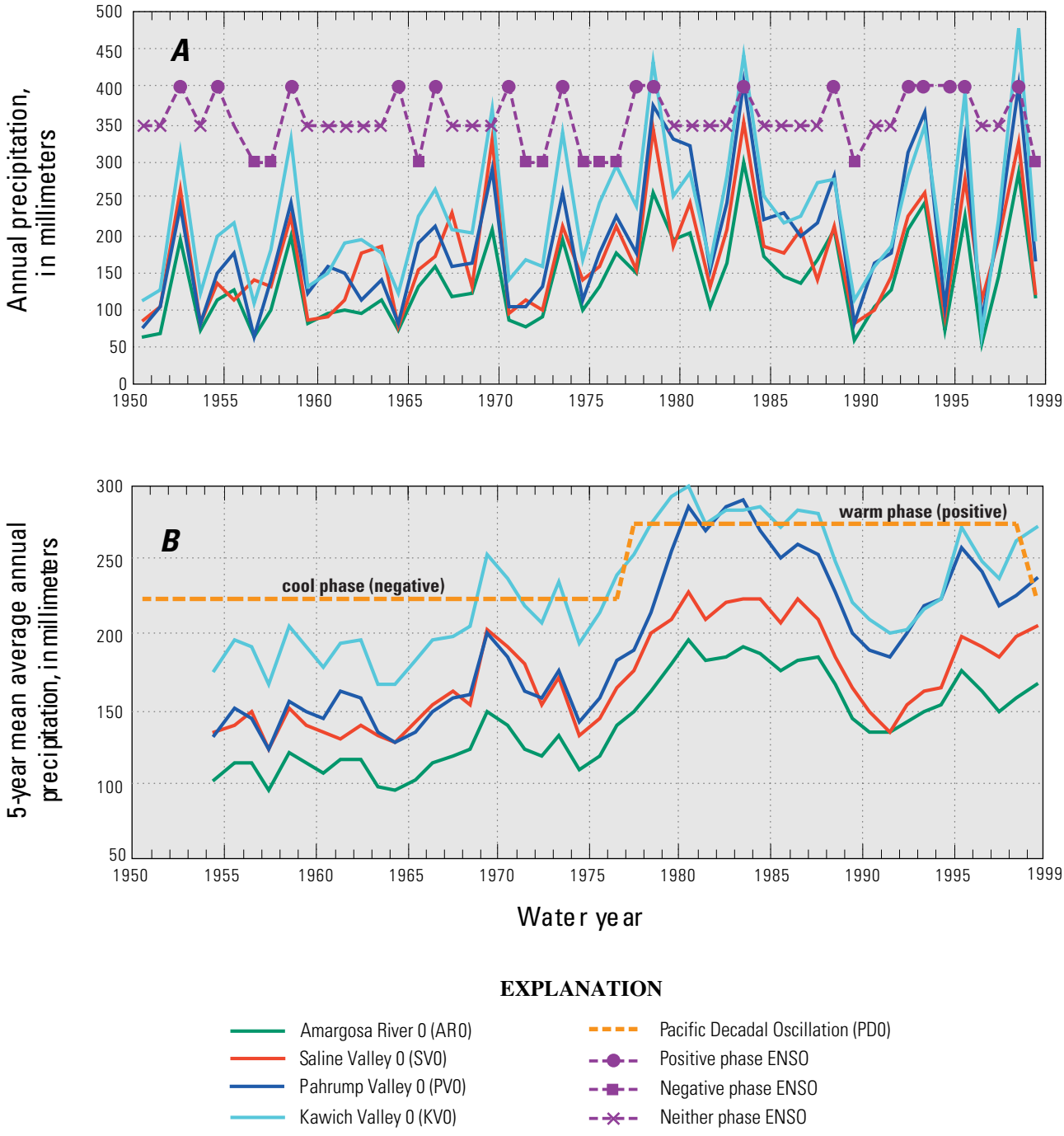

Figure 36. Annual precipitation and mean annual precipitation for selected watershed model domains and the Pacific Decadal Oscillation, Death Valley region, Nevada and California.

Temporal distribution of the 1950–99 simulation results showing: *A*, Simulated annual precipitation for four selected model areas and phases of the El Niño Southern Oscillation (ENSO). *B*, Simulated 5-year mean precipitation for four selected model areas and phases of the Pacific Decadal Oscillation (PDO). *C*, Simulated annual net infiltration, 5-year mean net infiltration, 10-year mean net infiltration, and 50-year mean net infiltration, averaged for all 61 model areas. *D*, Simulated 5-year mean net infiltration, averaged for all 61 model areas and the simulated 5-year mean net infiltration for four selected model areas.

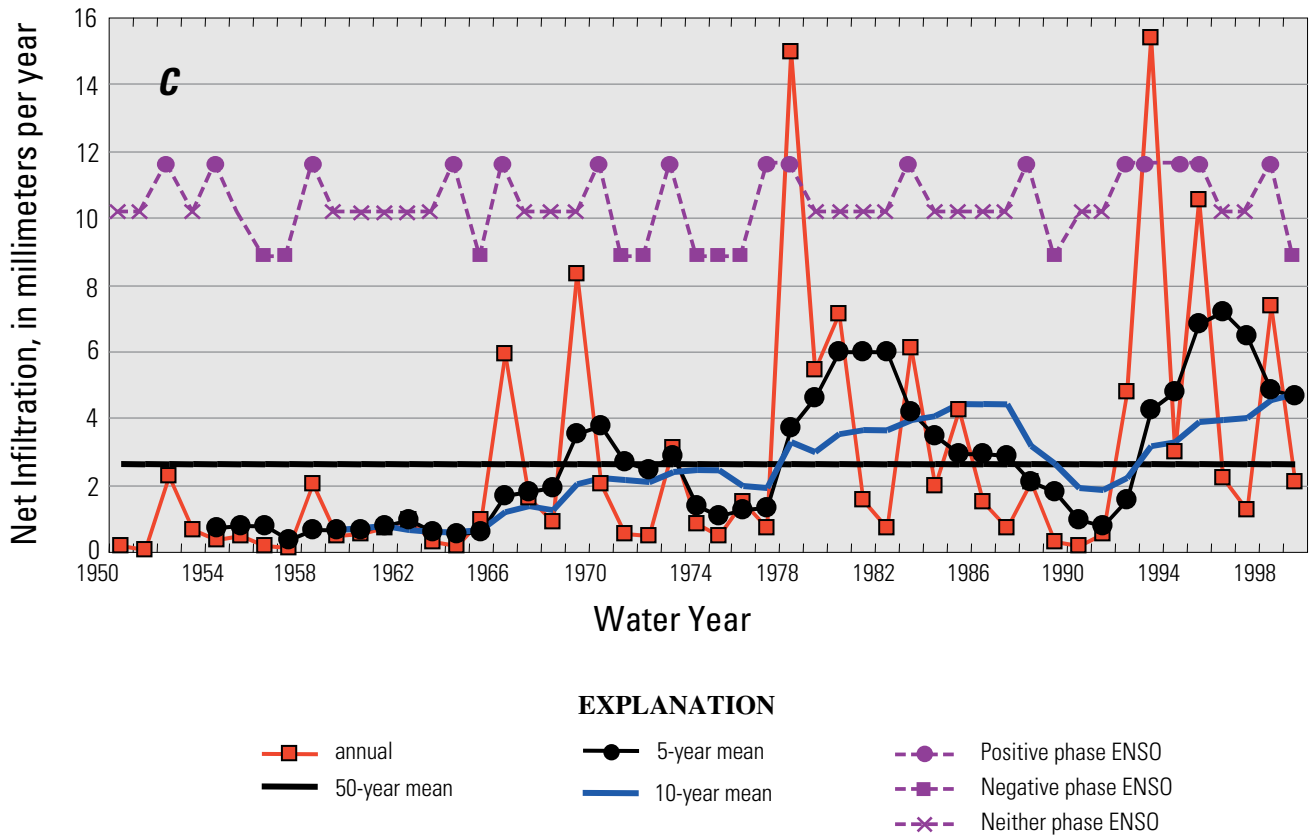

Figure. 36—Continued.

Results for the Death Valley Regional Flow System

Results for all simulated water-balance terms are summarized for the area of the DVRFS (table 19, at back of report). The spatially distributed, time-averaged results were developed using the four INFILv3 models (models 1 through 4) analyzed during model calibration and applied to the 50-year simulation. The four models were analyzed to evaluate model uncertainty and to quantify the contribution of simulated surface-water flow to simulated net infiltration and potential recharge. The basinwide water-balance results for the four models include inflows (precipitation, snowmelt, and infiltrated run-on), storage components (snowfall, change in root-zone water content, and runoff generation) and outflows (sublimation, evapotranspiration, run-on net infiltration, net infiltration, and surface-water outflow either to playas or out of the DVRFS).

Adjustments were made to the simulated net-infiltration results to account for mapped ground-water discharge zones and playa lakebeds. Net infiltration was set to 0 for all grid cells in the areas of ground-water discharge zones identified in D'Agnese and others (2002) because the contribution of ground-water discharge to the water balance is not represented by the INFILv3 model (fig. 3). In a second adjustment to the net-infiltration results, net infiltration was set to 0 for all areas identified as playas (fig. 3) to evaluate potential contributions to recharge from playas not currently identified as ground-water discharge zones. In performing these adjustments, an assumption was made that the amount of net infiltration subtracted could be added to the evapotranspiration component of the basinwide water balance.

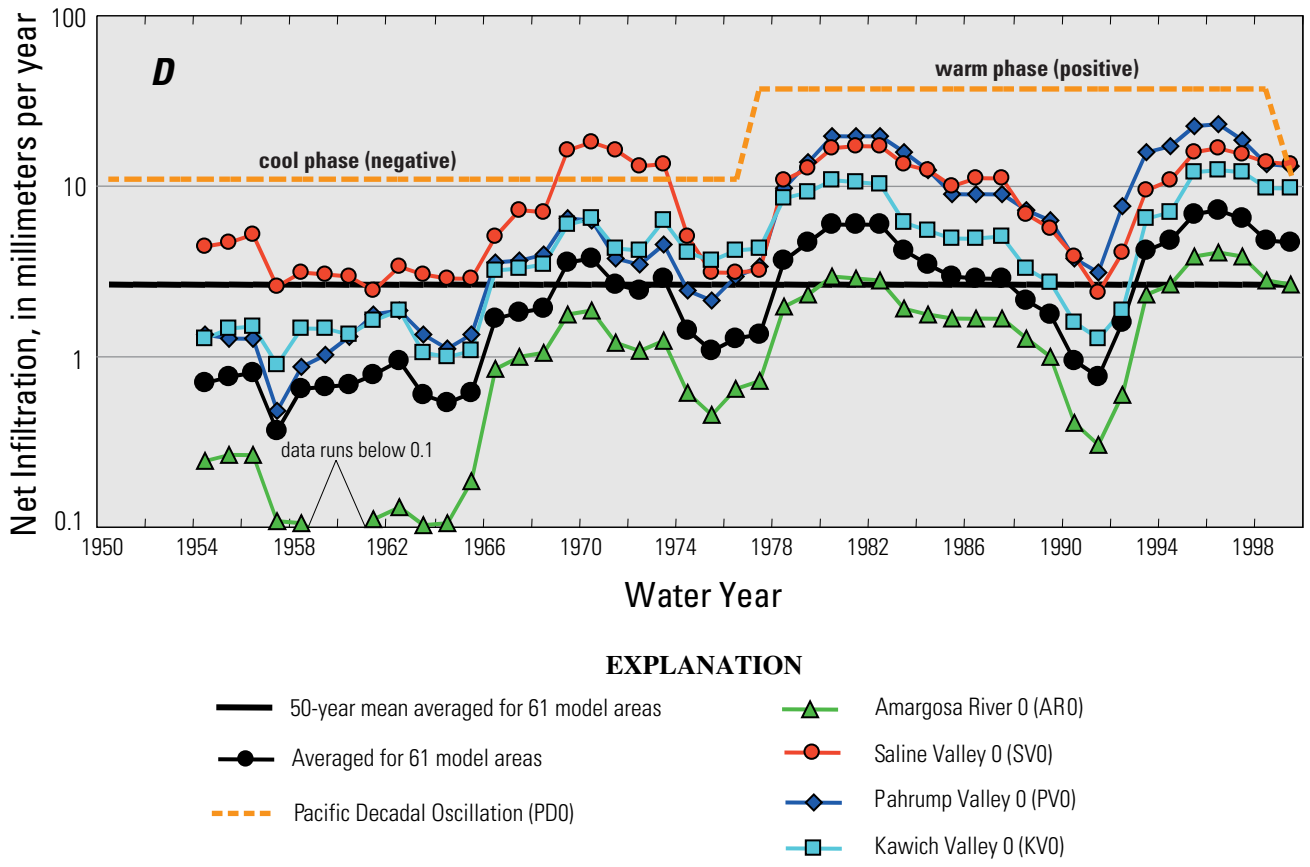

Figure. 36—Continued.

In addition to the simulation results of INFILv3 models 1, 2, 3, and 4, results from previous studies are included in table 19 at back of report. These results include PRISM estimates of annual precipitation, results for precipitation and net infiltration obtained in the preliminary application of INFIL to the Death Valley region (Hevesi and others, 2002), previous estimates of basinwide recharge for the 42 hydrographic areas (table 1), and a more recent estimate of total recharge to the DVRFS obtained in the process of calibrating a three-dimensional, steady-state ground-water flow model to measured water levels and estimated discharge (D'Agnese and others, 2002).

Results from the preliminary INFIL model include a basinwide average annual precipitation rate of 195.1 mm/yr and an average annual net-infiltration rate of 7.8 mm/yr (D'Agnese and others, 2002). These results are high relative to the PRISM estimate of 181.5 mm/yr for average annual precipitation and to the average annual recharge rate of 2.6 mm/yr obtained using previous estimates of recharge and the more recent recharge estimate of 2.1 mm/yr from D'Agnese and others (2002). As discussed by D'Agnese and others (2002) and Hevesi and others (2002), the estimate of net infiltration obtained using the INFIL model represents a preliminary result that is approximately four times greater than what can be approximately accounted for using the total ground-water discharge estimates for the DVRFS.

Results from INFILv3 model 1 for the DVRFS include a total net-infiltration volume, adjusted for ground-water discharge zones, of 342,100 m^3/d (table 19, at back of report). The adjusted net-infiltration volume is 1,900 m^3/d less than the simulated net infiltration volume of 344,000 m^3/d (1,900 m^3/d was subtracted from the ground-water discharge zones). The total net-infiltration result adjusted for playas (340,500 m^3/d) indicates that only 1,600 m^3/d, or less than 1 percent, was subtracted as net infiltration in the playa areas not defined as ground-water discharge zones. The total net-infiltration volume adjusted for ground-water discharge zones corresponds to the spatially averaged net-infiltration rate of 2.8 mm/yr; this rate is in close agreement with previous recharge estimates (2.6 mm/yr) and the more recent recharge estimate (2.1 mm/yr) from D'Agnese and others (2002). The INFILv3 model 1 simulation results also include an average precipitation rate of 171.3 mm/yr, a runoff generation rate of 2.2 mm/yr, and a surface-water outflow rate of 0.2 mm/yr. The surface-water outflow rate corresponds to a total surface-water discharge volume of 25, 900 m^3/d assumed to evaporate from playas or discharge as surface water outflow from the DVRFS.

A comparison of the simulation results of INFILv3 model 1 with the results of INFILv3 models 2, 3, and 4 indicates that model 1 simulated the highest net-infiltration volume. The simulation results of model 2, which is identical to model 1 except that surface-water run-on is not allowed to infiltrate, simulated an average annual net-infiltration rate (adjusted for discharge zones) of 2.4 mm/yr and a total net-infiltration volume of 293,100 m^3/d. Model 3, which uses lower estimates of bedrock hydraulic conductivity, simulated an average annual net-infiltration rate of 1.4 mm/yr, which corresponds to a total net-infiltration volume of 178,700 m^3/d. Model 4, which uses the lower estimates of bedrock hydraulic conductivity but a higher root density (which increases transpiration from the lower part of the root zone), simulated an average annual net infiltration rate of 1.2 mm/yr and a total net-infiltration volume of 144,700 m^3/d. Although models 1 and 4 provide similar results in terms of simulated streamflow, potential recharge volumes predicted using model 4 are less than half that predicted using model 1. This result illustrates the non-uniqueness of models that are calibrated by fitting to streamflow data, and the need to incorporate additional constraints during the model calibration process. The simulation results of models 1, 3, and 4 can be interpreted as realizations representative of uncertainty in model inputs: A more robust result may be developed by taking the average result from multiple realizations. For example, the average net infiltration simulated by models 1 and 3 is 2.1 mm/yr and the average net-infiltration volume is 260,400 m^3/d. This net-infiltration volume is a good match to the recharge volume of 266,800 m^3/d estimated by D'Agnese and others (2002).

Simulation results for INFILv3 models 1, 2, 3, and 4 also were evaluated by comparing simulated runoff and infiltration between upland areas that have thin soils with that for the alluvial fan and basin areas that have deep soils. The upland areas were identified as areas where the root zone extends into the underlying consolidated rock layer, whereas alluvial fan basin areas were identified as areas where the root zone is underlain by unconsolidated material (deep soils). Results of all four INFILv3 models indicate that net infiltration for the DVRFS primarily is controlled by net infiltration in upland areas that have thin soils (table 19 at back of report). For example, simulation results for model 1 show that net infiltration in the upland areas is 309,800 m^3/d but only 32,300 m^3/d (adjusted for discharge zones) in the alluvial fan and basin areas. A comparison of results between model 1 and model 2 indicated that most of the net infiltration for the alluvial fan and basin areas is due to surface-water flow and stream-channel losses. When surface-water run-on is removed from the root-zone water balance (surface water is not allowed to infiltrate during the routing process), net infiltration for alluvial fans and basins decreases from 32,300 m^3/d to 1,400 m^3/d. In all cases, adjustment of net infiltration to account for ground-water discharge zones had a negligible effect on the total net-infiltration volume, even when the adjusted result included all playa areas and the areas of the identified discharge zones. The average annual simulation results for selected components of the water balance obtained using INFILv3 model 1 are given in figures 37 through 43 and are summarized in table 19 at back of report. The figures illustrate the high degree of spatial variability in the simulated water-balance components, which include precipitation, snowfall, evapotranspiration, runoff, surface-water run-on, infiltrated run-on, and net infiltration.

INFILv3 Model 1 Simulated 50-Year Average Precipitation

INFILv3 model 1 simulated 50-year average annual precipitation (fig. 37) reflects expected orographic influences in the Death Valley region. The maximum precipitation rate (552 mm/yr) was simulated in the summit area of the Spring Mountains and the minimum rates (50 to 100 mm/yr) were simulated in locations of Death Valley and Panamint Valley. The relatively high precipitation rates (400 mm/yr and higher) were simulated in the summit areas of the Sheep Range, the Panamint Range, and the Timpahute Range. Precipitation rates simulated for the Yucca Mountain area range from 100 to 250 mm/yr; these rates are in good agreement with existing precipitation data for Yucca Mountain (Flint and Davies, 1997), which were not included in the model. The average precipitation rate for the entire INFILv3 model area is 182 mm/yr. A comparison of the 50-year average precipitation simulated by INFILv3 model 1 with estimates simulated by PRISM (fig. 6) indicates a generally good agreement between the two models in terms of orographic effects on the estimated spatial distribution of precipitation in the INFILv3 model area.

INFILv3 Model 1 Simulated 50-Year Average Snowfall

The spatial distribution for the average annual snowfall simulated by INFILv3 model 1 indicates the increased contribution of snow accumulation, sublimation, and melting to the water balance for the higher elevations where recharge is more likely to occur (fig. 38). For the summit area of the Spring Mountains, the average annual snowfall depth is more than 400 mm/yr (in terms of a water equivalent depth), which is approximately 80 percent of the average annual precipitation. Simulated average annual snowfall for Rainier Mesa, in the northern part of the NTS, exceeds 100 mm/yr. For these locations, factors controlling the seasonal accumulation and melting of snow are likely to have a significant effect on the timing and magnitude of net infiltration. However, for most locations in the INFILv3 model area, estimated average annual snowfall is less than 20 mm/yr (in water equivalent depth), and the processes of snow accumulation, sublimation, and melting probably are not important factors in controlling net infiltration.

INFILv3 Model 1 Simulated 50-Year Average Runoff

Simulation results of INFILv3 model 1 for runoff indicate that runoff primarily occurs in areas of thin soils that area underlain by impermeable bedrock and in areas with soils that have higher percentages of clays (and thus relatively lower permeability) repeatedly influenced by severe summer storms (fig. 39). Locations having relatively high runoff rates (greater than 20 to 50 mm/yr) due to a combination of thin soils and relatively impermeable bedrock include the Panamint Range, Rainier Mesa, the Groom Range, and the Black Mountains (see figure 2 for physiographic features). In contrast, runoff from the Spring Mountains and the Sheep Range was much lower than that from other locations that have comparable precipitation rates; the lower runoff was due to the higher permeability of the Paleozoic carbonate rocks that constitute the bedrock at these two locations. For areas with thicker soils, simulated runoff occurred primarily in response to severe precipitation during summer storms; the spatial distribution of runoff during summer is dependent on a combination of localized high daily precipitation amounts and the soil-saturated hydraulic conductivity. However, simulated runoff in model areas having thick soils was limited because of the number of severe summer storms between 1950 and 1999.

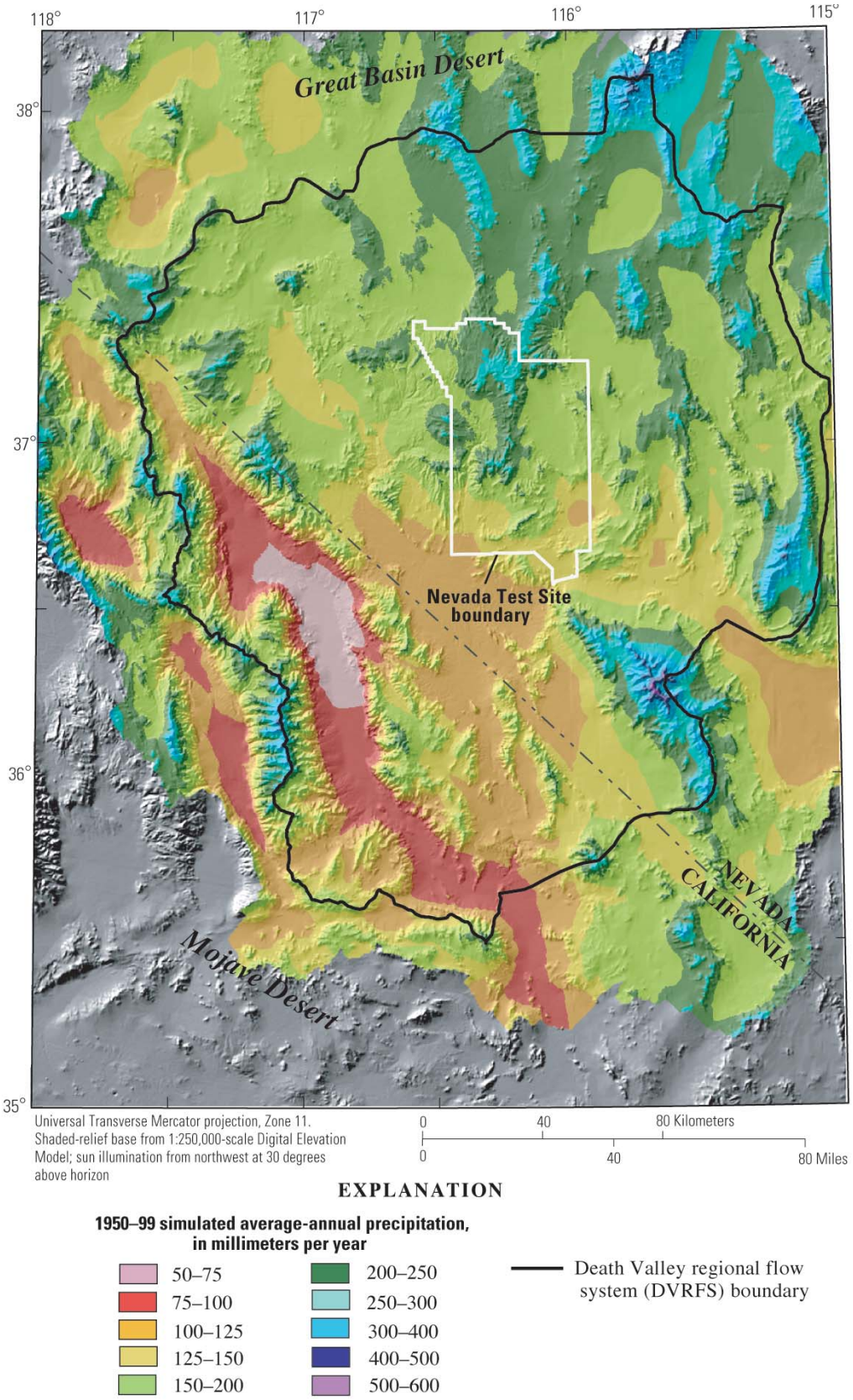

Figures 37. Average annual precipitation simulated by INFILv3 model 1, Death Valley region, Nevada and California, 1950–99.

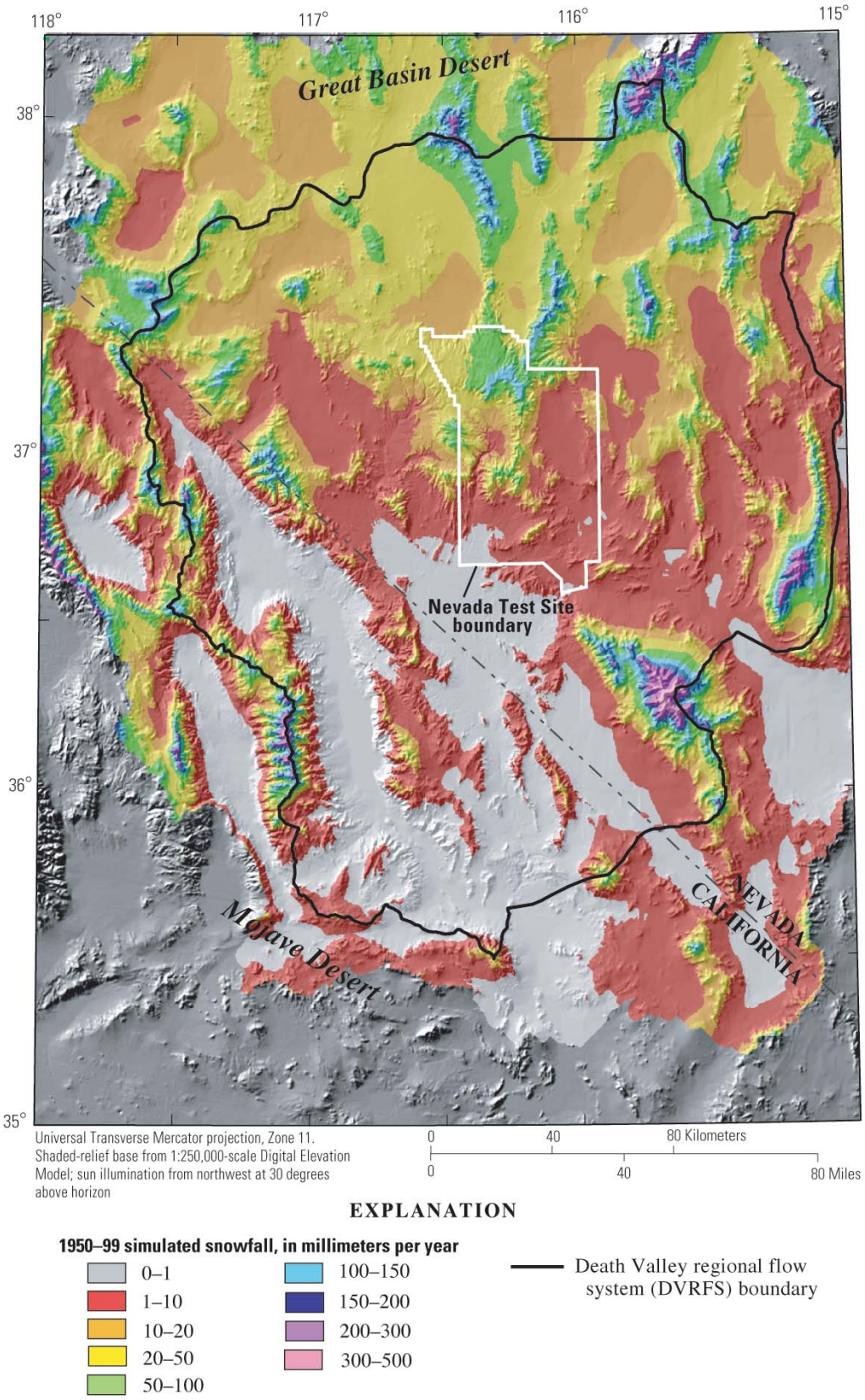

Figure 38. Average annual snowfall simulated by INFILv3 model 1, Death Valley region, Nevada and California, 1950–99.

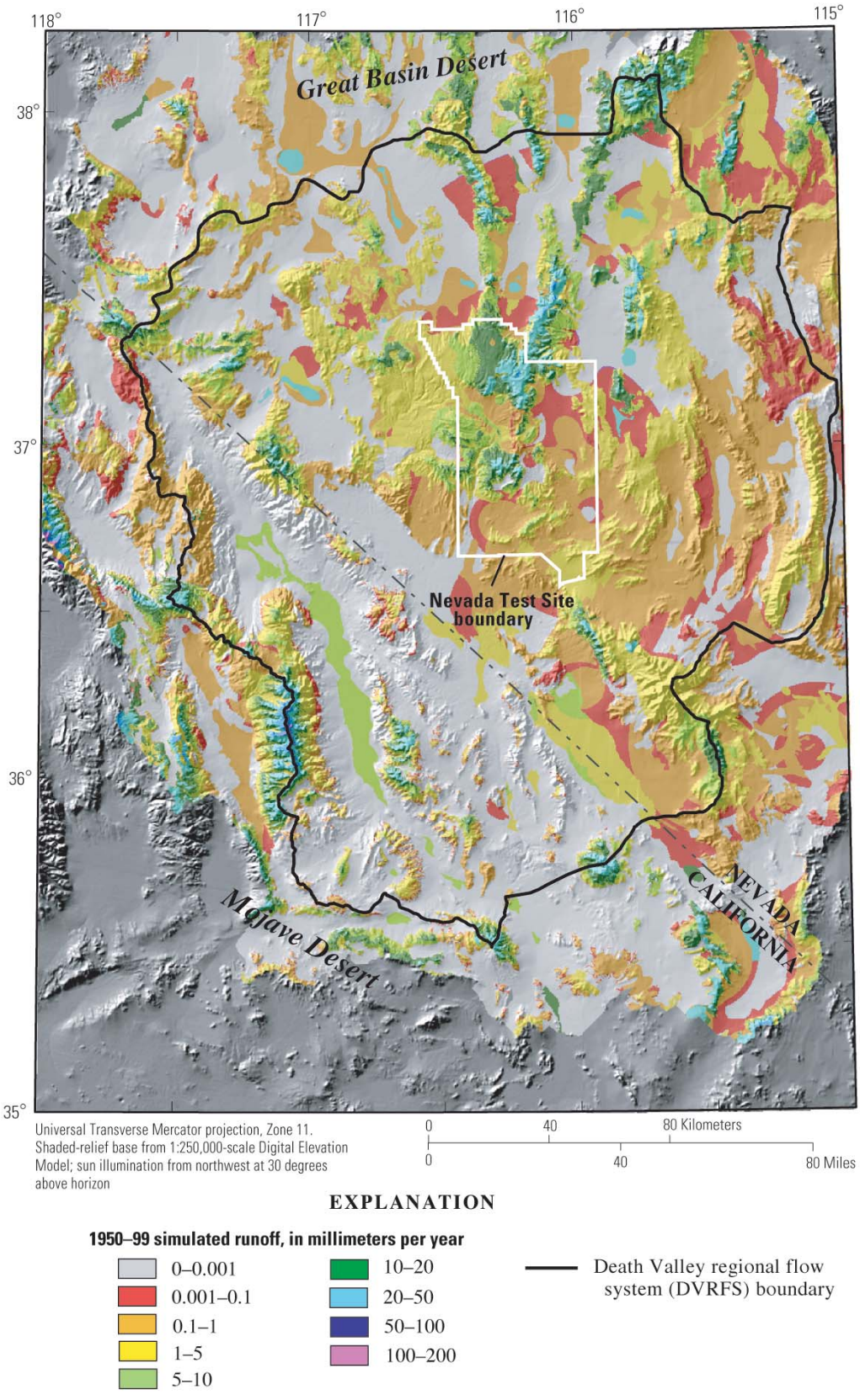

Figure 39. Average annual runoff simulated by INFILv3 model 1, Death Valley region, Nevada and California, 1950–99.

Simulated 50-Year Average Surface-Water Run-On

Simulated average annual surface-water run-on for 1950–99 (fig. 40) indicates the downstream redistribution of runoff as surface water. Areas having relatively high run-on values (greater than 1,000 mm/yr) generally correspond to stream channels downstream of areas having high runoff, such as the Panamint Range, the NTS, the Black Mountains, and Rainier Mesa (see figure 2 for physiographic features). Simulated run-on for some locations along the major stream channels in the Amargosa River drainage basin indicate simulated run-on depths exceeding 1,000 mm/yr. Locations having permeable bedrock, such as the Spring Mountains and the Sheep Range, are characterized by relatively lower values of run-on and runoff relative to the high precipitation and low potential evapotranspiration.

INFILv3 Model 1 Simulated 50-Year Average Infiltrated Run-On

Simulated average annual infiltrated run-on indicates areas where maximum average annual stream-channel infiltration losses occur in response to the downstream routing of surface-water runoff (fig. 41). The highest simulated values of infiltrated run-on in the area of the ground-water flow model (greater than 1,000 mm/yr) occur in the middle and lower sections of drainage basins in the Panamint Range where the relatively high frequency of simulated runoff was caused by a combination of thin soils, impermeable bedrock, and orographic effects on precipitation. Simulated infiltrated run-on (100 to 500 mm/yr) also was high for sections of the main stream channel in the Fortymile Wash drainage basin. East and south of Yucca Mountain, in the downstream section of the Fortymile Wash channel, values were much lower (20 to 50 mm/yr). The lower values are in good agreement with recharge estimates for Fortymile Wash from Savard (1998), which were based on an analysis of the streamflow records (including both peak flow and daily mean discharge records), field observations, and geophysical logs of boreholes in the wash.

Simulated 50-Year Average Evapotranspiration

The simulated average annual evapotranspiration values for 1950–99 indicate a general spatial distribution pattern that closely corresponds to the spatial distribution of average annual precipitation (figs. 37 and 42). Simulated evapotranspiration rates were highest for the summit area of the Spring Mountains (owing to the increase in available precipitation) and for the stream-channel locations (owing to the increase in available water from infiltrated run-on). These results indicate that following precipitation, evapotranspiration in recharge areas is the most dominant component of the water balance for net infiltration in the INFILv3 model area.

Simulated 50-Year Average Net Infiltration

Simulated average annual net infiltration for 1950–99 (fig. 43) indicates a spatially complex pattern that reflects the combined effects of precipitation, soil thickness, and bedrock permeability. The Spring Mountains is a dominant area of high net infiltration in the Death Valley region because of the combination of high precipitation, low potential evapotranspiration, thin soils, and high permeability of Paleozoic carbonate bedrock. Simulated net infiltration is between 20 to 50 mm/yr for most of the upland area of the Spring Mountains. Maximum rates of more than 100 mm/yr were simulated for the summit location; the high rates reflect the increased effect of spring snowmelt on promoting net infiltration. The maximum net-infiltration rates, however, are in the active channel locations and exceed 500 mm/yr for many locations, such as the mountain-front locations in the Panamint Range and the upper section of the Fortymile Wash drainage. The importance of the estimated bedrock hydraulic conductivity in controlling net infiltration is indicated by the results for the Panamint Range; net-infiltration estimates were less than 2 mm/yr for much of the summit area even though precipitation exceeds 400 mm/yr. In contrast, locations that have thin soils underlain by the Paleozoic carbonate rocks are characterized by relatively high net-infiltration rates, even for areas with relatively low precipitation rates, such as the southern Funeral Mountains.

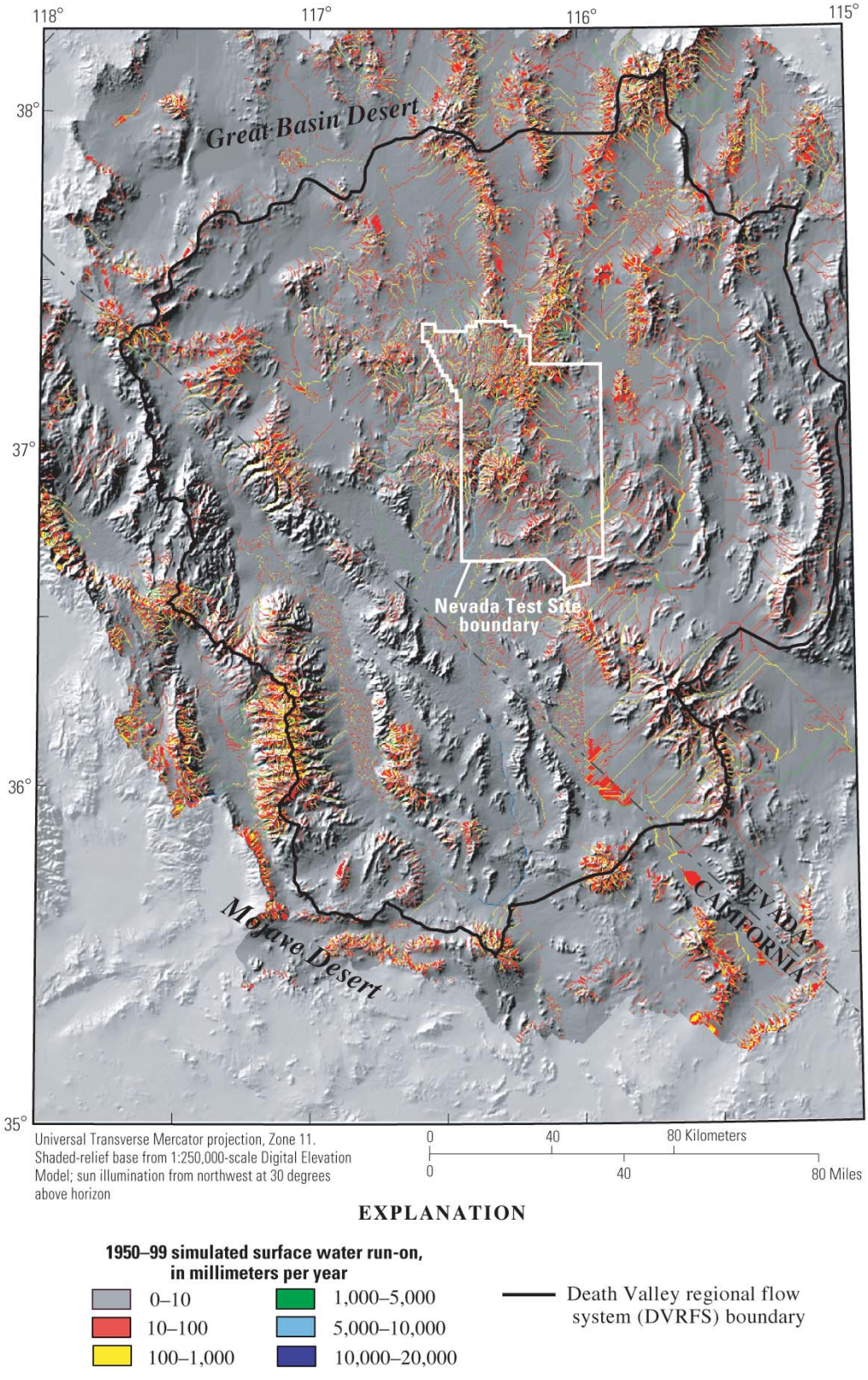

Figure 40. Average annual surface-water run-on simulated by INFILv3 model 1, Death Valley region, Nevada and California, 1950–99.

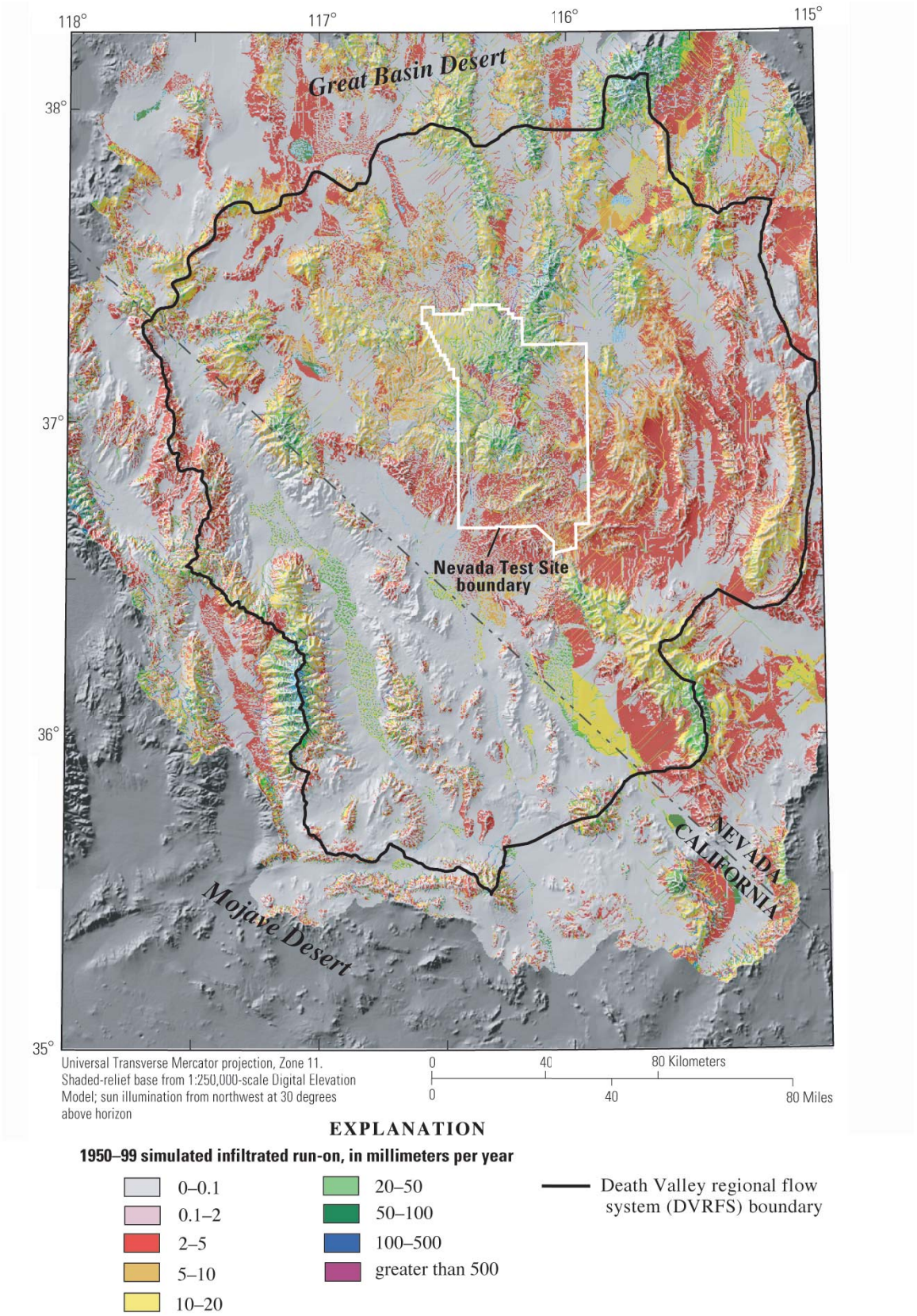

Figure 41. Simulated average annual infiltrated surface-water run-on for the Death Valley region, Nevada and California, 1950–99.

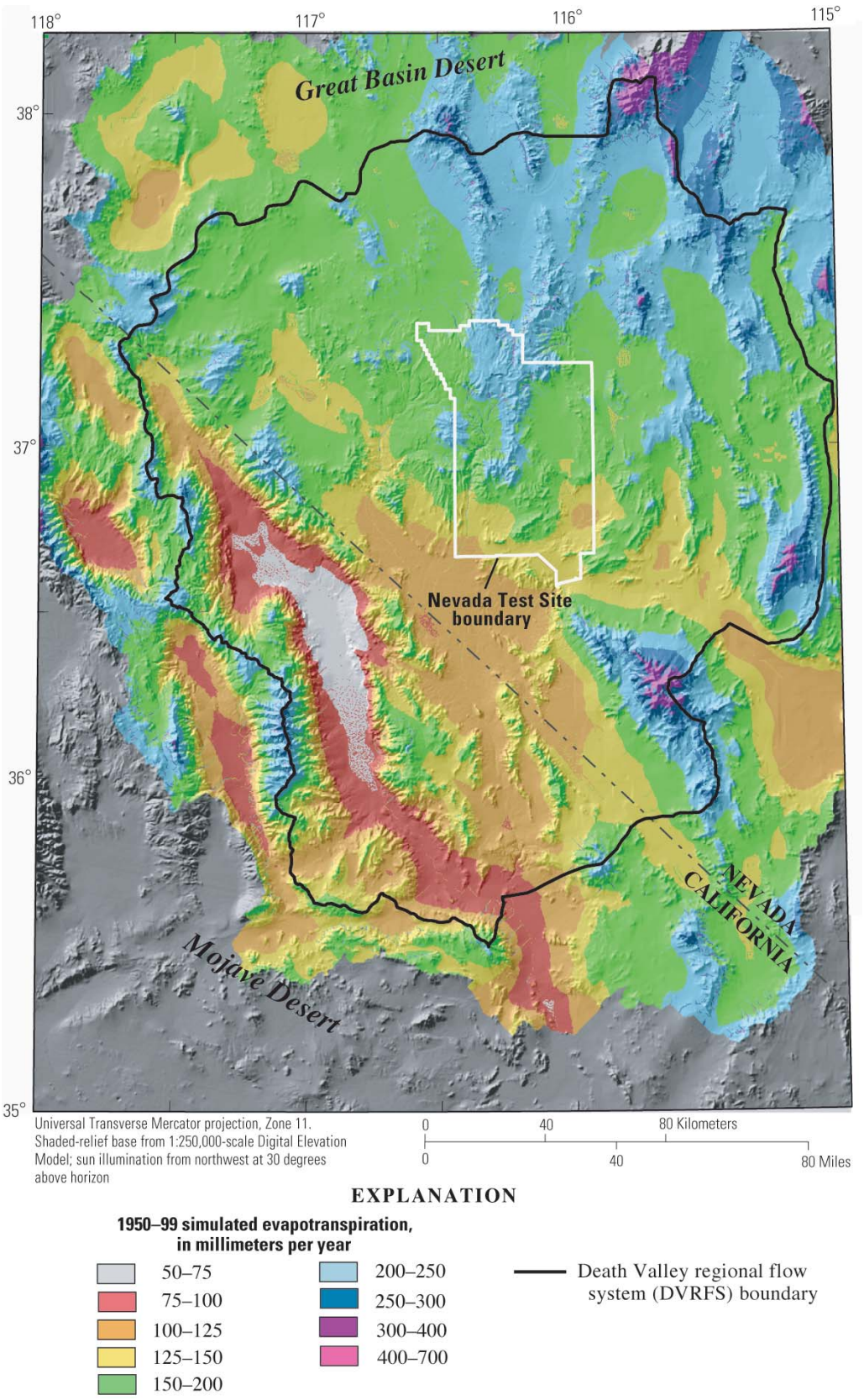

Figure 42. Simulated evapotranspiration for the Death Valley region, Nevada and California, 1950–99.

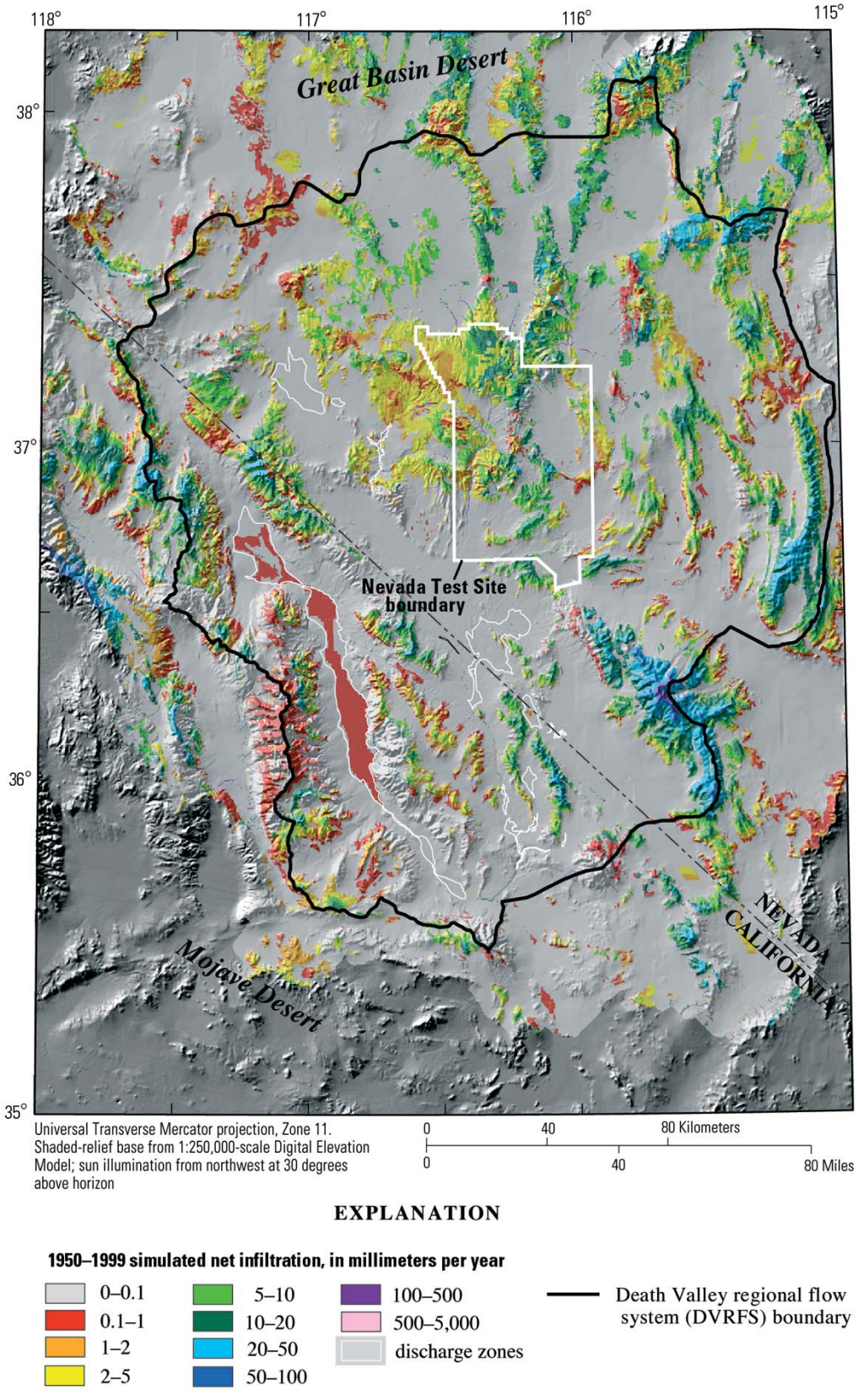

Figure 43. Simulated average annual net infiltration in the Death Valley region, Nevada and California, 1950–99.

Model Evaluation Using Hydrographic Areas

Model evaluation was done using averages simulated for the 42 hydrographic areas and subareas in and adjacent to the DVRFS (fig. 4). Simulated basinwide average annual precipitation rates were compared with basinwide rates estimated using PRISM. Simulated basinwide net-infiltration rates and total net-infiltration volumes were compared with previous estimates of basinwide recharge rates and volumes (fig. 5; table 1). Simulation results for the DVRFS area also were included in the analysis.

Comparison of Simulated Precipitation Estimates with PRISM Estimates

Average annual precipitation estimates simulated by the INFILv3 model were compared with estimates simulated by PRISM for the 42 hydrographic areas in the Death Valley region (table 20at back of report). The INFILv3 estimates are in general agreement with those estimated by PRISM for most of the hydrographic areas. The INFILv3 estimates closely match the PRISM estimates for five of the hydrographic areas (the lower Amargosa Valley, Shadow Valley, Chicago Valley, Crater Flat, and Death Valley). For some areas, average annual precipitation between the INFILv3 and the PRISM estimates for maximum basinwide precipitation exceeded 100 mm/yr. For example, the maximum PRISM estimate for the Garden Valley hydrographic area in the northern part of the model area is 686 mm/yr compared with 513 mm/yr for the INFILv3 estimate. For the Fortymile Canyon area, the maximum precipitation was 432 mm/yr for PRISM and 300 mm/yr for INFILv3. For this location, the precipitation estimates simulated using the INFILv3 model are considered fairly accurate because the model used daily precipitation data from the NTS monitoring network for several stations within and adjacent to the Fortymile Canyon area. Because PRISM does not include data from the NTS network, it tends to overestimate average annual precipitation for the NTS area. The PRISM-estimated average annual precipitation for all 42 hydrographic areas is 182 mm/yr, which is slightly greater than that estimated using INFILv3 (175 mm/yr) (table 20, at back of report).

Some of the differences between the PRISM estimates and the INFILv3 estimates may be attributed to differences in the period of records used in the models and to differences in the number and location of precipitation records. The PRISM estimates are for a 30-year period (1961–90); only stations that had a 30-year record were used to develop the estimates. The INFILv3 estimates are for a 50-year period, which includes the relatively dry 1950–60 period. Some stations included in the INFILv3 model have only 9 years of record. The shorter records were used to increase the spatial coverage and density of the daily climate records in the Death Valley region, which was assumed to improve the spatial interpolation of daily precipitation and air temperature.

Simulated Water Balance for Hydrographic Areas

The 50-year water-balance terms simulated using INFILv3 model 1 are summarized as basinwide average rates for the 42 hydrographic areas (table 21, at back of report). The results were used to explore differences in the hydrologic characteristics among the various basin areas. For example, basins that have higher precipitation rates also tend to have a higher percentage of precipitation as snow. A maximum snowfall rate of 71.7 mm/yr was simulated for Garden Valley. Garden Valley, the most northern area included in the analysis, is associated with the highest basinwide precipitation rate of 282.7 mm/yr and a moderately high net-infiltration rate of 3.50 mm/yr. The highest net-infiltration rates are in Pahrump Valley (5.66 mm/yr), Las Vegas Valley (4.97 mm/yr), and Kawich Valley (4.89 mm/yr).

Maximum simulated runoff rates include 7.70 mm/yr for Buckboard Mesa (area 227B) in northern Fortymile Canyon and 6.99 mm/yr for Kawich Valley (area 157) (table 21 at back of report). Buckboard Mesa, which includes a large part of the northern NTS area, also has the highest outflow rate (1.79 mm/yr). Outflow for Buckboard Mesa represents surface-water discharge downstream along the Fortymile Wash channel into Jackass Flats (area 227A) and the southern part of the Fortymile Wash drainage basin. Outflow for Jackass Flats is –0.77 mm/yr, indicating that the inflow from Buckboard Mesa along the Fortymile Wash channel exceeds the outflow from Jackass Flats along lower Fortymile Wash downstream into the Amargosa Desert (area 230). This result is consistent with the results of a study by Savard (1998) that shows significant channel losses during streamflow in Fortymile Wash.

In contrast to Buckboard Mesa (227B), the outflow rate of 0.40 mm/yr for Pahrump Valley (162) indicates discharge to playas in the closed basin. The negative outflow rates obtained for many of the areas indicate that surface-water inflows exceed outflows (either to a playa or to a downstream area). For areas such as southern Ivanpah Valley (164B), a negative outflow occurs because the area boundary does not adequately define the true topographic divide. The total outflow to all areas is 0.17 mm/yr and represents the total assumed evaporation loss from playas. Although not done for this study, a comparison of the assumed evaporation from playas with independent estimates of playa–lake water budgets could be used as part of model evaluation.

Adjusting the net-infiltration rates by setting the net infiltration in mapped discharge zones to 0 caused a reduction in basinwide net infiltration for only three of the hydrographic areas: Sarcobatus Flat, Death Valley, and Oasis Valley. The largest change was in Oasis Valley; net infiltration was reduced from 2.55 to 2.24 mm/yr. For this area, high net-infiltration rates were simulated in the channel of the Amargosa River upstream of Beatty, Nev. The location of the areas with high net-infiltration rates coincides with known discharge zones (springs) throughout this section of the channel.

Net-Infiltration Results for Hydrographic Areas

Net infiltration simulated using INFILv3 models 1, 2, 3, and 4 was averaged for the 42 hydrographic areas with previous estimates of recharge (fig. 5). The net-infiltration values used to develop the basinwide averages included the discharge-area adjustment to the INFILv3 simulation results (simulated net infiltration was set to 0 over mapped discharge zones).

The relative differences in net-infiltration rates among the hydrographic areas were fairly consistent between the four models (figs. 44–47; table 2, at back of report). For example, regardless of which model was used, net-infiltration rates tended to be high for Pahrump Valley (area 162), Las Vegas Valley (area 212), Kawich Valley (area 157), and Groom Lake Valley (area 158A), and low for Alkali Spring Valley (area 142), Jean Lake Valley (area 165), Lida Valley (area 144), the Amargosa Desert (area 230), and the Lower Amargosa Valley (area 242). A dominant factor controlling the relative magnitude of net infiltration for all four models is the percentage of upland area that has thin soils. In general, basins characterized by a higher percentage of upland areas that have thin soils have higher values of net infiltration. Maximum elevations in a basin and bedrock hydraulic conductivity also are important factors in determining relative differences in net infiltration between basins. Basins that have the higher elevation mountains tend to have higher basinwide net-infiltration rates.

For the four net-infiltration models analyzed in this study, the relatively high net-infiltration rates for Pahrump and Las Vegas Valleys occurred because the two areas share a common topographic divide along the crest of the Spring Mountains. Many factors tend to increase net infiltration in the Spring Mountains including high precipitation, permeable bedrock (Paleozoic carbonate rocks) underlying a widespread upland area of thin soils, north-facing slopes that have minimum potential evapotranspiration demand, areas of barren ground or shallow root zones, and a high percentage of precipitation as snow.

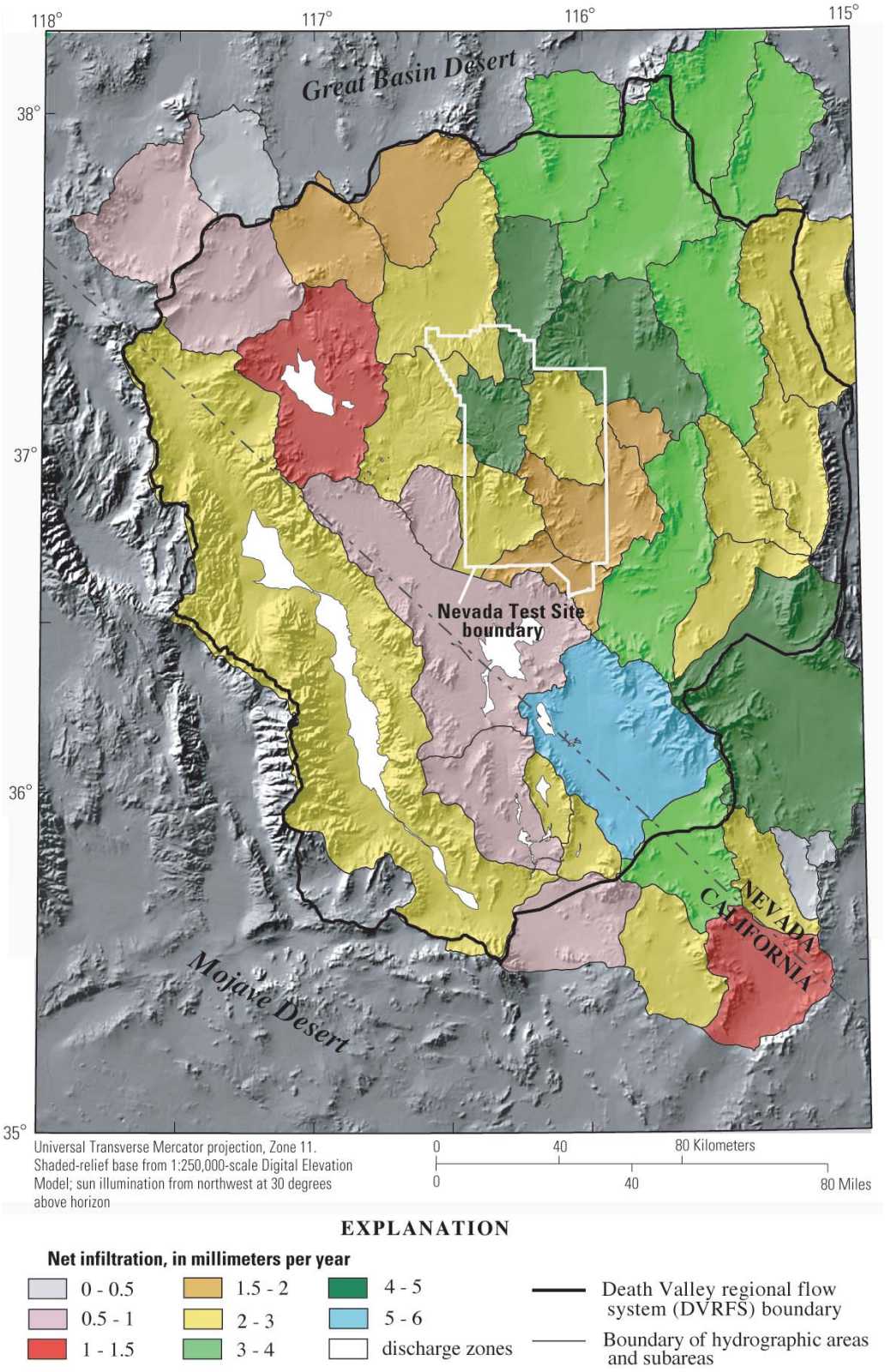

Figure 44. Average net infiltration simulated by INFILv3 model 1 for the 42hydrographic areas within and adjacent to the Death Valley region, Nevada and California, 1950–99.

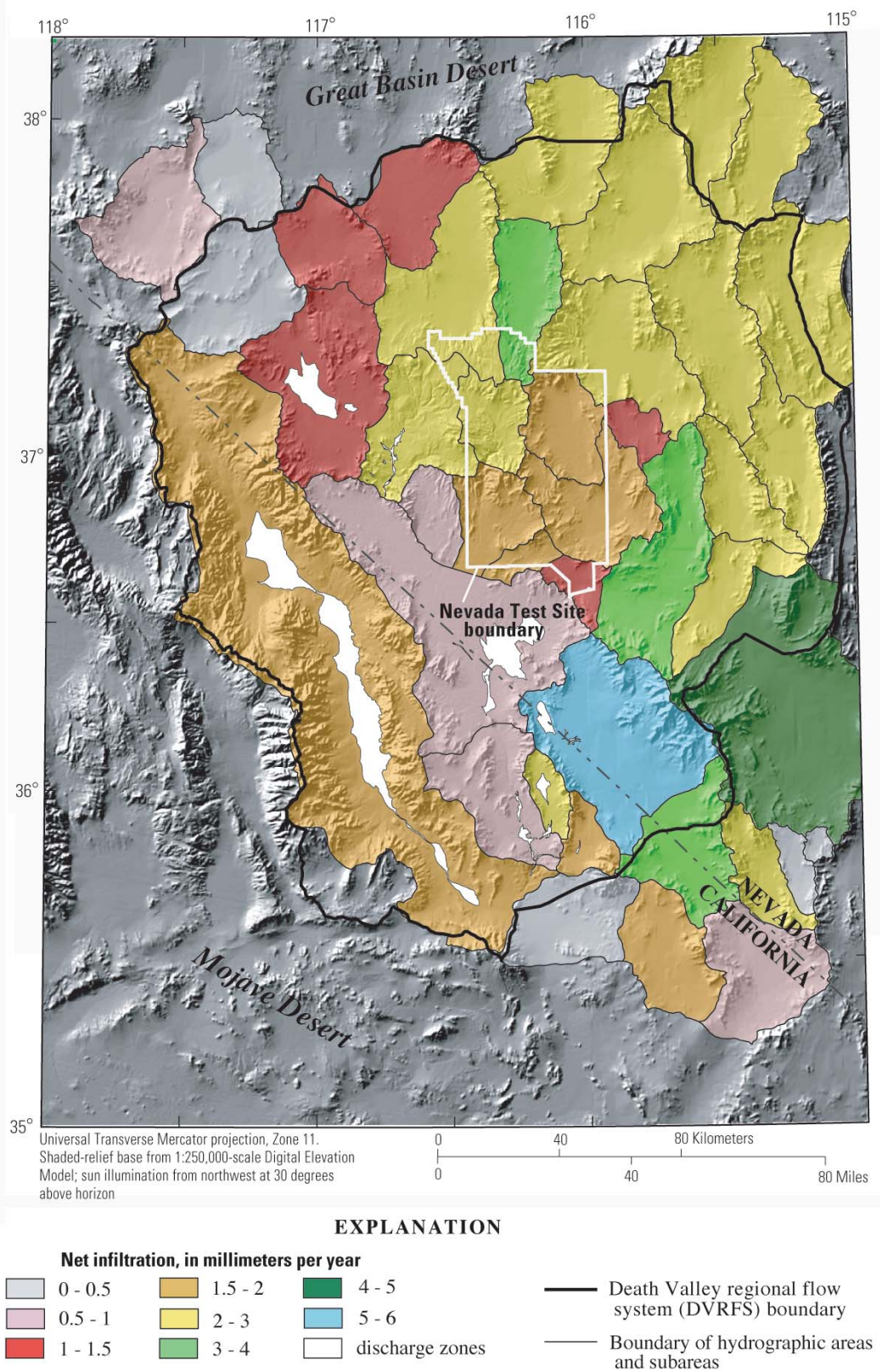

Figure 45. Average net infiltration simulated by INFILv3 model 2 for the 42 hydrographic areas within and adjacent to the Death Valley region, Nevada and California, 1950–99.

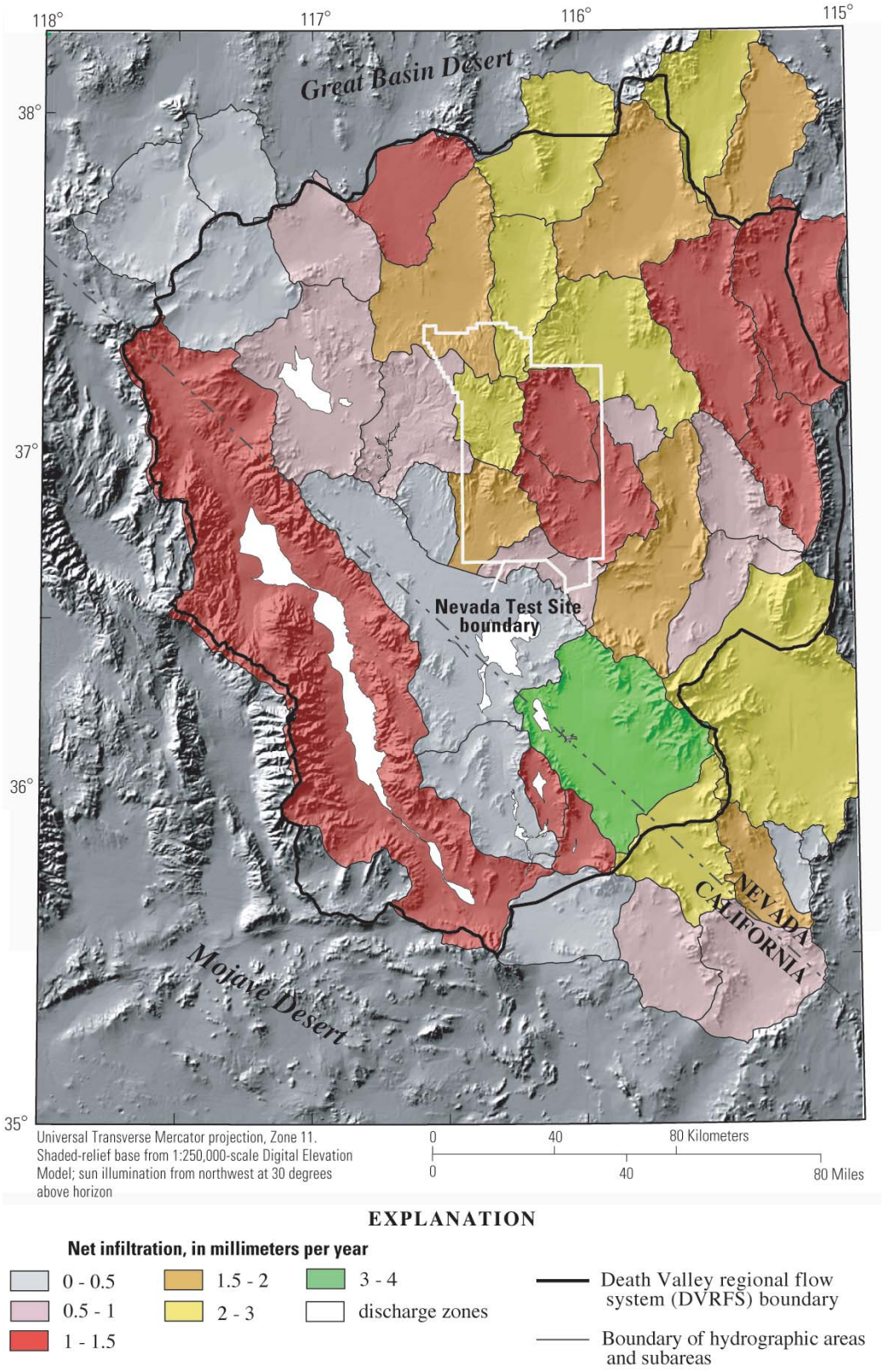

Figure 46. Average net infiltration simulated by INFILv3 model 3 for the 42 hydrographic areas within and adjacent to the Death Valley region, Nevada and California, 1950–99.

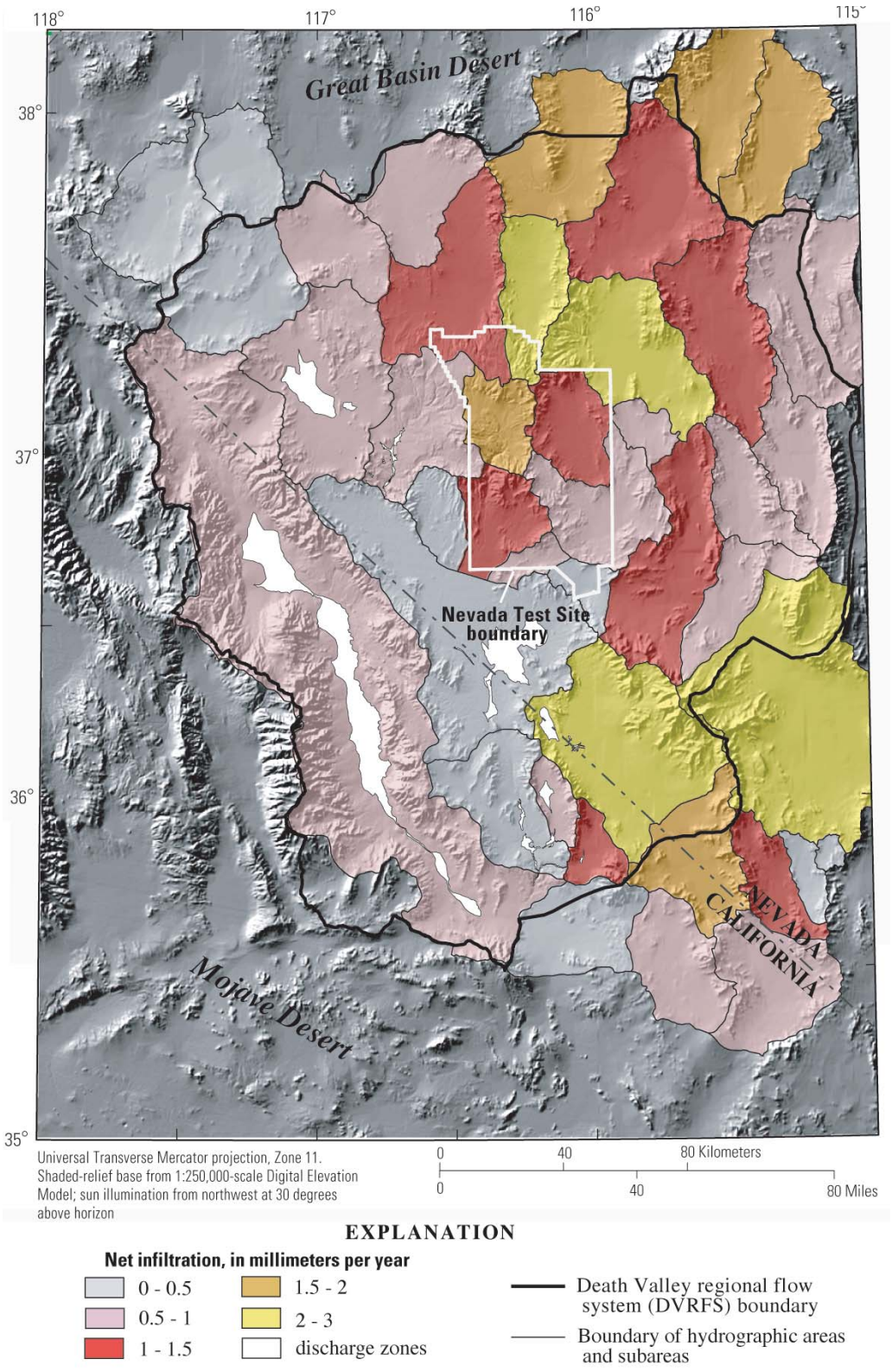

Figure 47. Average net infiltration simulated by INFILv3 model 4 for the 42 hydrographic areas within and adjacent to the Death Valley region, Nevada and California, 1950–99.

Differences in the spatial distribution of basinwide net infiltration between models 1 and 2 indicate areas where the streamflow contribution to net infiltration is important (figs. 44 and 45). For the NTS area, surface-water flow provides a significant contribution to total basinwide net infiltration for Buckboard Mesa (area 227B), which is the northern part of the Fortymile Canyon drainage basin. For Buckboard Mesa, direct (in-place) net infiltration from rain and snowmelt provides an average net-infiltration rate of 2.70 mm/yr (table 22, at back of report, model 2). Total net infiltration increases to 4.04 mm/yr when surface-water contributions are included (table 22 at back of report, model 1), indicating that net infiltration from infiltrating overland flow and streamflow accounts for approximately 33 percent of total net infiltration. For Jackass Flats (the downstream part of the Fortymile Wash drainage basin), net infiltration increases from 1.55 to 2.67 mm/yr, or approximately 42 percent, when infiltration of surface water is included in the root-zone water balance. These results for the Fortymile Wash drainage basin (Buckboard Mesa and Jackass Flats) are qualitatively supported by field studies, which indicate a strong correlation between streamflow in Fortymile Wash, deep infiltration of water beneath the stream channel, and significant increases in the elevation of the water table underlying the stream channel (Savard, 1995, 1998). Other areas where streamflow contributions are relatively high (greater than 20 percent of total net infiltration) include Kawich Valley (32 percent), Groom Lake (34 percent), Death Valley (25 percent), California Valley (35 percent), Jean Lake Valley (31 percent), Valjean Valley (92 percent), and southern Ivanpah Valley (45 percent). Areas where streamflow contributions to net infiltration are very low (less than 5 percent) include Alkali Springs Valley (4 percent), Pahranagat Valley (4 percent), southern Tikapoo Valley (0 percent), northern Three Lake Valley (0 percent), Rock Valley (3 percent), Pahrump Valley (2 percent), and Las Vegas Valley (1 percent).

Comparison of Simulated Net Infiltration with Previous Estimates of Recharge

Using the results obtained for the four net-infiltration models, the three goodness-of-fit statistics applied in the comparison of simulated and measured streamflow were applied to the comparison of net infiltration and previous estimates of recharge for the 42 hydrographic areas. Comparisons were made between basinwide average net infiltration and recharge rates (table 22, at back of report) and between total basinwide net infiltration and recharge volumes (table 23, at back of report). Comparisons involving rates eliminate the dependence of the results on basin area, which tends to greatly improve correlations based on volumes. On the other hand, incorporation of basin area has the affect of giving greater weight to the larger area basins, which also has benefits for analyzing results. For these reasons, both parameters were evaluated.

On the basis of an average estimation error (AEE) value of –0.07, a standardized mean-square error (SMSE) value of 0.61, and a correlation coefficient (CC) value of 0.67, net infiltration rates simulated using INFILv3 model 1 provide the best fit to the recharge rates (fig. 48; table 22, at back of report). Model 2, which does not account for net infiltration associated with streamflow, provides the strongest correlation with estimated recharge, but the SMSE and the absolute values of AEE are higher for model 2 than for model 1. Net infiltration simulated by models 3 and 4 do not compare well with basinwide recharge estimates because they tend to underpredict the recharge rates. All four models show a tendency to overpredict net infiltration relative to recharge for basins that have low recharge rates and to underpredict net infiltration relative to recharge for basins with high recharge rates (fig. 48). The largest underpredictions of net infiltration (using model 1) relative to estimated recharge were for (1) Pahrump Valley (net infiltration of 5.66 mm/yr and recharge estimate of 15.17 mm/yr), (2) Las Vegas Valley (net infiltration of 4.97 mm/yr and recharge of 8.87 mm/yr), (3) southern Three Lakes Valley (net infiltration of 2.05 and recharge of 9.48 mm/yr), (4) Indian Springs Valley (net infiltration of 3.27 mm/yr and recharge of 7.13 mm/yr), and (5) Garden Valley (net infiltration of 3.50 mm/yr compared to recharge of 9.97 mm/yr) (table 22, at back of report). The largest overpredictions of net infiltration (using model 1) relative to recharge were for (1) Chicago Valley (2.49 mm/yr net infiltration and 0.22 mm/yr recharge), (2) Mesquite Valley (3.77 mm/yr net infiltration and 1.68 mm/yr recharge), (3) Frenchman Flat (1.98 mm/yr net infiltration and 0.10 mm/yr recharge), and (4) Rock Valley (2.00 mm/yr net infiltration and 0.17 mm/yr recharge) (table 22, at back of report).

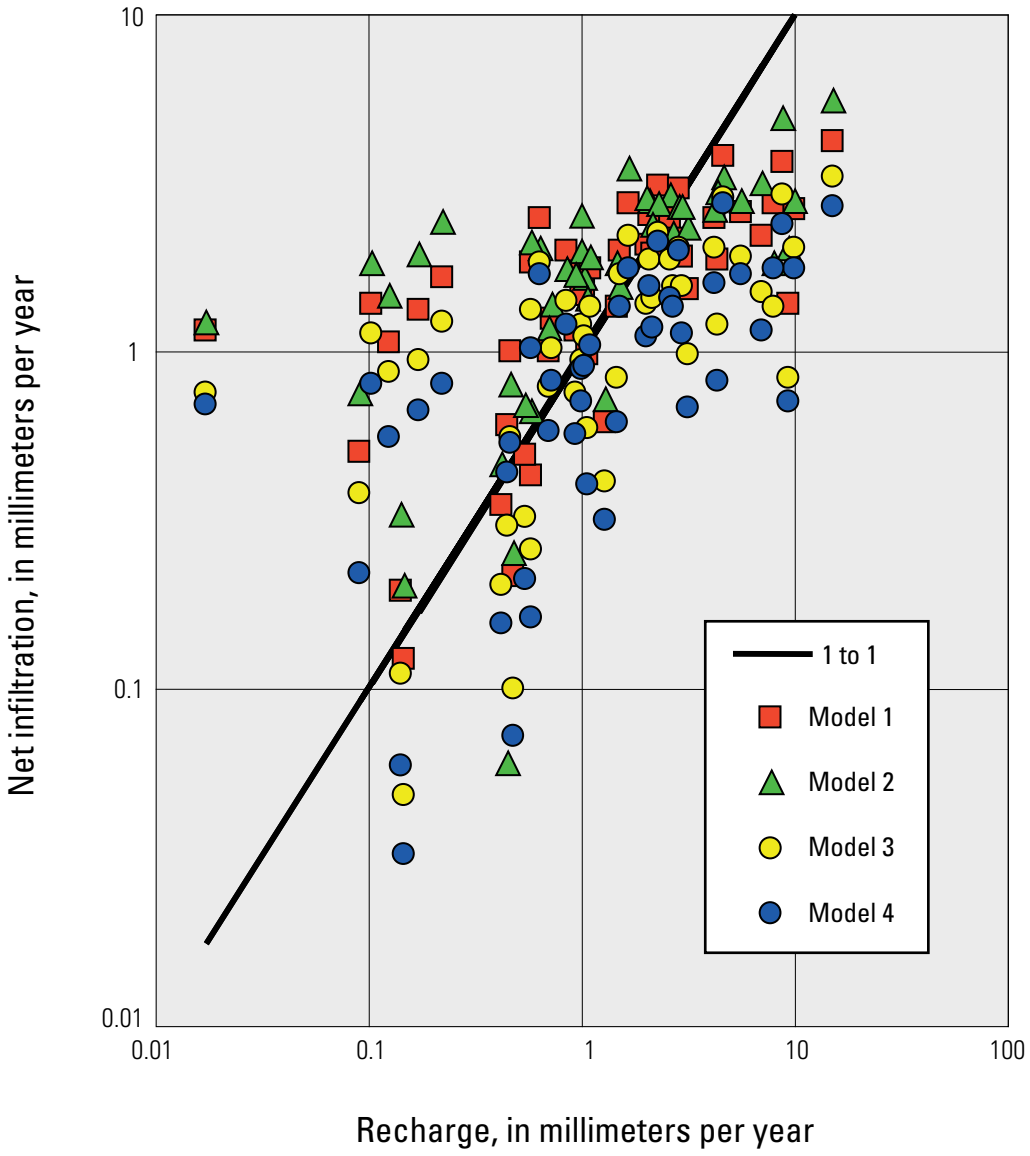

Figure 48. Net infiltration simulated using INFILv3 models 1, 2, 3, and 4 and previous estimates of basinwide recharge rates for hydrographic areas and subareas in the Death Valley region, Nevada and California.

A better match was obtained between simulated net infiltration and estimated recharge volumes (fig. 49) because these results were based on basin area and on the simulated net infiltration and estimated recharge rates. Overall, the simulated net-infiltration volumes are in good agreement with the estimated recharge volumes. In absolute terms, the largest differences between net infiltration and recharge are for Pahrump Valley and Las Vegas Valley (net infiltration volumes are approximately half the estimated recharge volumes) and for Death Valley (net infiltration volume is approximately twice the estimated recharge volume (table 23, at back of report). The simulation results of INFILv3 model 1 indicate that it has the best goodness-of-fit results, with an AEE of –317 m^3/d, a SMSE of 0.18, and a CC of 0.93. Although the SMSE of 0.12 for model 2 is lower than SMSE for model 1, the absolute AEE value is much higher at –2,954 m^3/d. Goodness-of-fit results for models 3 and 4 showed higher SMSE values and absolute AEE values. The CC values for all four models are very similar, ranging from 0.93 to 0.94.

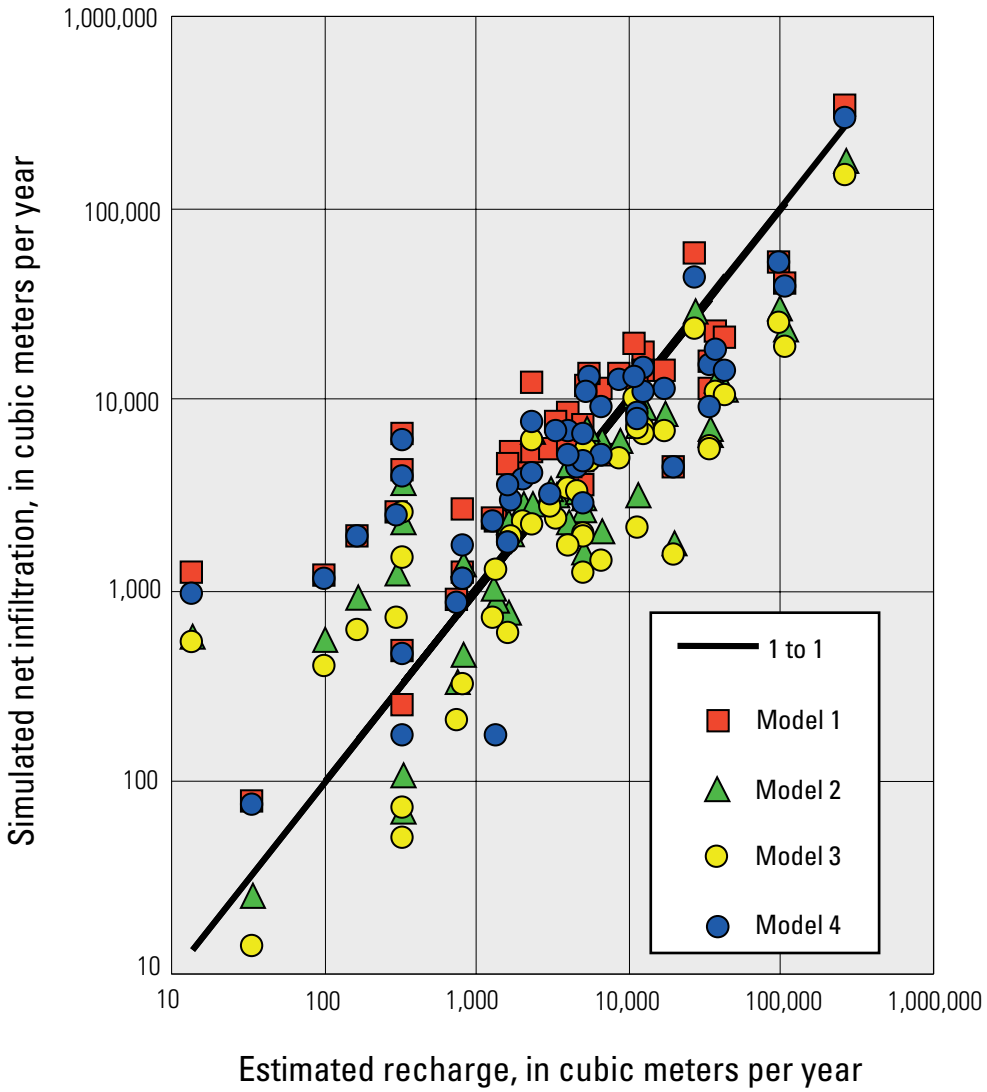

Figure 49. Net infiltration simulated using INFILv3 models 1, 2, 3, and 4 and previous estimates of basinwide recharge volumes for hydrographic areas and subareas in the Death Valley region, Nevada and California.

Comparison of the net-infiltration results for all four models using the sorted recharge estimates indicate that the net-infiltration estimates are a reasonable prediction of recharge; however, some areas have large relative differences, and the model consistently overpredicts the areas of estimated lower recharge volumes while underpredicting the areas of estimated higher recharge volumes (fig. 50). Simulation results for the four net-INFILv3 models show an improved fit to intermediate recharge volumes; (volumes between approximately 2,000 and 10,000 m^3/d).

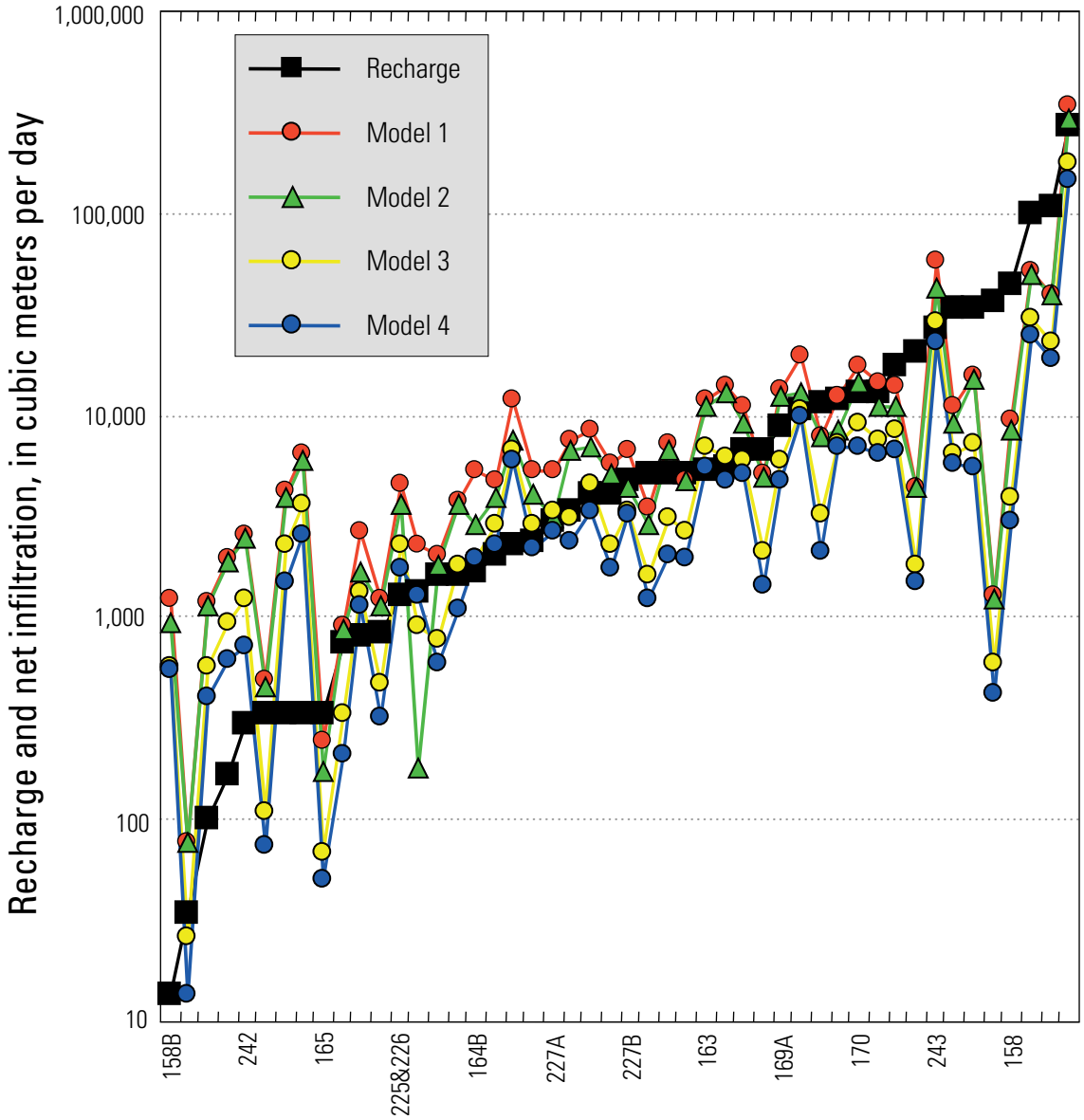

Figure 50. Recharge estimates and net-infiltration rates simulated using the INFILv3 models 1, 2, 3, and 4 for hydrographic areas and subareas in the Death Valley region, Nevada and California.

Model Uncertainty

Although the findings of this study are not sufficient for a rigorous quantification of model uncertainty, the simulation results of the four INFILv3 models were used in a qualitative assessment of model uncertainty. Uncertainty remains high for many critical model inputs such as bedrock permeability, soil thickness, root density as a function of depth, parameters defining stream-channel characteristics, parameters defining monthly spatial distribution models for climate inputs, and coefficients used in modeling potential evapotranspiration (table 3, at back of report). Overall model calibration remains problematic owing to the non-uniqueness of the models, which were fitted to measured streamflow. Constraining calibration results using previous estimates of basinwide recharge provides a higher degree of confidence in the simulated net-infiltration values, especially when combined with calibration results that were based on measured streamflow.

Differences between models 1 and 2 are used to represent uncertainty in net infiltration owing to infiltrated run-on. Uncertainty in infiltrated run-on remains high owing to the high uncertainty in channel characteristics and storm durations; both of these model components have a strong effect on simulated discharge. For the INFILv3 model area, uncertainty in the infiltrated run-on values is approximately ± 15 percent based on the differences between models 1 and 2. However, for the individual hydrographic areas and subareas within the area of the DVRFS, this uncertainty is much higher owing to a presumably greater contribution to net infiltration from surface-water flow. For example, uncertainty in the Fortymile Wash hydrographic area is about ± 40 percent.

Differences between model 1 and models 3 and 4 are more representative of the uncertainty in the inputs that strongly affect direct (in-place) net-infiltration rates. Differences between models 1 and 3 indicate that uncertainty in the net-infiltration results that are due to uncertainty in bedrock hydraulic conductivity may be about ± 50 percent for the area of the DVRFS. Differences between models 1 and 4 indicate that uncertainty in net infiltration owing to the combined uncertainty in bedrock hydraulic conductivity and root density may be about ± 60 percent.

SUMMARY

Spatially distributed estimates of time-averaged net infiltration were simulated for the Death Valley region, which includes the area of the Death Valley regional flow system (DVRFS), using the distributed parameter watershed model INFILv3. The model uses a daily water balance to simulate net infiltration, defined as the downward drainage across the lower boundary of the root zone. The daily water balance accounts for changes in the root-zone water content in response to rainfall, snowmelt, surface-water run-on, evapotranspiration, and net infiltration. Runoff is generated when the root-zone storage capacity is exceeded or when the rainfall, snowmelt, or run-on rate exceeds the soil or bedrock saturated hydraulic conductivity. Surface-water routing takes place when runoff is generated, allowing for the infiltration of surface-water run-on back into the root zone as the routing process moves downstream through the drainage basin.

The root zone is represented using a variable thickness, six-layer system, with the top five layers used to model the root zone in soils and the bottom layer used to model the extension of the root zone into fractured bedrock or to represent the unconsolidated deposits underlying the root zone for locations with thick (greater than 6 m) soils. The thickness of each model layer is dependent on estimated soil thickness. A maximum root-zone depth of 6 m was assumed for all locations that have a soil thickness greater than 6 m, and the thickness of the bedrock layer is set to 0 for all locations with a soil thickness greater than 3 m. For locations with soils less then 3 m thick, the depth to which the root zone is extended into the underlying bedrock ranges from 0 to 3 m, depending on the vegetation type assigned to the location.

Infiltration through the layered root-zone system is simulated using an assumed vertical unit gradient and a 1-dimensional continuous drainage function defined by soil texture data. Daily evapotranspiration from each root-zone layer is simulated as an empirical function of potential evapotranspiration, available root-zone water content, and estimated root densities. Daily potential evapotranspiration is estimated using simulated hourly net radiation and daily air temperature. Net radiation is estimated as a function of simulated incoming solar radiation, daily air temperature, terrain characteristics, and monthly atmospheric parameters.

Model inputs defining drainage basin characteristics, rock properties, soil properties, and root densities were developed using a combination of geographic information system (GIS) applications and FORTRAN routines. The GIS data included digitized maps defining hydrogeologic units, soil types, and vegetation types. A digital elevation model was used to define the model grid, to calculate surface-water flow routing parameters, to estimate shading parameters for modeling potential evapotranspiration, and to model the spatial distribution of climate inputs.

Historical streamflow records from 31 gaging sites were used to develop a composite model calibration based on a simultaneous fit to all records using a consistent set of model parameters across all drainage basins. Model calibration was based on a qualitative and quantitative comparison of the simulated and measured daily and annual hydrographs. A consistent calibration was difficult because of limitations in the daily climate records, estimated stream-channel characteristics, and, in some cases, baseflow contributions to the hydrograph. A set of parameters representing a calibrated model was selected, but was not considered as necessarily being an optimized parameter set.

Daily net infiltration for the area of the INFILv3 model was simulated from 1950 through 1999 using the calibrated model. The 50-year simulation used daily climate records from 132 stations located throughout the southern Nevada and southeastern California region. The time-averaged net-infiltration rate is considered representative of current climate conditions for the area of the Death Valley regional flow system.

The developed estimates of average annual net infiltration provide an indication of the spatial distribution of potential recharge to the Death Valley regional flow system under current climate conditions. Although the general magnitude of the estimated net-infiltration volume is consistent with discharge estimates and the general magnitude of previous basinwide recharge estimates throughout the Death Valley region, significant differences are observed between simulated net infiltration and recharge estimates for some basins. Average annual net infiltration was not as strongly correlated to precipitation as the previous basinwide recharge estimates. On average, the net-infiltration model underestimates higher recharge rates and overestimates lower recharge rates. These differences can be attributed to the many variables incorporated into the net-infiltration estimates, such as soil thickness, root-zone characteristics, and bedrock properties that are not directly accounted for in methods used to estimate basinwide recharge, especially in the case of Maxey–Eakin recharge estimates.

Model results obtained in this study represent a substantial improvement in estimating net infiltration and potential recharge in the Death Valley region compared with the previous model version used in the initial application of a deterministic daily water-balance approach. Model improvements include a better representation of hydrologic processes affecting net infiltration, such as surface-water flow, snowmelt, transpiration, and groundwater drainage in the root zone. The INFILv3 model improvements also include an algorithm for modeling spatially distributed daily precipitation and air temperature using all available daily climate records from a network of 132 historical and existing monitoring sites in and around the Death Valley region. Improvements in representing basin characteristics include the incorporation of available GIS databases for defining soil and vegetation characteristics and the vertical discretization of the root zone into a six-layer system.

If assumptions of steady-state, one-dimensional vertical flow are applied to the unsaturated zone, the net-infiltration estimates can represent the magnitude and spatial distribution of potential recharge for the Death Valley region. Compared to the preliminary estimates of net infiltration obtained using the earlier version of INFIL, results from the updated net-infiltration model, INFILv3, provide an improved representation of potential recharge under current climate conditions. This conclusion is based on (1) a model calibration indicating satisfactory performance in predicting the general timing and magnitude of streamflow recorded in the Death Valley region, (2) a satisfactory model evaluation based on a comparison with basinwide recharge estimates and the estimated overall discharge rate for the Death Valley region, and (3) a qualitative evaluation of the spatially distributed net-infiltration estimates. The uncertainty in the net infiltration estimates as indicators of current climate recharge would likely be reduced if (1) uncertainty in input parameters, such as bedrock permeability, soil properties, and vegetation cover, was reduced; (2) uncertainty in estimates of storm duration and intensity was reduced; (3) uncertainties in parameters used to define stream channel characteristics were reduced; (4) real-time streamflow was routed using both dispersive and convergent flow algorithms; (5) snowfall and snowmelt were simulated using a more detailed energy balance model, and (6) deep percolation through thick unsaturated zones and lateral flow through perched saturated zones were included in the model.

REFERENCES CITED

Avon, Lizanne, and Durbin, T.J., 1994, Evaluation of the Maxey–Eakin method for estimating recharge to ground-water basins in Nevada: American Water Resources Association, Water Resources Bulletin, v. 30, no. 1, p. 99–111.

Beatley, J.C., 1976, Vascular plants of the Nevada Test Site and central-southern Nevada: Ecological and geographical distributions: Springfield, Virginia, U.S. Department of Energy Research and Development Administration Report TID-26881, 308 p.

Bedinger, M.S., Langer, W.H., and Reed, J.E., 1989, Ground-water hydrology, *in* Bedinger, M.S., Sargent, K.A., and Langer, W.H., eds., Studies of geology and hydrology in the Basin and Range Province, southwestern United States, for isolation of high-level radioactive waste—Characterization of the Death Valley region, Nevada and California: U.S. Geological Survey Professional Paper 1370-F, 49 p.

Bowers, J.C., 1990, Potential hazards from floodflows in Grapevine Canyon, Death Valley National Monument, California and Nevada: U.S. Geological Survey Water-Resources Investigations Report 89-4063, 19 p.

Campbell, G.S., 1977, An introduction to environmental biophysics (2d ed.): New York, Springer–Verlag, 159 p.

———1985, Soil physics with BASIC: Transport models for soil plant systems: Amsterdam, The Netherlands, Elsevier, Developments in Soil Science, no. 14, 150 p.

Crippen, J.R., 1965, Natural water loss and recoverable water in mountainous basins of southern California: U.S. Geological Survey Professional Paper 417-E, 24 p.

———1981, Potential hazards from floodflows in Wildrose Canyon, Death Valley National Monument, California and Nevada: U.S. Geological Survey Open-File Report 81-407, 23 p.

D'Agnese, F.A., O'Brien, G.M, Faunt, C.C., Belcher, W.R., San Juan, C. A., 2002, A three-dimensional numerical model of predevelopment conditions in the Death Valley regional ground-water flow system, Nevada and California: U.S. Geological Survey Water-Resources Investigations Report 02-4102, 114 p.

D'Agnese, F.A., O'Brien, G.M., Faunt, C.C., San Juan, C.A., 1999, Simulated effects of climate change on the Death Valley regional ground-water flow system, Nevada and California: U.S. Geological Survey Water-Resources Investigations Report 98-4041, 40 p.

D'Agnese, F.A., Faunt, C.C., Turner, A.K., and Hill, M.C., 1997, Hydrogeologic evaluation and numerical simulation of the Death Valley regional ground-water flow system, Nevada and California: U.S. Geological Survey Water-Resources Investigations Report 96-4300, 124 p.

Daly, C., R.P. Neilson, and D.L. Phillips, 1994, A statistical-topographic model for mapping climatological precipitation over mountainous terrain: Journal of Applied Meteorology, v. 33, p. 140–158.

Davies, J.A., and Allen, C.D., 1973, Equilibrium, potential and actual evaporation from cropped surfaces in southern Ontario: Journal of Applied Meteorology, v. 12, p. 649–657.

de Bruin, H.A.R., 1988, Evaporation in arid and semi-arid regions, *in* Simmers, I., ed., Estimation of natural groundwater recharge: Boston, Reidel Publishing Company, p. 73–88.

Dettinger, M.D., 1989, Reconnaissance estimates of natural recharge to desert basins in Nevada, U.S.A., by using chloride-balance calculations: Journal of Hydrology, v. 106, p. 55–78.

Donovan, D.J., and Katzer, T., 2000, Hydrologic implications of greater ground-water recharge to Las Vegas Valley, Nevada: Journal of the American Water Resources Association, v. 36, no. 5, p. 1133–1148.

Eakin, T.E., 1963, Ground-water appraisal of Garden and Coal Valleys, Lincoln and Nye Counties, Nevada: Nevada Department of Conservation and Natural Resources Reconnaissance Report 18, 29 p.

Eichinger, W.E., Parlange, M.B., and Stricker, H., 1996, On the concept of equilibrium evaporation and the value of the Priestley–Taylor coefficient: Water Resources Research, v. 32, no. 1, p. 161–164.

Faunt, C.C., 1997, Effect of faulting on ground-water movement in the Death Valley region, Nevada and California, U.S. Geological Survey Water-Resources Investigations Report 95-4132, p. 42.

Faunt, C.C., D'Agnese, F.A., and Turner, A.K., 1997, A Hydrogeologic map of the Death Valley region, Nevada and California, developed using GIS techniques, U.S. Geological Survey Water-Resources Investigations Report 95-4016

Flint, A.L., and Childs, S.W., 1987, Calculation of solar radiation in mountainous terrain: Journal of Agricultural and Forest Meteorology, v. 40, p. 233–249.

———1991, Modification of the Priestley–Taylor equation for estimating evapotranspiration for soil water limited conditions: Journal of Agricultural and Forest Meteorology, v. 56, p. 247–260.

Flint, A.L., and Davies, W.J., 1997, Meteorological data for water years 1988–94 from 5 weather stations at Yucca Mountain, Nevada: U.S. Geological Survey Open-File Report 96-462, 31 p.

Flint, A.L., and Flint, L.E., 2000, Near surface infiltration monitoring using neutron moisture logging, Yucca Mountain, Nevada, *in* v. 1, Looney, B.B., and Falta, R.W., eds., Vadose Zone: Science and Technology Solutions: Columbus, OH, Battelle Press, p. 457–474.

Flint, A.L., Flint, L.E., Bodvarsson, G.S., Kwicklis, E.M., and Fabryka–Martin, J.M., 2001a, Evolution of the conceptual model of vadose zone hydrology for Yucca Mountain: Journal of Hydrology, 247(1-2), p. 1–30.

Flint, A.L., Flint, L.E., Bodvarsson, G.S., Kwicklis, E.M., and Fabryka–Martin, J.M., 2001b, Development of the conceptual model of vadose zone hydrology for Yucca Mountain, *in* Hsieh, P.A., Bahr, J.M., Doe, T.W., Flint, A.L., Gee, G.W., Gelhar, Solomon, D.K, van Genuchten, M. Th., and Wheatcraft, S.W., eds., 2001, Conceptual Models of Flow and Transport in the Fractured Vadose Zone: National Academy Press, Washington DC, p. 47–85.

Flint, A.L., Flint, L.E., Hevesi, J.A., D'Agnese, F.A., and Faunt, C.C., 2000, Estimation of regional recharge and travel time through the unsaturated zone in arid climate, *in* Faybishenko, B., Witherspoon, P.a., and Benson, S.M., eds., Dynamics of Fluids in Fractured Rock: American Geophysical Union Monograph 122, p. 115–128.

Flint, A.L., Flint, L.E., Hevesi, J.A., and Hudson, D.B., 2001c, Characterization of Arid Land Infiltration Processes at Yucca Mountain, Nevada, *in* Evans, D.D., Rasmussen, T.C., and Nicholson, T.J., eds., (2nd ed.) Flow and Transport through Unsaturated Fractured Rock: American Geophysical Union, Geophysical Monograph Series, v. 42, p.135–149.

French, R.H., 1983, Precipitation in southern Nevada: Journal of Hydraulic Engineering, v. 109, no. 7, July, p. 1023–1036.

Glancy, P.A., 1968, Water-resources appraisal of Mesquite–Ivanpah Valley area, Nevada and California: Nevada Division of Water Resources Reconnaissance Report 46, 57 p.

Glancy, P.A., 1994, Evidence of prehistoric flooding and the potential for future extreme flooding at Coyote Wash, Yucca Mountain, Nye County, Nevada: U.S. Geological Survey Open-File Report 92-458, 31 p.

Grasso, D.N., 1996, Hydrology of modern and late Holocene lakes, Death Valley, California: U.S. Geological Survey Water-Resources Investigations Report 95-4237, 54 p.

Grayson, D.K., 1993, The desert's past—A natural prehistory of the Great Basin: Washington, D.C., Smithsonian Institution Press, 356 p.

Grose, T.L., and Smith, G.I., 1989, Geology, *in* Bedinger, M.S., Sargent, K.A., and Langer, W.H., eds., Studies of geology and hydrology in the Basin and Range Province, southwestern United States, for isolation of high-level radioactive waste: U.S. Geological Survey Professional Paper 1370-F, p. 5–19.

Harrill, J.R., 1986, Ground-water storage depletion in Pahrump Valley, Nevada–California, 1962–1975; U.S. Geological Survey Water-Supply Paper 2279, 53 p.

Harrill, J.R., and Prudic, D.E., 1998, Aquifer systems in the Great Basin region of Nevada, Utah and adjacent states—Summary Report: U.S. Geological Survey Professional Paper 1409,66p.

Harrill, J.R., Gates, J.S., and Thomas, J.M., 1988, Major Ground-water flow systems in the Great Basin Region of Nevada, Utah, and adjacent states: U.S. Geological Survey Hydrologic Investigations Atlas HA-694-C, 2 sheets.

Hatton, T.J., 1998, Catchment scale recharge modeling, Part 4, *in* The Basics of Recharge and Discharge: CSIRO Publishing, Collingwood, Victoria, Australia, 19 p.

Hevesi, J.A., 2001, Simulation of net infiltration for modern and potential future climates: Analysis and Model Report ANL-NBS-HS-000032, Office of Civilian Radioactive Waste Management, Las Vegas, Nevada, 89p.

Hevesi, J.A., and Flint, A.L., 1998, Geostatistical estimates of future recharge for the Death Valley Region, *in* High Level Radioactive Waste Management, Proceedings of the Ninth Annual International Conference, Las Vegas, Nev., May 11-15, 1998: LaGrange Park, Ill., American Nuclear Society, p. 173–177.

Hevesi, J.A., Flint, A.L., and Flint, L.E., 2002, Preliminary estimates of spatially distributed net infiltration and recharge for the Death Valley region, Nevada-California: U.S. Geological Survey Water Resources Investigations Report 02-4010, 36 p.

Hevesi, J.A., Flint, A.L., and Istok, J.D., 1991, Precipitation estimation in mountainous terrain using multivariate geostatistics—II. Isohyetal maps: Journal of Applied Meteorology, v. 31, no. 7, p. 677–688.

Houghton, J.G., 1969, Characteristics of rainfall in the Great Basin: University of Nevada, Reno, Desert Research Institute, 205 p.

Hunt, C.B., Robinson, T.W., Bowles, W.A., and Washburn, A.L., 1966, Hydrologic basin, Death Valley, California: U.S. Geological Survey Professional Paper 494-B, 138 p.

Jury, W.A., Gardner, W.R., and Gardner, W.H., 1991, Soil Physics, 5th edition; John Wiley and Sons, Inc., 328 p.

Justus, P.S., and Stablein, N.K., 1989, Geoscientists help make 10,000-year decisions--U.S. Nuclear Regulatory Commission: Geotimes, January, p. 14–15.

Kirk, S.T., and Campana, M.E., 1990, A deuterium-calibrated ground-water flow model of a regional carbonate-alluvial system: Journal of Hydrology 119, p. 357–388.

LeCain, G.D., Lu, N., Kurzmack, M., 2002, Use of temperature, pressure, and water potential data to estimate infiltration and monitor percolation in Pagany Wash associated with the winter of 1997–98 El Nino precipitation, Yucca Mountain, Nevada: U.S. Geological Survey Water-Resources Investigations Report 02-4035, 31 p.

Lichty, R.W., and McKinley, P.W., 1995, Estimates of ground-water recharge rates for two small basins in central Nevada: U.S. Geological Survey Water-Resources Investigations Report 94-4104, 31 p.

Maidment, D.R., 1993, Handbook of Hydrology, McGraw-Hill, Inc, 889 p.

Malmberg, G.T., and Eakin, T.E., 1962, Ground-water appraisal of Sarcobatus Flat and Oasis Valley, Nye and Esmeralda Counties, Nevada: Nevada Department of Conservation and Natural Resources Ground-Water Resources Reconnaissance Report 10, 39 p.

Mantua, N.J., Hare, S.R., Zhang, Y., Wallace, J.M., and Francis, R.C., 1997, A Pacific interdecadal climate oscillation with impacts on Salmon production: Bulletin of the American Meteorological Society, v. 78, p. 1069–1079.

Maxey, G.B., and Eakin, T.E., 1950, Ground water in White River Valley, White Pine, Nye, and Lincoln Counties, Nevada: Nevada State Engineer, Water Resources Bulletin no. 8, 59 p.

Miller, G.A., 1977, Appraisal of the water resources of Death Valley, California–Nevada: U.S. Geological Survey Open-File Report 77-728, 68 p.

Munz, P.A., 1974, A flora of southern California: Berkeley, University of California Press, 1086 p.

Murray, Michael, 1997, Western cover type classification: U.S. Geological Survey, Gap Analysis Program data available on Web, accessed August 16, 2000, at http://www.gap.uidaho.edu/RegionalGAP/regionalftp.htm

Nichols, W.D., 1987, Geohydrology of the unsaturated zone at the burial site for low level radioactive waste near Beatty, Nye County, Nevada: U.S. Geological Survey Water-Supply Paper 2312, 52 p.

Peterson, F.F., 1981, Landforms of the Basin and Range province defined for soil survey: Reno, University of Nevada, Nevada Agricultural Bulletin no. 28, 53 p.

Philander, S.G., 1990, El Nino, La Nina, and the Southern Oscillation: Academic Press, Inc., New York, 291 p.

Priestley, C.H.B., and Taylor, R.J., 1972, On the assessment of surface heat flux and evaporation using large-scale parameters: Manual Weather Review, v. 100, p. 81–92.

Pyke, C.W., 1972, Some meteorological aspects of the seasonal distribution of precipitation in the Western United States and Baja California: University of California, Water Resources Center Contribution 139, 205 p.

Quiring, R.F., 1965, Annual precipitation amount as a function of elevation in Nevada south of 38-1/2 latitude, Las Vegas, Nevada: U.S. Weather Bureau Research Statistics, 14 p.

Rush, F.E., 1968, Water-resources appraisal of Clayton Valley–Stonewall Flat area, Nevada and California: Nevada Department of Conservation and Natural Resources Water Reconnaissance Report 45. 54 p.

———1971, Regional ground-water systems in the Nevada Test Site area, Nye, Lincoln, and Clark Counties, Nevada: Nevada Division of Water Resources Reconnaissnace Report 54, 25 p.

Savard, C.S, 1995, Selected Hydrologic Data from Fortymile Wash in the Yucca Mountain Area, Nevada, Water Year 1992: U.S. Geological Survey Open-File Report 94-317,

———1998, Estimated ground-water recharge from streamflow in Fortymile wash near Yucca Mountain, Nevada, U.S. Geological Survey Water-Resources Investigations Report 97-4273.

Schmidt, K.M, and Webb, R.H., 2001, Researchers consider U.S. Southwest's response to warmer, drier conditions, EOS Transactions, American Geophysical Union, v. 82, no. 41, p. 475-478.

Scott, B.R., Smales, T.J., Rush, F.E., and Van Denlburgh, A.S., 1971, Nevada's Water Resources: Nevada Division of Water Resources, Water for Nevada Report 3, 87 p.

Stannard, D.I., 1993, Comparison of Penman-Monteith, Shuttleworth-Wallace, and the modified Priestley–Taylor evapotranspiration models for wildland vegetation in semi-arid rangelands: Water Resources Research, v. 29, no. 5, p. 1379–1392.

Stewart, R.B., and Rouse, W.R., 1977, Substantiation of the Priestley and Taylor parameter =1.26 for potential evaporation in high latitudes: Journal of Applied Meteorology, v. 16, p. 649–s650.

Turner, A.K., D'Agnese, F.A., and Faunt, C.C., 1996, Digital elevation model (DEM) file of topographic elevations for the Death Valley region of southern Nevada and southeastern California processed from U.S. Geological Survey 1-degree digital elevation model data files: U.S. Geological Survey Open-File Report 95-287, 9 p.Wl

U.S. Department of Agriculture, 1994, State Soil Geographic (STATSGO) Data Base--Data use information, Misc. Pub. no. 1492.

Van Denburgh, A.S., and Rush, F.E., 1974, Water-resources appraisal of Railroad and Penoyer Valleys, east–central Nevada: Nevada Division of Water Resources Reconnaissance Report 60, 61 p.

Walker, G.E., and Eakin, T.E., 1963, Geology and ground water of Amargosa Desert, Nevada–California: Nevada Department of Conservation and Natural Resources Reconnaissance Report 14, 45 p.

Watson, P., Sinclair, P., and Waggoner, R., 1976, Quantitative evaluation of a method for estimating recharge to the desert basins of Nevada: Journal of Hydrology, v. 31, p. 335–357.

Winograd, I.J., Riggs, A.C., and Coplen, T.B., 1998, The relative contributions of summer and cool-season precipitation to groundwater recharge, Springs Mountains, Nevada, Hydrogeology Journal, v. 6, p. 77–93.

Winograd, I.J., 1981, Radioactive waste disposal in thick unsaturated zones: Science, v. 212, no. 4502, p. 1457–1464.

Winograd, I.J., and Thordarson, William, 1975, Hydrogeologic and hydrochemical framework, south-central Great Basin, Nevada–California, with special reference to the Nevada Test Site: U.S. Geological Survey Professional Paper 712-C, 126 p.

Table 2. Soil texture attributes and developed inputs to the INFILv3 model of the Death Valley region, Nevada and California

[Soil texture attributes developed for each map unit (MUID) of the digital elevation model (DEM) using State Soil Geographic (STATSGO) data. m, meter; mm/d, millimeter per day)

Soil type map code	STATSGO MUID code	Number of soil components	Soil texture attributes for MUIDs (weighted averages for sequences and layers)							Developed inputs (average values for soil layers)				
			Number of soil layers	Percent rock	Percent coarse sand, gravel, cobbles and boulders	Percent material finer than gravel	Grain size classes as a percentage of all material finer than gravel			Soil thickness (SOILTHCK) (m)	Porosity (SPOR) (dimensionless)	Wilting point (SWP) (dimensionless)	Drainage curve coefficient (SOILB)	Saturated hydraulic conductivity (SKS) (mm/d)
							Sand	Silt	Clay					
1	NV326	14	3	1	60	39	73	19	8	1.46	0.381	0.014	3.70	950
2	NV329	18	3	21	48	31	52	32	16	.24	.429	.041	3.70	341
3	NV307	20	3	27	47	26	50	31	19	.28	.435	.042	5.85	294
4	NV324	21	3	1	59	40	69	20	11	1.52	.393	.021	6.30	758
5	NV303	18	3	2	60	38	67	22	11	1.46	.403	.022	4.31	710
6	NV301	21	2	3	27	70	56	28	16	1.48	.401	.068	4.38	392
7	NV506	7	3	0	22	78	75	19	6	1.37	.397	.021	5.71	1,104
8	NV501	14	3	17	56	27	49	33	18	.38	.436	.039	3.29	287
9	NV224	7	2	3	63	34	47	34	19	.11	.441	.044	6.27	263
10	NV519	13	4	18	40	42	60	26	14	1.15	.415	.042	6.44	481
11	NV524	7	3	14	54	32	47	35	18	.21	.436	.045	5.23	266
12	NV523	19	4	7	44	49	65	22	13	1.40	.404	.036	6.32	612
13	NV521	12	2	0	15	85	50	33	17	1.54	.406	.087	4.77	317
14	NV388	12	3	0	11	89	45	37	18	1.54	.408	.104	5.97	243
15	NV514	14	4	4	44	52	65	23	12	1.47	.397	.035	6.45	620
16	NV500	21	3	21	50	29	40	41	18	.68	.472	.052	4.70	210
17	NV522	10	3	21	52	27	46	37	17	.47	.455	.041	6.55	271
18	NV508	12	2	1	12	87	42	42	16	1.50	.424	.102	6.17	234
19	NV313	12	4	20	36	44	54	33	13	.98	.401	.046	6.21	410
20	NV 25	15	4	26	34	40	48	36	17	1.03	.399	.056	5.28	289

Table 2. Soil texture attributes and developed inputs to the INFILv3 model of the Death Valley region, Nevada and California—Continued

Soil type map code	STATSGO MUID code	Number of soil components	Soil texture attributes for MUIDs (weighted averages for sequences and layers)							Developed inputs (average values for soil layers)				
			Number of soil layers	Percent rock	Percent coarse sand, gravel, cobbles and boulders	Percent material finer than gravel	Grain size classes as a percentage of all material finer than gravel			Soil thickness (SOILTHCK) (m)	Porosity (SPOR) (dimension-less)	Wilting point (SWP) (dimension-less)	Drainage curve coefficient (SOILB)	Saturated hydraulic conductivity (SKS) (mm/d)
							Sand	Silt	Clay					
21	NV317	9	3	14	33	53	69	19	12	1.03	0.403	0.036	6.05	727
22	NV 99	7	4	0	34	66	58	28	14	1.52	.416	.057	4.46	447
23	NV311	15	2	3	63	33	51	37	12	.23	.454	.032	5.32	383
24	NV308	18	3	13	59	28	49	31	20	.20	.435	.040	5.22	272
25	NV175	17	3	14	49	37	42	32	26	.43	.450	.070	6.52	173
26	NV244	21	4	8	49	43	47	36	17	1.39	.413	.051	7.72	274
27	NV306	13	2	1	58	41	69	21	10	1.49	.376	.020	6.15	772
28	NV507	10	3	16	47	37	40	38	22	.91	.434	.063	4.18	181
29	NV510	11	4	13	34	53	65	23	12	1.23	.405	.038	7.22	635
30	NV325	20	4	11	50	39	64	24	11	1.30	.406	.027	4.60	631
31	NV302	8	3	0	4	96	42	36	22	1.52	.437	.136	4.58	194
32	NV 26	17	3	2	6	92	32	43	25	1.50	.438	.152	7.10	125
33	NV233	5	2	4	62	34	51	37	12	.19	.450	.033	7.84	367
34	NV314	19	3	14	52	35	55	28	17	.24	.439	.041	5.33	380
35	NV312	16	3	17	51	32	41	40	19	.27	.443	.051	5.76	205
36	NV526	6	2	0	0	100	10	39	51	1.52	.365	.220	6.69	24
37	NV511	8	3	13	53	34	48	32	20	.54	.445	.051	13.70	255
38	NV315	14	3	15	54	31	65	23	12	.19	.422	.024	6.63	643
39	NV236	7	2	1	61	38	49	28	24	.25	.448	.056	4.58	238
40	NV221	15	4	14	30	56	63	23	15	1.36	.400	.050	7.15	533

Table 2. Soil texture attributes and developed inputs to the INFILv3 model of the Death Valley region, Nevada and California—Continued

Soil type map code	STATSGO MUID code	Number of soil components	Soil texture attributes for MUIDs (weighted averages for sequences and layers)							Developed inputs (average values for soil layers)				
			Number of soil layers	Percent rock	Percent coarse sand, gravel, cobbles and boulders	Percent material finer than gravel	Grain size classes as a percentage of all material finer than gravel			Soil thickness (SOILTHCK) (m)	Porosity (SPOR) (dimension-less)	Wilting point (SWP) (dimension-less)	Drainage curve coefficient (SOILB)	Saturated hydraulic conductivity (SKS) (mm/d)
							Sand	Silt	Clay					
41	NV223	4	3	0	29	71	52	31	17	1.22	0.413	0.072	5.13	341
42	NV310	16	3	30	44	26	62	23	15	.23	.418	.030	5.91	521
43	NV230	13	3	6	60	34	51	26	23	.44	.437	.049	5.18	260
44	NV 98	5	3	4	7	88	43	35	22	1.32	.386	.116	7.00	202
45	NV309	16	3	23	45	31	43	31	26	.52	.460	.067	7.12	183
46	NV231	13	3	8	25	68	49	37	14	1.13	.414	.069	7.65	333
47	NV305	13	4	24	43	32	63	24	13	1.08	.404	.031	5.58	559
48	NV304	17	3	7	52	41	65	25	10	1.44	.381	.024	4.95	673
49	NV238	3	4	18	29	53	72	22	7	.88	.372	.020	4.35	963
50	NV316	7	3	3	51	46	61	26	13	1.46	.397	.034	3.53	531
51	NV204	8	2	2	74	24	45	43	12	.38	.480	.026	4.93	306
52	NV242	7	2	1	23	76	58	34	8	1.36	.381	.041	5.47	567
53	NV200	7	2	5	38	57	41	42	17	.40	.464	.080	4.34	219
54	NV213	7	3	41	11	48	66	25	9	.66	.411	.041	6.41	732
55	NV513	10	3	17	60	23	43	40	16	.30	.459	.035	4.13	248
56	NV237	8	3	22	56	23	60	27	13	.45	.427	.023	6.19	505
57	NV512	14	4	9	36	55	64	24	12	1.32	.405	.039	5.05	613
58	CA783	18	3	2	60	38	67	22	11	1.46	.403	.022	4.64	710
59	NV205	9	3	7	54	39	59	31	10	.78	.382	.025	4.38	548
60	CA738	17	3	17	46	38	57	29	15	.36	.376	.036	4.59	426

Table 2. Soil texture attributes and developed inputs to the INFILv3 model of the Death Valley region, Nevada and California—Continued

Soil type map code	STATSGO MUID code	Number of soil components	Soil texture attributes for MUIDs (weighted averages for sequences and layers)							Developed inputs (average values for soil layers)				
			Number of soil layers	Percent rock	Percent coarse sand, gravel, cobbles and boulders	Percent material finer than gravel	Grain size classes as a percentage of all material finer than gravel			Soil thickness (SOILTHCK) (m)	Porosity (SPOR) (dimension-less)	Wilting point (SWP) (dimension-less)	Drainage curve coefficient (SOILB)	Saturated hydraulic conductivity (SKS) (mm/d)
							Sand	Silt	Clay					
61	CA784	8	3	0	4	96	42	36	22	1.52	0.437	0.136	5.40	194
62	NV536	17	3	19	49	31	36	43	21	.77	.479	.063	7.10	159
63	CA780	21	3	16	39	45	75	18	7	.37	.404	.016	7.22	1,080
64	CA905	15	1	43	36	21	59	32	9	.27	.398	.021	3.40	566
65	CA782	19	3	14	52	35	55	28	17	.24	.439	.041	4.43	380
66	CA744	19	3	11	41	49	63	25	12	1.29	.388	.036	5.76	576
67	CA785	14	3	15	54	31	65	23	12	.19	.422	.024	4.77	643
68	CA750	17	3	12	53	35	45	38	17	.42	.422	.046	4.58	261
69	CA786	17	3	7	52	41	65	25	10	1.44	.381	.024	6.21	673
70	NV202	8	3	4	64	32	55	31	14	.88	.406	.029	4.35	412
71	CA740	13	2	1	58	40	79	14	6	1.51	.368	.009	5.37	1,278
72	CA741	9	2	1	53	46	73	20	8	1.48	.366	.015	3.12	964
73	CA751	19	3	8	62	30	55	30	15	1.08	.379	.028	3.63	402
74	CA787	16	3	30	44	26	62	23	15	.23	.418	.030	5.52	521
75	NV381	5	2	0	9	91	51	30	19	1.52	.384	.095	5.18	302
76	CA788	20	3	27	47	26	50	31	19	.28	.435	.042	6.33	294
77	NV215	3	3	6	72	21	60	24	15	.90	.391	.019	6.30	478
78	CA909	17	1	35	29	36	67	22	11	.33	.387	.030	5.36	709
79	CA739	9	2	24	47	29	62	23	15	.43	.387	.029	4.38	529
80	NV543	17	1	35	29	36	67	22	11	.33	.387	.030	5.15	709

Table 2. Soil texture attributes and developed inputs to the INFILv3 model of the Death Valley region, Nevada and California—Continued

Soil type map code	STATSGO MUID code	Number of soil components	Soil texture attributes for MUIDs (weighted averages for sequences and layers)							Developed inputs (average values for soil layers)				
			Number of soil layers	Percent rock	Percent coarse sand, gravel, cobbles and boulders	Percent material finer than gravel	Grain size classes as a percentage of all material finer than gravel			Soil thickness (SOILTHCK) (m)	Porosity (SPOR) (dimension-less)	Wilting point (SWP) (dimension-less)	Drainage curve coefficient (SOILB)	Saturated hydraulic conductivity (SKS) (mm/d)
							Sand	Silt	Clay					
81	NV387	11	2	5	63	32	55	31	14	1.08	0.414	0.030	4.38	411
82	CA902	12	3	2	67	31	74	19	6	1.50	.369	.009	5.40	1,063
83	NV539	12	3	2	67	31	74	19	6	1.50	.369	.009	3.38	1,063
84	NV394	21	4	27	39	34	63	26	11	.76	.387	.028	3.38	607
85	CA906	16	3	17	51	32	41	40	19	.27	.443	.051	4.58	205
86	NV389	19	2	6	61	33	68	23	9	1.43	.388	.016	6.69	784
87	CA910	20	3	16	30	54	68	23	9	.95	.370	.027	4.03	795
88	NV390	5	3	33	51	16	55	36	9	.23	.411	.016	4.00	482
89	NV396	13	3	0	31	69	46	41	13	1.52	.408	.066	4.65	301
90	CA935	6	2	1	64	35	83	14	3	1.45	.343	.003	5.62	1,630
91	CA743	9	3	12	50	38	57	28	15	.35	.399	.037	2.52	428
92	NV544	15	1	43	36	21	59	32	9	.27	.398	.021	5.47	566
93	CA761	7	2	5	48	48	67	23	11	1.50	.356	.025	4.43	703
94	CA742	6	4	3	5	91	54	32	14	1.36	.378	.078	4.35	389
95	NV545	12	2	0	53	47	80	16	4	1.60	.370	.007	5.45	1,388
96	NV216	2	2	4	56	40	51	33	16	.31	.458	.046	2.82	338
97	CA923	6	2	0	0	100	14	37	49	1.53	.360	.207	5.77	30
98	NV385	14	3	17	46	37	56	33	12	1.07	.429	.036	12.87	447
99	CA901	12	2	0	53	47	80	16	4	1.60	.370	.007	5.04	1,388
100	CA921	14	2	0	18	82	84	13	4	1.53	.354	.008	2.82	1,638

Table 2. Soil texture attributes and developed inputs to the INFILv3 model of the Death Valley region, Nevada and California—Continued

Soil type map code	STATSGO MUID code	Number of soil components	Soil texture attributes for MUIDs (weighted averages for sequences and layers)							Developed inputs (average values for soil layers)				
			Number of soil layers	Percent rock	Percent coarse sand, gravel, cobbles and boulders	Percent material finer than gravel	Grain size classes as a percentage of all material finer than gravel			Soil thickness (SOILTHCK) (m)	Porosity (SPOR) (dimension-less)	Wilting point (SWP) (dimension-less)	Drainage curve coefficient (SOILB)	Saturated hydraulic conductivity (SKS) (mm/d)
							Sand	Silt	Clay					
101	NV393	14	4	15	40	45	59	32	9	1.36	0.388	0.031	2.55	547
102	CA760	18	2	3	53	44	68	21	11	1.49	.362	.022	4.51	729
103	CA650	7	2	0	2	98	17	36	47	1.52	.358	.197	4.33	36
104	CA765	8	4	0	21	79	70	19	10	1.57	.359	.035	12.26	809
105	CA917	14	1	25	46	29	47	38	14	.30	.468	.043	4.13	303
106	CA767	8	4	0	6	94	54	27	18	1.59	.400	.097	5.76	349
107	NV392	5	4	5	34	61	45	36	20	1.51	.429	.081	6.09	233
108	CA764	10	4	1	25	74	76	18	6	1.70	.330	.015	6.63	1,169
109	NV384	14	4	4	24	73	37	39	24	1.38	.430	.114	3.18	156
110	NV383	10	3	7	7	87	28	43	29	1.35	.430	.166	7.54	94
111	CA937	10	3	7	7	87	28	43	29	1.35	.430	.166	8.69	94
112	NV209	11	3	21	33	46	57	31	12	.82	.418	.044	8.69	482
113	CA911	20	2	16	21	63	68	22	10	.79	.377	.037	4.93	740
114	CA916	19	1	30	40	30	58	28	14	.36	.414	.035	4.23	471
115	CA907	18	1	49	25	25	65	26	9	.19	.360	.022	5.17	715
116	NV212	9	2	3	15	83	39	41	21	1.37	.437	.120	4.13	181
117	NV538	7	2	0	2	98	17	36	47	1.52	.358	.197	7.01	36
118	CA334	15	3	9	28	64	80	14	6	.81	.401	.014	12.26	1,362
119	NV210	11	2	9	48	43	62	29	9	1.31	.415	.027	2.98	630
120	NV211	9	3	7	4	90	35	46	19	1.33	.425	.130	4.30	167

Table 2. Soil texture attributes and developed inputs to the INFILv3 model of the Death Valley region, Nevada and California—Continued

Soil type map code	STATSGO MUID code	Number of soil components	Soil texture attributes for MUIDs (weighted averages for sequences and layers)							Developed inputs (average values for soil layers)				
			Number of soil layers	Percent rock	Percent coarse sand, gravel, cobbles and boulders	Percent material finer than gravel	Grain size classes as a percentage of all material finer than gravel			Soil thickness (SOILTHCK) (m)	Porosity (SPOR) (dimension-less)	Wilting point (SWP) (dimension-less)	Drainage curve coefficient (SOILB)	Saturated hydraulic conductivity (SKS) (mm/d)
							Sand	Silt	Clay					
121	CA913	15	1	56	17	27	69	21	10	0.21	0.367	0.028	6.91	780
122	NV218	10	3	13	59	28	69	22	9	1.27	.391	.014	4.13	821
123	NV220	7	2	1	71	28	57	36	8	.33	.404	.017	3.97	535
124	NV229	8	2	4	64	32	63	27	10	1.12	.410	.020	4.40	625
125	CA635	21	5	1	16	83	69	21	10	1.56	.355	.037	4.42	772
126	CA922	15	3	0	50	50	77	15	8	1.63	.359	.014	4.17	1,091
127	CA388	8	2	29	9	62	81	15	4	.80	.364	.012	3.51	1,464
128	CA927	12	3	7	43	50	59	26	15	1.53	.443	.051	2.74	449
129	CA919	14	3	27	18	55	63	24	13	.41	.373	.048	5.43	578
130	NV222	5	4	31	43	26	60	23	17	.47	.403	.035	4.81	440
131	CA930	17	3	2	57	41	72	20	8	1.53	.364	.014	5.71	930
132	CA931	19	4	0	28	72	78	17	5	1.53	.352	.013	3.71	1,284
133	CA339	13	3	4	12	84	56	26	18	1.51	.367	.080	3.00	372
134	NV227	11	2	7	18	75	55	34	12	1.46	.401	.062	5.96	433
135	NV217	9	3	2	20	78	59	27	14	1.52	.439	.069	5.06	478
136	CA934	11	2	7	18	75	55	34	12	1.46	.401	.062	5.20	433
137	NV226	8	4	10	52	39	56	31	13	1.16	.394	.035	5.06	426
138	NV228	6	3	1	68	31	46	28	27	.48	.440	.049	5.28	195
139	CA933	9	3	2	20	78	59	27	14	1.52	.439	.069	7.70	478
140	CA932	8	4	10	52	39	56	31	13	1.16	.394	.035	5.20	426

Table 2. Soil texture attributes and developed inputs to the INFILv3 model of the Death Valley region, Nevada and California—Continued

Soil type map code	STATSGO MUID code	Number of soil components	Soil texture attributes for MUIDs (weighted averages for sequences and layers)							Developed inputs (average values for soil layers)				
			Number of soil layers	Percent rock	Percent coarse sand, gravel, cobbles and boulders	Percent material finer than gravel	Grain size classes as a percentage of all material finer than gravel			Soil thickness (SOILTHCK) (m)	Porosity (SPOR) (dimension-less)	Wilting point (SWP) (dimension-less)	Drainage curve coefficient (SOILB)	Saturated hydraulic conductivity (SKS) (mm/d)
							Sand	Silt	Clay					
141	NV542	14	3	27	18	55	63	24	13	0.41	0.373	0.048	5.28	578
142	CA389	9	2	38	19	43	60	23	17	.40	.360	.055	4.81	460
143	CA926	19	3	18	49	33	56	28	16	.20	.439	.041	5.56	386
144	CA341	12	2	30	15	56	65	22	13	.51	.380	.050	5.73	607
145	CA340	8	5	3	21	76	69	18	13	1.46	.357	.041	4.79	722
146	CA643	14	3	20	14	66	66	22	12	.79	.369	.045	4.53	671
147	CA651	14	4	2	13	84	72	17	10	1.55	.360	.036	4.51	875
148	CA920	13	2	0	10	90	84	13	3	1.52	.352	.008	4.03	1,677
149	CA918	15	3	13	60	27	54	31	15	.48	.463	.032	2.46	377

Table 3. Summary of input parameters used in the INFILv3 model of the Death Valley region, Nevada and California

[Source data: DEM, digital-elevation model; STATSGO, State Soil Geographic database; GAP, Gap Analysis Program, Biological Resources; NOAA, National Oceanic and Atmospheric Administration; NCDC, National Climatic Data Center; GIS, geographic information system; NWS, National Weather Service. Parameter name: r, row; c, column. Parameter units: m, meter; u, unitless; dd, decimal degrees; d, degree; mm/d, millimeter per day; cm, centimeter; mm; millimeter; na, not applicable]

Source data	Preprocessing routines	Input file	Parameter name	Parameter description	Parameter use	Parameter units	Parameter accuracy
DEM and topographic parameters developed using the DEM							
DEM	GIS calculated	Watershed file	ELEV(r,c)	Land-surface elevation	Potential evapotranspiration, spatial interpolation models	m	High
		Watershed file	SLP(r,c)	Land-surface slope	Potential evapotranspiration, streamflow routing	u	High
		Watershed file	ASP(r,c)	Land-surface aspect	Potential evapotranspiration	u	High
		Watershed file	EAST(r,c)	DEM grid cell east–west coordinate	Grid cell location, spatial interpolation models	m	High
		Watershed file	NORTH(r,c)	DEM grid cell east–west coordinate	Grid cell location, spatial interpolation models	m	High
		Watershed file	LAT(r,c)	DEM grid cell latitude	Potential evapotranspiration	dd	High
		Watershed file	LON(r,c)	DEM grid cell latitude	Potential evapotranspiration	dd	High
	SKYVIEW calculated	Watershed file	RIDGE(r,c,36)	36 blocking ridge angles	Potential evapotranspiration	d	Medium
		Watershed file	SKYVIEW(r,c)	Reduction in total skyview	Potential evapotranspiration	u	Medium
	GRDSORT01 calculated	Watershed file	LOCID(r,c)	Location identifier for upstream cell	Streamflow routing	u	Medium
	ROUTER03 calculated	Watershed file	IROUT(r,c)	Location identifier for downstream cell	Streamflow routing	u	Medium
		Watershed file	UPCELLS(r,c)	Number of upstream cells	Streamflow routing	u	Medium
Soil properties associated with the STATSGO database							
STATSGO	GIS	Watershed file	SOILTYPE(r,c)	Map code for STATSGO soil units	Spatial distribution of soil properties	u	Medium
	STATSGO34	Watershed file	SOILTHCK(r,c)	Estimated soil thickness for root zone	Root-zone layer thickness	m	Low
		Soil attribute table	SPOR(soiltype)	Soil porosity	Root-zone storage capacity	u	Medium
		Soil attribute table	SWP(soiltype)	Wilting point	Root-zone storage capacity, evapotranspiration model	u	Medium
		Soil attribute table	SKS(soiltype)	Soil saturated hydraulic conductivity	Root-zone infiltration and drainage function	mm/d	Medium
		Soil attribute table	SOILB(soiltype)	Soil drainage function coefficient	Root-zone infiltration and drainage function	u	Medium
Bedrock and deep alluvium properties associated with the digital map of hydrogeologic units							
Faunt and others (1997)	GIS	Watershed file	ROCKTYPE(r,c)	Map code for hydrogeologic units	Spatial distribution of bedrock and deep properties	u	Medium
User defined		Bedrock attribute table	RKPOR(rocktype)	Effective root-zone porosity for bedrock layer	Defines storage capacity of root zone in bedrock layer	u	Low
		Bedrock attribute table	RK_{LO}(rocktype)	Effective unsaturated hydraulic conductivity for hydrogeologic unit	Defines lower bedrock hydraulic conductivity	mm/d	Low
		Bedrock attribute table	RK_{HI}(rocktype)	Effective saturated hydraulic conductivity for hydrogeologic unit	Defines upper bedrock and deep alluvium hydraulic conductivity	mm/d	Low

Table 3. Summary of input parameters used in the INFILv3 model of the Death Valley region, Nevada and California—Continued

Source data	Preprocessing routines	Input file	Parameter name	Parameter description	Parameter use	Parameter units	Parameter accuracy
Vegetation and root-zone properties associated with the GAP database							
GAP	GIS	Watershed file	VEGTYPE(r,c)	Map code for GAP vegetation units	Spatial distribution of vegetation properties, root- zone layer properties	u	Medium
User defined	GIS	Watershed file	VEGCOV(r,c)	Vegetation cover	Evapotranspiration model	percent	Medium
User defined	None	Vegetation attribute table	RZDEN(vegtype,l)	Root density for layer l	Evapotranspiration model	percent	Low
User defined	None	Vegetation attribute table	RZDPTH(vegtype,l)	Root-zone layer thickness	Evapotranspiration model, root-zone drainage model	m	Low
Snowmelt and sublimation parameters							
Maidment (1993)	None	Control file	SNODAY1	Day number 1 for snowmelt model	Define timing of early spring snowmelt model	Day number	Medium
		Control file	SNOPAR1	Snowmelt parameter 1	Degree-day snowmelt rate	mm/d	Medium
		Control file	SNODAY2	Day number 2 for snowmelt model	Define timing of late spring snowmelt model	Day number	Medium
		Control file	SNOPAR2	Snowmelt parameter 2	Degree-day snowmelt rate	mm/d	Medium
User defined	None	Control file	MELTIME	Duration of daily snowmelt	Controls intensity of snowmelt	Hours	Medium
		Control file	SUBPAR1	Sublimation rate parameter 1	Sublimation	u	Low
		Control file	SUBPAR2	Sublimation rate parameter 2	Sublimation	u	Low
Simulation-time parameters							
User defined	None	Control file	YRSTART	Simulation start year	Identifies simulation start date	u	na
		Control file	MOSTART	Simulation start month	Identifies simulation start date	u	na
		Control file	DYSTART	Simulation start day	Identifies simulation start date	u	na
		Control file	YREND	Simulation end year	Identifies simulation end date	u	na
		Control file	MOEND	Simulation end month	Identifies simulation end date	u	na
		Control file	DYEND	Simulation end day	Identifies simulation end date	u	na
Storm duration parameters							
		Control file	DYSUMBEG	Start day number for summer storms	Defines beginning day number for a summer storm	Day	Medium
User defined	None	Control file	DYSUMEND	End day number for summer storms	Defines ending day number for a summer storm	Day	Medium
		Control file	STORMSUM	Duration of summer precipitation and streamflow	Defines precipitation and streamflow intensity for summer storms	Hours	Low
User defined	None	Control file	STORMWIN	Duration of winter precipitation and streamflow	Defines precipitation and streamflow intensity for winter storms	Hours	Low
Evapotranspiration parameters							
Flint and Childs (1987)	None	Control file	BSEA	Priestley–Taylor model coefficient 1 for bare soil evaporation	Evapotranspiration model coefficient for modified Priestley–Taylor equation, for bare-soil evaporation	u	Medium

Table 3. Summary of input parameters used in the INFILv3 model of the Death Valley region, Nevada and California—Continued

Source data	Preprocessing routines	Input file	Parameter name	Parameter description	Parameter use	Parameter units	Parameter accuracy
		Control file	BSEB	Priestley–Taylor model coefficient 2 for bare soil evaporation	Evapotranspiration model coefficient for modified Priestley–Taylor equation, for bare-soil evaporation	u	Medium
		Control file	HSTEP	Potential evapotranspiration time step	Define hourly time-step for potential evapotranspiration model	Hours	na
		Control file	ETA	Priestley–Taylor model coefficient 1 for transpiration	Evapotranspiration model coefficient for modified Priestley–Taylor equation, for transpiration	u	Medium
User defined	None	Control file	ETB	Priestley–Taylor model coefficient 2 for transpiration	Evapotranspiration model coefficient for modified Priestley–Taylor equation, for transpiration	u	Medium
				Stream-channel parameters			
User defined	None	Control file	CHAN1	Surface-water minimum wetted area factor	Defines wetted area for stream-channel grid cell	u	Low
		Control file	CHAN2	Surface-water wetted area model coefficient	Defines wetted area for stream-channel grid cell	u	Low
		Control file	CHAN3	Surface-water headwater wetted area factor	Defines wetted area for stream-channel grid cell	u	Low
		Control file	CHAN4	Surface-water maximum wetted area factor	Defines wetted area for stream-channel grid cell	u	Low
		Control file	KSCHN1	Model coefficient for stream-channel characteristics	Minimum number of upstream cells for using KSCHN2	u	Low
User defined	None	Control file	KSCHN2	Model coefficient for stream-channel characteristics	Scaler for adjusting soil saturated hydraulic conductivity in channels	u	Low
		Control file	KSCHN3	Soil saturated hydraulic conductivity	Maximum soil saturated hydraulic conductivity in channels	u	Low
				Daily climate inputs developed from NOAA/NCDC			
		Control file	INITOPT	Initial condition option	Defines method for setting initial conditions	u	na
		Control file	VWCFACT	Scaler for setting initial water content for root zone	Defines initial water content for soil layers in root zone	u	Low
NOAA/ NCDC	DAYINP14	Precipitation. file	PPT(day, st)	Daily precipitation	Daily precipitation input	mm	High
		Maximum air temperature file	TMAX(day, st)	Maximum daily air temperature	Snowfall, snowmelt, sublimation, potential evapotranspiration	Degrees Celsius	High
		Minimum air temperature file	TMIN(day, st)	Minimum daily air temperature	Snowfall, snowmelt, sublimation, potential evapotranspiration	Degrees Celsius	High
User defined	EXCEL	Monthly climate model	PPTMOD (month)	Model type for monthly precipitation-elevation regression model	Defines model type for daily precipitation spatial interpolation model	u	Medium
				Daily climate inputs developed from NOAA/NCDC—Continued			
		Monthly climate model	PPTA(month)	Regression model coefficient for precipitation-elevation regression model	Coefficient for daily precipitation spatial interpolation model	u	Medium

Table 3. Summary of input parameters used in the INFILv3 model of the Death Valley region, Nevada and California—Continued

Source data	Preprocessing routines	Input file	Parameter name	Parameter description	Parameter use	Parameter units	Parameter accuracy
		Monthly climate model	PPTB(month)	Regression model coefficient for precipitation-elevation regression model	Coefficient for daily precipitation spatial interpolation model	u	Medium
		Monthly climate model	PPTC(month)	Regression model coefficient for precipitation-elevation regression model	Coefficient for daily precipitation spatial interpolation model	u	Medium
		Monthly climate model	TMAXMOD(month)	Model type for monthly maximum air temperature-elevation regression model	Defines model type for maximum daily air temperature spatial interpolation model	u	High
		Monthly climate model	TMAXA(month)	Regression model coefficient for maximum air temperature-elevation model	Coefficient for maximum daily air temperature spatial interpolation model	u	High
		Monthly climate model	TMAXB(month)	Regression model coefficient for maximum air temperature-elevation model	Coefficient for maximum daily air temperature spatial interpolation model	u	High
		Monthly climate model	TMAXC(month)	Regression model coefficient for maximum air temperature-elevation model	Coefficient for maximum daily air temperature spatial interpolation model	u	High
		Monthly climate model	TMINMOD(month)	Model type for monthly Minimum air temperature-elevation regression model	Defines model type for minimum daily air temperature spatial interpolation model	u	High
		Monthly climate model	TMINA(month)	Regression model coefficient for minimum air temperature-elevation model	Coefficient for minimum daily air temperature spatial interpolation model	u	High
		Monthly climate model	TMINB(month)	Regression model coefficient for minimum air temperature-elevation model	Coefficient for minimum daily air temperature spatial interpolation model	u	High
		Monthly climate model	TMINC(month)	Regression model coefficient for minimum air temperature-elevation model	Coefficient for minimum daily air temperature spatial interpolation model	u	High
Monthly atmospheric parameters							
NWS	None	Monthly atmospheric parameter	OZONE (month)	Ozone layer thickness	Potential evapotranspiration model, incoming solar radiation	cm	Medium
		Monthly atmospheric parameter	WP (month)	Precipitable water in atmosphere	Potential evapotranspiration model, incoming solar radiation	cm	Medium
		Monthly atmospheric parameter	BETA (month)	Mean atmospheric turbidity	Potential evapotranspiration model, incoming solar radiation, net radiation	u	Medium
		Monthly atmospheric parameter	CSR(month)	Circumsolar radiation	Potential evapotranspiration model, incoming solar radiation, net radiation	u	Medium
		Monthly atmospheric parameter	PG (month)	Surface reflectivity	Potential evapotranspiration model, incoming solar radiation, net radiation	u	Medium

Table 4. Estimated root-zone water storage capacities and effective hydraulic conductivities for deep soils and bedrock underlying the root zone of the Death Valley region, Nevada and California

[Hydrogeologic unit from D'Agnese and others (2002). Hydrogeologic unit description modified from Faunt and others (1997). mm/d, millimeter per day]

Deep soils/bedrock set	Hydrogeologic unit	Hydrogeologic unit description	Estimated root-zone storage capacity (RKPOR)	Estimated effective hydraulic conductivity	
				Low (RK_{LO}) (mm/d)	High (RK_{HI}) (mm/d)
Set A: (for models 1 and 2)	Qtal	Quaternary and Tertiary valley fill	0.35	500.00	500.00
	Tv	Quaternary and Tertiary lava flows	.05	.01	1.00
	Tv	Tertiary volcanic rocks	.05	.02	2.00
	TSDVS	Tertiary volcaniclastic rocks	.05	.005	.50
	TJi	Tertiary and late Jurassic granitic rocks	.001	.00005	.005
	Mvs	Mesozoic sedimentary and metavolcanic rocks	.10	.05	5.00
	LCA/UCA	Paleozoic carbonate rocks	.10	.2	20.00
	LCCU	Paleozoic and Precambrian clastic rocks	.02	.001	.10
	pCgm	Precambrian igneous and metamorphic rocks	.002	.0001	.01
	QTp	Quaternary playa deposits	.45	.20	.20
	UCCU	Paleozoic clastic rocks	.01	.0005	.05
Set B: (for models 3 and, 4)	Qtal	Quaternary and Tertiary valley fill	.35	500.00	500.00
	Tv	Quaternary and Tertiary lava flows	.05	.001	1.00
	Tv	Tertiary volcanic rocks	.05	.002	2.00
	TSDVS	Tertiary volcaniclastic rocks	.05	.0005	.50
	TJi	Tertiary and late Jurassic granitic rocks	.001	.000005	.005
	Mvs	Mesozoic sedimentary and metavolcanic rocks	.10	.005	5.00
	LCA/UCA	Paleozoic carbonates rocks	.10	.02	20.00
	LCCU	Paleozoic and Precambrian clastic rocks	.02	.0001	.10
	pCgm	Precambrian igneous and metamorphic rocks	.002	.00001	.01
	QTp	Quaternary playa deposits	.45	.20	.20
	UCCU	Paleozoic clastic rocks	.01	.00005	.05

Table 5. Estimated vegetation type or land-surface characteristics and estimated root densities used to define the root-zone parameters for root-zone model A of the INFILv3 model of the Death Valley region, Nevada and California

[Root-zone parameter set A used in INFILv3 models 1, 2, and 3. Vegetation types from U.S. Geological Survey, National Gap Analysis Program (GAP), western region vegetation map (WESTVEG), (Murray, 1997, accessed March 16, 2000). Map code identifiers 1 and 2 used for vegetation types identified as unknown in GAP. Map code identifiers for the purposes of this study only. The term association does not necessarily relate to any established vegetation associations, only to the groupings used for this study. m, meter]

Map code identifier for vegetation type or land-surface characteristic (locations on figure 7)	Vegetation type or land-surface characteristic (VEGTYPE)	Estimated vegetation type or land-surface characteristic			Estimated root density (RZDEN), in percent						Rock layer maximum thickness (RZTHCK) (m)
		Vegetation type or land-surface characteristic	Vegetation cover (VEGCOV), in percent	Maximum root depth (m)	Soil layer 1 (0 – 0.1 m)	Soil layer 2 (0.1 – 0.3 m)	Soil layer 3 (0.3 – 1.0 m)	Soil layer 4 (1.0 – 3.0 m)	Soil layer 5 (3.0 – 6.0 m)	Rock layer (0–3.0 m)	
3	Subalpine pine	Coniferous forest	50	6	50	50	50	50	50	50	3
4	Ponderosa pine	Coniferous forest	60	6	60	60	60	60	60	60	3
5	Jeffrey pine	Coniferous forest	60	6	60	60	60	60	60	60	3
6	White fir	Coniferous forest	60	6	60	60	60	60	60	60	3
7	Meadow	Grasslands	70	.3	70	70	40	20	10	5	1.5
8	Riparian wetland	Discharge one	90	3	90	90	90	90	90	90	3
9	Ash	Deciduous forest	50	6	50	50	50	50	40	30	3
10	California chaparral	Desert shrubs	40	3	40	40	40	40	30	10	2
11	Mountain shrub–clear cut	Mountain shrub	70	3	70	70	70	70	20	10	1.5
12	Alpine–subalpine meadows	Grasslands	60	.3	60	60	30	20	10	5	1.5
13	Juniper	Coniferous forest	40	6	40	40	40	40	30	30	2.5
14	Pinyon pine	Coniferous forest	50	6	50	50	50	50	40	30	2.5
15	Pinyon–juniper	Coniferous forest	40	6	40	40	40	40	30	30	2.5
16	Mountain mahogany	Mountain shrub	60	3	60	60	50	50	30	20	2
17	Sagebrush	Desert shrubs	30	3	30	30	30	30	20	10	1.5
18	Sagebrush–perennial grass	Desert shrubs	50	1	50	50	50	30	20	10	1.5
19	Rabbitbrush	Desert shrubs	30	1	30	30	30	20	10	10	1.5
20	Great Basin grassland	Grasslands	50	1	50	50	50	20	10	5	1.5
21	California disturbed grassland	Grasslands	40	.3	40	40	20	20	10	5	1.5
22	Foothills grassland	Grasslands	70	1	70	70	70	30	20	5	1.5

Table 5. Estimated vegetation type or land-surface characteristics and estimated root densities used to define the root-zone parameters for root-zone model A of the INFILv3 model of the Death Valley region, Nevada and California—*Continued*

Map code identifier for vegetation type or land-surface characteristic (locations on figure 7)	Vegetation type or land-surface characteristic (VEGTYPE)	Estimated vegetation type or land-surface characteristic			Estimated root density (RZDEN), in percent						Rock layer maximum thickness (RZTHCK) (m)
		Vegetation type or land-surface characteristic	Vegetation cover (VEGCOV), in percent	Maximum root depth (m)	Soil layer 1 (0 – 0.1 m)	Soil layer 2 (0.1 – 0.3 m)	Soil layer 3 (0.3 – 1.0 m)	Soil layer 4 (1.0 – 3.0 m)	Soil layer 5 (3.0 – 6.0 m)	Rock layer (0–3.0 m)	
23	Salt desert shrub	Desert shrubs	20	1	20	20	20	10	10	5	1.5
24	Blackbrush	Desert shrubs	30	.3	30	30	10	10	5	5	1.5
25	Creosote–bursage	Desert shrubs	30	6	30	30	30	30	30	10	2.5
26	Greasewood	Desert trees/shrubs	30	6	30	30	30	30	30	20	2.5
27	Hopsage	Desert shrubs	20	1	20	20	20	10	5	5	1.5
28	Mesquite	Desert trees/shrubs	30	6	30	30	30	30	30	10	2.5
29	Mojave mixed shrub	Desert shrubs	20	1	20	20	20	10	5	5	1.5
30	Joshua tree	Desert trees/shrubs	30	3	30	30	30	30	20	10	2
31	Shadescale	Desert shrubs	20	1	20	20	20	10	5	5	1.5
32	Catclaw acacia	Desert trees/shrubs	20	3	20	20	20	20	10	10	1.5
33	Water	Discharge zone	0	0	0	0	0	0	0	0	.0
34	Agriculture	Agriculture	90	1	90	90	90	30	20	5	1.5
35	Highly developed	Highly developed	50	6	50	50	50	50	50	50	2.5
36	Inland dune	Barren	0	0	0	0	5	5	5	5	1.5
37	Barren	Barren	0	0	0	0	5	5	5	5	1.5

Table 6. Estimated vegetation type or land-surface characteristic and estimated root density used to define the root-zone parameters for root-zone model B of the INFILv3 model of the Death Valley region, Nevada and California

[Root-zone parameter set B used in INFILv3 models 1, 2, and 3. Vegetation types from U.S. Geological Survey, National Gap Analysis Program (GAP), western region vegetation map (WESTVEG), (Murray, 1997, accessed March 16, 2000). Map code identifiers 1 and 2 used for vegetation types identified as unknown in GAP. Map code identifiers for the purposes of this study only. The term association does not necessarily relate to any established vegetation associations, only to the groupings used in this study. m, meter]

Map code identifier for vegetation type or land-surface characteristic (locations on figure 7)	Vegetation type or land-surface characteristic (VEGTYPE)	Estimated vegetation type or land-surface characteristic			Estimated root density (RZDEN), in percent						Rock layer maximum thickness (RZTHCK) (m)
		Vegetation or land-use association	Vegetation cover (VEGCOV), in percent	Maximum root depth (m)	Soil layer 1 (0 – 0.1 m)	Soil layer 2 (0.1 – 0.3 m)	Soil layer 3 (0.3 – 1.0 m)	Soil layer 4 (1.0 – 3.0 m)	Soil layer 5 (3.0 – 6.0 m)	Rock layer (0–3.0 m)	
3	Subalpine pine	Coniferous forest	50	6	50	50	50	50	50	50	3
4	Ponderosa pine	Coniferous forest	60	6	60	60	60	60	60	60	3
5	Jeffrey pine	Coniferous forest	60	6	60	60	60	60	60	60	3
6	White fir	Coniferous forest	60	6	60	60	60	60	60	60	3
7	Meadow	Grasslands	70	.3	70	70	40	20	10	10	1.5
8	Riparian wetland	Discharge zone	90	3	90	90	90	90	90	90	3
9	Ash	Deciduous forest	50	6	50	50	50	50	40	40	3
10	California chaparral	Desert shrubs	40	3	40	40	40	40	30	20	2
11	Mountain shrub–clear cut	Mountain shrub	70	3	70	70	70	70	20	20	1.5
12	Alpine–subalpine meadows	Grasslands	60	.3	60	60	30	20	10	10	1.5
13	Juniper	Coniferous forest	40	6	40	40	40	40	40	40	2.5
14	Pinyon pine	Coniferous forest	50	6	50	50	50	50	40	40	2.5
15	Pinyon–juniper	Coniferous forest	40	6	40	40	40	40	40	40	2.5
16	Mountain mahogany	Mountain shrub	60	3	60	60	50	50	30	30	2
17	Sagebrush	Desert shrubs	30	3	30	30	30	30	20	15	1.5
18	Sagebrush–perennial grass	Desert shrubs	50	1	50	50	50	30	20	20	1.5
19	Rabbitbrush	Desert shrubs	30	1	30	30	30	20	20	20	1.5
20	Great Basin grassland	Grasslands	50	1	50	50	50	20	10	10	1.5
21	California disturbed grassland	Grasslands	40	.3	40	40	20	20	10	10	1.5
22	Foothills grassland	Grasslands	70	1	70	70	70	30	20	10	1.5

Table 6. Estimated vegetation type or land-surface characteristic and estimated root density used to define the root-zone parameters for root-zone model B of the INFILv3 model of the Death Valley region, Nevada and California, Nevada and California—*Continued*

Map code identifier for vegetation type or land-surface characteristic (locations on figure 7)	Vegetation type or land-surface characteristic (VEGTYPE)	Estimated vegetation type or land-surface characteristic			Estimated root density (RZDEN), in percent						Rock layer maximum thickness (RZTHCK) (m)
		Vegetation or land-use association	Vegetation cover (VEGCOV), in percent	Maximum root depth (m)	Soil layer 1 (0 – 0.1 m)	Soil layer 2 (0.1 – 0.3 m)	Soil layer 3 (0.3 – 1.0 m)	Soil layer 4 (1.0 – 3.0 m)	Soil layer 5 (3.0 – 6.0 m)	Rock layer (0–3.0 m)	
23	Salt desert shrub	Desert shrubs	20	1	20	20	20	10	10	10	1.5
24	Blackbrush	Desert shrubs	30	.3	30	30	10	10	10	10	1.5
25	Creosote–bursage	Desert shrubs	30	6	30	30	30	30	30	20	2.5
26	Greasewood	Desert trees/shrubs	30	6	30	30	30	30	30	30	2.5
27	Hopsage	Desert shrubs	20	1	20	20	20	10	10	10	1.5
28	Mesquite	Desert trees/shrubs	30	6	30	30	30	30	30	30	2.5
29	Mojave mixed shrub	Desert shrubs	20	1	20	20	10	10	10	20	1.5
30	Joshua tree	Desert trees/shrubs	30	3	30	30	30	20	20	30	2
31	Shadescale	Desert shrubs	20	1	20	20	10	10	10	20	1.5
32	Catclaw acacia	Desert trees/shrubs	20	3	20	20	20	20	20	20	1.5
33	Water	Discharge zone	0	0	0	0	0	0	0	0	.0
34	Agriculture	Agriculture	90	1	90	90	90	30	20	20	1.5
35	Highly developed	Highly developed	50	6	50	50	50	50	50	50	2.5
36	Inland dune	Barren	0	0	0	10	10	10	10	10	1.5
37	Barren	Barren	0	0	0	10	10	10	10	10	1.5

Table 7. Summary of daily climate records used as input to the INFILv3 model of the Death Valley region, Nevada and California

[See figure 23 for location of climate recording stations. [UTM, Universal Transverse Mercator coordinates; NAD27, North American Datum of 1927; NWS, National Weather Service. m, meter; mm/yr, millimeters per year, °C, degrees Celsius; —, not available]

Daily climate recording station			Station location coordinates (UTM zone 11, NAD27)		Station elevation (m)	Daily precipitation		Daily maximum air temperature		Daily minimum air temperature	
Station identifier	Station name	Station code	Easting (m)	Northing (m)		Number years of record	Annual average (mm/yr)	Number years of record	Daily average (°C)	Number years of record	Daily average (°C)
1	Twentynine Palms	49099	588,807	3,776,455	602	50	105	50	29	50	11
2	Adaven	260046	624,188	4,219,501	1,905	51	324	51	18	51	1
3	Adelanto	40024	461,786	3,826,721	869	17	91	0	—	0	—
4	Amargosa Farms Garey	260150	548,143	4,047,290	747	25	114	25	28	25	9
5	Apple Valley	40244	480,113	3,819,271	894	27	132	0	—	0	—
6	Backus Ranch	40418	391,948	3,867,940	808	13	123	13	25	13	8
7	Baker	40436	584,263	3,902,719	287	20	109	20	30	20	12
8	Baker 9 NNW	40437	580,231	3,915,714	320	17	69	17	29	17	13
9	Barstow	40519	496,955	3,861,757	659	48	113	48	27	48	9
10	Barstow Fire Station	40521	497,919	3,860,401	707	19	124	19	27	18	10
11	Beatty	260714	522,269	4,085,454	1,007	23	105	22	25	22	7
12	Beatty 8 N	260718	525,064	4,094,152	1,082	26	161	26	24	26	6
13	Beaver Dam	20672	772,454	4,087,604	572	32	193	31	28	31	10
14	Benton Inspection ST	40684	369,923	4,189,196	1,664	34	203	0	—	0	—
15	Big Pines Park FC83B	40779	437,179	3,804,676	2,086	47	632	0	—	0	—
16	Bishop AP	40822	379,749	4,136,703	1,250	51	136	51	24	51	3
17	Bishop Creek Intake	40819	359,576	4,123,577	2,485	39	316	0	—	0	—
18	Blythe	40924	722,656	3,722,044	82	67	100	67	31	67	13
19	Blythe FCWOS	40927	711,830	3,721,798	119	50	94	50	31	50	15
20	Bodie	40943	323,659	4,231,043	2,551	32	350	33	13	33	–7

Table 7. Summary of daily climate records used as input to the INFILv3 model of the Death Valley region, Nevada and California—*Continued*

Daily climate recording station			Station location coordinates (UTM zone 11, NAD27)		Station elevation (m)	Daily precipitation		Daily maximum air temperature		Daily minimum air temperature	
Station identifier	Station name	Station code	Easting (m)	Northing (m)		Number years of record	Annual average (mm/yr)	Number years of record	Daily average (°C)	Number years of record	Daily average (°C)
21	Boulder City	261071	694,423	3,983,464	770	66	146	66	25	66	14
22	Bouse	20949	775,048	3,759,638	282	47	143	47	31	47	12
23	Bullhead City	21050	721,590	3,891,202	165	22	171	22	31	22	15
24	Caliente	261358	719,256	4,166,013	1,341	68	229	65	22	65	2
25	Cantil	41488	412,110	3,906,543	613	19	104	18	27	18	9
26	China Lake Armitage	41733	438,166	3,948,842	677	20	111	0	—	0	—
27	Cow Creek	42092	510,444	4,042,910	–46	12	41	12	33	12	18
28	Daggett FCWOS	42257	518,918	3,856,539	586	50	101	51	28	51	12
29	Davis Dam No. 2	22439	721,532	3,897,737	201	19	110	17	29	17	15
30	Death Valley	42319	512,221	4,035,025	–59	38	58	38	33	38	17
31	Deep Canyon Laboratory	42327	557,825	3,723,485	366	36	151	0	—	0	—
32	Deep Springs College	42331	412,926	4,135,799	1,593	45	158	42	20	42	3
33	Desert National Wildlife Range	262243	646,408	4,033,051	890	50	112	49	26	49	8
34	Desert Rock AP	262251	586,936	4,053,019	1,006	12	157	12	25	12	10
35	Duckwater	262390	611,846	4,309,346	1,710	28	188	28	18	27	1
36	Dunn Siding	42570	551,679	3,878,537	491	11	87	0	—	0	—
37	Dyer	262431	404,475	4,171,028	1,493	48	129	47	21	47	1
38	Eagle Mountain	42598	643,484	3,740,867	297	51	93	51	29	51	17
39	Llano Eberle Ranch	45002	431,118	3,813,960	1,165	17	168	16	23	16	9
40	Ehrenberg	22787	728,886	3,720,341	98	27	90	27	31	27	14

Table 7. Summary of daily climate records used as input to the INFILv3 model of the Death Valley region, Nevada and California—*Continued*

Daily climate recording station			Station location coordinates (UTM zone 11, NAD27)		Station elevation (m)	Daily precipitation		Daily maximum air temperature		Daily minimum air temperature	
Station identifier	Station name	Station code	Easting (m)	Northing (m)		Number years of record	Annual average (mm/yr)	Number years of record	Daily average (°C)	Number years of record	Daily average (°C)
41	Ehrenberg 2 E	22790	739,761	3,718,756	142	22	133	22	31	22	17
42	Elgin	262557	717,633	4,136,081	1,042	14	315	13	24	13	6
43	Elgin 3 SE	262562	721,539	4,132,729	1,006	18	349	17	24	17	8
44	El Mirage	42771	442,122	3,827,531	899	27	152	27	24	27	6
45	Enterprise	422558	790,668	4,163,305	1,622	44	358	0	—	0	—
46	Goldfield	263285	479,457	4,173,245	1,734	41	164	42	18	41	4
47	Goldstone Echo No. 2	43498	519,603	3,904,072	899	25	150	0	—	0	—
48	Greenland Ranch	43603	511,949	4,033,669	–51	12	37	12	33	11	17
49	Gunlock Powerhouse	423506	790,077	4,130,812	1,253	50	317	0	—	0	—
50	Haiwee	43710	414,276	3,999,573	1,166	50	171	50	23	50	8
51	Hayfield Pumping PLA	43855	626,658	3,729,538	418	51	95	51	29	50	13
52	Hesperia	43935	472,431	3,808,202	976	17	164	0	34	0	15
53	Independence	44232	392,620	4,072,943	1,204	68	133	61	24	61	7
54	Indian Springs	263980	617,794	4,049,257	952	15	74	15	27	15	6
55	Indio Fire Station	44259	572,716	3,729,931	–6	67	82	67	32	66	15
56	Inyokern	44278	426,069	3,945,237	744	49	104	49	27	48	8
57	Inyokern Armitage	44280	438,166	3,948,842	682	29	88	0	—	0	—
58	Iron Mountain	44297	672,128	3,778,319	281	51	88	50	30	51	16
59	Joshua Tree	44405	563,008	3,776,956	830	14	123	0	—	0	—
60	Kee Ranch	44467	543,013	3,780,539	1,321	27	211	0	—	0	—

Table 7. Summary of daily climate records used as input to the INFILv3 model of the Death Valley region, Nevada and California—*Continued*

Daily climate recording station			Station location coordinates (UTM zone 11, NAD27)		Station elevation (m)	Daily precipitation		Daily maximum air temperature		Daily minimum air temperature	
Station identifier	Station name	Station code	Easting (m)	Northing (m)		Number years of record	Annual average (mm/yr)	Number years of record	Daily average (°C)	Number years of record	Daily average (°C)
61	Kingman	24639	768,637	3,897,163	1,025	63	263	60	25	61	8
62	Kingman No. 2	24645	771,618	3,899,103	1,079	25	266	25	24	25	9
63	Lake Valley Steward	264384	705,452	4,243,358	1,935	27	401	27	16	27	3
64	Lancaster FSS	44749	388,613	3,843,949	713	25	196	25	24	25	9
65	Lancaster	44747	397,707	3,838,298	732	24	128	24	25	24	7
66	Las Vegas AP	264436	666,108	3,994,073	648	50	106	50	27	50	12
67	Las Vegas	264429	667,897	4,003,848	613	27	111	26	28	26	10
68	Lake Havasu	24759	741,929	3,815,003	147	22	117	13	30	13	16
69	Logandale	264651	725,069	4,055,097	430	23	131	21	28	22	9
70	Lake Sabrina	44705	356,556	4,119,929	2,763	24	429	0	—	0	—
71	Lucerne Valley 1 WSW	45182	504,593	3,811,858	903	23	101	22	26	22	7
72	Mitchell Caverns	45721	632,693	3,867,556	1,326	41	270	41	23	41	12
73	Mecca Fire Station	45502	585,697	3,714,823	–55	49	74	49	32	49	13
74	Mina	265168	403,419	4,249,090	1,387	70	120	68	21	68	4
75	Mount San Jacinto WS	45978	533,941	3,739,847	2,568	9	655	8	13	8	–1
76	Mojave	45756	393,600	3,879,012	834	50	149	33	24	33	10
77	Morongo Valley	45863	538,464	3,765,736	781	18	199	0	—	0	—
78	Mountain Pass	45890	632,115	3,926,003	1,442	41	221	36	21	36	7
79	Needles FCWOS	46118	717,726	3,849,272	279	50	118	50	30	50	16
80	North Las Vegas	265705	668,726	4,008,765	573	19	107	19	28	19	10

Table 7. Summary of daily climate records used as input to the INFILv3 model of the Death Valley region, Nevada and California—*Continued*

Daily climate recording station			Station location coordinates (UTM zone 11, NAD27)		Station elevation (m)	Daily precipitation		Daily maximum air temperature		Daily minimum air temperature	
Station identifier	Station name	Station code	Easting (m)	Northing (m)		Number years of record	Annual average (mm/yr)	Number years of record	Daily average (°C)	Number years of record	Daily average (°C)
81	Overton	265846	727,504	4,047,635	381	27	109	26	29	26	10
82	Pahranagat Wildlife Refuge	265880	666,720	4,126,186	1,036	34	164	32	24	33	7
83	Pahrump	265890	589,539	4,015,111	815	42	120	40	26	40	7
84	Palmdale	46624	399,113	3,827,191	791	67	199	67	25	67	8
85	Palmdale CAA Airport	46627	400,701	3,832,720	767	25	131	25	25	25	7
86	Palm Springs	46635	545,369	3,742,944	130	70	147	69	32	69	14
87	Parker	26250	749,182	3,782,449	125	97	123	95	31	95	13
88	Parker Reservoir	46699	760,825	3,797,011	225	51	139	51	30	51	17
89	Pierce Ferry 17 SSW	26538	763,301	3,974,739	1,176	20	268	20	23	20	9
90	Pioche	266252	722,660	4,202,474	1,884	48	344	48	17	48	4
91	Quartzsite	26865	756,534	3,728,439	267	28	103	27	30	26	14
92	Randsburg	47253	440,725	3,913,980	1,088	51	155	51	24	50	10
93	Rattlesnake	266630	572,718	4,255,868	1,803	14	126	13	19	12	3
94	Red Rock Canyon State Park	266691	638,660	3,992,455	1,152	22	301	22	24	22	9
95	Reese River O'Toole	266746	464,287	4,323,585	1,996	24	207	23	16	23	–4
96	Sarcobatus	267319	498,522	4,124,252	1,226	12	85	12	24	12	3
97	Searchlight	267369	688,588	3,926,521	1,079	51	194	50	24	50	11
98	Shoshone	48200	565,819	3,980,883	479	25	132	0	—	0	—
99	Silverpeak	267463	450,209	4,179,348	1,298	31	115	31	22	31	4
100	Snowball Ranch	267640	569,333	4,321,344	2,182	32	228	32	15	32	–2

Table 7. Summary of daily climate records used as input to the INFILv3 model of the Death Valley region, Nevada and California—*Continued*

Daily climate recording station			Station location coordinates (UTM zone 11, NAD27)		Station elevation (m)	Daily precipitation		Daily maximum air temperature		Daily minimum air temperature	
Station identifier	Station name	Station code	Easting (m)	Northing (m)		Number years of record	Annual average (mm/yr)	Number years of record	Daily average (°C)	Number years of record	Daily average (°C)
101	South Lake	48406	360,559	4,114,498	2,920	24	506	0	—	0	—
102	ST George	427516	805,068	4,111,957	844	70	209	69	26	69	8
103	Sunrise Manor Las Vegas	267925	672,321	4,007,633	555	27	109	27	29	27	8
104	Tempiute 4 NW	267983	613,161	4,171,251	1,490	13	200	12	21	12	1
105	Thermal FAA Airport	48892	577,288	3,721,620	–34	49	77	49	32	49	14
106	Tonopah	268160	479,532	4,213,032	1,836	26	126	26	17	26	5
107	Tonopah FCWOS	268170	492,226	4,212,085	1,655	44	136	44	19	44	3
108	Trona	49035	464,669	3,957,601	517	50	100	49	28	49	12
109	Twin Springs FALLINI	268443	572,162	4,228,491	1,615	12	155	12	19	12	–1
110	Valyermo Fire Station 79	49250	420,387	3,812,198	1,098	12	276	11	23	11	4
111	Valyermo Ranger Station	49251	421,918	3,812,185	1,129	22	223	20	24	20	5
112	Valley Of Fire State Park	268588	722,847	4,034,283	610	26	174	26	27	26	14
113	Veyo Powerhouse	429136	795,265	4,138,957	1,402	42	359	41	20	41	5
114	Victorville Pump Palza	49325	471,935	3,821,325	871	51	140	51	25	51	7
115	Wildrose R S	49671	483,357	4,013,218	1,250	29	180	29	22	29	7
116	Willow Beach	29376	711,171	3,971,702	226	31	140	31	30	31	15
117	Yucca 1 NNE	29645	761,920	3,863,008	594	46	195	45	27	45	12
118	Rainier Mesa	990001	569,647	4,116,362	2,283	40	310	0	—	0	—
119	Buster Jangle Y	990002	584,237	4,102,256	1,240	39	163	0	—	0	—
120	Cane Springs	990003	581,044	4,074,427	1,219	35	198	0	—	0	—

Table 7. Summary of daily climate records used as input to the INFILv3 model of the Death Valley region, Nevada and California—*Continued*

Daily climate recording station			Station location coordinates (UTM zone 11, NAD27)		Station elevation (m)	Daily precipitation		Daily maximum air temperature		Daily minimum air temperature	
Station identifier	Station name	Station code	Easting (m)	Northing (m)		Number years of record	Annual average (mm/yr)	Number years of record	Daily average (°C)	Number years of record	Daily average (°C)
121	Desert Rock	990005	587,107	4,053,284	991	36	147	0	—	0	—
122	Jackass Flats	990007	563,450	4,071,227	1,043	41	140	0	—	0	—
123	40 Mile Canyon	990008	563,355	4,100,564	1,469	39	208	0	—	0	—
124	Little Feller 2	990009	561,842	4,108,195	1,560	23	210	0	—	0	—
125	Mercury	990010	588,477	4,057,705	1,149	28	149	0	—	0	—
126	Mid Valley	990011	573,704	4,092,142	1,420	35	231	0	—	0	—
127	Pahute Mesa 1	990012	549,886	4,122,631	1,996	36	199	0	—	0	—
128	PHS Farm	990013	585,307	4,118,478	1,391	35	190	0	—	0	—
129	Rock Valley	990014	572,169	4,060,264	1,036	36	156	0	—	0	—
130	Tippipah Springs 2	990015	571,898	4,101,064	1,518	39	220	0	—	0	—
131	Well 5 B	990016	592,305	4,073,401	939	36	127	0	—	0	—
132	Yucca Dry Lake	990017	584,799	4,090,458	1,196	41	171	0	—	0	—

Table 8. Monthly regression coefficients used to spatially distribute daily precipitation and air temperature using elevation in the INFILv3 model of the Death Valley region, Nevada and California

[Model types: 1, linear regression model; 3, quadratic regression model. PPTMOD, precipitation model; PPTA, PPTB, PPTC: regression coefficients for estimating precipitation; TMAXMOD, maximum daily air temperature model; TMAXA, TMAXB, TMAXC: regression coefficients for estimating maximum daily air temperatures; TMINMOD, minimum daily air temperature model; TMINA, TMINB, TMINC: regression coefficients for estimating minimum daily air temperatures. na, not applicable]

Parameter	Month	Model type	Regression model coefficients			r-square
			A	B	C	
		PPTMOD	PPTA	PPTB	PPTC	
Average monthly precipitation (PPT), in millimeters	January	3	8.0×10^{-6}	–0.0041	17.93	0.32
	February	3	7.0×10^{-6}	–.0003	15.11	.38
	March	3	5.0×10^{-6}	.0037	12.04	.41
	April	3	1.0×10^{-6}	.0059	2.96	.62
	May	3	5.0×10^{-7}	.0075	–.05	.64
	June	3	8.0×10^{-7}	.0035	–.28	.60
	July	3	-1.0×10^{-6}	.0091	4.50	.25
	August	[1] 0	na	na	na	na
	September	3	3.0×10^{-6}	–.0009	9.01	.41
	October	3	1.0×10^{-6}	.0024	5.23	.35
	November	3	4.0×10^{-6}	.0004	8.78	.49
	December	3	7.0×10^{-6}	.0052	13.25	.38
		TMAXMOD	TMAXA	TMAXB	TMAXC	
Monthly average maximum daily air temperature (TMAX), in degrees Celsius)	January	1	-7.3×10^{-3}	19.7	0	0.91
	February	1	-7.9×10^{-3}	23.1	0	.96
	March	1	-8.1×10^{-3}	26.5	0	.97
	April	1	-8.3×10^{-3}	31.2	0	.96
	May	1	-8.0×10^{-3}	35.8	0	.95
	June	1	-7.8×10^{-3}	41.2	0	.94
	July	1	-7.1×10^{-3}	44.0	0	.93
	August	1	-7.2×10^{-3}	43.1	0	.95
	September	1	-7.8×10^{-3}	39.8	0	.97
	October	1	-7.8×10^{-3}	33.4	0	.97
	November	1	-7.4×10^{-3}	25.2	0	.95
	December	1	-7.0×10^{-3}	19.9	0	.91

Table 8. Monthly regression coefficients used to spatially distribute daily precipitation and air temperature using elevation in the INFILv3 model of the Death Valley region, Nevada and California

[Model types: 1, linear regression model; 3, quadratic regression model. PPTMOD, precipitation model; PPTA, PPTB, PPTC: regression coefficients for estimating precipitation; TMAXMOD, maximum daily air temperature model; TMAXA, TMAXB, TMAXC: regression coefficients for estimating maximum daily air temperatures; TMINMOD, minimum daily air temperature model; TMINA, TMINB, TMINC: regression coefficients for estimating minimum daily air temperatures. na, not applicable]

Parameter	Month	Model type	Regression model coefficients			r-square
			A	B	C	
		TMINMOD	TMINA	TMINB	TMINC	
Monthly average minimum daily air temperature (TMIN) in degrees Celsius	January	1	-6.7×10^{-3}	4.9	0	0.75
	February	1	-7.1×10^{-3}	7.5	0	.83
	March	1	-7.5×10^{-3}	10.3	0	.87
	April	1	-8.0×10^{-3}	14.2	0	.86
	May	1	-8.1×10^{-3}	18.6	0	.85
	June	1	-8.2×10^{-3}	23.2	0	.80
	July	1	-8.4×10^{-3}	27.2	0	.79
	August	1	-8.6×10^{-3}	26.5	0	.81
	September	1	-8.4×10^{-3}	22.3	0	.80
	October	1	-7.7×10^{-3}	15.7	0	.78
	November	1	-6.8×10^{-3}	8.9	0	.75
	December	1	-6.5×10^{-3}	4.8	0	.72

Table 9. Monthly values for atmospheric parameters used to simulate potential evapotranspiration in the INFILv3 model of the Death Valley region, Nevada and California

[For the INFILv3 model version used in this study, surface reflectivity was not adjusted to account for the absence or presence of snow cover. cm, centimeter]

Month	Atmospheric parameters				
	Ozone layer thickness (OZONE) (cm)	Precipitable water in atmosphere (WP) (cm)	Mean atmospheric turbidity (BETA) (dimensionless)	Circumsolar radiation (CSR) (dimensionless)	Surface reflectivity (PG) (dimensionless)
January	0.29	1	0.075	0.85	0.24
February	.31	1	.075	.85	.24
March	.32	1.05	.075	.85	.24
April	.33	1.1	.085	.85	.24
May	.33	1.5	.085	.74	.24
June	.32	1.8	.09	.74	.24
July	.3	2.2	.09	.57	.24
August	.29	2.44	.084	.57	.24
September	.28	2	.077	.66	.24
October	.27	1.4	.075	.74	.24
November	.27	1.05	.075	.9	.24
December	.28	0.95	.075	.9	.24

Table 10. Stream gages and streamflow records used for calibrating the INFILv3 model of the Death Valley region, Nevada and California

[Stream-gage station number, location, elevation, and upstream drainage area from the U.S. Geological Survey National Water Information System (NWIS) database. Data are presented in order of decreasing drainage area. Stream-gage map identifier assigned for purpose of this study only; see figures 27 and 28 for location of gages. Elevation of stream gages in meters above sea level. m, meter; km^2, square kilometer; na, not available]

Stream-gage station number	Stream-gage map identifier	Stream-gage location	Universal Transverse Mercator coordinate (UTM zone 11, NAD27)		Elevation of stream gage (m)	Upstream drainage basin area (km^2)	Number of upstream model cells	Calibration watershed model area (km^2)	Period of record
			easting (m)	northing (m)					
10251300	ART	Amargosa River at Tecopa	569,608	3,967,232	399	8,000	105,544	8,185.9	1961–95
10251259	AR127	Amargosa River at Hwy 127 near California–Nevada line	551,770	4,026,790	628	3,992	52,610	4,080.4	1993–95
10251100	SC	Salt Creek near Stovepipe Wells	498,857	4,050,237	na	na	51,417	3,987.9	1974–88
10251220	ARNB	Amargosa River near Beatty	521,441	4,080,090	863	1,217	15,771	1,223.2	1963–68
10251218	AR95	Amargosa River at Hwy 95 below Beatty	522,180	4,081,510	975	1,217	15,743	1,221.0	1991–95
10251217	ARAB	Amargosa River at Beatty	521,701	4,084,775	1,006	1,186	15,333	1,189.2	1993–96
10251258	FMAV	Fortymile Wash near Amargosa Valley	550,563	4,058,397	824	818	11,032	855.6	1983–96
10251255	FMJ13	Fortymile Wash near well J13	553,497	4,073,483	988	788	10,351	802.8	1983–97
10247901	YL (YL01)	Yucca Lake 01 3024	587,573	4,087,725	na	na	10,165	788.4	1977–77
10247902	YL (YL02)	Yucca Lake 02 2415	587,573	4,087,725	na	na	10,165	788.4	1977–77
10251250	FMN	Fortymile Wash at Narrows	555,199	4,082,307	1,122	667	8,678	673.1	1983–96
10250800	DC	Darwin Creek near Darwin	453,048	4,019,429	na	448	5,803	450.1	1962–89
10251215	BW	Beatty Wash near Beatty	525,007	4,088,451	1,055	245	3,258	252.7	1988–95
10251249	FMSW	Stockade Wash near Fortymile Wash	558,697	4,102,638	1,442	177	2,359	183.0	1991–95
10251242	FMCC	Fortymile Wash above East Cat Canyon	558,028	4,102,911	1,454	106	2,334	181.0	1991–95
10251980	LW	Lovell Wash near Blue Diamond	622,225	3,984,906	1,170	137	1,383	107.3	1966–77
10250600	WC	Wildrose Canyon near Wildrose Station	484,031	4,013,155	na	61	831	64.5	1960–75
10251243	ECC	East Cat Canyon Wash at Fortymile Wash	558,029	4,102,849	1,454	34	475	36.8	1991–95
10252330	WW	Wheaton Wash near Mountain Pass	637,364	3,925,651	na	26	424	32.9	1964–68
09419610	LC	Lee Canyon near Charleston Park	621,154	4,022,336	2,383	24	313	24.3	1963–94

Table 10. Stream gages and streamflow records used for calibrating the INFILv3 model of the Death Valley region, Nevada and California —Continued

Stream-gage station number	Stream-gage map identifier	Stream-gage location	Universal Transverse Mercator coordinate (UTM zone 11, NAD27)		Elevation of stream gage (m)	Upstream drainage basin area (km^2)	Number of upstream model cells	Calibration watershed model area (km^2)	Period of record
			easting (m)	northing (m)					
10251350	HTC	Horsethief Canyon near Tecopa, Calif.	599,669	3,960,032	na	8	110	8.5	1960–70
10251248	SWUT	Stockade Wash, unnamed tributary	565,120	4,115,166	1,823	10	67	5.2	1984–95
10247860	PV	Penoyer Valley Tributary near Tempiute	616,548	4,160,417	1,670	4	57	4.4	1965–77
102512535	DHU	Upper Drillhole Wash	548,405	4,079,924	1,314	2	46	3.6	1994–95
10252300	CHI	China Spring C Nr Mountain Pass, Calif.	635,346	3,925,774	na	2	43	3.3	1960–72
10252550	CC	Caruthers Creek near Ivanpah, Calif.	654,852	3,901,342	1,719	2	33	2.6	1963–99
102512533	PWL	Pagany Wash Number 1, NTS, Nev.	550,315	4,079,380	1,176	2.12	32	2.5	1992–95
10251000	BDC	Big Dip Creek near Stovepipe Wells Ca	473,896	4,085,619	na	2	27	2.1	1963–69
102512533	PWU	Pagany Wash near the Prow at Yucca Mtn	550,315	4,079,380	1,176	2	18	1.4	1992–95
102512537	USW	Upper Split Wash at Yucca Mountain	549,183	4,078,079	1,274	.85	11	0.9	1993–95
102512536	WREN	Wren Wash At Yucca Mountain	548,657	4,079,216	1,286	.6	8	0.6	1994–95

Table 11. Model coefficients used to simulate streamflow and net infiltration in INFILv3 models 1–4 of the Death Valley region, Nevada and California

[na, not applicable]

Parameter description	Parameter name	Model 1	Model 2	Model 3	Model 4
Sublimation rate parameter 1	SUBPAR1	0.4	0.4	0.35	0.4
Surface-water flow coupled to root zone	na	yes	no	yes	yes
Surface-water minimum wetted area factor	CHAN1	.10	.10	.05	.05
Surface-water wetted area model coefficient	CHAN2	10,000	10,000	10,000	5,000
Surface-water headwater wetted area factor	CHAN3	.8	.8	.8	.8
Surface-water maximum wetted area factor	CHAN4	2.0	2.0	1.0	1.0
Model coefficient for stream-channel characteristics	KSCHN1	20.0	20.0	20.0	2.0
Model coefficient for stream-channel characteristics	KSCHN2	2,000	2,000	2,000	4,000
Soil saturated hydraulic conductivity	KSCHN3	4.0	4.0	2.0	2.0
Potential evapotranspiration time step (hours)	HSTEP	2.0	2.0	2.0	1.0
Duration of summer precipitation and streamflow (hours)	STORMSUM	2.0	2.0	1.0	2.0
Duration of winter precipitation and streamflow (hours)	STORMWIN	12.0	12.0	8.0	12.0
Bedrock properties input file[1]	na	A	A	B	B
Root-zone parameters input file[2]	na	A	A	A	B

[1]Refer to table 4 for description of bedrock properties input files A and B.

[2]Refer to table 5 for description of root-zone parameters input file A and table 6 for description of root-zone parameters input file B.

Table 12. Measured and simulated streamflow frequency (number of days with streamflow) using INFILv3 models 1–4 of the Death Valley region, Nevada and California

[Stream-gage station number and location from the U.S. Geological Survey National Water Information System (NWIS) database. Stream-gage map identifier assigned for purpose of this study only; see figures 27 and 28 for location of gages. Elevation of stream gages in meters above sea level. m^3/d, cubic meters per day]

Stream-gage station number	Stream-gage map identifier	Stream-gage location	Number of days of record	Number of days with flow	Estimated baseflow (m^3/d)	Number of days with flow greater than estimated baseflow	Simulated number of days with flow			
							Model 1	Model 2	Model 3	Model 4
10251300	ART	Amargosa River at Tecopa	9,133	6,947	10,000	683	4	689	18	5
10251259	AR127	Amargosa River at Hwy 127 near California–Nevada line	760	28	100	17	0	54	2	0
10251100	SC	Salt Creek near Stovepipe Wells	5,344	5,344	3,000	56	41	571	87	41
10251220	ARNB	Amargosa River near Beatty	1,827	87	0	87	0	55	3	0
10251218	AR95	Amargosa River at Hwy 95 below Beatty	1,675	41	0	41	0	107	3	1
10251217	ARAB	Amargosa River at Beatty	840	840	5,000	8	0	29	3	1
10251258	FMAV	Fortymile Wash near Amargosa Valley	2,191	13	0	13	0	164	6	1
10251255	FMJ13	Fortymile Wash near well J13	5,054	10	0	10	3	255	22	7
10247901	YL (YL01)	Yucca Lake 01 3024	128	5	0	5	1	1	1	1
10247902	YL (YL02)	Yucca Lake 02 2415	203	3	0	3	1	2	1	1
10251250	FMN	Fortymile Wash at Narrows	4,759	13	0	13	12	245	31	13
10250800	DC	Darwin Creek near Darwin	9,862	9,862	2,500	66	10	1262	18	12
10251215	BW	Beatty Wash near Beatty	2,556	3	0	3	2	97	6	4
10251249	FMSW	Stockade Wash near Fortymile Wash	1,501	4	0	4	8	138	19	9
10251242	FMCC	Fortymile Wash above East Cat Canyon	1,515	6	0	6	4	109	9	5
10251980	LW	Lovell Wash near Blue Diamond	3,653	153	5,000	82	2	5	3	3
10250600	WC	Wildrose Canyon near Wildrose Station	5,478	25	0	25	1	633	3	1
10251243	ECC	East Cat Canyon Wash at Fortymile Wash	1,523	3	0	3	5	74	7	7
10252330	WW	Wheaton Wash near Mountain Pass	1,461	0	0	0	8	41	13	10
09419610	LC	Lee Canyon near Charleston Park	11,323	49	0	49	4	14	19	5
10251350	HTC	Horsethief Canyon near Tecopa, California	3,652	13	0	13	0	108	5	4
10251248	SWUT	Stockade Wash, unnamed tributary	4,148	153	0	153	51	92	62	51
10247860	PV	Penoyer Valley tributary near Tempiute	4,383	7	0	7	1	17	11	1
102512535	DHU	Upper Drillhole Wash	402	1	0	1	2	4	3	3
10252300	CHI	China Spring C Near Mountain Pass, Calif.	4,383	7	0	7	8	40	20	15

Table 12. Measured and simulated streamflow frequency (number of days with streamflow) using INFILv3 models 1–4 of the Death Valley region, Nevada and California—Continued

Stream-gage station number	Stream-gage map identifier	Stream-gage location	Number of days of record	Number of days with flow	Estimated baseflow (m^3/d)	Number of days with flow greater than estimated baseflow	Simulated number of days with flow			
							Model 1	Model 2	Model 3	Model 4
10252550	CC	Caruthers Creek near Ivanpah, Calif.	12,937	1,909	500	812	459	696	471	449
102512533	PWL	Pagany Wash Number 1, NTS, Nev.	1,095	2	0	2	0	6	0	0
10251000	BDC	Big Dip Creek near Stovepipe Wells, Calif.	2,375	10	0	10	0	0	0	0
102512533	PWU	Pagany Wash near the Prow at Yucca Mountain	401	2	0	2	0	3	3	0
102512537	USW	Upper Split Wash at Yucca Mountain	751	3	0	3	0	0	0	0
102512536	WREN	Wren Wash At Yucca Mountain	403	3	0	3	0	0	0	0
		Average estimation error (AEE) days				0.0	–50	107	–43	–50
		Standardized mean-squared error (SMSE)				.0	.59	2.16	.56	.59
		Pearson correlation coefficient (CC)				1.0	.57	.26	.57	.56

Table 13. Measured and simulated total discharge at 31 stream gages using INFILv3 models 1–4 of the Death Valley region, Nevada and California

[Stream-gage station number and location from the U.S. Geological Survey National Water Information System (NWIS) database. Stream-gage map identifiers assigned for purpose of this study only; see figures 27 and 28 for location of gages. Elevation of stream gages in meters above sea level. m^3/d, cubic meters per day]

Stream-gage station number	Stream-gage map identifier	Stream-gage location	Measured total discharge (m^3/d)	Simulated total discharge (m^3/d)			
				Model 1	Model 2	Model 3	Model 4
10251300	ART	Amargosa River at Tecopa	71,543,027	47,274,526	513,667,685	229,642,493	78,525,258
10251259	AR127	Amargosa River at Hwy 127 near California–Nevada line	206,340	0	39,682,778	2,373,191	0
10251100	SC	Salt Creek near Stovepipe Wells	761,243	8,289,442	163,864,728	34,009,787	10,041,015
10251220	ARNB	Amargosa River near Beatty	943,434	0	1,951,977	324,330	0
10251218	AR95	Amargosa River at Hwy 95 below Beatty	1,723,161	0	22,109,760	3,475,201	417,017
10251217	ARAB	Amargosa River at Beatty	729,231	0	11,953,658	2,996,323	573,996
10251258	FMAV	Fortymile Wash near Amargosa Valley	843,194	0	54,296,498	6,022,982	1,699,820
10251255	FMJ13	Fortymile Wash near well J13	881,851	2,509,943	79,398,147	35,683,359	7,696,393
10247901	YL (YL01)	Yucca Lake 01 3024	32,883	1,102,673	8,572,858	11,789,119	2,050,554
10247902	YL (YL02)	Yucca Lake 02 2415	367	1,102,673	8,600,019	11,789,119	2,050,554
10251250	FMN	Fortymile Wash at Narrows	958,897	7,374,068	68,932,916	38,702,403	13,162,113
10250800	DC	Darwin Creek near Darwin	3,195,738	266,189	101,782,598	10,169,435	552,792
10251215	BW	Beatty Wash near Beatty	508,270	211,743	10,576,626	3,041,036	597,971
10251249	FMSW	Stockade Wash near Fortymile Wash	286,333	1,557,364	19,067,938	6,457,569	2,747,882
10251242	FMCC	Fortymile Wash above East Cat Canyon	880,310	747,607	5,875,083	2,175,907	1,191,201
10251980	LW	Lovell Wash near Blue Diamond	2,080,949	436,272	3,722,207	809,586	592,979
10250600	WC	Wildrose Canyon near Wildrose Station	252,520	13,094	12,473,917	118,081	68,887
10251243	ECC	East Cat Canyon Wash at Fortymile Wash	45,557	531,838	1,037,585	734,132	636,328
10252330	WW	Wheaton Wash near Mountain Pass	0	317,146	2,003,650	841,651	587,574
09419610	LC	Lee Canyon near Charleston Park	486,739	593,295	1,920,154	2,157,998	616,712
10251350	HTC	Horsethief Canyon near Tecopa, Calif.	161,480	0	1,120,704	184,212	61,952
10251248	SWUT	Stockade Wash, unnamed tributary	241,633	931,892	1,175,789	1,044,571	926,235
10247860	PV	Penoyer Valley Trib. near Tempiute	19,696	20,912	128,509	46,230	22,371
102512535	DHU	Upper Drillhole Wash	12,233	8,523	95,275	58,432	40,912
10252300	CHI	China Spring C near Mountain Pass, Calif.	10,986	51,940	195,476	147,623	108,927

Table 13. Measured and simulated total discharge using INFILv3 models 1–4 of the Death Valley region, Nevada and California—Continued

Stream-gage station number	Stream-gage map identifier	Stream-gage location	Measured total discharge (m^3/d)	Simulated total discharge (m^3/d)			
				Model 1	Model 2	Model 3	Model 4
10252550	CC	Caruthers Creek near Ivanpah, Calif.	3,250,785	2,252,006	2,712,257	2,478,590	2,211,634
102512533	PWL	Pagany Wash Number 1, NTS, NV	21,066	0	31,660	0	0
10251000	BDC	Big Dip Creek near Stovepipe Wells, Calif.	38,511	0	0	0	0
102512533	PWU	Pagany Wash near the Prow at Yucca Mtn	33,519	0	17,349	2,735	0
102512537	USW	Upper Split Wash at Yucca Mountain	11,255	0	0	0	0
102512536	WREN	Wren Wash At Yucca Mountain	10,325	0	0	0	0
		Total (m^3/d)	90,171,534	75,593,146	1,136,967,802	407,276,093	127,181,078
		Average estimation error (AEE) (m^3/d)	.0	–470,271	33,767,622	10,229,179	1,193,856
		Standardized mean-squared error (SMSE)	.0	.14	49.14	5.77	.07
		Pearson correlation coefficient (CC)	1.0	.95	.86	.94	.95

Table 14. Measured and simulated maximum daily discharge using INFILv3 models 1–4 of the Death Valley region, Nevada and California

[Stream-gage station number and location from the U.S. Geological Survey National Water Information Service (NWIS) database. Stream-gage identifiers assigned for the purpose of this study; see figures 27 and 28 for the location of gages. Elevation of stream gages in meters above sea level. m^3, cubic meters]

Stream-gage station number	Stream-gage map identifier	Stream-gage location	Measured maximum daily discharge (m^3)	Simulated maximum daily discharge (m^3)			
				Model 1	Model 2	Model 3	Model 4
10251300	ART	Amargosa River at Tecopa	3,659,997	37,389,028	107,854,200	136,552,416	54,265,728
10251259	AR127	Amargosa River at Hwy 127 near California–Nevada line	61,067	0	17,020,672	2,372,991	0
10251100	SC	Salt Creek near Stovepipe Wells	138,907	2,405,267	15,761,368	9,221,677	2,708,877
10251220	ARNB	Amargosa River near Beatty	638,579	0	269,015	311,151	0
10251218	AR95	Amargosa River at Hwy 95 below Beatty	1,338,326	0	6,174,311	2,635,134	417,017
10251217	ARAB	Amargosa River at Beatty	560,180	0	6,160,303	2,742,566	573,996
10251258	FMAV	Fortymile Wash near Amargosa Valley	440,400	0	10,032,231	4,694,524	1,699,820
10251255	FMJ13	Fortymile Wash near well J13	562,733	1,085,760	10,033,452	8,082,901	3,994,744
10247901	YL (YL01)	Yucca Lake 01 3024	18,839	1,102,673	8,572,858	11,789,119	2,050,554
10247902	YL (YL02)	Yucca Lake 02 2415	196	1,102,673	8,572,858	11,789,119	2,050,554
10251250	FMN	Fortymile Wash at Narrows	611,666	2,937,097	9,265,382	6,659,115	4,985,582
10250800	DC	Darwin Creek near Darwin	1,054,459	79,888	5,029,695	3,883,204	212,057
10251215	BW	Beatty Wash near Beatty	489,333	210,230	2,725,665	1,429,018	529,695
10251249	FMSW	Stockade Wash near Fortymile Wash	278,920	815,838	2,701,112	1,854,073	1,173,406
10251242	FMCC	Fortymile Wash above East Cat Canyon	489,333	560,431	1,555,324	1,102,922	758,876
10251980	LW	Lovell Wash near Blue Diamond	1,022,599	341,259	1,338,775	520,573	401,505
10250600	WC	Wildrose Canyon near Wildrose Station	112,547	13,094	274,599	104,651	68,887
10251243	ECC	East Cat Canyon Wash at Fortymile Wash	39,147	398,584	480,255	447,503	408,635
10252330	WW	Wheaton Wash near Mountain Pass	0	157,931	266,914	210,408	183,941
09419610	LC	Lee Canyon near Charleston Park	146,800	202,608	512,948	636,010	199,125

Table 14. Measured and simulated maximum daily discharge using INFILv3 models 1–4 of the Death Valley region, Nevada and California—Continued

Stream-gage station number	Stream-gage map identifier	Stream-gage location	Measured maximum daily discharge (m^3)	Simulated maximum daily discharge (m^3)			
				Model 1	Model 2	Model 3	Model 4
10251350	HTC	Horsethief Canyon near Tecopa Ca	44,040	0	135,815	73,920	40,620
10251248	SWUT	Stockade Wash, unnamed tributary	31,807	134,588	136,807	134,883	134,900
10247860	PV	Penoyer Valley Trib. near Tempiute	6,606	20,912	96,687	35,370	22,371
102512535	DHU	Upper Drillhole Wash	12,233	7,136	34,322	22,447	17,407
10252300	CHI	China Spring C Nr Mountain Pass Ca	5,872	16,173	24,177	21,727	19,629
10252550	CC	Caruthers Creek near Ivanpah Ca	195,233	66,211	71,293	81,179	66,124
102512533	PWL	Pagany Wash Number 1, NTS, NV	21,041	0	7,152	0	0
10251000	BDC	Big Dip Creek near Stovepipe Wells Ca	29,360	0	0	0	0
102512533	PWU	Pagany Wash near the Prow at Yucca Mtn	29,360	0	6,906	2,007	0
102512537	USW	Upper Split Wash at Yucca Mountain	7,340	0	0	0	0
102512536	WREN	Wren Wash At Yucca Mountain	6,361	0	0	0	0
		Average estimation error (AEE) (m^3/d)	0.0	1,193,358	6,550,381	6,301,849	2,094,541
		Standardized mean-squared error (SMSE)	.0	74.93	770.03	1,177.36	169.37
		Pearson correlation coefficient (CC)	1.0	.74	.74	.74	.75

Table 15. Measured and simulated monthly streamflow using INFILv3 models 1–4 of the Death Valley region, Nevada and California

[m^3, cubic meters; $(m^3)^2$, cubic meter squared]

Parameter	Measured streamflow	Simulated streamflow			
		Model 1	Model 2	Model 3	Model 4
Average number of days with streamflow per month	0.61	0.18	1.59	0.24	0.17
Maximum number of days with streamflow per month	31	29	31	29	29
Total discharge (m^3)	89,667,928	74,481,948	1,128,131,154	395,438,207	123,283,134
Average monthly discharge (m^3)	25,863	21,483	325,391	114,058	35,559
Maximum monthly discharge (m^3)	7,682,689	37,389,028	110,249,454	136,631,600	54,265,728
Variance in monthly discharge $(m^3)^2$	8.08×10^{10}	4.42×10^{11}	8.37×10^{12}	6.77×10^{12}	1.02×10^{12}
Average estimation error (AEE)	0.0	–4,380	299,528	88,194	9,696
Standardized mean-square error (SMSE)	.0	4.11	91.22	74.45	9.86
Pearson correlation coefficient (CC)	1.0	.50	.71	.57	.53

Table 16. Measured and simulated total discharge and flow-period statistics using INFILv3 models 1–4 of the Death Valley region, Nevada and California

[m^3, cubic meters; $(m^3)^2$, cubic meter squared]

Parameter	Model 1	Model 2	Model 3	Model 4
Measured streamflow				
Total number of days in records	108,229	108,229	108,229	108,229
Number of days with measured streamflow	2,104	2,104	2,104	2,104
Number of flow periods compared	599	999	696	616
Average number of days with measured streamflow per flow period	3.51	2.11	3.02	3.42
Maximum number of days with measured streamflow per flow period	80	80	80	80
Variance in number of days measured streamflow per flow period	50.42	38.61	44.88	49.36
Total measured discharge (m^3)	89,697,287	89,697,287	89,697,287	89,697,287
Average measured discharge per flow period (m^3)	149,745	89,787	128,875	145,612
Maximum measured discharge per flow period (m^3)	9,385,239	9,418,853	9,385,239	9,385,239
Variance of measured discharge per flow period $(m^3)^2$	5.36×10^{11}	3.58×10^{11}	4.64×10^{11}	5.22×10^{11}
Simulated streamflow				
Total number of days with simulated streamflow	625	5511	849	650
Average number of days with simulated streamflow per flow period	1.04	5.52	1.22	1.06
Maximum number of days with simulated streamflow per flow period	40	125	40	40
Variance in number of days measured streamflow per flow period	13.07	160.14	11.41	12.34
Average estimation error for number of days with streamflow	–2.47	3.41	–1.80	–2.36
Standardized mean square error for number of days with streamflow	.96	4.04	.92	.95
Pearson correlation coefficient for number of days with streamflow	.41	.35	.40	.41
Total simulated discharge (m^3)	75,584,621	1,136,967,802	407,276,093	127,181,077
Average simulated discharge per flow period (m^3)	126,185	1,138,106	585,167	206,463
Maximum simulated discharge per flow period (m^3)	37,389,028	109,864,729	136,631,600	54,265,728
Variance of discharge per flow period $(m^3)^2$	2.55×10^{12}	1.49×10^{29}	4.09×10^{29}	5.72×10^{29}
Average estimation error for discharge per flow period (m^3)	–23,560	1,048,319	456,291	60,850
Standardized mean square error for discharge per flow period	3.75	92.58	65.35	8.79
Pearson correlation coefficient for discharge per flow period	.46	.72	.50	.48

Table 17. Selected basin characteristics of the INFILv3 watershed model domains in the Death Valley region, Nevada and California

[See figure 35 for location of watershed model domains. Elevation in meters above sea level. km^2, square kilometer; m, meter]

Map code for watershed model domain	Watershed model domain	Number of model grid cells	Area of watershed model domain (km^2)	Elevation (m)			Slope		Average root-zone layer thickness (m)				
									Soil layers				Rock layer
				Average	Maximum	Minimum	Average	Maximum	All layers	Layer 3	Layer 4	Layer 5	
1	Amargosa River 0	203,149	15,757	944	2,336	–77	4.8	42.0	3.77	0.47	1.22	1.80	0.58
2	Alkali Springs Valley 0	9,074	704	1,675	2,441	1,523	2.2	17.7	4.08	.51	1.33	1.95	.36
3	Alkali Springs Valley 1	1,245	97	1,621	2,249	1,523	3.0	13.1	4.41	.56	1.45	2.11	.26
4	Alkali Springs Valley 2	3	.2	1,523	1,523	1,523	.0	.0	6.00	.70	2.00	3.00	.00
5	Alkali Springs Valley 3	2	.2	1,523	1,523	1,523	.0	.0	6.00	.70	2.00	3.00	.00
6	Beatty Wash 1	119	9	1,712	1,910	1,558	4.7	14.6	0.69	.06	.17	.25	1.19
7	Cactus Flat 0	7,993	620	1,773	2,757	1,621	2.0	20.1	4.46	.54	1.47	2.18	.36
8	Cactus Flat 1	6,330	491	1,817	2,790	1,623	2.6	27.0	4.41	.53	1.45	2.16	.46
9	Clayton Valley 0	14,917	1,157	1,724	2,833	1,310	5.0	27.8	3.39	.44	1.09	1.58	.56
10	Clayton Valley 1	4,485	348	1,645	2,617	1,310	4.5	22.7	4.03	.50	1.32	1.93	.37
11	Coal Valley 0	30,608	2,374	1,781	3,060	1,483	4.0	31.1	3.98	.51	1.29	1.91	.54
12	Coyote Spring Valley 0	7,442	577	1,441	2,908	794	7.7	37.7	3.32	.43	1.04	1.56	.70
13	Coyote Spring Valley 1	1,203	93	1,503	2,192	1,045	9.1	26.1	1.57	.25	.41	.61	.95
14	Death Valley 0	8,938	693	877	2,743	–70	9.1	40.3	3.42	.42	1.09	1.62	.66
15	Death Valley 1	5,924	459	612	3,127	–77	10.6	39.4	3.37	.43	1.07	1.57	.65
16	Death Valley 2	7,957	617	668	2,546	–73	9.3	39.4	3.23	.38	1.03	1.55	.67
17	Death Valley 3	4,005	311	703	3,302	–75	10.8	38.8	3.25	.40	1.03	1.53	.63
18	Fish Lake Valley 0	5,576	432	1,978	2,786	1,575	4.4	16.9	3.30	.47	1.03	1.51	.62
19	Frenchman Flat	29,127	2,259	1,370	2,315	958	3.9	27.7	3.76	.48	1.21	1.79	.43
20	Gold Flat	22,502	1,745	1,752	2,638	1,531	2.8	25.2	3.34	.40	1.09	1.61	.64
21	Groom Lake 0	11,934	926	1,737	2,767	1,401	4.7	26.7	3.22	.39	1.04	1.55	.74
22	Groom Lake 1	7,200	558	1,535	2,241	1,401	3.0	21.0	3.71	.46	1.19	1.78	.46
23	Groom Lake 2	2,038	158	1,470	1,874	1,401	2.9	16.7	4.23	.50	1.38	2.06	.36
24	Hot Creek Valley	10,993	853	1,895	2,807	1,584	4.1	30.5	3.34	.42	1.08	1.60	.71
25	Indian Springs Valley 1	21,784	1,690	1,346	3,110	906	5.2	31.6	3.99	.50	1.28	1.92	.47

Table 17. Selected basin characteristics of the INFILv3 watershed model domains in the Death Valley region, Nevada and California—Continued

Map code for watershed model domain	Watershed model domain	Number of model grid cells	Area of watershed model domain (km^2)	Elevation (m)			Slope		Average root-zone layer thickness (m)				
									Soil layers				Rock layer
				Average	Maximum	Minimum	Average	Maximum	All layers	Layer 3	Layer 4	Layer 5	
26	Ivanpah Valley North	9,289	720	1,117	2,366	801	4.6	24.8	3.93	.50	1.25	1.87	.44
27	Ivanpah Valley South	16,413	1,273	1,195	2,332	800	4.6	31.5	3.95	.49	1.28	1.90	.52
28	Jean Lake Valley	4,221	327	1,020	1,701	853	3.7	19.4	4.00	.54	1.28	1.88	.46
29	Kawich Valley	12,331	956	1,852	2,586	1,615	4.2	28.4	3.59	.42	1.17	1.75	.65
30	Las Vegas Valley 0	50,593	3,924	1,209	3,500	479	5.0	43.4	3.88	.49	1.24	1.85	.53
31	Las Vegas Valley 1	8	1	819	853	792	1.4	1.8	6.00	.70	2.00	3.00	.00
32	Lida Valley	16,850	1,307	1,713	2,699	1,431	3.5	24.6	3.91	.51	1.26	1.85	.42
33	Mesquite Valley	12,877	999	1,080	2,455	792	4.9	26.5	3.78	.46	1.22	1.81	0.54
34	North Death Valley	64,372	4,993	1,029	2,702	–70	8.3	43.9	3.08	.38	.97	1.44	.89
35	North Saline Valley	18,349	1,423	1,500	3,052	883	7.7	34.1	3.07	.41	.95	1.41	.65
36	Panamint Valley 0	21,902	1,699	990	2,671	301	7.2	35.6	2.95	.36	.93	1.38	1.02
37	Panamint Valley 1	13,381	1,038	1,186	3,247	302	10.0	34.7	3.28	.41	1.03	1.54	.81
38	Panamint Valley 2	15,371	1,192	1,439	2,644	464	7.1	35.0	2.88	.36	.90	1.33	1.11
39	Panamint Valley 3	3,911	303	1,014	2,256	465	7.7	31.4	4.61	.56	1.50	2.24	.47
40	Penoyer Valley 0	16,795	1,303	1,686	2,447	1,462	2.9	27.2	3.90	.47	1.27	1.89	.52
41	Penoyer Valley 1	6,792	527	1,775	2,757	1,462	4.5	28.3	3.98	.52	1.28	1.90	.59
42	Pahranagat Valley	32,647	2,532	1,471	2,558	776	4.7	27.5	3.68	.45	1.18	1.76	.52
43	Pahrump Valley 0	24,328	1,887	1,341	3,486	747	5.1	31.0	4.08	.50	1.32	1.97	.51
44	Pahrump Valley 1	9,947	771	1,091	2,611	729	5.4	31.4	4.45	.55	1.45	2.16	.41
45	Pahrump Valley 2	1,119	87	877	1,499	735	5.4	26.7	3.53	.51	1.14	1.60	.61
46	Ralston Valley	43,760	3,394	1,799	2,824	1,565	2.7	28.8	4.12	.51	1.35	2.00	.44
47	Railroad Valley North 0	2,509	195	1,857	3,038	1,493	4.9	27.6	3.43	.47	1.09	1.60	.72
48	Railroad Valley North 2	1,852	144	1,970	3,046	1,476	9.4	33.2	3.14	.45	.97	1.44	.97
49	Railroad Valley North 3	315	24	1,633	2,424	1,484	2.3	13.4	5.08	.62	1.69	2.50	.20
50	Railroad Valley North 4	2,047	159	1,621	2,199	1,485	3.2	30.5	4.47	.54	1.48	2.19	.32
51	Railroad Valley South	20,778	1,611	1,766	2,623	1,468	3.7	26.7	4.06	.49	1.33	1.99	.51

Table 17. Selected basin characteristics of the INFILv3 watershed model domains in the Death Valley region, Nevada and California—Continued

Map code for watershed model domain	Watershed model domain	Number of model grid cells	Area of watershed model domain (km^2)	Elevation (m)			Slope		Average root-zone layer thickness (m)				
									Soil layers				Rock layer
				Average	Maximum	Minimum	Average	Maximum	All layers	Layer 3	Layer 4	Layer 5	
52	Sarcobatus Flat 0	30,110	2,335	1,493	2,574	1,188	3.7	27.2	3.75	.47	1.22	1.79	.45
53	Sarcobatus Flat 1	768	60	1,312	1,770	1,205	4.3	23.8	4.05	.48	1.33	1.98	.42
54	Saline Valley	26,015	2,018	1,318	3,277	309	10.9	43.1	2.56	.35	.77	1.13	.91
55	Shadow Valley 0	526	41	1,205	1,401	958	3.9	14.6	1.24	.20	.31	.44	1.27
56	Stonewall Flat	12,161	943	1,645	2,385	1,402	3.0	26.0	3.40	.40	1.10	1.63	.56
57	Tikapoo Valley North	2,027	157	1,438	2,044	1,218	5.0	24.7	3.72	.46	1.19	1.78	.45
58	Tikapoo Valley South	31,388	2,434	1,488	2,838	991	4.9	34.9	3.54	.44	1.12	1.68	.58
59	Three Lakes Valley N	9,551	741	1,421	2,948	1,066	5.9	32.3	3.54	.45	1.12	1.68	.53
60	Three Lakes Valley S	11,336	879	1,362	3,121	914	4.8	27.6	4.24	.53	1.36	2.04	.45
61	Tonopah Flat 0	22,471	1,743	1,649	2,723	1,403	3.1	37.2	4.43	.53	1.45	2.15	.31

Table 18. Simulation results of INFILv3 model 1 for watershed model domains in the the Death Valley region, Nevada and California, 1950–99

[See figure 35 for location of watershed model domains. °C, degrees Celsius]

Map code for watershed model domain	Watershed model domain	Average air temperature (°C)	Simulation results (average for the watershed model domain), in millimeters per year										
			Potential evapotranspiration	Precipitation	Snow	Sublimation	Evapotranspiration	Change in root-zone water content	Runoff (A)	Infiltrated run-on (B)	Run-on net infiltration (C)	Total net infiltration	Surface-water outflow (E) (A–B–C=E)
1	Amargosa River 0	16.7	1,582	140.4	5.3	0.5	138.4	0.07	1.59	1.52	0.018	1.34	.047
2	Alkali Springs Valley 0	10.9	1,348	159.7	24.1	2.8	156.8	–.13	.39	.39	.000	.23	.000
3	Alkali Springs Valley 1	11.1	1,343	153.9	20.3	2.1	151.8	–.16	.22	.22	.000	.06	.000
4	Alkali Springs Valley 2	12.0	1,406	147.0	13.9	1.4	145.8	–.18	.00	.00	.000	.00	.000
5	Alkali Springs Valley 3	12.0	1,389	147.0	14.0	1.4	145.8	–.18	.00	.00	.000	.00	.000
6	Beatty Wash 1	10.5	1,351	211.5	29.1	2.8	196.6	.11	8.74	2.45	.041	5.72	6.245
7	Cactus Flat 0	10.0	1,322	206.2	40.6	4.4	199.7	.01	2.29	2.03	.015	1.81	.249
8	Cactus Flat 1	9.6	1,314	207.2	48.2	5.8	199.8	–.07	2.05	1.94	.013	1.58	.095
9	Clayton Valley 0	10.0	1,310	168.6	38.1	4.5	163.1	–.08	1.05	1.04	.008	1.08	.000
10	Clayton Valley 1	10.7	1,357	156.3	26.1	3.0	153.2	–.13	.40	.40	.000	.21	.000
11	Coal Valley 0	10.1	1,316	267.8	57.0	6.1	257.8	.01	4.49	4.15	.023	3.54	.324
12	Coyote Spring Valley 0	12.6	1,396	208.1	32.1	3.3	198.5	–.14	.49	.48	.000	6.35	.007
13	Coyote Spring Valley 1	12.2	1,377	209.0	23.8	2.1	201.1	–.16	.43	.43	.001	5.98	.003
14	Death Valley 0	17.4	1,564	123.5	7.1	.5	120.1	.14	2.12	1.89	.003	2.44	.230
15	Death Valley 1	19.4	1,629	120.3	16.0	1.8	115.2	.41	6.22	5.44	.005	2.10	.775
16	Death Valley 2	18.8	1,625	124.1	6.4	.6	120.3	.49	4.78	4.24	.005	2.18	.526
17	Death Valley 3	18.8	1,603	125.0	24.4	2.8	117.1	.27	7.53	6.82	.027	4.04	.682
18	Fish Lake Valley 0	8.3	1,268	210.1	68.3	8.3	200.3	.00	2.90	2.89	.002	1.43	.002
19	Frenchman Flat	13.2	1,448	174.6	10.8	.9	171.3	.20	2.27	2.15	.011	2.08	.107
20	Gold Flat	10.2	1,330	204.2	36.9	3.8	197.0	.05	3.81	3.39	.035	2.94	.387
21	Groom Lake 0	10.3	1,341	219.3	42.8	4.6	208.8	.27	7.56	7.00	.163	5.24	.391
22	Groom Lake 1	11.8	1,397	197.4	17.6	1.5	191.9	.32	2.79	2.43	.004	3.32	.356
23	Groom Lake 2	12.4	1,398	183.9	10.7	.8	182.3	.17	1.96	1.91	.002	.61	.046
24	Hot Creek Valley	8.8	1,262	224.8	60.2	6.9	214.5	–.06	3.60	3.56	.033	3.49	.012
25	Indian Springs Valley 1	13.4	1,447	168.7	16.6	1.4	164.2	.00	1.16	1.07	.003	2.92	.086

Table 18. Simulation results of INFILv3 model 1 for watershed model domains in the the Death Valley region, Nevada and California, 1950–99—Continued

Map code for watershed model domain	Watershed model domain	Average air temperature (°C)	Simulation results (average for the watershed model domain), in millimeters per year										
			Potential evapotran-spiration	Precipi-tation	Snow	Sublimation	Evapotrans-piration	Change in root-zone water content	Runoff (A)	Infiltrated run-on (B)	Run-on net infiltration (C)	Total net infiltration	Surface-water outflow (E) (A–B–C=E)
26	Ivanpah Valley North	16.0	1,570	178.6	5.9	0.6	175.7	0.11	0.96	0.88	0.000	02.17	0.078
27	Ivanpah Valley South	15.8	1,551	194.9	6.8	.6	192.6	.27	4.55	4.38	.003	1.32	.167
28	Jean Lake Valley	16.6	1,581	163.4	1.8	.1	163.0	.00	.15	.15	.000	.31	.000
29	Kawich Valley	9.4	1,294	227.6	52.8	5.4	216.6	.25	7.17	6.63	.069	4.89	.467
30	Las Vegas Valley 0	14.6	1,508	174.4	25.3	2.9	166.8	–.20	.91	.86	.002	4.82	.043
31	Las Vegas Valley 1	17.5	1,615	121.1	.4	.0	121.3	–.21	.00	.00	.000	.00	.000
32	Lida Valley	10.5	1,345	180.2	33.3	3.8	176.0	–.10	0.98	.98	.002	.53	.000
33	Mesquite Valley	16.1	1,560	170.4	5.6	.5	166.6	.15	1.62	1.61	.002	3.16	.001
34	North Death Valley	16.0	1,531	140.6	16.7	1.6	136.1	.12	1.69	1.56	.009	2.56	.117
35	North Saline Valley	12.1	1,391	168.8	28.3	2.8	163.0	.29	1.25	1.25	.009	2.71	.000
36	Panamint Valley 0	16.2	1,555	144.4	10.6	1.1	141.2	.15	4.28	4.13	.093	1.91	.054
37	Panamint Valley 1	14.9	1,494	166.6	37.6	4.3	157.0	.40	9.52	9.05	.014	4.42	.457
38	Panamint Valley 2	12.9	1,446	187.1	31.0	3.1	179.7	.18	4.88	4.85	.014	4.12	.019
39	Panamint Valley 3	16.3	1,546	142.5	12.1	1.2	139.3	.28	1.04	.91	.002	1.60	.122
40	Penoyer Valley 0	10.5	1,332	217.5	34.6	3.3	209.5	–.02	4.18	3.69	.039	4.36	.454
41	Penoyer Valley 1	10.0	1,334	248.1	56.0	6.5	239.6	–.26	4.30	3.97	.018	1.82	.315
42	Pahranagat Valley	12.2	1,401	216.9	23.1	2.2	211.9	–.11	.89	.89	.007	2.82	.000
43	Pahrump Valley 0	13.6	1,484	194.4	37.5	5.0	181.7	–.05	2.08	1.79	.004	7.51	.289
44	Pahrump Valley 1	15.0	1,528	147.1	12.8	1.4	142.7	.02	2.82	2.16	.000	2.25	.666
45	Pahrump Valley 2	16.8	1,575	126.1	1.1	.0	124.0	–.08	1.64	.87	.000	1.31	.773
46	Ralston Valley	9.8	1,310	186.0	40.2	4.8	179.5	–.11	1.77	1.69	.012	1.68	.070
47	Railroad Valley North 0	9.4	1,272	257.6	75.8	8.9	244.0	–.15	8.27	7.85	.065	4.50	.352
48	Railroad Valley North 2	8.6	1,188	289.6	102.4	10.6	270.2	–.16	9.68	8.88	.135	8.35	.670
49	Railroad Valley North 3	11.1	1,326	223.1	32.9	3.0	217.6	–.35	2.79	2.69	.080	2.76	.021
50	Railroad Valley North 4	10.9	1,356	199.6	24.4	2.5	195.8	–.40	2.08	2.02	.018	1.63	.034

Table 18. Simulation results of INFILv3 model 1 for watershed model domains in the the Death Valley region, Nevada and California, 1950–99—Continued

Map code for watershed model domain	Watershed model domain	Average air temperature (°C)	Simulation results (average for the watershed model domain), in millimeters per year										
			Potential evapotran-spiration	Precipi-tation	Snow	Sublimation	Evapotrans-piration	Change in root-zone water content	Runoff (A)	Infiltrated run-on (B)	Run-on net infiltration (C)	Total net infiltration	Surface-water outflow (E) (A–B–C=E)
51	Railroad Valley South	9.9	1,307	222.4	44.7	4.6	214.5	–0.05	3.62	3.36	0.042	3.13	0.218
52	Sarcobatus Flat 0	12.1	1,401	171.5	19.2	1.8	168.0	.01	2.17	2.01	.009	1.55	.157
53	Sarcobatus Flat 1	13.4	1,464	149.5	6.9	.6	148.0	–.10	1.06	1.01	.000	1.00	.048
54	Saline Valley	13.8	1,422	170.8	36.2	3.5	158.1	.49	4.59	4.51	.053	8.70	.030
55	Shadow Valley 0	15.2	1,549	181.7	3.3	.3	180.8	.03	.55	.54	.002	.62	.000
56	Stonewall Flat	11.1	1,365	177.6	26.2	2.7	173.3	–.09	1.12	1.08	.007	1.59	.030
57	Tikapoo Valley North	12.5	1,387	192.0	14.6	1.1	187.7	–.15	.55	.51	.000	3.38	.043
58	Tikapoo Valley South	12.1	1,398	203.5	24.6	2.4	198.0	–.08	.96	.96	.005	3.14	.002
59	Three Lakes Valley North	12.8	1,429	188.9	19.7	1.9	183.9	–.04	.51	.49	.000	3.18	.011
60	Three Lakes Valley South	13.3	1,435	176.5	26.6	2.8	171.1	–.16	.34	.34	.000	2.71	.000
61	Tonopah Flat 0	10.7	1,338	163.8	24.8	2.7	160.6	–.13	.85	.79	.000	.54	.057
	All areas	12.7	1,421	183.0	27.3	2.9	177.1	.02	2.72	2.43	.018	2.71	.271

Table 19. Summary of INFILv3 model results for the Death Valley regional flow system, Nevada and California

[Total volumes are rounded to nearest 100 cubic meters per day. m^3/d, cubic meter per day; mm/yr, millimeter per year; <, less than; na, not available]

Model or method	Parameter	Total volume (m^3/d)	Average annual rate (mm/yr)	Maximum average annual rate (mm/yr)	Minimum average annual rate (mm/yr)	Absolute percentage of total precipitation
PRISM annual precipitation	Precipitation (rain and snow)	22,501,500	181.5	584.2	25.4	na
Previous recharge estimates	Recharge (basinwide)	327,300	2.6	12.5	<.1	na
MODFLOW ground-water flow model (D'Agnese and others, 2002)	Recharge (basinwide)	266,800	2.1	na	na	na
Preliminary INFIL model (Hevesi and others, 2002)	Precipitation (rain and snow)	24,094,100	195.1	765.4	76.0	na
	Total net infiltration	963,300	7.8	362.6	.0	4.00
INFILv3, model 1	Results for the entire area within the INFILv3 watershed model boundary					
	Potential evapotranspiration	142,767,500	1,151.4	1,615.8	465.0	672.0
	Inflows					
	Precipitation (rain and snow)	21,242,200	171.3	551.7	53.5	100.0
	Snowmelt	2,432,000	19.6	388.8	.0	11.4
	Infiltrated run-on[1]	249,400	2.0	1,513.6	.0	1.17
	Storage					
	Snowfall	2,717,100	21.9	467.7	.0	12.8
	Change in root-zone water content[2]	4,200	.03	37.2	–4.0	.02
	Runoff generation[3]	275,300	2.2	136.3	.0	1.30
	Outflows					
	Sublimation	285,100	2.3	92.8	.0	1.34
	Evapotranspiration	20,585,400	166.0	580.9	44.9	96.9
	Run-on net infiltration[4]	2,400	.02	125.5	.0	.01
	Net infiltration	344,000	2.8	1,262.3	.0	1.62
	Surface water outflow (inflow to playas)[5]	25,900	.2	na	na	.12
	Adjusted net infiltration					
	Net infiltration adjusted for discharge zones[6]	342,100	2.8	1,262.3	.0	1.61
	Net infiltration adjusted for all playas[7]	340,500	2.7	1,262.3	.0	1.60
	Net infiltration for playa areas[8]	1,600	.01	na	na	.01
	Results for upland areas[9]					
	Runoff generation	226,100	4.3	136.3	.0	1.06
	Infiltrated run-on	87,600	1.7	303.0	.0	.41
	Run-on net infiltration	1,300	.02	19.8	.0	.01
	Net surface water outflow[10]	138,500	2.7	na	na	.65
	Net infiltration	309,800	5.9	256.8	.0	1.46

See footnotes at end of table.

Table 19. Summary of INFILv3 model results for the Death Valley regional flow system, Nevada and California —Continued

Model or method	Parameter	Total volume (m^3/d)	Average annual rate (mm/yr)	Maximum average annual rate (mm/yr)	Minimum average annual rate (mm/yr)	Absolute percentage of total precipitation
	Results for alluvial fan and basin areas[11]					
	Runoff generation	49,100	.7	37.01	0	.23
	Infiltrated run-on	161,800	2.3	1,513.6	0	.76
	Run-on net infiltration	1,000	.01	125.5	0	.005
	Net surface water outflow	–112,700	–1.6	na	na	1.03
	Net infiltration	34,200	.5	1,262.3	.0	.16
	Net infiltration adjusted for discharge zones	32,300	0.5	1,262.3	0.0	0.15
INFILv3, model 2	Results for the entire area within the INFILv3 watershed model boundary					
	Potential evapotranspiration	142,767,500	1,151.4	1,615.8	465.0	672.0
	Inflows					
	Precipitation (rain and snow)	21,242,200	171.3	551.7	53.5	100.0
	Snowmelt	2,432,000	19.6	388.8	.0	11.4
	Infiltrated run-on	0	.0	.0	.0	.00
	Storage					
	Snowfall	2,717,100	21.9	467.7	.0	12.8
	Change in root-zone water content	–6,300	–.05	14.8	–2.6	.26
	Runoff generation	263,700	2.1	136.3	.0	1.24
	Outflows					
	Sublimation	285,100	2.3	92.8	.0	1.34
	Evapotranspiration	20,406,200	164.6	403.7	44.9	96.1
	Run-on net infiltration	0	.0	.0	.0	.00
	Net infiltration	293,500	2.4	210.2	.0	1.38
	Surface-water outflow (inflow to playas)	263,700	2.1	na	na	1.24
	Adjusted net infiltration					
	Net infiltration adjusted for discharge zones	293,100	2.4	210.2	.0	1.38
	Net infiltration adjusted for all playas	291,900	2.4	210.2	.0	1.37
	Net infiltration for playa areas	1,200	.01	.0	.0	.001
	Results for upland areas					
	Runoff generation	214,600	4.1	136.3	.0	1.01
	Infiltrated run-on	0	.0	.0	.0	.00
	Run-on net infiltration	0	.0	.0	.0	.00
	Net surface water outflow	214,600	4.1	na	na	1.01
	Net infiltration	291,700	5.6	210.2	.0	1.37
	Results for alluvial fan and basin areas					
	Runoff generation	49,100	.7	37.0	.0	.23
	Infiltrated run-on	0	.0	.0	.0	.00
	Run-on net infiltration	0	.0	.0	.0	.00
	Net surface water outflow	49,100	.7	na	na	.23
	Net infiltration	1,700	.02	12.8	.0	.01
	Net infiltration adjusted for discharge zones	1,400	.02	12.8	.0	.01

Table 19. Summary of INFILv3 model results for the Death Valley regional flow system, Nevada and California —Continued

Model or method	Parameter	Total volume (m^3/d)	Average annual rate (mm/yr)	Maximum average annual rate (mm/yr)	Minimum average annual rate (mm/yr)	Absolute percentage of total precipitation
INFILv3, model 3	Results for the entire area within the INFILv3 watershed model boundary					
	Potential evapotranspiration	142,767,500	1,151.4	1,615.8	465.0	672.0
	Inflows					
	Precipitation (rain and snow)	21,242,200	171.3	551.7	53.5	100.0
	Snowmelt	2,464,100	19.9	397.8	.0	11.6
	Infiltrated run-on	404,200	3.3	828.0	.0	1.90
	Storage					
	Snowfall	2,717,100	21.9	467.7	.0	12.8
	Change in root-zone water content	8,700	.07	39.4	–2.5	.04
	Runoff generation	500,600	4.0	139.8	.0	2.36
	Outflows					
	Sublimation	252,900	2.0	82.6	.0	1.19
	Evapotranspiration	20,705,600	167.0	488.4	40.1	97.5
	Run-on net infiltration	1,100	.009	50.7	.0	.01
	Total net infiltration	179,800	1.4	697.4	.0	.85
	Surface-water outflow (inflow to playas)	96,300	.8	na	na	.45
	Adjusted net infiltration					
	Net infiltration adjusted for discharge zones	178,700	1.4	697.4	.0	.84
	Net infiltration adjusted for all playas	177,700	1.4	697.4	.0	.84
	Net infiltration for playa areas	1,200	.01	na	na	.006
	Results for upland areas					
	Runoff generation	363,400	7.0	139.8	.0	1.71
	Infiltrated run-on	178,100	3.4	267.6	.0	.84
	Run-on net infiltration	1,100	.02	11.9	.0	.01
	Net surface water outflow	185,300	.8	na	na	.87
	Net infiltration	164,000	3.1	215.8	.0	.77
	Results for alluvial fan and basin areas					
	Runoff generation	137,200	1.9	56.0	.0	.65
	Infiltrated run-on	226,100	3.1	828.0	.0	1.06
	Run-on net infiltration	< 100	<.001	50.7	.0	<.001
	Net surface water outflow	–88,900	.8	na	na	.42
	Net infiltration	15,700	.2	697.4		.07
	Net infiltration adjusted for discharge zones	14,700	.2	697.4	.0	.07
INFILv3, model 4	Results for the entire area within the INFILv3 watershed model boundary					
	Potential evapotranspiration	145,330,400	1,172.1	1,624.2	479.2	684.16
	Inflows					
	Precipitation (rain and snow)	21,242,200	171.3	551.7	53.5	100.00
	Snowmelt	2,426,800	19.6	387.0	.0	11.42
	Infiltrated run-on	238,800	1.9	1,015.7	.0	1.12

Table 19. Summary of INFILv3 model results for the Death Valley regional flow system, Nevada and California —Continued

Model or method	Parameter	Total volume (m^3/d)	Average annual rate (mm/yr)	Maximum average annual rate (mm/yr)	Minimum average annual rate (mm/yr)	Absolute percentage of total precipitation
	Storage					
	Snowfall	2,717,100	21.9	467.7	.0	12.79
	Change in root-zone water content	4,200	<.1	37.2	-3.7	.02
	Runoff generation	270,800	2.2	136.3	.0	1.27
	Outflows					
	Sublimation	290,300	2.3	93.9	.0	1.37
	Evapotranspiration	20,771,300	167.5	530.9	45.0	97.78
	Run-on net infiltration	1,100	.01	39.9	.0	.01
	Total net infiltration	145,700	1.2	882.6	.0	.69
	Surface water discharge to playas	32,000	.3	na	na	.15
	Adjusted net infiltrations					
	Net infiltration adjusted for discharge zones	144,700	1.2	882.6	.0	.68
	Net infiltration adjusted for all playas	143,100	1.2	882.6	.0	.67
	Net infiltration for playa areas	1,600	.01	.0	.0	.001
	Results for upland areas					
	Runoff generation	221,700	4.25	136.3	.0	1.04
	Infiltrated run-on	85,200	1.63	264.4	.0	.40
	Run-on net infiltration	900	.02	12.7	.0	.004
	Net surface water outflow	136,500	2.6	na	na	.64
	Net infiltration	124,100	2.4	224.7	.0	.58
	Results for alluvial fan and basin areas					
	Runoff generation	49,100	.7	37.0	.0	.23
	Infiltrated run-on	153,600	2.1	1,015.7	.0	.72
	Run-on net infiltration	200	.003	39.9	.0	.001
	Net surface water outflow	–104,400	–1.4	na	na	–.49
	Net infiltration	21,600	.3	882.6	.0	.10
	Net infiltration adjusted for discharge zones	20,600	.3	882.6	.0	.10
Average for models 1, 2, 3, 4	Net infiltration adjusted for discharge zones	239,700	1.9	542.2	.0	1.1
Average for models 1, 3, 4	Net infiltration adjusted for discharge zones	221,800	1.8	722.9	.0	1.0
Average for models 1, 3	Net infiltration adjusted for discharge zones	260,400	2.1	764.6	.0	1.2

[1]Infiltrated run-on is runoff that has been routed to downstream grid cells and has infiltrated into the root zone causing an increase in the root-zone water content.

[2]Change in root-zone water content indicates difference in water content between the first and last day of the simulation; positive values indicate an increase relative to the first day, and negative values indicate a decrease relative to the first day.

[3]Runoff generation indicates in-place runoff calculated as excess rain or snowmelt.

[4]Run-on net infiltration is net infiltration in direct response to the downstream routing and infiltration of surface water (runoff).

[5]Surface-water outflow indicates either inflow to playa lakes (all of which is assumed to evaporate) or streamflow into or out of a basin. Positive values indicate a net loss of surface water, while negative values indicate a net gain of surface water (inflow to basin).

[6]Net infiltration is set to zero for all areas identified as discharge zones in D'Agnese and others (2002).

[7]Net infiltration is set to zero for all areas identified as playas (figure 3).

Table 20. Average annual precipitation simulated using the INFILv3 model and estimated using PRISM for hydrographic areas and subareas in the Death Valley region, Nevada and California

[See figure 4 for location of hydrographic areas and subareas. PRISM, parameter-elevation regressions on independent slopes model (Daly and others, 1994). mm/yr, millimeters per year]

Hydrographic areas and subareas		Simulated precipitation using INFILv3 (mm/yr)			Estimated precipitation using PRISM (mm/yr)		
Name	Identifier	Average	Maximum	Minimum	Average	Maximum	Minimum
Alkali Spring Valley	142	159	246	143	145	178	127
Amargosa Desert	230	126	265	104	132	330	76
Cactus Flat	148	207	355	177	189	330	127
California Valley	241	153	290	118	148	330	127
Chicago Valley	240	131	236	110	134	229	127
Clayton Valley	143	164	312	118	159	279	127
Coal Valley	171	251	418	221	253	432	178
Crater Flat	229	146	247	112	145	279	127
Death Valley	243	132	488	54	130	483	25
Emigrant Valley (Groom Lake)	158A	208	388	175	230	330	178
Emigrant Valley (Papoose Lake)	158B	190	228	177	232	279	178
Fortymile Canyon (Buckboard Mesa)	227B	212	300	163	301	432	178
Fortymile Canyon (Jackass Flats)	227A	157	275	113	170	381	127
Frenchman Flat	160	163	277	120	185	381	127
Garden Valley	172	282	513	235	292	686	178
Gold Flat	147	204	334	179	219	432	127
Hidden Valley (south)	166	161	189	151	143	178	127
Indian Springs Valley	161	172	453	123	213	533	127
Ivanpah Valley (north)	164A	184	384	147	169	381	127
Ivanpah Valley (south)	164B	189	357	148	178	330	127
Jean Lake Valley	165	168	298	146	147	279	127
Kawich Valley	157	226	341	196	246	432	178
Las Vegas Valley	212	174	551	104	195	584	76
Lida Valley	144	179	316	152	155	279	127
Lower Amargosa Valley	242	125	211	99	121	229	76
Mercury Valley	225	148	267	125	171	330	127
Mesquite Valley	163	175	394	139	168	432	127
Oasis Valley	228	178	273	127	226	381	127
Pahranagat Valley	209	210	375	152	225	381	127
Pahrump Valley	162	176	547	115	201	584	127
Penoyer Valley	170	225	429	186	229	483	178
Railroad Valley (south)	173A	226	348	186	208	330	127
Rock Valley	226	144	226	115	146	229	127
Sarcobatus Flat	146	170	325	140	169	381	127
Shadow Valley	245	186	358	141	186	330	127
Stonewall Flat	145	178	273	151	150	279	127

Table 20. Average annual precipitation simulated using the INFILv3 model and estimated using PRISM for hydrographic areas and subareas in the Death Valley region, Nevada and California—Continued

Hydrographic areas and subareas		Simulated precipitation using INFILv3 (mm/yr)			Estimated precipitation using PRISM (mm/yr)		
Name	Identifier	Average	Maximum	Minimum	Average	Maximum	Minimum
Three Lakes Valley (north)	168	182	430	147	200	381	127
Three Lakes Valley (south)	211	171	431	125	195	533	127
Tikapoo Valley (north)	169A	209	394	167	229	330	178
Tikapoo Valley (south)	169B	189	380	149	200	381	127
Valjean Valley	244	127	302	92	137	279	76
Yucca Flat	159	184	300	153	217	432	127
Total area covered by all hydrographic areas and subareas		175	551	54	182	686	25

Table 21. Simulation results using INFILv3 model 1 for hydrographic areas and subareas in the Death Valley region, Nevada and California, 1950–99

[Net infiltration over designated discharge zones set to 0. Positive outflow indicates net discharge from area to playa or to downstream drainage; negative outflow indicates net inflow to area. All values are in millimeters per year. na, not applicable]

Hydrographic areas and subareas		Potential evapotranspiration	Precipitation	Snowfall	Sublimation	Evapotranspiration	Change in storage	Runoff	Infiltrated run-on	Net infiltration	Adjusted net infiltration [1]	Outflow
Name	Identifier											
Alkali Spring Valley	142	1,060	159.8	24.2	2.81	156.9	–0.13	0.39	0.38	0.21	0.21	0.01
Amargosa Desert	230	1,244	125.8	2.4	.18	124.9	–.02	.52	.58	.77	.77	–.05
Cactus Flat	148	1,039	207.0	43.9	4.99	200.1	–.01	2.21	2.06	1.70	1.70	.15
California Valley	241	1,222	153.1	4.7	.35	149.7	.14	2.91	2.82	2.75	2.75	.09
Chicago Valley	240	1,277	131.4	1.3	.09	128.8	–.03	.32	.33	2.49	2.49	–.01
Clayton Valley	143	1,042	164.8	34.5	4.01	160.0	–.09	.89	.88	.90	.90	.00
Coal Valley	171	1,051	251.6	40.9	3.91	243.7	.24	3.88	3.51	3.47	3.47	.37
Crater Flat	229	1,196	146.6	5.5	.47	145.3	.07	.92	.84	.70	.70	.08
Death Valley	243	1,243	132.5	13.9	1.42	128.4	.16	2.48	2.16	2.22	2.19	.32
Emigrant Valley (Groom Lake)	158A	1,074	208.8	31.4	3.21	200.7	.27	5.35	4.80	4.14	4.14	.55
Emigrant Valley (Papoose Lake)	158B	1,104	190.7	13.5	1.04	187.0	.26	3.90	3.10	1.61	1.61	.80
Fortymile Canyon (Buckboard Mesa)	227B	1,057	212.7	35.3	3.68	203.0	.20	7.70	5.92	4.04	4.04	1.79
Fortymile Canyon (Jackass Flats)	227A	1,184	157.2	8.0	.73	154.4	.32	2.79	3.56	2.67	2.67	–.77
Frenchman Flat	160	1,161	163.3	7.0	.54	160.8	.07	1.41	1.44	1.98	1.98	–.03
Garden Valley	172	1,022	282.7	71.7	8.11	271.1	–.22	5.08	4.82	3.50	3.50	.27
Gold Flat	147	1,047	204.4	37.2	3.84	197.2	.05	3.84	3.37	2.94	2.94	.47
Hidden Valley (south)	166	1,247	161.3	1.4	.12	160.9	–.02	.00	.00	.33	.33	.00
Indian Springs Valley	161	1,134	172.0	20.1	1.88	166.7	–.02	1.09	.98	3.27	3.27	.11
Ivanpah Valley (north)	164A	1,223	184.6	8.0	.78	181.0	.00	.65	.53	2.73	2.73	.12
Ivanpah Valley (south)	164B	1,234	189.2	5.8	.51	187.1	.35	3.93	4.09	1.47	1.47	–.16
Jean Lake Valley	165	1,236	168.7	2.8	.21	168.3	.06	.46	.67	.36	.36	–.21
Kawich Valley	157	1,021	226.8	51.8	5.30	216.1	.25	6.99	6.62	4.89	4.89	.37
Las Vegas Valley	212	1,188	174.5	26.8	3.13	166.6	–.21	.94	.89	4.97	4.97	.04
Lida Valley	144	1,063	179.7	32.7	3.73	175.6	–.11	.98	.96	.54	.54	.02
Lower Amargosa Valley	242	1,286	125.7	1.0	.06	125.0	–.02	.22	.33	.79	.79	–.11

Table 21. Simulation results using INFILv3 model 1 for hydrographic areas and subareas in the Death Valley region, Nevada and California, 1950–99—Continued

Hydrographic areas and subareas		Potential evapotranspiration	Precipitation	Snowfall	Sublimation	Evapotranspiration	Change in storage	Runoff	Infiltrated run-on	Net infiltration	Adjusted net infiltration [1]	Outflow
Name	Identifier											
Mercury Valley	225	1,177	148.8	5.0	0.38	146.2	0.04	2.29	1.68	1.54	1.54	0.61
Mesquite Valley	163	1,224	175.1	7.4	.69	170.5	.22	1.66	1.73	3.77	3.77	–.07
Oasis Valley	228	1,105	178.2	19.1	1.87	173.3	.10	2.94	2.50	2.55	2.24	.44
Pahranagat Valley	209	1,107	210.2	20.9	1.99	205.8	–.14	.52	.52	2.61	2.61	.00
Pahrump Valley	162	1,181	176.7	29.7	3.88	166.9	–.08	2.19	1.80	5.66	5.66	.40
Penoyer Valley	170	1,050	225.5	40.0	4.12	217.7	–.09	4.07	3.79	3.55	3.55	.28
Railroad Valley (south)	173A	1,025	226.9	48.8	5.16	218.1	–.02	4.05	3.64	3.32	3.32	.41
Rock Valley	226	1,220	144.0	3.0	.24	141.5	–.01	1.08	.80	2.00	2.00	.28
Sarcobatus Flat	146	1,106	170.2	18.2	1.67	166.9	.00	2.17	1.97	1.44	1.43	.20
Shadow Valley	245	1,218	186.6	5.9	.53	184.1	.20	1.00	1.33	2.11	2.11	–.33
Stonewall Flat	145	1,071	178.2	26.8	2.79	173.8	–.09	1.13	1.08	1.56	1.56	.05
Three Lakes Valley (north)	168	1,136	182.2	13.8	1.14	178.7	–.04	.45	.45	2.36	2.36	.00
Three Lakes Valley (south)	211	1,141	170.9	21.0	2.09	167.0	–.16	.29	.31	2.05	2.05	–.02
Tikapoo Valley (north)	169A	1,087	209.8	27.8	2.77	204.1	–.12	1.28	1.27	3.07	3.07	.01
Tikapoo Valley (south)	169B	1,125	188.9	15.7	1.36	184.7	–.03	.35	.37	2.96	2.96	–.02
Valjean Valley	244	1,320	127.4	2.1	.19	126.4	.10	2.23	2.37	.77	.77	–.14
Yucca Flat	159	1,126	184.4	15.1	1.42	180.1	.37	3.07	2.96	2.48	2.48	.11
All hydrogaphic areas and subareas	na	1,153	175.0	21.7	2.29	169.9	.03	2.19	2.02	2.60	2.59	.17

[1]Net infiltration is slightly reduced in some basins to account for ground-water discharge zones.

Table 22. Previous estimates of recharge rates and simulated net-infiltration rates using INFILv3 models 1–4 for hydrographic areas and subareas in the Death Valley region, Nevada and California, 1950–99

[See figure 4 for locations of areas and subareas (by identifier). For areas having more than one estimate of recharge (see table 1), the average recharge estimate was used. AVG, average; D, Deuterium mixing model; GFM, ground-water flow model; ME, Maxey–Eakin. mm/yr, millimeters per year; na, not applicable]

Hydrographic areas and subareas		Estimated modern-day recharge (mm/year)	Recharge estimation method	Simulated net infiltration, in millimeters per year				
Name	Identifier			Model 1	Model 2	Model 3	Model 4	Average for models 1 and 3
Alkali Spring Valley	142	0.15	ME	0.21	0.20	0.05	0.03	0.12
Amargosa Desert	230	.54	ME	.77	.70	.33	.21	.49
Cactus Flat	148	.72	ME	1.70	1.37	1.03	.81	1.26
California Valley	241	.85	ME	2.75	1.78	1.42	1.20	1.98
Chicago Valley	240	.22	ME	2.49	2.45	1.22	.80	1.65
Clayton Valley	143	1.29	ME	.90	.72	.41	.32	.61
Coal Valley	171	2.09	ME	3.47	2.82	1.88	1.57	2.52
Crater Flat	229	.57	ME	.70	.66	.26	.16	.43
Death Valley	243	1.04	ME	2.22	1.65	1.11	.90	1.54
Emigrant Valley (Groom Lake)	158A	2.31	ME	4.14	2.74	2.25	2.12	3.13
Emigrant Valley (Papoose Lake)	158B	.02	ME	1.61	1.23	.75	.70	1.15
Fortymile Canyon (Buckboard Mesa)	227B	2.89	ME	4.04	2.70	2.02	1.99	3.02
Fortymile Canyon (Jackass Flats)	227A	1.51	ME	2.67	1.55	1.69	1.35	2.01
Frenchman Flat	160	.10	ME	1.98	1.85	1.14	.79	1.39
Garden Valley	172	9.97	ME	3.50	2.80	2.02	1.77	2.64
Gold Flat	147	2.66	ME	2.94	2.26	1.57	1.36	2.15
Hidden Valley (south)	166	.14	ME	.33	.33	.11	.06	.20
Indian Springs Valley	161	7.13	ME	3.27	3.16	1.50	1.16	2.22
Ivanpah Valley (north)	164A	2.92	ME	2.73	2.69	1.55	1.12	1.92
Ivanpah Valley (south)	164B	.47	ME	1.47	.81	.55	.54	1.00
Jean Lake Valley	165	.48	ME	.36	.25	.10	.07	.21
Kawich Valley	157	4.64	ME	4.89	3.31	2.85	2.76	3.82
Las Vegas Valley	212	8.87	AVG	4.97	4.91	2.94	2.39	3.68
Lida Valley	144	.42	GFM	.54	.47	.20	.16	.35
Lower Amargosa Valley	242	.09	GFM	.79	.75	.38	.22	.50
Mercury Valley	225	1.07	ME	1.54	1.45	.59	.41	.97
Mesquite Valley	163	1.68	AVG	3.77	3.50	2.22	1.75	2.76
Oasis Valley	228	1.01	ME	2.55	2.01	.94	.71	1.47
Pahranagat Valley	209	1.01	AVG	2.61	2.51	1.20	.89	1.75
Pahrump Valley	162	15.17	AVG	5.66	5.53	3.30	2.70	4.18

Table 22. Previous estimates of recharge rates and simulated net-infiltration rates using INFILv3 models 1–4 for hydrographic areas and subareas in the Death Valley region, Nevada and California, 1950–99 —Continued

Hydrographic areas and subareas		Estimated modern-day recharge (mm/year)	Recharge estimation method	Simulated net infiltration, in millimeters per year				
Name	Identifier			Model 1	Model 2	Model 3	Model 4	Average for models 1 and 3
Penoyer Valley	170	2.59	AVG	3.55	2.93	1.87	1.42	2.49
Railroad Valley (south)	173A	4.18	AVG	3.32	2.66	2.01	1.60	2.46
Rock Valley	226	.17	ME	2.00	1.94	.94	.67	1.33
Sarcobatus Flat	146	.70	ME	1.44	1.18	.79	.58	1.01
Shadow Valley	245	1.46	ME	2.11	1.82	.83	.62	1.36
Stonewall Flat	145	.13	ME	1.56	1.46	.86	.56	1.06
Three Lakes Valley (north)	168	3.16	ME	2.36	2.35	.97	.68	1.52
Three Lakes Valley (south)	211	9.48	ME	2.05	2.03	.84	.71	1.38
Tikapoo Valley (north)	169A	2.01	ME	3.07	2.84	1.37	1.10	2.08
Tikapoo Valley (south)	169B	4.37	ME	2.96	2.95	1.21	.81	1.88
Valjean Valley	244	.46	ME	.77	.06	.30	.44	.60
Yucca Flat	159	1.11	ME	2.48	1.91	1.34	1.05	1.76
Combined areas:								
California and Chicago Valleys	241 and 240	.58	GFM	2.64	2.10	1.32	1.02	1.83
Emigrant Valley	158	8.04	GFM	3.78	1.83	1.35	1.76	2.77
Fortymile Canyon	227	.63	GFM	3.28	2.05	1.83	1.70	2.49
Garden and Coal Valleys	172 and 171	5.61	D	3.49	2.81	1.92	1.68	2.58
Mercury and Rock Valleys	225 and 226	0.94	GFM	1.74	1.69	0.76	0.57	1.15
Death Valley regional flow system (DVRFS) model	na	2.15	GFM	2.77	2.36	1.44	1.17	1.96
Average estimation error (m^3/d)				–.07	–.49	–1.26	–1.47	–.77
Standardized mean square error				.61	.64	.89	.97	.73
Pearson correlation coefficient				.67	.70	.63	.64	.66

Table 23. Previously estimated recharge volumes and simulated net infiltration volumes using INFILv3 models 1–4 for hydrographic areas and subareas in the Death Valley region, Nevada and California, 1950–99

[See figure 4 for locations of areas and subareas (by identifier). For areas having more than one estimate of recharge (see table 1), the average recharge estimate was used. AVG, average; D, Deuterium mixing model; GFM, ground-water flow model; ME, Maxey–Eakin. m^3/d, cubic meters per day. na, not applicable]

Hydrographic areas and subareas		Estimated modern-day recharge (m^3/d)	Recharge estimation method	Simulated net infiltration (m^3/d)				
Name	Identifier			Model 1	Model 2	Model 3	Model 4	Average for models 1 and 3
Alkali Spring Valley	142	338	ME	480	459	109	73	294
Amargosa Desert	230	5,066	ME	7,225	6,602	3,065	2,009	5,145
Cactus Flat	148	2,026	ME	4,761	3,840	2,873	2,271	3,817
California Valley	241	814	ME	2,617	1,689	1,353	1,142	1,985
Chicago Valley	240	169	ME	1,920	1,887	936	615	1,428
Clayton Valley	143	5,066	ME	3,549	2,842	1,606	1,252	2,577
Coal Valley	171	6,754	ME	11,219	9,100	6,060	5,081	8,640
Crater Flat	229	743	ME	904	860	335	209	620
Death Valley	243	27,017	ME	57,041	42,865	28,872	23,374	42,956
Emigrant Valley (Groom Lake)	158A	10,807	ME	19,382	12,810	10,520	9,906	14,951
Emigrant Valley (Papoose Lake)	158B	14	ME	1,243	954	579	540	911
Fortymile Canyon (Buckboard Mesa)	227B	4,728	ME	6,616	4,416	3,301	3,260	4,959
Fortymile Canyon (Jackass Flats)	227A	3,039	ME	5,347	3,114	3,389	2,701	4,368
Frenchman Flat	160	338	ME	6,426	5,998	3,681	2,573	5,054
Garden Valley	172	33,771	ME	11,223	8,969	6,469	5,677	8,846
Gold Flat	147	12,833	ME	14,201	10,922	7,603	6,569	10,902
Hidden Valley (south)	166	34	ME	78	77	26	14	52
Indian Springs Valley	161	33,771	ME	15,505	14,979	7,113	5,493	11,309
Ivanpah Valley (north)	164A	5,066	ME	4,723	4,659	2,680	1,938	3,702
Ivanpah Valley (south)	164B	1,689	ME	5,299	2,909	1,987	1,930	3,643
Jean Lake Valley	165	338	ME	248	175	70	51	159
Kawich Valley	157	11,820	ME	12,454	8,428	7,253	7,022	9,854
Las Vegas Valley	212	97,936	AVG	51,154	50,557	30,233	24,650	40,694
Lida Valley	144	1,600	GFM	2,059	1,781	773	594	1,416
Lower Amargosa Valley	242	300	GFM	2,591	2,470	1,245	719	1,918
Mercury Valley	225	844	ME	1,214	1,139	464	319	839
Mesquite Valley	163	5,234	AVG	11,719	10,861	6,888	5,443	9,303
Oasis Valley	228	3,377	ME	7,459	6,689	3,141	2,371	5,300
Pahranagat Valley	209	5,572	AVG	13,663	13,129	6,292	4,675	9,978
Pahrump Valley	162	106,378	AVG	39,712	38,772	23,171	18,969	31,441

Table 23. Previously estimated recharge volumes and simulated net infiltration volumes using INFILv3 models 1–4 for hydrographic areas and subareas in the Death Valley region, Nevada and California, 1950–99—Continued

Hydrographic areas and subareas		Estimated modern-day recharge (m^3/d)	Recharge estimation method	Simulated net infiltration (m^3/d)				
Name	Identifier			Model 1	Model 2	Model 3	Model 4	Average for models 1 and 3
Penoyer Valley	170	12,720	AVG	17,427	14,346	9,167	6,984	13,297
Railroad Valley (south)	173A	17,561	AVG	13,964	11,181	8,456	6,736	11,210
Rock Valley	226	101	ME	1,189	1,157	560	398	874
Sarcobatus Flat	146	4,053	ME	8,329	6,866	4,560	3,357	6,445
Shadow Valley	245	4,053	ME	5,847	5,051	2,296	1,711	4,071
Stonewall Flat	145	338	ME	4,191	3,912	2,306	1,504	3,248
Three Lakes Valley (north)	168	6,754	ME	5,031	5,014	2,078	1,446	3,555
Three Lakes Valley (south)	211	20,263	ME	4,382	4,350	1,798	1,509	3,090
Tikapoo Valley (north)	169A	8,780	ME	13,410	12,400	6,004	4,798	9,707
Tikapoo Valley (south)	169B	11,482	ME	7,751	7,743	3,168	2,122	5,460
Valjean Valley	244	1,351	ME	2,266	178	891	1,291	1,579
Yucca Flat	159	2,364	ME	5,257	4,051	2,852	2,223	4,054
Combined areas:								
California and Chicago Valleys	241 and 240	1,600	GFM	4,538	3,576	2,289	1,757	3,413
Emigrant Valley	158	43,900	GFM	20,625	13,764	11,099	10,446	15,862
Fortymile Canyon	227	2,300	GFM	11,963	7,530	6,690	5,961	9,327
Garden and Coal Valleys	172 and 171	37,148	D	22,442	18,069	12,529	10,758	17,485
Mercury and Rock Valleys	225 and 226	1,300	GFM	2,402	2,296	1,024	718	1,713
Death Valley regional flow system (DVRFS) model	na	266,800	GFM	342,098	293,121	178,675	144,700	260,387
Average estimation error (m^3/d)				–317	–2,954	–8,371	–10,010	–4,344
Standardized mean-squared error				.18	.12	.26	.37	.14
Pearson correlation coefficient				.93	.94	.94	.94	.93